МИСИС
УНИВЕРСИТЕТ НАУКИ И ТЕХНОЛОГИЙ

СибГИУ
Сибирский государственный индустриальный университет

ISSN 0368-0797
eISSN 2410-2091

ИЗВЕСТИЯ ВЫСШИХ УЧЕБНЫХ ЗАВЕДЕНИЙ ЧЕРНАЯ МЕТАЛЛУРГИЯ

IZVESTIYA. FERROUS METALLURGY

fermet.misis.ru

2024 Том Vol. 67 № No. 6

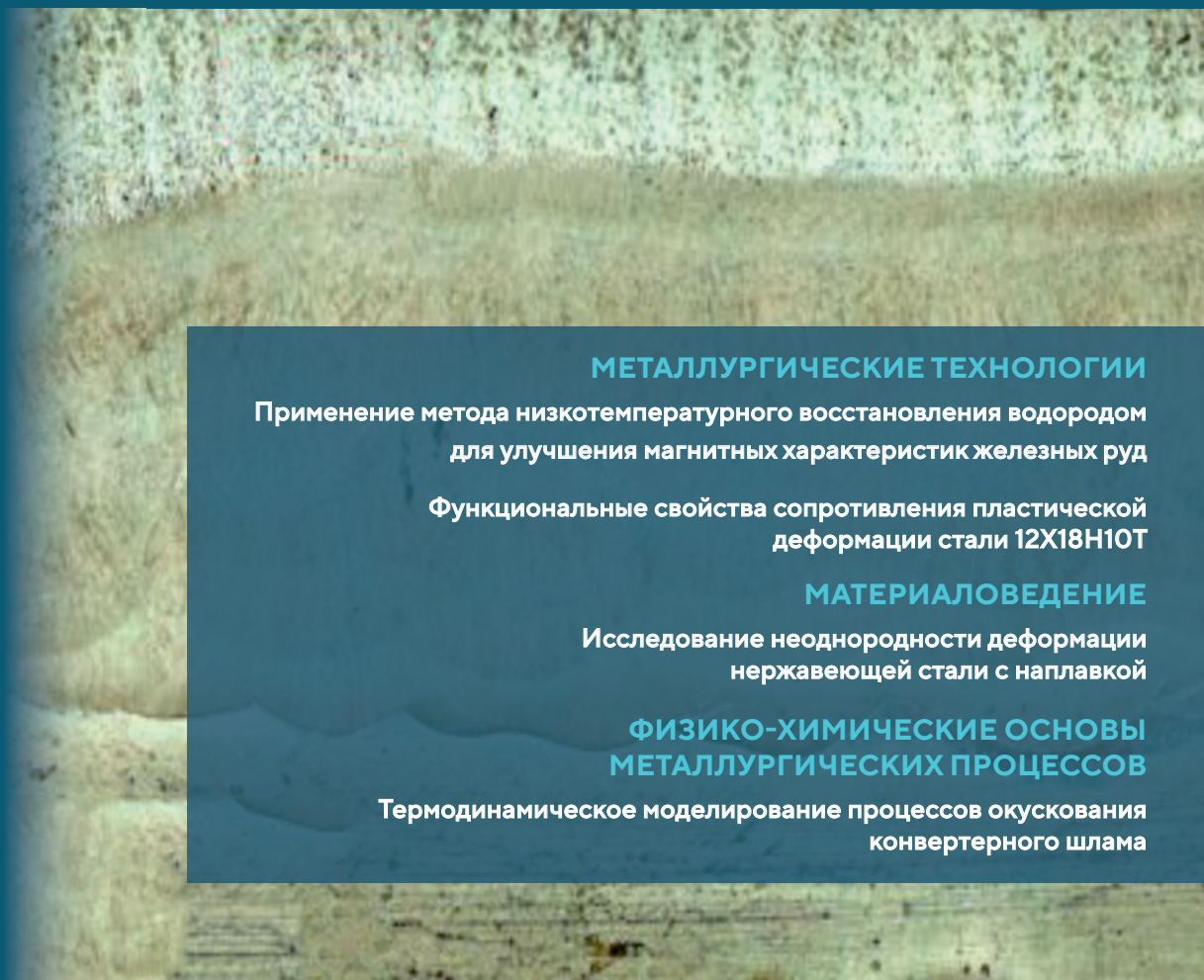

МИСИС УНИВЕРСИТЕТ

СибГИУ
Сибирский государственный индустриальный университет

ISSN 0368-0797
eISSN 2410-2091

ИЗВЕСТИЯ ВЫСШИХ УЧЕБНЫХ ЗАВЕДЕНИЙ ЧЕРНАЯ МЕТАЛЛУРГИЯ

Научно-технический журнал

Издается с января 1958 г. Выпускается 6 раз в год

2024 Том Vol. 67 № No. 6

IZVESTIYA FERROUS METALLURGY

Scientific and Technical Journal

Published since January 1958. Issued 6 times a year

IZVESTIYA FERROUS METALLURGY

www.fermet.misis.ru

ISSN 0368-0797 *(Print)* ISSN 2410-2091 *(Online)*

Alternative title:

Izvestiya vuzov. Chernaya metallurgiya

Founders:

MISIS
UNIVERSITY OF SCIENCE AND TECHNOLOGY

SibSIU
Siberian State Industrial University

Publisher:

National University of Science and Technology "MISIS"

Editorial Office Address:

in Moscow
4 Leninskii Ave., Moscow 119049, Russian Federation
National University of Science and Technology "MISIS"
Tel.: +7 (495) 638-44-11
E-mail: fermet.misis@mail.ru, ferrous@misis.ru

in Novokuznetsk
42 Kirova Str., Novokuznetsk, Kemerovo Region – Kuzbass
654007, Russian Federation
Siberian State Industrial University
Tel.: +7 (3843) 74-86-28 *E-mail*: redjizvz@sibsiu.ru

In accordance with paragraph 5 of the Rules for the formation of the Higher Attestation Comission list journal "Izvestiya. Ferrous metallurgy" is included in the list of leading peer-reviewed scientific journals, publication in which is taken into account in the defense of candidate and doctoral dissertations, as indexed in internatonal data bases.

Indexed: Scopus, Russian Science Citation Index (RSCI), Research Bible, Chemical Abstracts, OCLC and Google Scholar

Registered in Federal Service for Supervision in the Sphere of Mass Communications **PI number FS77-35456**.

ИЗВЕСТИЯ
ВЫСШИХ УЧЕБНЫХ ЗАВЕДЕНИЙ
ЧЕРНАЯ МЕТАЛЛУРГИЯ

www.fermet.misis.ru

ISSN 0368-0797 *(Print)* ISSN 2410-2091 *(Online)*

Варианты названия:

Известия вузов. Черная металлургия

Izvestiya. Ferrous Metallurgy

Учредители:

МИСИС
УНИВЕРСИТЕТ НАУКИ И ТЕХНОЛОГИЙ

СибГИУ
Сибирский государственный индустриальный университет

Издатель:

Национальный исследовательский технологический университет «МИСИС»

Адреса подразделений редакции:

в Москве
Россия, 119049, Москва, Ленинский просп., д. 4, стр. 1
Национальный исследовательский технологический университет «МИСИС»
Тел.: +7 (495) 638-44-11 *E-mail*: ferrous@misis.ru

в Новокузнецке
Россия, 654007, Новокузнецк,
Кемеровская обл. – Кузбасс, ул. Кирова, зд. 42
Сибирский государственный индустриальный университет
Тел.: +7 (3843) 74-86-28 *E-mail:* redjizvz@sibsiu.ru

В соответствии п. 5 Правил формирования перечня ВАК журнал «Известия вузов. Черная металлургия» входит в перечень ведущих рецензируемых научных журналов и изданий, публикация в которых учитывается при защитах кандидатских и докторских диссертаций как индексируемый в МБД.

Индексирование: Scopus, Russian Science Citation Index (RSCI), Research Bible, Chemical Abstracts, OCLC и Google Scholar

Зарегистрирован Федеральной службой по надзору в сфере связи и массовых коммуникаций **ПИ № ФС77-35456**.

Izvestiya. Ferrous Metallurgy.
2024;67(6)

Известия вузов. Черная металлургия.
2024;67(6)

CONTENTS / СОДЕРЖАНИЕ

METALLURGICAL TECHNOLOGIES

ECOLOGY AND RATIONAL USE OF NATURAL RESOURCES

MATERIALS SCIENCE

МЕТАЛЛУРГИЧЕСКИЕ ТЕХНОЛОГИИ

ЭКОЛОГИЯ И РАЦИОНАЛЬНОЕ ПРИРОДОПОЛЬЗОВАНИЕ

МАТЕРИАЛОВЕДЕНИЕ

CONTENTS *(Continuation)* / СОДЕРЖАНИЕ *(продолжение)*

PHYSICO-CHEMICAL BASICS OF METALLURGICAL PROCESSES

ФИЗИКО-ХИМИЧЕСКИЕ ОСНОВЫ МЕТАЛЛУРГИЧЕСКИХ ПРОЦЕССОВ

INNOVATIONS IN METALLURGICAL INDUSTRIAL AND LABORATORY EQUIPMENT, TECHNOLOGIES AND MATERIALS

ИННОВАЦИИ В МЕТАЛЛУРГИЧЕСКОМ ПРОМЫШЛЕННОМ И ЛАБОРАТОРНОМ ОБОРУДОВАНИИ, ТЕХНОЛОГИЯХ И МАТЕРИАЛАХ

INFORMATION TECHNOLOGIES AND AUTOMATIC CONTROL IN FERROUS METALLURGY

ИНФОРМАЦИОННЫЕ ТЕХНОЛОГИИ И АВТОМАТИЗАЦИЯ В ЧЕРНОЙ МЕТАЛЛУРГИИ

UDC 621.771.65
DOI 10.17073/0368-0797-2024-6-637-643

Original article
Оригинальная статья

Influence of chemical composition of steels for production of grinding balls on their deformation characteristics

A. A. Umanskii ✉, **V. V. Baidin**, **A. S. Simachev**

Siberian State Industrial University (42 Kirova Str., Novokuznetsk, Kemerovo Region – Kuzbass 654007, Russian Federation)

✉ umanskii@bk.ru

Abstract. The conducted studies determined the patterns of influence of chemical composition and deformation parameters of ball steels with experimental chemical composition on their deformability. The development of experimental chemical compositions of ball steels was carried out based on the existing experience of domestic and foreign researchers, taking into account the possibility of further application of the obtained results for ball steels of standard grades. The studies were carried out using a specialized laboratory installation by the method of hot-rolling samples. An increase in the carbon content in the range of 0.72 – 0.85 %, manganese in the range from 0.72 to 0.85 %, chromium in the range of 0.38 – 1.71 % and nickel in the range from 0.08 to 0.87 % has a significant effect on increasing the deformation resistance of steels. At the same time, the quantitative effect of carbon content in the steels on their deformation resistance is much more pronounced in relation to manganese, chromium and nickel. It was determined that a decrease in the deformation temperature from 1200 to 900 °C, an increase in the deformation rate in the range from 1 to 10 s^{-1} and true deformation in the range 0.05 – 0.35 cause an increase in the deformation resistance of ball steels, regardless of their chemical composition. The influence of all these parameters on the deformation resistance of steels has a pronounced nonlinear character and the deformation temperature has the greatest relative influence on the deformation resistance. The data obtained are summarized in the form of a multiple regression equation, which establishes the quantitative relationship between the resistance of steel to deformation with its chemical composition and deformation parameters. Verification of the adequacy of the obtained equation in relation to the rolling conditions of ball steel billets of standard grades at the continuous medium-grade mill 450 of JSC EVRAZ United West Siberian Metallurgical Plant confirmed the possibility of using it to predict the energy-power parameters of rolling ball steels of various chemical composition.

Keywords: deformation resistance, grinding balls, long billet, hot torsion, chemical composition, temperature and velocity parameters of deformation

For citation: Umanskii A.A., Baidin V.V., Simachev A.S. Influence of chemical composition of steels for production of grinding balls on their deformation characteristics. *Izvestiya. Ferrous Metallurgy*. 2024;67(6):637–643. https://doi.org/10.17073/0368-0797-2024-6-637-643

Исследование влияния химического состава сталей для производства мелющих шаров на их деформационные характеристики

А. А. Уманский ✉, **В. В. Байдин**, **А. С. Симачев**

Сибирский государственный индустриальный университет (Россия, 654007, Кемеровская обл. – Кузбасс, Новокузнецк, ул. Кирова, 42)

✉ umanskii@bk.ru

Аннотация. Авторы определили закономерности влияния химического состава и параметров деформации шаровых сталей экспериментального химического состава на их деформируемость. Разработку экспериментальных химических составов шаровых сталей вели, опираясь на имеющийся опыт отечественных и зарубежных исследователей, с учетом возможности дальнейшего применения полученных результатов для шаровых сталей стандартных марок. Исследования проводились с использованием специализированной лабораторной установки методом горячего кручения образцов. Повышение содержания углерода в диапазоне 0,72 – 0,85 %, марганца в интервале от 0,72 до 0,85 %, хрома в диапазоне 0,38 – 1,71 % и никеля в интервале от 0,08 до 0,87 % оказывает значимое влияние на увеличение сопротивления деформации сталей. При этом количественное влияние содержания углерода в сталях на их сопротивление деформации является значительно более выраженным по отношению к марганцу, хрому и никелю. Определено, что снижение температуры деформации с 1200 до 900 °С, увеличение скорости деформации в интервале от 1 до 10 $с^{-1}$ и истинной деформации в диапазоне 0,05 – 0,35 обуславливают

повышение сопротивления деформации шаровых сталей вне зависимости от их химического состава. Влияние всех перечисленных параметров на сопротивление сталей деформированию имеет выраженный нелинейный характер и наибольшее относительное влияние на сопротивление деформации оказывает температура деформации. Полученные данные обобщены в виде уравнения множественной регрессии, устанавливающего количественную взаимосвязь сопротивления стали деформированию с ее химическим составом и параметрами деформации. Проверка адекватности полученного уравнения применительно к условиям прокатки заготовок шаровых сталей стандартных марок на непрерывном среднесортном стане 450 АО «ЕВРАЗ Объединенный Западно-Сибирский металлургический комбинат» подтвердила возможность его использования для прогнозирования энергосиловых параметров прокатки шаровых сталей различного химического состава.

Ключевые слова: сопротивление деформации, мелющие шары, сортовые заготовки, горячее кручение, химический состав, температурно-скоростные параметры деформации

Для цитирования: Уманский А.А., Байдин В.В., Симачев А.С. Исследование влияния химического состава сталей для производства мелющих шаров на их деформационные характеристики. *Известия вузов. Черная металлургия*. 2024;67(6):637–643.
https://doi.org/10.17073/0368-0797-2024-6-637-643

Introduction

Currently, one of the main approaches to improving the hardness, wear resistance, and impact resistance of steel grinding balls involves refining their chemical composition [1 – 3]. This is due to the inability of standard ball steels to meet the required levels of these quality parameters [4 – 6].

A series of developments aim to improve the chemical composition of steels to enhance the operational properties of grinding balls. In studies [7; 8], pilot-industrial trials were conducted for the production of 35 mm diameter balls from the fifth hardness group using steel alloyed with manganese and chromium to concentrations of 0.90 – 1.05 and 0.40 %, respectively. The resulting grinding balls, after heat treatment, exhibited the following characteristics:

– surface hardness of 59 – 64 HRC;

– hardness at half of the radius of 55 – 60 HRC;

– coercive force (indicative of internal stresses) of 44 – 50 units.

A significant number of patents [9 – 11] propose varying the qualitative and quantitative composition of alloying elements in ball steels within a wide range. In Russian inventions, manganese and chromium are the primary alloying elements, with their content in steels reaching up to 0.90 and 0.60 %, respectively. In contrast, foreign patents distinguish themselves by including a broader range of alloying elements, such as silicon, nickel, molybdenum, and niobium, alongside manganese and chromium, with higher levels of manganese and chromium alloying (upper concentration limits of 2.0 and 1.5 %, respectively).

Currently, there is no consensus on the optimal chemical composition of steel for grinding ball production. However, there is a general trend toward increased alloying levels in these steels. Increasing the concentration of alloying elements in most cases enhances deformation resistance during rolling [12 – 14], leading to a corresponding increase in loads on rolling mill equipment [15; 16].

Given the significant inaccuracies that arise when extrapolating deformation resistance data for standard steel grades to steels with new chemical compositions [17 – 19], experimental studies are needed to evaluate these parameters for new grades of ball steels. In addition to cross-helical rolling mills, multi-stand large or medium-grade rolling mills used for producing initial round-section billets are also integral to the technological cycle of grinding ball production.

Research methodology

The study examined five steel samples, each representing a different variant of chemical composition, previously analyzed in [20] to investigate the microstructure formation processes in grinding balls after heat treatment. The key distinguishing features of these compositions were as follows (Table 1):

1) presence and degree of alloying with chromium and nickel;

2) carbon and manganese content in the steel.

The development of these chemical compositions for ball steels drew on the experience of both domestic and international researchers. The concentration ranges for carbon, manganese, chromium, and nickel in the experimental steels were chosen to facilitate the generalization of results. This allowed for the establishment of relationships between mechanical and deformation characteristics and the content of these elements, as well as their potential application to standard grade ball steels (Table 2).

The deformation resistance of the ball steels was studied using a specialized laboratory installation (Fig. 1) through the hot torsion method. The installation includes a movable and a fixed shaft located inside a resistance furnace. Cylindrical samples with additional heads at their ends are secured in grooves on the shafts. After being heated to the target temperature, the samples are subjected to torsion testing by rotating the movable shaft.

Table 1. **Chemical composition of experimental steel samples**

Таблица 1. **Химический состав образцов опытных сталей**

Element	Content, wt. %, steel (variant)				
	1	*2*	*3*	*4*	*5*
C	0.73 – 0.75	0.70 – 0.74	0.83 – 0.85	0.72 – 0.76	0.75 – 0.78
Si	0.31 – 0.38	0.32 – 0.36	0.34 – 0.37	0.36 – 0.39	0.30 – 0.32
Mn	0.75 – 0.84	0.75 – 0.78	0.80 – 0.85	0.76 – 0.78	0.72 – 0.75
Cr	0.38 – 0.42	1.43 – 1.49	0.81 – 0.83	1.63 – 1.71	1.06 – 1.10
Ni	0.08 – 0.11	0.73 – 0.75	0.19 – 0.21	0.85 – 0.87	0.46 – 0.48
Cu	0.09 – 0.12	0.10 – 0.12	0.11 – 0.13	0.09 – 0.11	0.11 – 0.13
Ti	0.004 – 0.006	0.004 – 0.005	0.007	0.014 – 0.016	0.007
V	0.03 – 0.04	0.04	0.07 – 0.08	0.04	0.04
S	0.010 – 0.014	0.010 – 0.013	0.015 – 0.018	0.009 – 0.011	0.009 – 0.010
P	0.009 – 0.012	0.009 – 0.013	0.009 – 0.012	0.005 – 0.008	0.008 – 0.010

The control unit of the installation, which records the torque and accumulated strain, enables the determination of deformation resistance using the following equation:

$$\sigma = \frac{12\sqrt{3}}{\pi d_0^3} M, \quad (1)$$

where d_0 is the diameter of the sample before testing, and M is the torque.

The adequacy of this installation for determining the plastic and deformation characteristics of steels has been confirmed by previous studies on rail steels [21].

During the experimental research, the deformation temperature was varied between 900 and 1200 °C in increments of 50 °C, while the relative deformation ranged from 5 to 35 % in increments of 5 %. Deformation rates of 1, 5, and 10 s^{-1} were used. The selected range of deformation parameters corresponds to their variation during the production of section billets and grinding balls under industrial rolling mill conditions.

Results and discussion

The analysis of the experimental research results revealed (Fig. 2) that, regardless of the combination of temperature-velocity parameters and deformation degree, Steel *4* is the most difficult to deform among the samples studied, while, Steel *1* demonstrates significantly lower deformation resistance. Meanwhile, the deformation resistance of Steels *2*, *3*, and *5* is approximately at the same level, occupying an intermediate position.

These results can be interpreted as follows: for Steels *1*, *2*, *4*, and *5*, the most significant factor influencing deformation resistance was the chromium and nickel

Table 2. **Chemical composition of standard grade ball steels**

Таблица 2. **Химический состав шаровых сталей стандартных марок**

Steel grade	Element content. wt. %								
	C	Si	Mn	Cr	Ni	Ti	Cu	S	P
Sh2.1	0.60 – 0.69	0.20 – 0.30	0.60 – 0.70	–	–	–	–	≤ 0.025	≤ 0.030
Sh2.2	0.70 – 0.80	0.20 – 0.30	0.60 – 0.70	–	–	–	–	≤ 0.015	≤ 0.020
Sh2.3	0.65 – 0.75	0.20 – 0.35	0.70 – 0.80	0.30 – 0.40	≤ 0.30	–	≤ 0.30	≤ 0.020	≤ 0.030
Sh2.4	0.65 – 0.75	0.20 – 0.35	0.70 – 0.80	0.35 – 0.45	≤ 0.30	–	≤ 0.30	≤ 0.020	≤ 0.030
Sh2.Л	0.65 – 0.75	0.20 – 0.35	0.70 – 0.80	0.50 – 0.60	≤ 0.30	–	≤ 0.30	≤ 0.015	≤ 0.020
Sh1	0.50 – 0.65	0.17 – 0.37	0.60 – 0.70	≤ 0.30	≤ 0.25	≤ 0.03	≤ 0.25	≤ 0.020	≤ 0.030
Sh2	0.60 – 0.75	0.17 – 0.37	0.65 – 0.80	≤ 0.30	≤ 0.25	≤ 0.03	≤ 0.25	≤ 0.020	≤ 0.030
Sh4.1	0.60 – 0.70	0.35 – 0.45	0.65 – 0.75	0.35 – 0.45	≤ 0.25	≤ 0.03	≤ 0.25	≤ 0.020	≤ 0.030
Sh4.2	0.55 – 0.65	0.35 – 0.45	0.65 – 0.75	0.50 – 0.60	0.30 – 0.40	0.02 – 0.05	≤ 0.25	≤ 0.020	≤ 0.030
Sh5	0.65 – 0.75	0.35 – 0.45	0.75 – 0.85	0.55 – 0.60	0.40 – 0.50	0.02 – 0.05	≤ 0.25	≤ 0.020	≤ 0.030

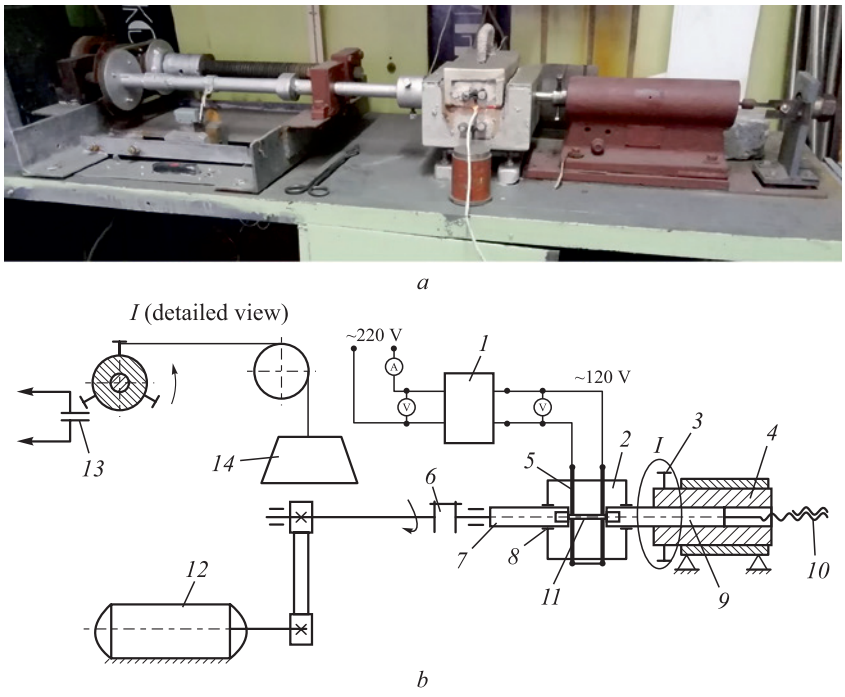

Fig. 1. General view (*a*) and diagram (*b*) of the installation for testing samples for hot torsion:
1 – transformer; *2* – resistance furnace; *3* – locking screw; *4* – fixed shaft housing; *5* – device for fixing the number of revolutions; *6* – silite heaters; *7* – movable shaft; *8* – seal; *9* – fixed shaft; *10* – screw nut; *11* – steel sample; *12* – electric motor; *13* – opening contact; *14* – load

Рис. 1. Общий вид (*a*) и схема (*b*) установки для испытаний образцов на горячее кручение:
1 – трансформатор; *2* – печь сопротивления; *3* – стопорный винт; *4* – корпус неподвижного вала; *5* – устройство для фиксации количества оборотов; *6* – силитовые нагреватели; *7* – подвижный вал; *8* – уплотнение; *9* – неподвижный вал; *10* – винт-гайка; *11* – стальной образец; *12* – электродвигатель; *13* – размыкающий контакт; *14* – груз

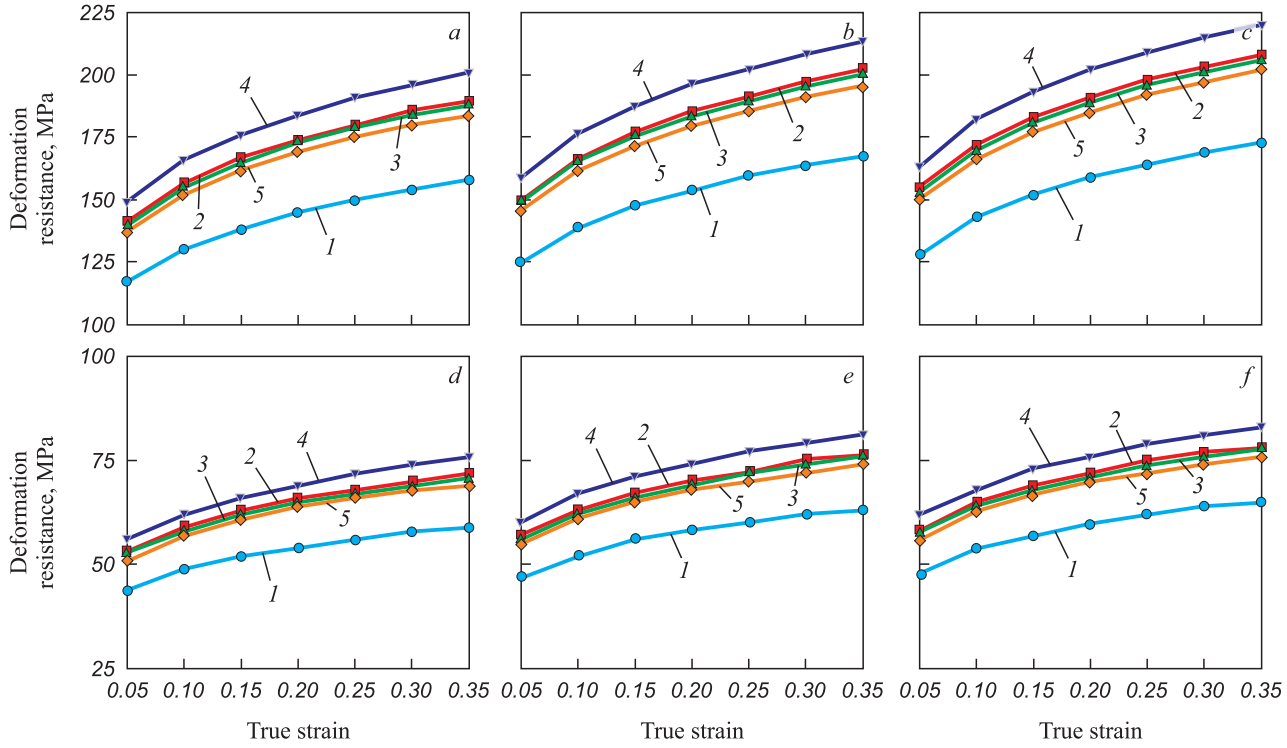

Fig. 2. Flow curves for ball steels at deformation temperatures of 900 (*a* – *c*) and 1200 °C (*d* – *f*) and deformation rates of 1 (*a*, *d*), 5 (*b*, *e*) and 10 s^{-1} (*c*, *f*)

Рис. 2. Кривые течения для шаровых сталей при температуре деформации 900 (*a* – *c*) и 1200 °C (*d* – *f*) и скорости деформации 1 (*a*, *d*), 5 (*b*, *e*) и 10 $с^{-1}$ (*c*, *f*)

content. The deformation resistance of these steels is directly proportional to the concentration of these elements. This relationship is particularly evident given the minimal variations in the concentrations of other elements. Across the samples, the average deviations in carbon, silicon, and manganese content do not exceed 0.045, 0.065, and 0.060 %, respectively (Table 1). For Steel *3*, however, chromium and nickel content are not the determining factors for its deformability. Despite significantly lower concentrations of these elements in Steels *2* and 5 (Table 1), Steel *3* exhibits similar deformation resistance. This behavior in Steel *3* can likely be attributed to its higher carbon content, exceeding that of Steels *2* and *5* by 0.120 and 0.075 %, respectively, and its higher manganese content, exceeding those of Steels *2* and *5* by 0.06 and 0.09 %, respectively. Overall, the findings suggest that carbon content plays a quantitatively dominant role in influencing the deformation resistance of ball steels compared to other elements studied.

It was also determined that, for all the analyzed steel compositions, increasing the deformation degree and deformation rate, as well as decreasing the deformation temperature, reduces deformability (i.e., increases deformation resistance). Additionally, the influence of these parameters on deformation resistance exhibits a distinctly nonlinear pattern, aligning qualitatively with widely accepted principles. Among the deformation parameters, temperature has the greatest impact on deformation resistance. For example, lowering the deformation temperature from 1200 to 900 °C increases deformation resistance by an average of 2.7 times, with deformation rate and deformation degree held constant. In comparison, increasing the true deformation from 0.05 to 0.35 results in only 36 % average increase in deformation resistance under similar temperature-velocity parameters, while changes in deformation rate contribute to a maximum increase of approximately 9 %.

The comprehensive analysis and processing of the experimental results facilitated the development of a regression equation that quantitatively describes the relationship between the deformation resistance of steels used in grinding ball production, their chemical composition, and rolling parameters:

$$\sigma_s = (4032[C] + 336[Mn] + 546[Cr] + \\ + 364[Ni])3689e^{-3.255\left(\frac{t}{1000}\right)}\varepsilon^{0.153}u^{0.004}, \quad (2)$$

where σ_s is the deformation resistance of steel (MPa); [C], [Mn], [Cr] and [Ni] are the contents of carbon, manganese, chromium, and nickel in the steel (%); t is the rolling temperature (°C); ε is the true strain; and u is the deformation rate (s^{-1}).

The validity of the equation was confirmed by comparing the rolling force calculated based on the computed deformation resistances with the actual rolling forces measured during the production of 60 mm diameter grinding ball billets from Sh2.1 and Sh2.3 steel grades (Table 2) at the continuous medium-grade mill 450 of JSC EVRAZ United West Siberian Metallurgical Combine. The observed deviations did not exceed 10 % (Fig. 3), demonstrating the reliability of the equation and its suitability for designing and optimizing rolling modes for both grinding balls and initial billets.

Conclusions

Based on the experimental studies, the relationships between the chemical composition of ball steels, their deformation parameters, and deformation resistance were analyzed both qualitatively and quantitatively. The findings were consolidated into a multiple regression equa-

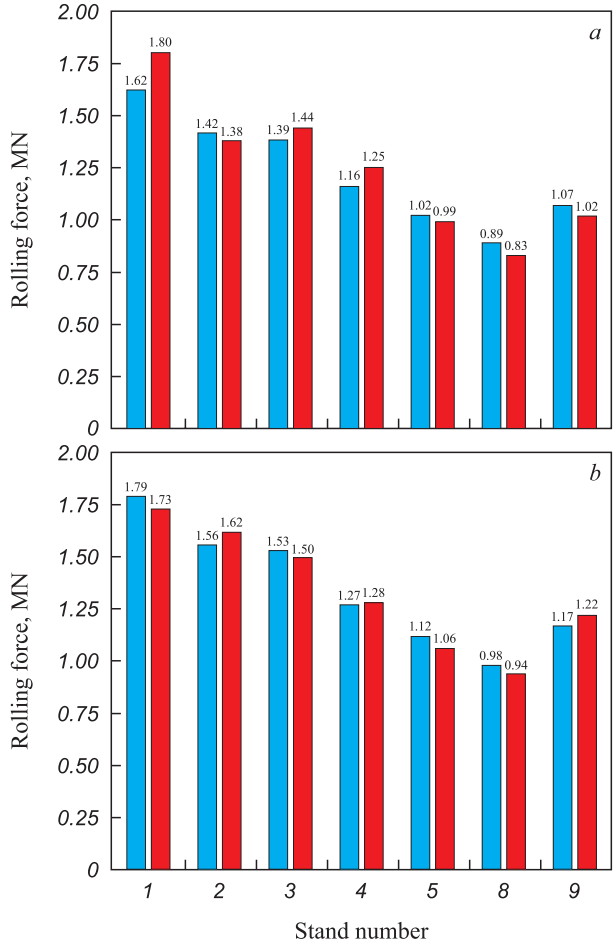

Fig. 3. Rolling force in the roughing stands of the medium-grade mill 450 of JSC EVRAZ United West Siberian Metallurgical Plant in the production of a ball furnace with a diameter of 60 mm made of steel grades Sh2.1 (*a*) and Sh2.3 (*b*):
■ – calculation; ■ – fact

Рис. 3. Усилие прокатки в черновых клетях среднесортного стана 450 АО «ЕВРАЗ Объединенный Западно-Сибирский металлургический комбинат» при производстве шаровой заготовки диаметром 60 мм из стали марок Ш2.1 (*a*) и Ш2.3 (*b*):
■ – расчет; ■ – факт

tion, whose validity was confirmed under production conditions for ball steel billets at the continuous medium-grade mill 450 of JSC EVRAZ United West Siberian Metallurgical Plant.

References / Список литературы

1. Aldrich C. Consumption of steel grinding media in mills. *Minerals Engineering*. 2013;49:77–91. https://doi.org/10.1016/j.mineng.2013.04.023
2. Bai X., Jin Y. Heat treatment of wear resistant steel ball for large ball mill. *Jinshu Rechuli / Heat Treatment of Metals*. 2017;42(5):193–196. https://doi.org/10.13251/j.issn.0254-6051.2017.05.040
3. Kotenok V.I., Podobedov S.I. Energy-efficient design of rolls for ball-rolling mills. *Metallurgist*. 2001;45(9-10):363–367. https://doi.org/10.1023/A:1017920006038
4. Song Z., Pu Y., Liu Z., Wang B. Analysis of failure of grinding balls during service. *Metal Science and Heat Treatment*. 2022;64(12):127–133. https://doi.org/10.1007/s11041-022-00772-3
5. Li T., Peng Y., Zhu Z., Zou S., Liu S., Yin Z., Ni X., Chang X. Multi-layer kinematics and collision energy in a large-scale grinding mill-the largest semi-autogenous grinding mill in China. *Advances in Mechanical Engineering*. 2016;8(12):1–10. https://doi.org/10.1177/1687814016681371
6. Rakhutin M.G., Boyko P.F. Ways to improve assessment methods of the main characteristics of grinding balls. *Ugol'–Russian Coal Journal*. 2017;(12(1101)):49–52. (In Russ.). https://doi.org/10.18796/0041-5790-2017-12-49-52

   Рахутин М.Г., Бойко П.Ф. Пути совершенствования методов оценки основных характеристик мелющих шаров. *Уголь*. 2017;(12(1101)):49–52. https://doi.org/10.18796/0041-5790-2017-12-49-52
7. Bykov P.O., Kasimgazinov A.D. Research and approbation of production technology for rolled grinding balls of the 5th group of hardness in the PB LLP "Casting". *Nauka i tekhnika Kazakhstana*. 2018;(1):31–40. (In Russ.).

   Быков П.О., Касимгазинов А.Д. Исследование и апробация технологии получения катаных помольных шаров 5 группы твердости в условиях ПФ ТОО «Кастинг». *Наука и техника Казахстана*. 2018;(1):31–40.
8. Naizabekov A.B., Mukhametkaliev B.S., Arbuz A.S., Lezhnev S.N. Reducing consumption of steel grinding balls by improving their production technology. *Vesti vysshikh uchebnykh zavedenii Chernozem'ya*. 2016;(4(46)):78–86. (In Russ.).

   Найзабеков А.Б., Мухаметкалиев Б.С., Арбуз А.С., Лежнев С.Н. Снижение расхода стальных мелющих шаров путем улучшения технологии их производства. *Вести высших учебных заведений Черноземья.* 2016;(4(46)):78–86.
9. Pavlov V.V., Korneva O.V., Atkonova O.P Steel for grinding balls. Pat. 2340699 RF. *Bulleten' izobretenii*. 2008;34.

   Пат. 2340699 РФ. Сталь для мелющих шаров / В.В. Павлов, О.В. Корнева, О.П. Атконова; заявл. 31.10.2006; опубл. 10.12.2008. Бюл. 34.
10. Yur'ev A.B., Mukhatdinov N.Kh., Atkonova O.P., etc. Steel. Pat. 2425168 RF. *Bulleten' izobretenii*. 2011;21.

    Пат. 2425168 РФ. Сталь / А.Б. Юрьев, Н.Х. Мухатдинов, О.П. Атконова и др.; заявл. 05.10.2009; опубл. 27.07.2011. Бюл. № 21.
11. Yur'ev A.B., Mukhatdinov N.Kh., Kozyrev N.A., etc. Pat. 2425169 RF. Steel. *Bulleten' izobretenii*. 2011;21.

    Пат. 2425169 РФ. Сталь / А.Б. Юрьев, Н.Х. Мухатдинов, Н.А. Козырев и др.; заявл. 05.10.2009; опубл. 27.07.2011. Бюл. № 21.
12. Rodriguez-Ibabe J.M., Gutiérrez I., López B., Iza-Mendia A. Modeling of the resistance to hot deformation and the effects of microalloying in high-Al steels under industrial conditions. *Materials Science Forum*. 2005;500-501:195–202. https://doi.org/10.4028/www.scientific.net/MSF.500-501.195
13. Konovalov A.V., Smirnov A.S., Parshin V.S., Dronov A.I., Karamyshev A.P., Nekrasov I.I., Fedulov A.A., Serebryakov A.V. Study of the resistance of steels 18KhMFB and 18Kh3MFB to hot deformation. *Metallurgist*. 2016;59(11-12):1118–1121. https://doi.org/10.1007/s11015-016-0279-6
14. Safronov A.A., Belskiy S.M., Chernyj V.A., Mazur I.P. Modeling of temperature influence on resistance to plastic deformation of electrotechnical steels in hot rolling. *Journal of Physics: Conference Series*. 2018;1134:012050.
15. Umanskii A.A., Dorofeev V.V., Dumova L.V. Theoretical foundations for energy-efficient production of railway rails with improved performance properties. *Izvestiya. Ferrous Metallurgy*. 2020;63(5):318–326. (In Russ.). https://doi.org/10.17073/0368-0797-2020-5-318-326

    Уманский А.А., Дорофеев В.В., Думова Л.В. Разработка теоретических основ энергоэффективного производства железнодорожных рельсов с повышенными эксплуатационными свойствами. *Известия вузов. Черная металлургия*. 2020;63(5):318–326. https://doi.org/10.17073/0368-0797-2020-5-318-326
16. Ostapenko A.L., Perekhodchenko V.A., Kushnir O.N., Plastun D.A. On the applicability of deformation resistance calculation methods for evaluating energy conditions of hot strip rolling. *Stal'*. 2014;(5):41–52. (In Russ.).

    Остапенко А.Л., Переходченко В.А., Кушнир О.Н., Пластун Д.А. О применимости методик расчета сопротивления деформации для оценки энергосиловых условий горячей прокатки полос. *Сталь*. 2014;(5):41–52.
17. Gladkovsky S.V., Potapov A.I., Lepikhin S.V. Studying the deformation resistance of Ep679 maraging steel. *Diagnostics, Resource and Mechanics of Materials and Structures*. 2015;(4):18–28. https://doi.org/10.17804/2410-9908.2015.4.018-028
18. Umanskii A.A., Golovatenko A.V., Temlyantsev M.V., Dorofeev V.V. Experimental studies of plasticity and deformation resistance of chromium rail steels. *Chernye metally*. 2019;(6):24–28. (In Russ.).

    Уманский А.А., Головатенко А.В., Темлянцев М.В., Дорофеев В.В. Экспериментальные исследования пластичности и сопротивления деформации хромистых рельсовых сталей. *Черные металлы*. 2019;(6):24–28.
19. Adigamov R.R., Nikishin I.A., Zhitelev P.S., Andreev A.R., Karlina A.I. Experience of implementing steel crushing balls manufacture in the PJSC "SEVERSTAL". *Stal'*. 2022;(3):13–18. (In Russ.).

Адигамов Р.Р., Никишин И.А., Жителев П.С., Андреев А.Р., Карлина А.И. Опыт освоения производства стальных мелющих шаров в ПАО «СЕВЕРСТАЛЬ». *Сталь*. 2022;(3):13–18.

20. Umanskii A.A., Baidin V.V., Simachev A.S., Dumova L.V. Features of the formation of the microstructure of grinding media produced from rail steels of various chemical compositions. In: *Metallurgy: Technologies, Innovations, Quality. Proceedings of the XXIII Int. Sci. and Pract. Conf*. Novokuznetsk: SibSIU, 2022:21–28.

Уманский А.А., Байдин В.В., Симачев А.С., Думова Л.В. Особенности формирования микроструктуры мелющих тел, произведенных из рельсовых сталей различного химического состава. В кн.: *Металлургия: технологии, инновации, качество. Труды XXIII Международной научно-практической конференции*. Новокузнецк: ИЦ СибГИУ; 2022:21–28.

Information about the Authors / Сведения об авторах

Aleksandr A. Umanskii, *Dr. Sci. (Eng.), Prof. of the Chair of Ferrous Metallurgy and Chemical Technology*, Siberian State Industrial University
ORCID: 0000-0003-4403-9006
E-mail: umanskii@bk.ru

Vadim V. Baidin, *Candidates for a degree of Cand. Sci. (Eng.) of the Chair of Ferrous Metallurgy and Chemical Technology*, Siberian State Industrial University
E-mail: 5745426@gmail.com

Artem S. Simachev, *Cand. Sci. (Eng.), Assist. Prof. of the Chair "Metal Forming and Metal Science. OJSC "EVRAZ ZSMK"*, Siberian State Industrial University
ORCID: 0000-0002-9712-3757
E-mail: simachev_as@mail.ru

Александр Александрович Уманский, *д.т.н., профессор кафедры металлургии черных металлов и химической технологии*, Сибирский государственный индустриальный университет
ORCID: 0000-0003-4403-9006
E-mail: umanskii@bk.ru

Вадим Викторович Байдин, *соискатель степени к.т.н. кафедры металлургии черных металлов и химической технологии*, Сибирский государственный индустриальный университет
E-mail: 5745426@gmail.com

Артем Сергеевич Симачев, *к.т.н., доцент кафедры «Обработка металлов давлением и металловедение. ЕВРАЗ ЗСМК»*, Сибирский государственный индустриальный университет
ORCID: 0000-0002-9712-3757
E-mail: simachev_as@mail.ru

Contribution of the Authors / Вклад авторов

A. A. Umanskii – development of a research plan, generalization and interpretation of the results, editing the article.
V. V. Baidin – conducting experiments and processing their results.
A. S. Simachev – analysis of literary sources, writing the main text of the article.

А. А. Уманский – разработка плана исследований, обобщение и интерпретация результатов, редактирование статьи.
В. В. Байдин – проведение экспериментов и обработка их результатов.
А. С. Симачев – анализ литературных источников, написание основного текста статьи.

Received 15.04.2024
Revised 21.08.2024
Accepted 17.10.2024

Поступила в редакцию 15.04.2024
После доработки 21.08.2024
Принята к публикации 17.10.2024

METALLURGICAL TECHNOLOGIES / МЕТАЛЛУРГИЧЕСКИЕ ТЕХНОЛОГИИ

UDC 669.094.1
DOI 10.17073/0368-0797-2024-6-644-652

Original article
Оригинальная статья

Application of low-temperature reduction by hydrogen for enhancing the magnetic characteristics of several iron ores

Yu. V. Konyukhov[1], R. Khanna[2], N. A. Maslennikov[1], K. Li[3], Z. Liang[3], I. N. Burmistrov[1], D. Yu. Karpenkov[4], S. V. Kashevskii[1], M. V. Kravchenko[5]

[1] **National University of Science and Technology "MISIS"** (4/1 Leninskii Ave., Moscow 119049, Russian Federation)
[2] **University of New South Wales, Institute of Materials Science and Engineering** (Sydney, NSW 2052, Australia)
[3] **School of Metallurgical and Ecological Engineering, University of Science and Technology Beijing** (Beijing 100083, China)
[4] **M.V. Lomonosov Moscow State University** (1 Leninskie Gory, Moscow 119991, Russian Federation)
[5] **National Research University "Moscow Power Engineering Institute"** (14 Krasnokazarmennaya Str., Moscow 119049, Russian Federation)

martensit@mail.ru

Abstract. The conversion of non-magnetic or weakly magnetic constituents of iron ores into the magnetic 'magnetite' phase was investigated using partial reduction by hydrogen at temperatures below 400 °C. The examined four commercial iron ores from Russian and Chinese deposits have significant differences in their compositions and morphologies. All ore samples were crushed using mechanical abrasion in a stamp and sieved with a mesh size of 1.5 mm. Reduction was carried out in a tube furnace under isothermal conditions at 375 and 400 °C for one hour. To study the kinetics of the reduction process, non-isothermal studies of selected ores were conducted using a thermogravimetric analyzer with heating to 800 °C at a heating rate of 10 °C/min in hydrogen flow. The authors made a detailed characterization of the annealed products using *X*-ray diffraction, scanning electron microscopy and energy dispersive spectroscopy to determine the magnetic characteristics of initial and partially reduced ores. *X*-ray diffraction patterns showed hematite peaks in the initial samples; both magnetite and metallic iron peaks were detected in the samples reduced at 375 and 400 °C. Such behavior was observed for all four samples under investigation. The most important result of the study is the confirmation of an order of magnitude increase in saturation magnetization for hematite ores, in addition the reduced ore samples show soft magnetic properties with average coercive force values of approximately 20 kA/m. Application of the low-temperature reduction by hydrogen to iron-containing ores is very promising for production of the materials that could later be subjected to enrichment using magnetic separation methods.

Keywords: iron ores, reduction by hydrogen, hematite, magnetite, metallization kinetics, "green" metallurgy, mineral processing, magnetic properties

Acknowledgements: The work was supported by the Russian Science Foundation (project No. 24-29-00672).

For citation: Konyukhov Yu.V., Khanna R., Maslennikov N.A., Li K., Liang Z., Burmistrov I.N., Karpenkov D.Y., Kashevskii S.V., Kravchenko M.V. Application of low-temperature reduction by hydrogen for enhancing the magnetic characteristics of several iron ores. *Izvestiya. Ferrous Metallurgy*. 2024;67(6):644–652. https://doi.org/10.17073/0368-0797-2024-6-644-652

Применение метода низкотемпературного восстановления водородом для улучшения магнитных характеристик железных руд

Ю. В. Конюхов[1], Р. Ханна[2], Н. А. Масленников[1], К. Ли[3], Ц. Лян[3], И. Н. Бурмистров[1], Д. Ю. Карпенков[4], С. В. Кашевский[1], М. В. Кравченко[5]

[1] **Национальный исследовательский технологический университет «МИСИС»** (Россия, 119049, Москва, Ленинский пр., 4, стр. 1)
[2] **Университет Нового Южного Уэльса, Институт материаловедения и инженерии** (Австралия, 2052, Новый Южный Уэльс, Сидней)
[3] **Пекинский университет науки и технологии, Институт металлургической и экологической инженерии** (Китай, 100083, Пекин)
[4] **Московский государственный университет им. М.В. Ломоносова** (Россия, 119991, Москва, Ленинские горы, 1)
[5] **Национальный исследовательский университет «МЭИ»** (Россия, 111250, Москва, ул. Красноказарменная, 14, стр. 1)

martensit@mail.ru

Аннотация. В работе исследовали превращения немагнитных или слабомагнитных компонентов железных руд в магнитную фазу «магнетит» в результате частичного восстановления водородом при температурах ниже 400 °С. Исследованные четыре вида промышленных железных руд российских и китайских месторождений существенно различаются по составу и морфологии. Для подготовки образцов руды измельчали с помощью механического истирания в ступке и просеивали через сита с размером ячеек 1,5 мм. Восстановление проходило в изотермических условиях в трубчатой печи при температурах 375 и 400 °С в течение одного часа. Для изучения кинетики процесса восстановления были проведены неизотермические исследования выбранных руд с использованием термогравиметрического анализатора при нагреве до 800 °С со скоростью нагрева 10 °С/мин в токе водорода. Детальная характеризация исходных и частично восстановленных руд осуществлялась с использованием рентгеновской дифракции, сканирующей электронной микроскопии и энергодисперсионной спектроскопии для определения магнитных характеристик. На рентгеновских дифрактограммах исходных образцов присутствуют пики гематита, а в восстановленных как при 400 °С, так и при 375 °С – пики магнетита и металлического железа. Аналогичное поведение наблюдалось для всех четырех рудных образцов. Наиболее важным результатом исследования является подтверждение увеличения намагниченности насыщения на порядок для гематитовых руд, при этом восстановленные образцы руды показали магнитомягкие свойства со средними значениями коэрцитивной силы примерно 20 кА/м. Таким образом показано, что применение метода низкотемпературного восстановления водородом на железных рудах с низким содержанием магнитных фаз является весьма перспективным для получения материалов, которые в дальнейшем могут быть подвергнуты обогащению методами магнитной сепарации.

Ключевые слова: железные руды, водородное восстановление, гематит, магнетит, кинетика металлизации, «зеленая» металлургия, обогащение полезных ископаемых, магнитные свойства

Благодарности: Исследование выполнено за счет гранта Российского научного фонда (проект № 24-29-00672).

Для цитирования: Конюхов Ю.В., Ханна Р., Масленников Н.А., Ли К., Лян Ц., Бурмистров И.Н., Карпенков Д.Ю., Кашевский С.В., Кравченко М.В. Применение метода низкотемпературного восстановления водородом для улучшения магнитных характеристик железных руд. *Известия вузов. Черная металлургия*. 2024;67(6):644–652. https://doi.org/10.17073/0368-0797-2024-6-644-652

Introduction

Humanity is currently deeply concerned about the issue of global warming, which is primarily linked to carbon dioxide emissions [1; 2]. Approximately 7 % of global CO_2 emissions are attributed to the metallurgical industry [3]. On average, producing one ton of crude steel generates 1.9 tons of CO_2 emissions [4]. According to the World Steel Association, steel production in the Russian Federation reached 71.5 million tons in 2022, while China produces over 1 billion tons of crude steel annually [5].

Under increasing pressure from environmental groups and society, the metallurgical industry will soon need to reduce its CO_2 emissions, necessitating a shift to more environmentally friendly and energy-efficient production technologies. Among the most promising approaches is the direct reduction of iron by hydrogen [6; 7], as this process generates water vapor (H_2O) instead of carbon-containing gaseous byproducts (CO/CO_2).

The widespread adoption of direct reduction by hydrogen is currently limited by the high cost of hydrogen, which depends on the methods used for its production [8]. The main methods for producing hydrogen include steam reforming of methane and natural gas, coal gasification, water electrolysis, pyrolysis, partial oxidation, biotechnology, and atomic hydrogen processes [9]. According to [10], global hydrogen consumption in 2020 was 115 million tons, and forecasts predict this figure will rise to 530 million tons by 2030.

Producing one ton of steel requires approximately 51 kg of hydrogen [11]. Calculations indicate that converting hematite to magnetite consumes only 4.31 kg of hydrogen per ton of Fe_3O_4. Therefore, during the initial transition to hydrogen metallurgy, it seems practical to focus on the partial reduction of iron-bearing materials during the beneficiation stage, rather than fully reducing them to metallic iron.

In many iron ores, iron is entirely or partially present as hematite, which is challenging to extract. In such cases, reduction by hydrogen can convert hematite into magnetite, allowing its subsequent extraction through magnetic separation [12; 13]. Magnetite-based super-concentrates, with an iron content exceeding 72 % [14; 15], can be injected into the lower part of blast furnaces [16; 17]. This approach can reduce CO_2 emissions by altering the mass and thermal balance of the furnace and eliminating the sintering stage. Additionally, these super-concentrates have potential as the primary raw material for direct iron reduction processes in shaft and hearth furnaces [18]. Using partially reduced oxides as feedstock is expected to shorten the time required for full iron reduction [19], thereby improving production energy efficiency.

Most research on the kinetics of reduction by hydrogen of iron ore materials focuses on processes at temperatures between 500 and 1000 °C, culminating in the production of metallic iron [4; 20]. In these studies, magnetite formation is treated as an intermediate reaction in the overall reduction process leading to pure iron. However, studies on the low-temperature (below 400 °C) reduction of iron ores by hydrogen are rare. This study aimed to investigate the feasibility of converting non-magnetic or weakly magnetic components of iron ores into magnetite through partial reduction in a hydrogen flow at temperatures below 400 °C.

Sample preparation and research methods

The study focused on hematite ore (sinter ore) from the Varichev Mikhailovsky GOK (ore *A*), iron ore from the Pechegubsky deposit of the Olenegorsk GOK (ore *B*), and ores provided by partners from China (ores *C* and *D*).

For the Russian ores, gangue material was separated using laboratory sieves. All ores were then mechanically ground in a laboratory mortar and sieved through a mesh with 1.5 mm openings.

Isothermal reduction experiments were conducted in a Carbolite Gero KST/KZS tube furnace (UK) at 375 and 400 °C. Ceramic boats with dimensions of 100×20×15 mm were used, and the thickness of the powder layer was maintained at 2 – 3 mm. Samples were preheated in a helium flow, after which the helium flow was replaced with hydrogen. Hydrogen was supplied by SAM-1 and TsvetChrom hydrogen generators (Russia) with a combined capacity of 80 L/h and dried beforehand using a silica gel system. After holding the samples at the target temperature, they were cooled in a helium flow.

Reduction studies under linear heating modes were performed at a rate of 10 °C/min in a hydrogen atmosphere using an SDT Q600 thermogravimetric analyzer (USA).

The phase composition of the samples was analyzed using a TDM-20 tabletop *X*-ray diffractometer (China) equipped with a copper anode. Diffraction data were processed using Match!3 software (Crystal Impact, Germany).

The gas atmosphere generated during oxidative annealing at 800 °C was studied using a ChemBet Pulsar flow chemisorption analyzer (USA), which also regulated the air flow rate. During the experiments, a *U*-shaped quartz reactor was heated in an air flow at a rate of 50 °C/min up to 500 °C. The gas-air mixture was then heated further to 800 °C at a rate of 30 °C/min and directed to a Pfeiffer Vacuum OmniStar GSD 320 quadrupole mass spectrometer (Germany). The mass spectrometer analyzed a range of 1 to 300 atomic mass units (amu). Since no significant signals were observed in the ranges of 1 – 10 and 45 – 300 amu, the analysis focused on the range of 10 – 45 amu.

Micrographs were obtained using a TESCAN VEGA3 SB scanning electron microscope (Czech Republic). Elemental analysis was conducted via energy-dispersive spectroscopy (EDS) using an INCA Energy 450 attachment (UK). The probe diameter for elemental composition measurements was 300 nm, with an accuracy ±1 %.

Magnetic properties were measured using a VSM-130 vibrating sample magnetometer (Dexing Magnet Company, China) with a magnetic moment measurement accuracy of $1 \cdot 10^{-6}$ A·m^2.

Results and discussion

Fig. 1 presents micrographs of the initial materials. The ore particles of Russian origin predominantly have a rounded shape (Fig. 1, *a*, *b*), which is typical of natural materials that have not been subjected to intensive grinding. The particle size distribution in ore *A* is relatively narrow, ranging from 10 to 160 μm. In ore *B*, most particles are within the range of 50 – 800 μm, with some exceeding 1 mm in diameter. Ore *C* (of Chinese origin) contains particles with flaky and fractured shapes (Fig. 1, *c*). The fractured particles are small, ranging from 3 to 35 μm, while the flaky particles are much larger, measuring between 10 and 100 μm in size and 1 – 3 μm in thickness. This microstructure suggests that ore *C* is like a mixture of two or more types of iron ore materials. Ore *D* (also of Chinese origin) consists of fractured and spherical particles (Fig. 1, *d*) of submicron size,

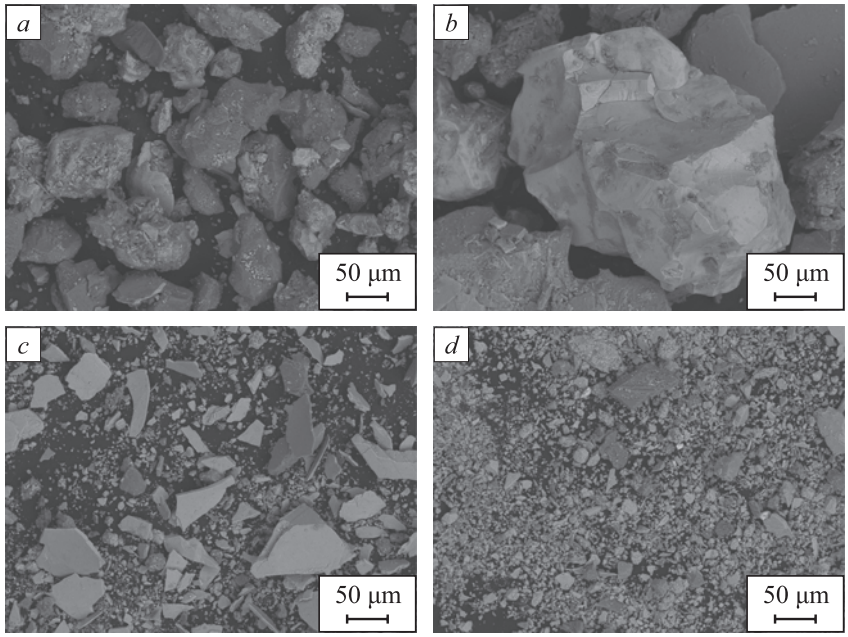

Fig. 1. SEM photos: ore *A* (*a*), *B* (*b*), *C* (*c*) and *D* (*d*)

Рис. 1. Микрофотографии: руда *A* (*a*), *B* (*b*), *C* (*c*) и *D* (*d*)

ranging from 3 to 35 μm. It is well-known that magnetite ores are generally difficult to grind, and grinding is one of the most cost-intensive operations in mineral beneficiation. The submicron size of the particles in ore *D* may indicate that the material underwent preliminary conditioning to extract more valuable elements.

Table 1 summarizes the elemental composition of the initial and hydrogen-treated ores (processed for 1 h at 375 °C), as determined by energy-dispersive *X*-ray spectroscopy (EDX). The results reveal similar compositions among the studied materials. The Russian ores are characterized by high silicon content (over 20 wt. %), as they had not undergone prior beneficiation. Sodium, at concentrations of 0.7 – 0.8 wt. %, is present only in ore *B*. Sulfur, in amounts ranging from 0.2 to 0.6 wt. %, is found in all samples except ore *C*, where no sulfur was

Table 1. **Elemental composition of iron ore materials in the initial state and after processing in hydrogen flow at a temperature of 375 °C for 1 h**

Таблица 1. **Элементный состав железорудных материалов в исходном состоянии и после обработки в токе водорода при температуре 375 °С в течение 1 ч**

Material state	Element content, wt. %											
	O	Na	Mg	Al	Si	S	K	Ca	Fe	Mn	Ti	Ba
Ore *A*												
Initial state	41.74	–*	0.45	2.91	20.10	0.61	0.46	0.53	33.21	–	–	–
After processing	26.76	–	0.51	2.55	21.10	1.37	0.52	1.16	46.03	–	–	–
Ore *B*												
Initial state	46.73	0.81	2.38	3.42	21.88	0.18	1.05	1.92	21.48	–	0.15	–
After processing	41.37	0.71	2.33	3.14	27.40	0.43	1.02	2.35	21.34	–	–	–
Ore *C*												
Initial state	33.10	–	1.02	1.23	1.43	–	0.26	5.28	57.67	–	–	–
After processing	23.16	–	1.35	1.73	2.70	–	0.37	6.36	64.32	–	–	–
Ore *D*												
Initial state	33.69	–	–	1.55	3.20	0.35	0.40	2.81	56.76	0.85	–	0.39
After processing	29.23	–	0.65	1.85	4.39	0.52	0.52	4.52	57.14	1.18	–	–

* – below the detection limit of the EDX method for the respective element.

detected. The absence of sulfur in ore *C* may be due to its high calcium content, which could either have been intentionally added or naturally present in the raw material as carbonates or other compounds.

The presence of carbon in the studied iron ore materials was examined by analyzing the gases released during calcination in air. The spectra confirmed that at 800 °C, CO_2 is released at $m/z = 44$, resulting from the decomposition of carbonates. As an example, Fig. 2 shows the mass spectrum of the gas phase generated during the calcination of a sample from ore *C* in air at 800 °C. The total mass loss during oxidative annealing was 3.52 % for ore *A* and 3.16 % for ore *B*. In contrast, the Chinese iron ores exhibited significantly higher mass losses: 19.59 % for ore *C* and 12.45 % for ore *D*. These higher values for the Chinese ores can be attributed to their higher carbonate content and lower silica content.

The interaction of iron ore materials with hydrogen under non-isothermal conditions showed noticeable differences in mass-change patterns. A comparative analysis of the thermogravimetric curves (Fig. 3) revealed both common trends and distinctive features in the metallization process of iron ores from different sources in a hydrogen stream. Metallization refers to the partial or complete decomposition of oxides and their reduction to metals or lower oxides.

For ore *A*, the first two peaks on the thermogram (Fig. 3, *a*, DTG curve) correspond to the removal of adsorbed moisture. The peak near 300 °C likely represents the decomposition of hydroxides, which may have formed during the ore's exposure to moisture. In the temperature range of 350 – 450 °C, hematite is reduced to magnetite. In subsequent stages, magnetite is reduced to metallic iron (below 570 °C), bypassing the formation of wüstite. Since mass loss does not cease at 570 °C, it is possible that an intermediate FeO product forms in the 570 – 800 °C range. A small peak near 800 °C is likely due to the decomposition of carbonates. The maximum reaction rate occurs at 570 °C.

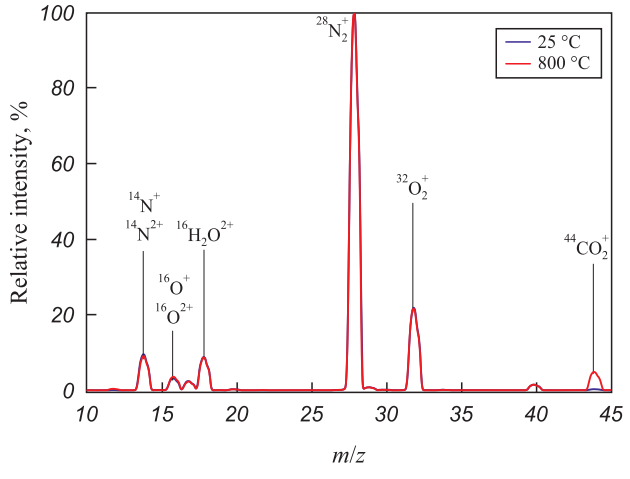

Fig. 2. Mass spectra of the gas phase formed during air blowing of ore *A* at 25 and 800 °C

Рис. 2. Масс-спектры газовой фазы, образующейся при продувке воздухом руды *A* при температурах 25 и 800 °C

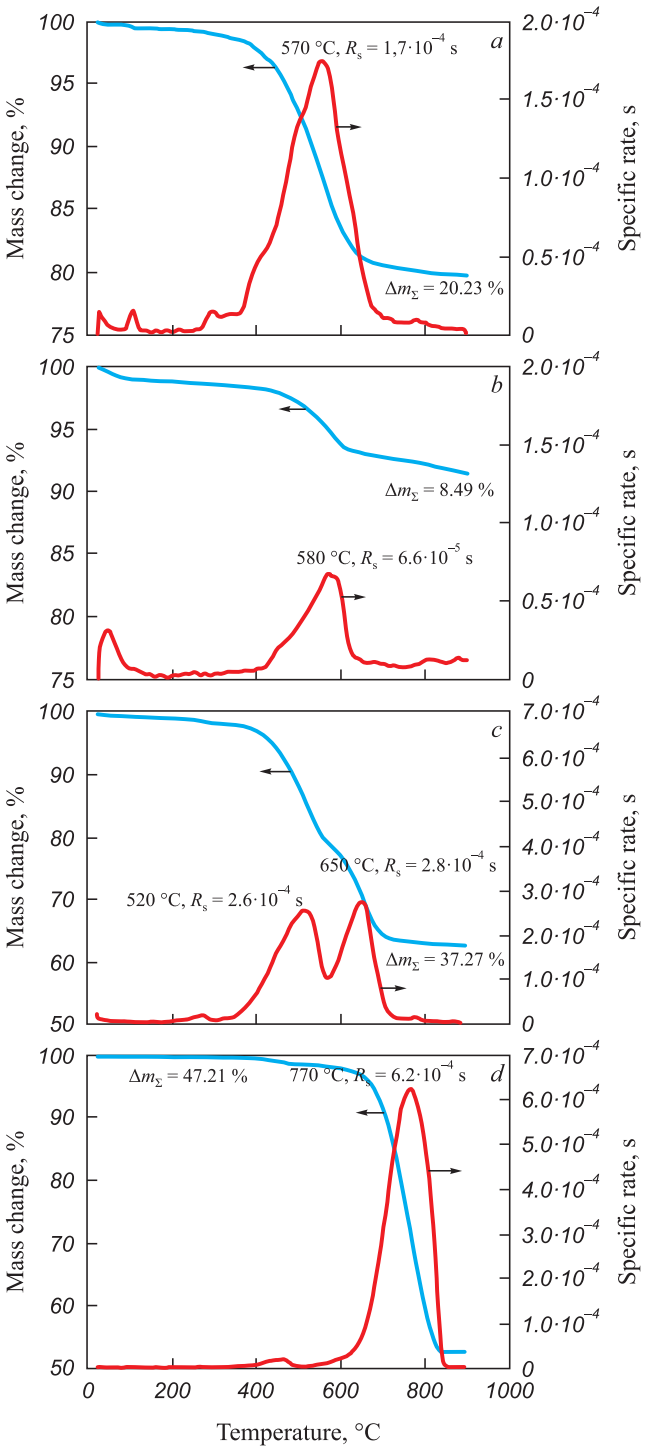

Fig. 3. Thermogravimetric curves of iron ore processing in hydrogen flow in linear heating mode at a rate of 10 °C/min:
a – ore *A*; *b* – ore *B*; *c* – ore *C*; *d* – ore *D*

Рис. 3. Термогравиметрические кривые обработки железных руд в токе водорода в режиме линейного нагрева со скоростью 10 °C/мин:
a – руда *A*; *b* – руда *B*; *c* – руда *C*; *d* – руда *D*

The temperature ranges for the metallization of ores *B* and *A* are similar (Fig. 3, *b*), despite ore *B* being classified as a magnetite type. Its composition includes small amounts of iron hydroxide and hematite. At the final stage, a significant mass loss occurs due to its higher calcium content and, consequently, a greater amount of carbonates. The maximum reaction rate is observed at 580 °C.

The thermogram of ore *C* (Fig. 3, *c*) shows two primary peaks, supporting the earlier hypothesis that this sample was produced by mechanically mixing two different iron ore materials (likely natural ore and a beneficiation byproduct). The maximum reaction rates are observed at 520 and 650 °C. The lower temperature for the first peak can be attributed to the high dispersion of particles, which enhances the reactivity of some of the ore material.

The metallization process for ore *D* (Fig. 3, *d*) differs from the other three samples. Despite the high dispersion of this material, reduction begins only at 550 °C, with the maximum reaction rate occurring at 770 °C. This suggests that this iron ore material is not a concentrate but is more likely a byproduct obtained during mineral processing [21].

To investigate sample behavior under isothermal conditions, temperatures of 375 and 400 °C were chosen, and samples of ores *A* and *D* were processed in hydrogen for 1 h at these temperatures. The diffraction patterns of the initial materials show peaks corresponding to the hematite phase (Fig. 4). Treatment at 375 °C resulted in the complete transformation of the hematite phase into magnetite for all samples. Additionally, peaks for metallic iron appeared in the diffraction patterns, demonstrating the feasibility of producing metallic iron at temperatures below 400 °C. No significant differences were observed between the diffraction patterns obtained at 375 and 400 °C, indicating that the processes at these temperatures are qualitatively similar, differing only slightly in the extent of their completion.

Fig. 5 presents the results of magnetic property measurements for the initial materials and those processed at 375 °C in a hydrogen flow for one hour.

Magnetization measurements were conducted on non-compacted isotropic powders of both the initial ores and the reduction products. The key magnetic characteristics of the samples are summarized in Table 2.

An analysis of the field dependence curves indicates that all samples exhibit soft magnetic properties, with average coercive force values around 20 kA/m. The rectangularity coefficient of the hysteresis loops (M_r/M_s) suggests that the samples are composed of isotropic magnetic phases. Reduction annealing significantly increased the saturation magnetization of all samples (except ore *B*) by an order of magnitude. This increase is attributed to the formation of numerous iron-containing phases with high magnetic properties during thermal treatment. This observation is supported by *X*-ray phase analysis results. It is important to note that high saturation magnetization is a critical parameter for optimizing magnetic separation conditions for iron-containing ores.

Thus, the significant enhancement in magnetic properties underscores the potential of low-temperature reduction by hydrogen for producing materials that can be further processed using magnetic separation methods.

Conclusions

The study demonstrated the feasibility of partial reduction of selected types of iron ore materials by hydrogen

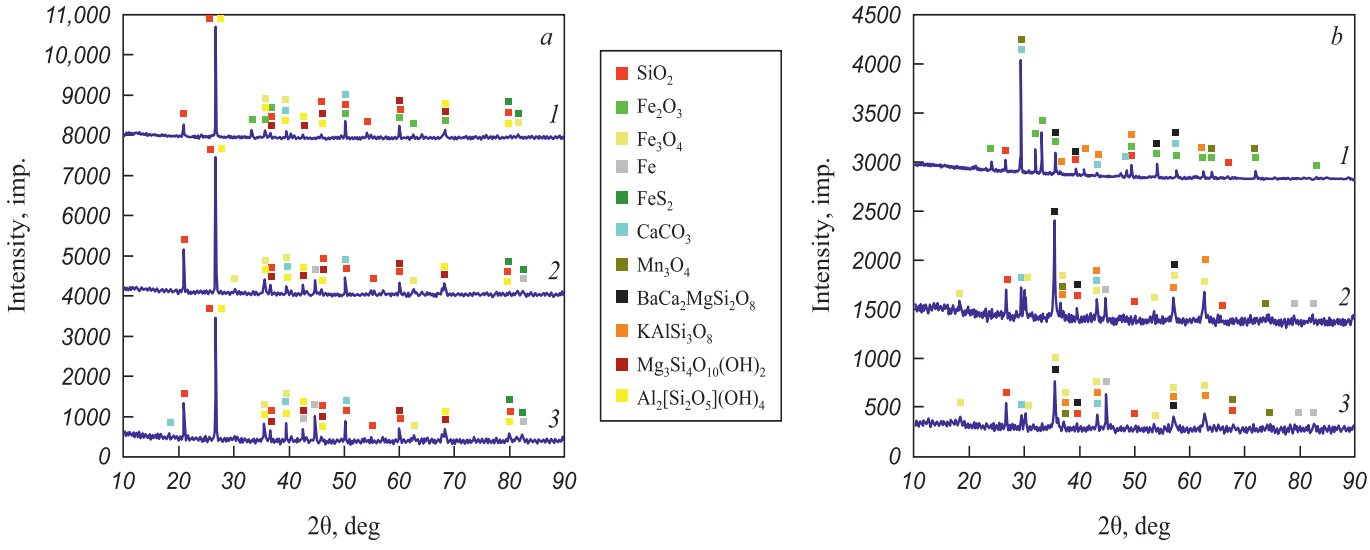

Fig. 4. XRD curves of ore *A* (*a*) and ore *D* (*b*) in the initial state (*1*) and processed at temperatures of 375 (*2*) and 400 °C (*3*)

Рис. 4. Дифрактограммы руды *A* (*a*) и руды *D* (*b*) в исходном состоянии (*1*) и обработанных при температурах 375 (*2*) и 400 °C (*3*)

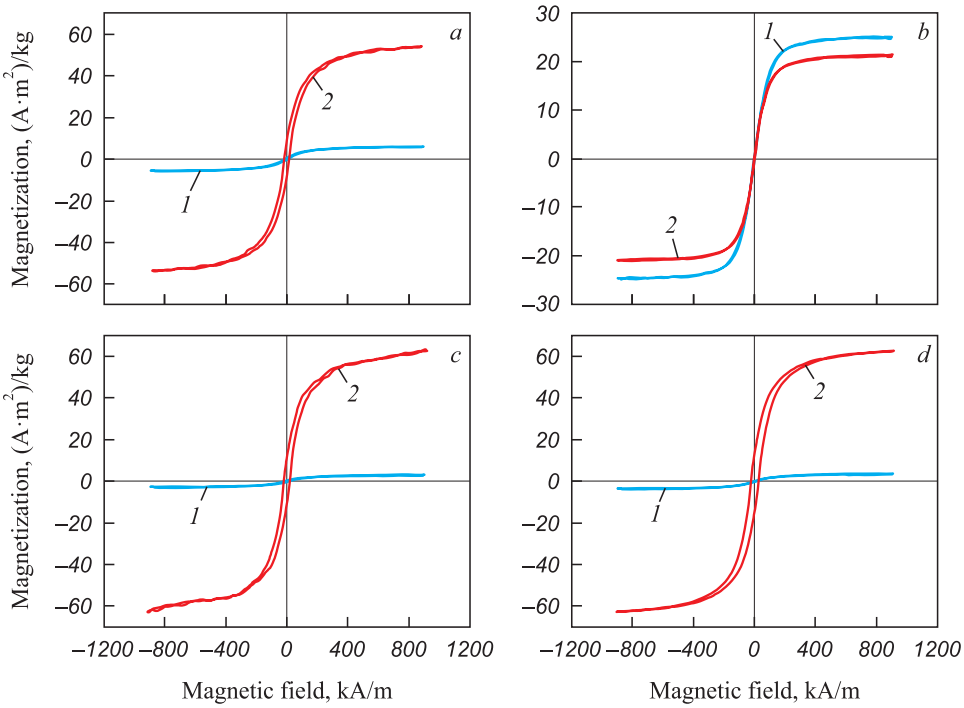

Fig. 5. Hysteresis loops of ore materials in the initial state (*1*) and processed at a temperature of 375 °C (*2*): *a* – ore *A*; *b* – ore *B*; *c* – ore *C*; *d* – ore *D*

Рис. 5. Петли гистерезиса рудных материалов в исходном состоянии (*1*) и обработанных при температуре 375 °С (*2*): *a* – руда *A*; *b* – руда *B*; *c* – руда *C*; *d* – руда *D*

Table 2. **Magnetic characteristics for ore materials in the initial state and processed at a temperature of 375 °C**

Таблица 2. **Магнитные характеристики для рудных материалов в исходном состоянии и обработанных при температуре 375 °С**

Ore sample		Saturation magnetization, $(A \cdot m^2)/kg$	Residual magnetization, $(A \cdot m^2)/kg$	Coercive force, kA/m	M_r/M_s
A	initial	5.50	0.49	12.7	0.09
	after reduction	53.80	8.37	15.8	0.16
B	initial	24.80	0.51	2.4	0.02
	after reduction	21.30	0.49	2.3	0.02
C	initial	2.65	10.90	19.5	4.11
	after reduction	62.00	0.48	20.1	0.01
D	initial	3.76	0.28	10.9	0.07
	after reduction	62.90	13.90	24.9	0.22

at temperatures below 400 °C, including those with a high SiO_2 content (over 20 wt. %) and large average particle sizes (over 1 mm).

It was established that processing the studied iron ore samples in a hydrogen flow at 375 °C for one hour results in the formation of magnetite phases and partially reduced iron. No residual hematite phases were detected in the diffraction patterns of the samples.

The processing of hematite iron ores with hydrogen at 375 °C significantly enhances their magnetic properties, making the material promising for enrichment using magnetic separation methods.

References / Список литературы

1. Rebonato R., Kainth D., Melin L., O'kane D. Optimal climate policy with negative emissions. *International Journal of Theoretical and Applied Finance*. 2024;27(01):2450012. https://doi.org/10.1142/S0219024924500122
2. Zou C., Wu S., Yang Z., Pan S., Wang G., Jiang X., Guan M., Yu C., Yu Z., Shen Y. Progress, challenge and significance of building a carbon industry system in the context of carbon neutrality strategy. *Petroleum Exploration and Development*. 2023;50(1):210–228. https://doi.org/10.1016/S1876-3804(22)60382-3

3. Holappa L. A general vision for reduction of energy consumption and CO_2 emissions from the steel industry. *Metals*. 2020;10(9):1117. https://doi.org/10.3390/met10091117
4. Heidari A., Niknahad N., Lijana M., Fabritius T. A review on the kinetics of iron ore reduction by hydrogen. *Materials*. 2021;14(24):7540. https://doi.org/10.3390/ma14247540
5. Qiao Y., Wang G. Recent status of production, administration policies, and low-carbon technology development of China's steel industry. *Metals*. 2024;14(4):480. https://doi.org/10.3390/met14040480
6. Spreitzer D., Schenk J. Reduction of iron oxides with hydrogen – A review. *Steel Research International*. 2019;90(10): 1900108. https://doi.org/10.1002/srin.201900108
7. Zhang J., Li K., Liu Z., Yang T. Primary Exploration of Hydrogen Metallurgy. Springer Singapore; 2024:391.
8. Lagioia G., Spinelli M.P., Amicarelli V. Blue and green hydrogen energy to meet European Union decarbonisation objectives. An overview of perspectives and the current state of affairs. *International Journal of Hydrogen Energy*. 2023;48(4):1304–1322. https://doi.org/10.1016/j.ijhydene.2022.10.044
9. Dash S.K., Chakraborty S., Elangovan D. A brief review of hydrogen production methods and their challenges. *Energies*. 2023;16(3):1141. https://doi.org/10.3390/en16031141
10. Zhiznin S.Z., Shvets N.N., Timakhov V.M., Gusev A.L. Economics of hydrogen energy of green transition in the world and Russia. Part I. *International Journal of Hydrogen Energy*. 2023;48(57):21544–21567. https://doi.org/10.1016/j.ijhydene.2023.03.069
11. Kukushkin A.B., Kukushkin A.S., Levashova M.G., Lisitsa V.S., Neverov V.S., Pshenov A.A., Sdvizhenskii P.A., Tolstikhina I.Yu., Khusnutdinov R.I., Serov S.V., Tugarinov S.N. The effect of thermodynamic nonequilibrium of hydrogen recycling on the charge-exchange spectroscopy of tokamak edge plasma. *Problems of Atomic Science and Technology. Series: Thermonuclear Fusion*. 2022;45(3):12–22.

    Кукушкин А.Б, Кукушкин А.С., Левашова М.Г., Лисица В.С., Неверов В.С., Пшенов А.А., Сдвиженский П.А., Толстихина И.Ю., Хуснутдинов Р.И., Серов С.В., Тугаринов С.Н. Влияние термодинамической неравновесности рециклинга водорода на перезарядочную спектроскопию периферийной плазмы токамака. *Вопросы атомной науки и техники. Серия: термоядерный синтез*. 2022;45(3):12–22.
12. Svoboda J. Magnetic Techniques for the Treatment of Materials. Springer Science & Business Media; 2004:642. https://doi.org/10.1007/1-4020-2107-0
13. Yuan S., Wang R., Zhang Q., Li Y., Gao P. Extraction and phase transformation of iron in fine-grained complex hematite ore by suspension magnetizing roasting and magnetic separation. *Korean Journal of Chemical Engineering*. 2022; 39:1891–1901. https://doi.org/10.1007/s11814-022-1116-1
14. Zelenova I.M. Iron-ore concentrates in iron-powder production. *Steel in Translation*. 2009;39(9):827–830 (2009). https://doi.org/10.3103/S0967091209090216
15. Syrkov A.G., Prokopchuk N.R. Dispersed iron obtaining by the method of solid state hydride synthesis and the problem of hydrophobicity of metal. *CIS Iron and Steel Review*. 2021;21:16–22. https://doi.org/10.17580/cisisr.2021.01.03
16. Moskalina A.A., Chaika A.L., Kornilov B.V., Lebed' V.V., Dzhigota M.G. Improvement of blast furnace energy efficiency by injection of preheated pulverized coal fuel with iron oxides. *Steel in Translation*. 2021;51(7):468–474. https://doi.org/10.3103/S0967091221070056

    Москалина А.А., Чайка А.Л., Корнилов Б.В., Лебедь В.В., Джигота М.Г. Повышение энергоэффективности доменной печи путем вдувания предварительно нагретого ПУТ с оксидами железа. *Сталь*. 2021;(7):8–13.
17. Borodulin A.V., Chaika A.L., Sokhatskii A.A., Kornilov B.V. Investigation of impact of injection of pulverized ferric oxides and preheated pulverized-coal fuel in hearth to indexes of heat operation of blast furnace. *Ecologiya i promyshlennost'*. 2016;(2(47)):48–53. (In Russ.).

    Бородулин А.В., Чайка А.Л., Сохацкий А.А., Корнилов Б.В. Исследование влияния вдувания в горн пылевидных оксидов железа и предварительно нагретого пылеугольного топлива на показатели тепловой работы доменной печи. *Экология и промышленность*. 2016;(2(47)):48–53.
18. Yusfin Y.S., Pashkov N.F. Metallurgy of Iron. Moscow: Akademkniga; 2007:464.

    Юсфин Ю.С., Пашков Н.Ф. Металлургия железа. Москва: Академкнига; 2007:464.
19. Bogdandy L., Engell H.-J. Die Reduktion der Eisenerze. Düsseldorf: Springer Verlag; 1967:539. (In Germ.).

    Богданди Л.Ф., Энгель Г.-Ю. Восстановление железных руд/ Пер. с нем. Е.Ф. Вегмана, Ю.С. Юсфина, под ред. А.Н. Похвиснева. Москва: Металлургия; 1971:519.
20. He J., Li K., Zhang J., Conejo A.N. Reduction kinetics of compact hematite with hydrogen from 600 to 1050 °C. *Metals*. 2023;13(3):464. https://doi.org/10.3390/met13030464
21. Lileev A.S., Konyukhov Yu.V., Zhukov D.G., Khanna R. Properties of nanocrystalline magnetic powders of the Fe–O system Obtained from iron ore dust using magnetic pulse processing. *Inorganic Materials: Applied Research*. 2024; 15(3):883–888. https://doi.org/10.1134/S2075113324700333

Information about the Authors / Сведения об авторах

Yurii V. Konyukhov, *Dr. Sci. (Eng.), Prof., Head of the Chair of Mineral Processing and Industrial Wastes Recycling*, National University of Science and Technology "MISIS"
ORCID: 0000-0003-0219-4809
E-mail: ykonukhov@misis.ru

Rita Khanna, *PhD, Prof.,* University of New South Wales, Institute of Materials Science and Engineering
ORCID: 0009-0004-3629-6891
E-mail: rita.khanna66@gmail.com

Юрий Владимирович Конюхов, *д.т.н., профессор, заведующий кафедрой обогащения и переработки полезных ископаемых и техногенного сырья*, Национальный исследовательский технологический университет «МИСИС»
ORCID: 0000-0003-0219-4809
E-mail: ykonukhov@misis.ru

Рита Ханна, *PhD, профессор*, Университет Нового Южного Уэльса, Институт материаловедения и инженерии
ORCID: 0009-0004-3629-6891
E-mail: rita.khanna66@gmail.com

Nikita A. Maslennikov, *Assistant of the Chair of Mineral Processing and Industrial Wastes Recycling*, National University of Science and Technology "MISIS"
E-mail: masl.nik2000@gmail.com

Kejiang Li, *PhD, Prof.*, School of Metallurgical and Ecological Engineering, University of Science and Technology Beijing
ORCID: 0000-0002-7807-8241
E-mail: likejiang@ustb.edu.cn

Zeng Liang, *PhD Student*, School of Metallurgical and Ecological Engineering, University of Science and Technology Beijing
E-mail: zeng_l99@163.com

Igor' N. Burmistrov, *Dr. Sci. (Eng.), Leading Expert of the Chair of Functional Nanosystems and High-Temperature Materials*, National University of Science and Technology "MISIS"
ORCID: 0000-0003-0776-2465
E-mail: burmistrov.in@misis.ru

Dmitrii Yu. Karpenkov, *Cand. Sci. (Phys.-Math.), Senior Researcher of the Chair of Magnetism*, M.V. Lomonosov Moscow State University
ORCID: 0000-0001-8686-2303
E-mail: karpenkov_d_y@mail.ru

Sergei V. Kashevskii, *MA Student of the Chair of Functional Nanosystems and High-Temperature Materials*, National University of Science and Technology "MISIS"
E-mail: serg.kashevsky@gmail.com

Maksim V. Kravchenko, *Cand. Sci. (Eng.), Director of Branch in Tashkent*, National Research University "Moscow Power Engineering Institute"
E-mail: Kravchenkomv@mpei.ru

Никита Андреевич Масленников, *ассистент кафедры обогащения и переработки полезных ископаемых и техногенного сырья*, Национальный исследовательский технологический университет «МИСИС»
E-mail: masl.nik2000@gmail.com

Кэцзян Ли, *PhD, профессор, Пекинский университет науки и технологии*, Институт металлургической и экологической инженерии
ORCID: 0000-0002-7807-8241
E-mail: likejiang@ustb.edu.cn

Цзэн Лян, *аспирант*, Пекинский университет науки и технологии, Институт металлургической и экологической инженерии
E-mail: zeng_l99@163.com

Игорь Николаевич Бурмистров, *д.т.н., ведущий эксперт кафедры функциональных наносистем и высокотемпературных материалов*, Национальный исследовательский технологический университет «МИСИС»
ORCID: 0000-0003-0776-2465
E-mail: burmistrov.in@misis.ru

Дмитрий Юрьевич Карпенков, *к.ф.-м.н., старший научный сотрудник кафедры магнетизма*, Московский государственный университет имени М.В. Ломоносова
ORCID: 0000-0001-8686-2303
E-mail: karpenkov_d_y@mail.ru

Сергей Владимирович Кашевский, *магистрант кафедры функциональных наносистем и высокотемпературных материалов*, Национальный исследовательский технологический университет «МИСИС»
E-mail: serg.kashevsky@gmail.com

Максим Владимирович Кравченко, *к.т.н., директор Ташкентского филиала*, Национальный исследовательский университет «МЭИ»
E-mail: Kravchenkomv@mpei.ru

Contribution of the Authors / Вклад авторов

Yu. V. Konyukhov – formation of the article idea, scientific guidance, writing the final version of the manuscript.

R. Khanna – conceptualization, review and editing.

N. A. Maslennikov – carrying out research, data analysis and processing.
K. Li – participation in draft writing, review and editing.

Z. Liang – review and editing.
I. N. Burmistrov – participation in the description and discussion of the results, review and editing.
D. Yu. Karpenkov – carrying out research, analysis, data processing and discussion.
S. V. Kashevskii – carrying out research, data processing.
M. V. Kravchenko – review and editing.

Ю. В. Конюхов – идея работы, научное руководство, разработка методологии исследования, написание окончательного варианта рукописи.
Р. Ханна – концептуализация, подготовка обзора и редактирование текста.
Н. А. Масленников – проведение исследований, анализ и обработка данных.
К. Ли – участие в написании черновой версии рукописи, рецензирование и редактирование.
Ц. Лян – рецензирование и редактирование.
И. Н. Бурмистров – участие в описании и обсуждении результатов, рецензирование и редактирование.
Д. Ю. Карпенков – проведение измерений, анализ, обработка данных и их обсуждение.
С. В. Кашевский – проведение измерений и обработка данных.
М. В. Кравченко – рецензирование и редактирование.

Received 11.10.2024
Revised 17.10.2024
Accepted 17.10.2024

Поступила в редакцию 11.10.2024
После доработки 17.10.2024
Принята к публикации 17.10.2024

Metallurgical technologies / Металлургические технологии

UDC 669.017.16:669.018.294.2
DOI 10.17073/0368-0797-2024-6-653-659

Original article
Оригинальная статья

On the results of tribological studies of railway rails

I. A. Olifirenko[1, 2], T. N. Oskolkova[1] ✉, E. V. Polevoi[2]

[1] **Siberian State Industrial University** (42 Kirova Str., Novokuznetsk, Kemerovo Region – Kuzbass 654007, Russian Federation)
[2] **JSC EVRAZ United West Siberian Metallurgical Plant** (16 Kosmicheskoe Route, Novokuznetsk, Kemerovo Region – Kuzbass 654007, Russian Federation)

✉ oskolkovatatiana@yandex.ru

Abstract. Metal resistance to the formation of contact fatigue defects and wear development has a great influence on the consumer properties of rails. The most significant factors limiting the service life of rails in curved sections of the railway track are wear of rails of the outer threads and development of contact fatigue defects in the inner threads of the track. In this regard, methods of reliable laboratory assessment of the rail metal resistance become important in the development of new products. The paper describes the change in the nature of damage to rails of various hardness categories by contact fatigue defects, and evaluates their wear resistance. The study of defects and forecasting of the rail resource require an integrated approach. The paper provides a brief description of modeling the conditions of formation and accumulation of contact fatigue defects. The parameters under consideration have an effect on the wear resistance of rail metal of various chemical compositions. During the testing, the rails microstructure and the nature of crack growth change. The authors made a comparative analysis of the data obtained characterizing the wear resistance of rail steels of various hardness categories. The basis of the methodology for assessing the wear resistance of railway rails is the physical modeling of adhesion-deformation mechanism of friction of the samples on a roller friction machine (tribometer). During laboratory tests of the studied categories of rails, the friction machine automatically outputs and records a number of computational parameters shown in the work. The conducted research is promising from a practical point of view. The results obtained can be used to develop a theory to increase the service life of differentially hardened rails produced by JSC EVRAZ United West Siberian Metallurgical Plant.

Keywords: tribometer, wear, wear resistance, rails, hardness, defects, friction, microstructure, deformed structure

For citation: Olifirenko I.A., Oskolkova T.N., Polevoi E.V. On the results of tribological studies of railway rails. *Izvestiya. Ferrous Metallurgy*. 2024;67(6):653–659. https://doi.org/10.17073/0368-0797-2024-6-653-659

О результатах трибологических исследований железнодорожных рельсов

И. А. Олифиренко[1, 2], Т. Н. Осколкова[1] ✉, Е. В. Полевой[2]

[1] **Сибирский государственный индустриальный университет** (Россия, 654007, Кемеровская обл. – Кузбасс, Новокузнецк, ул. Кирова, 42)
[2] **АО «ЕВРАЗ Объединенный Западно-Сибирский металлургический комбинат»** (Россия, 654043, Кемеровская обл. – Кузбасс, Новокузнецк, шоссе Космическое, 16)

✉ oskolkovatatiana@yandex.ru

Аннотация. Большое влияние на потребительские свойства рельсов оказывает стойкость металла к образованию дефектов контактной усталости и развитию износа. Наиболее значимыми факторами, лимитирующими срок службы рельсов в кривых участках железнодорожного пути, являются износ рельсов наружных нитей и развитие дефектов контактной усталости во внутренних нитях пути. В связи с этим при разработке новой продукции важное значение приобретают методы достоверной лабораторной оценки стойкости рельсового металла. В работе описывается изменение характера повреждаемости рельсов различных категорий твердости дефектами контактной усталости, проводится оценка их износостойкости. Исследование дефектов и прогнозирование ресурса рельсов требуют комплексного подхода. Приводится краткое описание моделирования условий образования и накопления контактно-усталостных дефектов. Рассматриваемые параметры оказывают влияние на износостойкость рельсового металла различного химического состава. В процессе испытаний изменяются микроструктура рельсов и характер роста трещин. Авторы провели сравнительный анализ полученных данных, характеризующих износостойкость рельсовых сталей различных категорий твердости. Основой методики оценки износостойкости железнодорожных рельсов является физическое моделирование процесса адгезионно-деформационного механизма трения образцов на роликовой машине трения (трибометр). При проведении лабораторных испытаний исследуемых категорий рельсов машина трения автоматически выдает и фиксирует целый ряд вычислительных параметров, показанных в работе. Проведенные исследования являются перспективными с практической точки зрения. Полученные результаты могут быть использованы для развития

теории по увеличению срока службы дифференцированно упрочненных рельсов производства АО «ЕВРАЗ Объединенный Западно-Сибирский металлургический комбинат».

Ключевые слова: трибометр, износ, износостойкость, рельсы, твердость, контактно-усталостные дефекты, трение, микроструктура, деформированная структура

Для цитирования: Олифиренко И.А., Осколкова Т.Н., Полевой Е.В. О результатах трибологических исследований железнодорожных рельсов. *Известия вузов. Черная металлургия*. 2024;67(6):653–659. https://doi.org/10.17073/0368-0797-2024-6-653-659

Introduction

According to GOST R 51685, the quality of rail steel is evaluated based on a range of mechanical properties, including yield strength (σ_y), ultimate tensile strength (σ_t), elongation (δ_5), reduction of area (φ), impact toughness, impact toughness, hardness of the running surface and cross-section, and the level of residual stresses. Additionally, compliance with requirements for micro- and macrostructure, non-metallic inclusions, surface quality, straightness, and other parameters is assessed. These factors influence the operational properties of rails; however, similar characteristics can be achieved through different approaches, such as alloying, heat treatment, and variations in force and temperature modes during rolling. Each treatment method activates distinct mechanisms of strengthening and structure formation, which directly impact resistance to contact fatigue defects and wear resistance. These differences become especially pronounced when rails are used on curved sections of the track. Rails on the outer threads of curves experience significant wear due to lateral forces from the wheel flanges of rolling stock. These forces arise from the interaction between the rotating wheels and the tangent to the curve of the rails [1 – 3].

Historically, hardness was considered the primary indicator of wear resistance in steel. However, recent studies [4; 5] suggest that the nature of wear is much more complex, and wear resistance cannot be evaluated solely based on hardness. Abrasive wear is influenced by the hardness, strength, and plasticity of the steel. Additionally, wear resistance depends on the chemical composition, production technology, and microstructure of the rails [6 – 8].

With the growth of heavy-duty transportation and the general trend toward increasing freight intensity, the issue of rail wear in curved sections and the formation of contact fatigue defects has become increasingly significant. Numerous studies [10 – 15] have been devoted to identifying the mechanisms of defect formation and progression, as well as understanding the structural changes in rails during operation. Additional research has focused on evaluating the operational properties of rails either directly in service [16 – 21] or through the use of specialized test rigs [22; 23] that simulate the wheel-rail interaction on a full scale. Full-scale wheel-rail test rigs provide precise assessments of rail wear resistance by testing the rail as an integrated structure, accounting for variations in structure and properties across the cross-section. These tests offer insights into rail performance at different stages of its life cycle. However, direct in-service measurements have significant limitations, including the substantial influence of specific operating conditions during field tests and the lengthy duration required for both field (~2.0 – 2.5 years) and laboratory stand (~0.5 – 1.0 years) tests. Furthermore, wheel-rail test rigs are expensive and currently unavailable in Russia.

Thus, a key challenge in modern railway rail production is developing and implementing new laboratory methods to assess the resistance of rail steel to wear and contact fatigue defects. These methods will allow for evaluating the effectiveness of technological solutions and expedite the development of high-demand products. Establishing a scientifically grounded methodology for assessing rail wear resistance is a priority, as no standardized approach currently exists in the available technical documentation.

Materials and methods

In this study, the focus was on differentially hardened R65 rails of compositions *1* and *2*, produced by JSC EVRAZ United West Siberian Metallurgical Plant (JSC EVRAZ ZSMK) using 76KhF steel in accordance with GOST R 51685 – 2022. The chemical composition of 76KhF steel, as per GOST R 51685 – 2022, is as follows (wt. %): C 0.71 – 0.84; Mn 0.75 – 1.25; Si 0.25 – 1.00; P ≥ 0.020; S ≥ 0.020; Al ≥ 0.004; Cr 0.20 – 0.60; V 0.03 – 0.15. The grades differ in carbon and manganese content: grade *1* – 0.76 % C, 0.79 % Mn; grade *2* – 0.81 % C, 0.97 % Mn.

Friction tests were performed using a roller friction machine with the following specifications:

– load: up to 5 kN;

– sample rotation speed: up to 3000 rpm;

– ability to test with or without lubricants, with heating of lubricants up to 100 °C.

The machine is equipped with wear sensors, an eddy current sensor, and two vibration sensors measuring in three planes (*x*, *y*, *z*).

All samples were tested under consistent conditions:

– load: 1.2 kN;

– rail roller rotation speed: 217 rpm;

– slip ratio: ~10 %;

– test duration: 120 min;

– contact roller hardness: HRC 59;

– no lubricants used.

The machine also recorded several computational parameters in the form of graphs, including the coefficient of friction, slip ratio, friction force, sliding speed, speed of increase, and the relationship between slip and roller diameter. Parameters were dynamically adjusted to reflect changes introduced during the tests.

During the experiments, the sliding speed of the contact roller was varied to maintain a consistent slip ratio of 10 %, accounting for changes in roller diameter due to friction.

For the laboratory evaluation of wear resistance, one sample was cut from rails of compositions *1* and *2* from current production according to the specified design (Fig. 1).

A thermally strengthened roller made of 31Mn4 steel with a hardness of (59 ÷ 59) ± 2 HRC in accordance with the European standard DIN 1544, was used as the contact sample. The diagram of the contact sample is shown in Fig. 2.

The evaluation of the wear rate of rail rollers was conducted over 52,000 to 156,000 revolutions to eliminate the influence of surface quality at the beginning

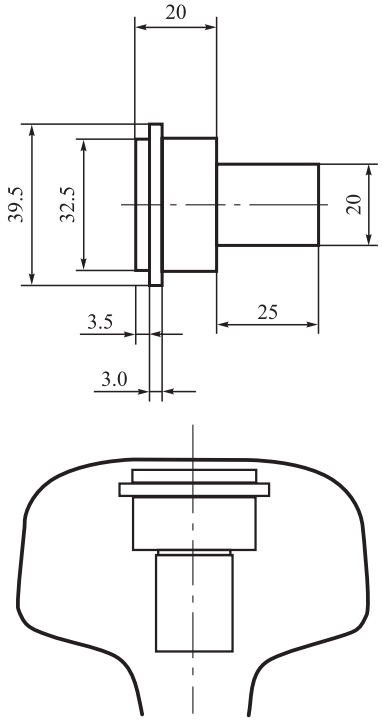

Fig. 1. Scheme and place of cutting samples

Рис. 1. Схема и место вырезки образцов

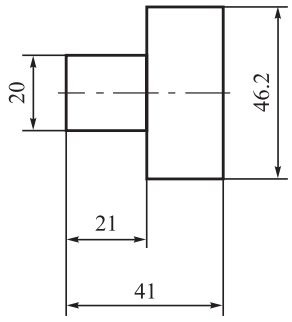

Fig. 2. Diagram of the contact sample

Рис. 2. Схема контактного образца

of the tests and the effect of metal delamination during the final test cycles.

Wear resistance was determined as the reciprocal of wear rate. Due to the minimal mass loss during testing, laboratory analytical scales with an accuracy of up to 0.0001 g were used:

$$W = \frac{m_1 - m_2}{N_{\text{cycle}}} \cdot 10^{-5},$$

where W is the wear resistance, g/cycle; m_1 and m_2 are sample masses before and after testing, g; N_{cycle} is the number of revolutions (1 cycle = 2600 revolutions).

The factors influencing the wear resistance of rail steel include a combination of several characteristics that allow for the assessment and improvement of rail steel performance in terms of wear resistance. These characteristics are: material hardness; chemical composition (carbide-forming carbon) and sulfur content (which determines the quantity of manganese and iron sulfides that act as stress concentrators in micro-damage zones during wear) [16]; microstructure parameters (interlamellar spacing, grain diameter, size of pearlite colonies, volumetric fraction of cementite); influence of carbides and carbonitrides (their quantity, shape, and distribution) [4].

Comparative analysis of the results

The hardness of the metal in the tested samples was measured using the Vickers method on a “Qness Q10A+” microhardness tester at seven points on the sample surface under a load of 50 N. The measurement results are presented in Table 1.

The data show that the hardness of the samples from rails with composition *2* is 7.85 % higher compared to those with composition *1*.

The microstructure of the rail steel was studied on transverse polished sections prepared from the fillet zone of the rail head after electropolishing and etching in a 4 % ethanol solution of nitric acid. The investigations were conducted using a scanning electron microscope (SEM).

Table 1. **Results of hardness measurements of the samples**

Таблица 1. **Результаты измерений твердости образцов**

Composition	Hardness, HV, at measurement points						
	1	*2*	*3*	*4*	*5*	*6*	*7*
1	405	395	384	387	392	402	402
2	433	426	432	439	437	428	436

The analyzed area was located 2 – 4 mm from the running surface of the rail head.

The results of these measurements are presented in Table 2 and Fig. 3.

The analysis of the data indicates that the interlamellar spacing in the microstructure of the steel from rails with composition *1* slightly exceeds that of rails with composition *2*. At the same time, the grain diameter in the steel

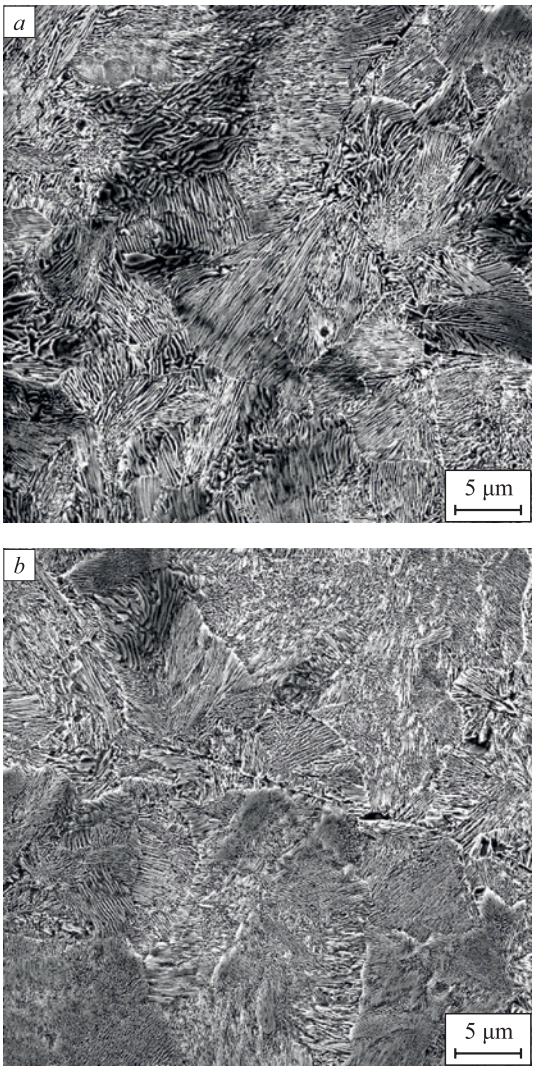

Fig. 3. Microstructure of metal of the rails of composition *1* (*a*) and composition *2* (*b*)

Рис. 3. Микроструктура металла рельсов состава *1* (*a*) и состава *2* (*b*)

Table 2. **Parameters of the rail microstructure**

Таблица 2. **Параметры микроструктуры рельсов**

Composition	Interlamellar spacing, μm	Grain diameter, μm	Grain number
1	0,109	24.20	8
2	0,091	19.50	9

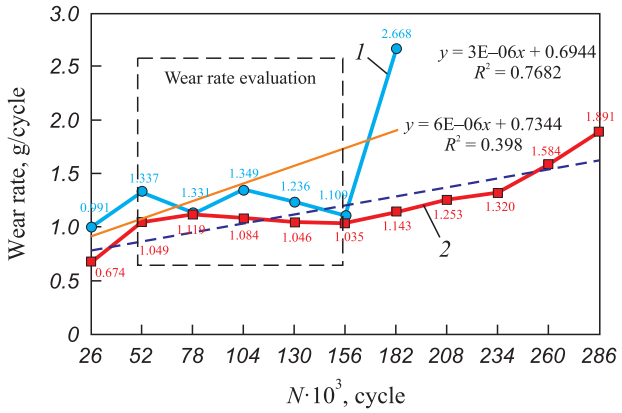

Fig. 4. Wear rate of the rail samples of composition *1* (●) and composition *2* (■)

Рис. 4. Интенсивность износа рельсов состава *1* (●) и состава *2* (■)

of rails with lower carbon and manganese content (composition *1*) is 1.0 grade larger than that of rails with composition *2*. The grain sizes correspond to 24.20 μm (grain number 8) for composition *1* and 19.50 μm (grain number 9) for composition *2*.

The average wear rate of samples from rails with composition *2* was $1.0665 \cdot 10^{-5}$ g/cycle, which is 13.5 % lower than the wear rate of samples from rails with composition *1*, measured at $1.2324 \cdot 10^{-5}$ g/cycle.

It is worth noting that after 182,000 revolutions, the samples cut from rails with composition *1* exhibited a sharp increase in mass loss (Fig. 4).

The microstructure of the samples after the friction test cycle was studied using an Olympus JX71 optical inverted microscope. Microstructural analysis revealed a fibrous-deformed structure with a layer thickness of up to 82.4 μm on the edges of samples with composition *2* and up to 103.9 μm on the edges of samples with composition *1* (Figs. 5, *a*, *b*). In the central part of the samples, the layer thickness reached up to 67.7 μm for composition *2* and up to 77.6 μm for composition *1* (Figs. 5, *c*, *d*).

CONCLUSIONS

An increase in carbon and manganese content in rail steel enhances its wear resistance and resistance to contact fatigue defects.

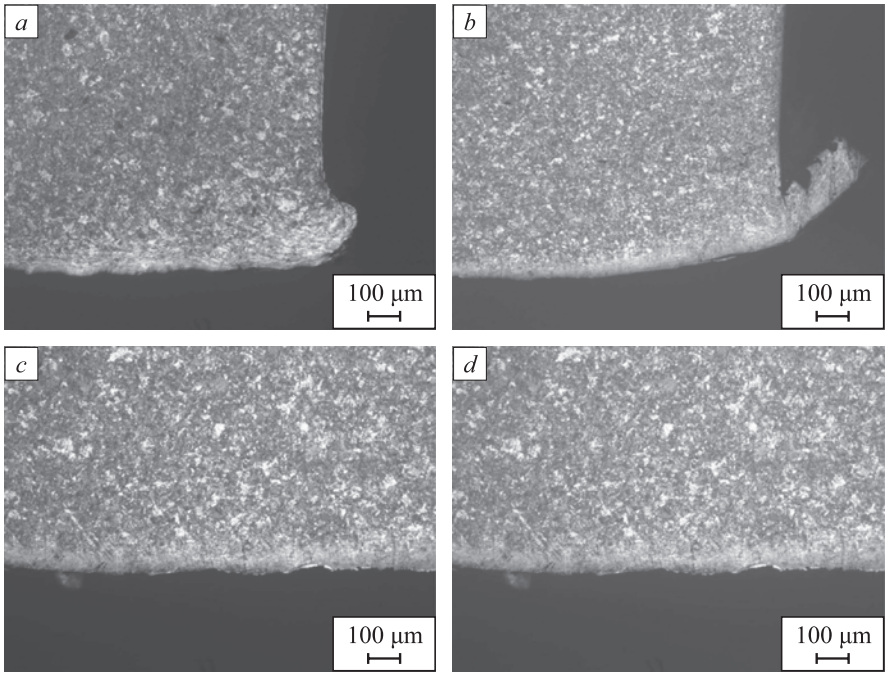

Fig. 5. Fibrous-deformed structure along the edges of the rail samples (*a*, *b*) and along the central part of the rail samples (*c*, *d*) of composition *1* (*a*, *c*) and composition *2* (*b*, *d*)

Рис. 5. Волокнисто-деформированная структура по краям образцов рельсов (*a*, *b*) и по центральной части образцов рельсов (*c*, *d*) состава *1* (*a*, *c*) и состава *2* (*b*, *d*)

The scientific findings of this study can be used to advance the theory of extending rail service life, reducing maintenance costs, and improving the reliability of differentially hardened rails produced by JSC EVRAZ United West Siberian Metallurgical Plant.

References / Список литературы

1. Yokoyama H., Mitao S., Yamamoto S. Wear and rolling contact fatigue behavior in pearlitic and bainitic rail steels. In: *7th International Heavy Haul Conf.* Fukuyama, Japan: Materials & Processing Research Center; 2001:551–557.
2. Goryacheva I.G., Shur E.A., Bortz A.I., Zakharov S.M. New generation rails damageability mechanisms evaluation and damage occurrence design. *Bulletin of the Joint Scientific Council of Russian Railways*. 2017;(4):25–27. (In Russ.).

   Горячева И.Г., Шур Е.А., Борц А.И., Захаров С.М. Исследование механизмов повреждаемости рельсов нового поколения и моделирование их возникновения. *Бюллетень Объединенного ученого совета ОАО РЖД*. 2017;(4):25–27.
3. Goryacheva I.G., Zakharov S.M., Kogan A.Ya., Torskaya E.V., Shur E.A., Abdurashitov A.Yu., Borts A.I., Zagranichek K.L. Complex approach to forecasting the operability and resource of new generation rails. *Bulletin of the Joint Scientific Council of Russian Railways*. 2017;(5-6): 16–26. (In Russ.).

   Горячева И.Г., Захаров С.М., Коган А.Я., Торская Е.В., Шур Е.А., Абдурашитов А.Ю., Борц А.И., Загранічек К.Л. Комплексный подход к прогнозированию работоспособности и ресурса рельсов нового поколения. *Бюллетень Объединенного ученого совета ОАО РЖД*. 2017;(5-6):16–26.
4. Polevoy E.V., Yunin G.N., Yunusov A.M., Dobuzhskaya A.B., Golitsyn G.A. On the issue of wear resistance of rails. *Stal'*. 2019;(7):62–65. (In Russ.).

   Полевой Е.В., Юнин Г.Н., Юнусов А.М., Добужская А.Б., Галицын Г.А. К вопросу об износостойкости рельсов. *Сталь*. 2019;(7):62–65.
5. Jendel T. Prediction of wheel profile wear – comparisons with field measurements. *Wear*. 2002;253(1-2):89–99. https://doi.org/10.1016/S0043-1648(02)00087-X
6. Zagranichek K.L., Bortz A.I., Peshkov I.E. Comparative assessment of wear resistance of differentially heat-strengthened rails for general and special purposes in laboratory conditions. In: *Improving the Quality and Operating Conditions of Rails and Rail Fasteners. Collection of Scientific Reports based on the Materials of the Meeting of the Non-Profit Partnership "Rail Commission" (Novokuznetsk, September 26-27, 2019).* Yekaterinburg: UIM; 2020:94-114. (In Russ.).

   Загранічек К.Л., Борц А.И., Перков И.Е. Сравнительная оценка сопротивления износу дифференцированно термоупрочненных рельсов общего и специального назначения в лабораторных условиях. В кн.: *Улучшение качества и условий эксплуатации рельсов и рельсовых скреплений. Сборник научных докладов по материалам заседания некоммерческого партнерства «Рельсовая комиссия» (Новокузнецк, 26–27 сентября 2019 г.)*. Екатеринбург: УИМ; 2020:94–114. (In Russ.).
7. Shur E.A., Borts A.I., Bazanova L.V. Fatigue life of damaged rails. *Journal of Physics: Conference Series*. 2020;1431(1):012071. https://doi.org/10.1088/1742-6596/1431/1/012071

8. Improvement of rail steels. *Zheleznye dorogi mira*. 2016;(1): 74–76. (In Russ.).

Совершенствование рельсовых сталей. *Железные дороги мира*. 2016;(1):74–76.

9. Generalization of the World Experience of Heavy-Weight Movement: Control of the Wheel – Rail System. Trans. from Eng. Zakharov S.M. ed. Moscow: Intext; 2017:420. (In Russ.).

Обобщение мирового опыта тяжеловесного движения: управление содержанием системы колесо – рельс / Пер. с англ. под ред. С.М. Захарова. Москва: Интекст; 2017:420.

10. Dang Van, Maitournam M.H., Moumni Z., Roger F. A comprehensive approach for modeling fatigue and fracture of rails. *Engineering Fracture Mechanics*. 2009;76(17):2626–2636. https://doi.org/10.1016/j.engfracmech.2008.12.020

11. Goryacheva I.G., Zakharov S.M., Torskaya E.V. Rolling contact fatigue and wear of wheel/rail simulation. In: *Proceedings of the Second Int. Conf. on Railway Technology Research Development and Maintenance. Stirlingshire,* Scotland: Civil-Comp Press; 2014:0123456789.

12. Kabo E., Ekberg A. Prediction of RCF from laboratory tests. In: *INNOTRACK Concluding Technical Report*. 2010:131–133.

13. Rodríguez-Arana B., Emeterio A.S., Panera M., Montes A., Alvarez D. Investigation of a relationship between twin-disc wear rates and the slipping contact area on R260 grade rail. *Tribology International*. 2022;168:107456. https://doi.org/10.1016/j.triboint.2022.107456

14. Kuznetsov R.V., Gromov V.E., Polevoy E.V., Rubannikova Yu.A., Kormyshev V.E. Evolution of structural-phase states and properties of differentially hardened 100-meter rails during extremely long-term operation. Message 3. Structure and properties of rails after the transported tonnage of 1.77 billion tons. *Problemy chernoi metallurgii i materialovedeniya*. 2021;(2):81–87. (In Russ.).

Кузнецов Р.В., Громов В.Е., Полевой Е.В., Рубанникова Ю.А., Кормышев В.Е. Эволюция структурно-фазовых состояний и свойств дифференцированно закаленных 100-метровых рельсов при экстремально длительной эксплуатации. Сообщение 3. Структура и свойства рельсов после пропущенного тоннажа 1,77 млрд т брутто. *Проблемы черной металлургии и материаловедения*. 2021;(2):81–87.

15. Pacey M.N., James M.N., Patterson E.A. A new photoelastic model studying fatigue cracks closure. *Experimental Mechanics*. 2005;45(1):42–45. https://doi.org/10.1007/BF02428989

16. Shur E.A., Tsvigun V.N., Koinov R.S. Models of formation of factographic reliefs on fatigue cracks. *Vestnik gorno-metallurgicheskoi sektsii Rossiiskoi akademii nauk. Otdelenie metallurgii*. 2018;(40):118–135. (In Russ.).

Шур Е.А., Цвигун В.Н., Койнов Р.С. Модели образования фрактографических рельефов на усталостных трещинах. *Вестник горно-металлургической секции Российской академии естественных наук. Отделение металлургии*. 2018;(40):118–135.

17. Goryacheva I.G., Bortz A.I., Zakharov S.M., Zagranichek K.L., Shur E.A. Investigation and modeling of the occurrence of surface contact fatigue damage in rails. In: *Tribology – machine structure. Proceedings of the XII Int. Sci. and Tech. Conf. dedicated to the 80th anniversary of IMASH RAS*. 2018:146–149. (In Russ.).

Горячева И.Г., Борц А.И., Захаров С.М., Заграничек К.Л., Шур Е.А. Исследование и моделирование возникновения поверхностных контактно-усталостных повреждений в рельсах. В кн.: *Трибология – машиностроению. Труды XII Международной научно-технической конференции, посвященной 80-летию ИМАШ РАН*. 2018:146–149.

18. Nekrasov D.B., Palagin S.V., Lykov K.Yu. On the expansion of landfills and the improvement of methods for monitoring and testing rails. *Railway Track and Facilities*. 2023;(4): 29–31. (In Russ.).

Некрасов Д.Б., Палагин С.В., Лыков К.Ю. О расширении полигонов и совершенствовании методик мониторинга и испытаний рельсов. *Путь и путевое хозяйство*. 2023;(4):29–31.

19. Shur E.A. How to compare the wear resistance of different rails correctly. *RSP Expert*. 2018;(1-2):20-25. (In Russ.).

Шур Е.А. Как правильно сравнивать износостойкость различных рельсов. *РСП-эксперт*. 2018;(1-2):20–25.

20. Nekrasov D.B., Borts A.I., Becher S.A., Bobrov A.L., Palagin S.V., Shlyakhtenko S.P. Ensuring the effectiveness of grinding based on the diagnosis of pre-defective conditions. *Railway Track and Facilities*. 2024;(3):17–19. (In Russ.).

Некрасов Д.Б., Борц А.И., Бехер С.А., Бобров А.Л., Палагин С.В., Шляхтенков С.П. Обеспечение эффективности шлифования на основе диагностирования преддефектных состояний. *Путь и путевое хозяйство*. 2024;(3):17–19.

21. Nekrasov D.B., Palagin S.V., Lykov K.Yu. Test results of rails of the DT400IK category. *Railway Track and Facilities*. 2023;(2):20–22. (In Russ.).

Некрасов Д.Б., Палагин С.В., Лыков К.Ю. Результаты испытаний рельсов категории ДТ400ИК. *Путь и путевое хозяйство*. 2023;(2):20–22.

22. Burstow M. A whole life rail model application and development for RSSB – Continued development of an RCF damage parameter. London: Rail Safety and Standards Board; 2004:74.

23. Chen Y.-T., Liu D.-Y., Fang H.-S., Bai B.-Z. Rolling contact fatigue of rail steel. *Journal of Iron and Steel Research International*. 2000;12(5):50–53.

Information about the Authors | Сведения об авторах

Ivan A. Olifirenko, *Chief Specialist in Physical Research Methods, Directorate for Rail Production of the Research and Production Center,* JSC EVRAZ United West Siberian Metallurgical Plant; *Postgraduate of the Chair of Ferrous Metallurgy and Chemical Technology,* Siberian State Industrial University
E-mail: Ivan.Olifirenko@evraz.com

Иван Андреевич Олифиренко, *главный специалист по физическим методам исследования дирекции по рельсовому производству научно-производственного центра,* АО «ЕВРАЗ Объединенный Западно-Сибирский металлургический комбинат»; *аспирант кафедры металлургии черных металлов и химической технологии,* Сибирский государственный индустриальный университет
E-mail: Ivan.Olifirenko@evraz.com

Tat'yana N. Oskolkova, *Dr. Sci. (Eng.), Prof. of the Chair of Ferrous Metallurgy and Chemical Technology*, Siberian State Industrial University
ORCID: 0000-0003-1310-1284
E-mail: oskolkovatatiana@yandex.ru

Egor V. Polevoi, *Cand. Sci. (Eng.), Head of Bureau of Metal Science and Heat Treatment of Technical Department of the Rail Site*, JSC EVRAZ United West Siberian Metallurgical Plant
E-mail: egor.polevoj@evraz.com

Татьяна Николаевна Осколкова, *д.т.н., профессор кафедры металлургии черных металлов и химической технологии*, Сибирский государственный индустриальный университет
ORCID: 0000-0003-1310-1284
E-mail: oskolkovatatiana@yandex.ru

Егор Владимирович Полевой, *к.т.н., начальник бюро металловедения и термической обработки технического отдела рельсовой площадки*, АО «ЕВРАЗ Объединенный Западно–Сибирский металлургический комбинат»
E-mail: egor.polevoj@evraz.com

Contribution of the Authors

I. A. Olifirenko – setting the task and goals of research, conducting tribological and mechanical tests, writing the text, conducting studies of samples using scanning electron microscopy, discussion and analysis of the results.

T. N. Oskolkova – setting the task and goals of research, discussion and analysis of the results.
E. V. Polevoi – analysis and summarizing of the results.

Вклад авторов

И. А. Олифиренко – постановка задачи и цели исследований, проведение трибологических и механических испытаний, написание текста статьи, проведение исследований образцов методами сканирующей электронной микроскопии, обсуждение и анализ результатов.
Т. Н. Осколкова – постановка задачи и цели исследований, обсуждение и анализ результатов.
Е. В. Полевой – анализ и обобщение результатов исследования.

Received 25.04.2024
Revised 05.06.2024
Accepted 17.09.2024

Поступила в редакцию 25.04.2024
После доработки 05.06.2024
Принята к публикации 17.09.2024

UDC 669.168.3:621.365.2
DOI 10.17073/0368-0797-2024-6-660-664

Original article
Оригинальная статья

Sub-electrode gap and specific electrical resistance of a ferroalloy furnace bath

A. P. Shkirmontov

Financial University under the Government of the Russian Federation (49/2 Leningradskii Ave., Moscow 125167, Russian Federation)

aps-panor@yandex.ru

Abstract. To increase the energy-technological efficiency of a ferroalloy furnace, the author studied the smelting of 45 % ferrosilicon by a carbon-thermal method. In some cases, methods for measuring and changing the specific electrical resistance of charge materials at temperatures up to 1900 K are used to study the technology of smelting ferroalloys for smelting manganese alloys from various ores, carbonaceous ferrochrome, ferrosilicon, ferrosilicon manganese and ferrosilicon aluminum. For a series of heats of 45 % ferrosilicon, measurements of the useful voltage, electrode current, and power factor were carried out. As smelting progressed, the bath resistance was calculated and for the reaction melting zone (melting crucible), the specific electrical resistance in the single-electrode version of the furnace was determined at various sub-electrode gaps. Smelting using technology with an increased sub-electrode gap was performed in a large-scale experimental electric furnace with a capacity of 130 – 290 kV·A. As a result, it was found that an increase in the sub-electrode gap from (0.6 ÷ 0.9) to 6.0 of electrode diameters leads to the effect of a 2.5-fold increase in resistance, voltage and power in the bath (each indicator), but at the same time to a slight decrease in the specific electrical resistance of the melting zone of the furnace with a constant diameter (150 mm) of the electrode. The optimal sub-electrode gap (electrode – substrate distance) in the bath of a single-electrode furnace was determined by changing the specific electrical resistance. The optimal value is 3.33 of the electrode diameter. Assuming deviations of about ±5 % of this value, it is possible to efficiently smelt 45 % ferrosilicon in the range of 3.2 – 3.5 electrode diameters for the sub-electrode gap during the ore recovery process with a closed arc.

Keywords: ferroalloys, electric furnace, sub-electrode gap, electrode current, operating voltage, bath resistance, power factor, recovery rate

For citation: Shkirmontov A.P. Sub-electrode gap and specific electrical resistance of a ferroalloy furnace bath. *Izvestiya. Ferrous Metallurgy*. 2024;67(6):660–664. *https://doi.org/10.17073/0368-0797-2024-6-660-664*

Подэлектродный промежуток и удельное электросопротивление ванны ферросплавной печи

А. П. Шкирмонтов

Финансовый университет при Правительстве Российской Федерации (Россия, 125167, Москва, Ленинградский пр., 49/2)

aps-panor@yandex.ru

Аннотация. Для повышения энерготехнологической эффективности работы ферросплавной печи проведены исследования выплавки 45 %-ного ферросилиция углеродотермическим способом. Для исследования технологии выплавки ферросплавов в ряде случаев применяют способы замера и изменения удельного электросопротивления шихтовых материалов при температурах до 1900 К для выплавки марганцевых сплавов из различных руд, углеродистого феррохрома, ферросилиция, ферросиликомарганца и ферросиликоалюминия. Для серии плавок 45 %-ного ферросилиция проводили замеры полезного напряжения, силы тока электрода, коэффициента мощности. По мере выплавки рассчитывали сопротивление ванны и для реакционной плавильной зоны (плавильного тигля) определяли удельное электросопротивление в одноэлектродной печи при различных подэлектродных промежутках. Выплавка по технологии с увеличенным подэлектродным промежутком выполнена в крупномасштабной опытной электропечи мощностью 130 – 290 кВ·А. Увеличение подэлектродного промежутка от (0,6 ÷ 0,9) до 6,0 диаметров электрода приводит к эффекту повышения в 2,5 раза сопротивления, напряжения и мощности в ванне (каждого показателя), но при этом несколько снижается удельное электросопротивление плавильной зоны печи при неизменном диаметре (150 мм) электрода. Определен оптимальный подэлектродный промежуток (расстояние электрод – подина) в ванне одноэлектродной печи по изменению удельного электросопротивления. Оптимальным является значение 3,33 диаметра электрода. При допущении отклонений около ±5 % от этой величины возможно проводить эффективную выплавку 45 %-ного ферросилиция в диапазоне 3,2 – 3,5 диаметров электрода для подэлектродного промежутка при рудовосстановительном процессе с закрытой дугой.

Ключевые слова: ферросплавы, электропечь, подэлектродный промежуток, сила тока электрода, рабочее напряжение, сопротивление ванны, коэффициент мощности, степень извлечения

Для цитирования: Шкирмонтов А.П. Подэлектродный промежуток и удельное электросопротивление ванны ферросплавной печи. *Известия вузов. Черная металлургия*. 2024;67(6):660–664. https://doi.org/10.17073/0368-0797-2024-6-660-664

Introduction

The smelting of ferroalloys using the carbon-thermal method is one of the most energy-intensive [1] and material-consuming processes [2] in ferrous metallurgy. The efficiency of a ferroalloy electric furnace depends on numerous factors, including the technological specifics of smelting from ore materials [3; 4]; electrical parameters and operating modes [5; 6]; energy technology parameters, particularly the thermal operation of the ferroalloy furnace bath; and the design features of melting units.

One of the key parameters in ferroalloy production is the sub-electrode gap – the distance between the electrode and the furnace substrate within the furnace bath. For traditional ferroalloy electric furnace designs, when smelting silicon, chromium, and manganese alloys using the carbon-thermal method, the sub-electrode gap typically ranges from approximately 0.6 to 0.9 electrode diameters [7]. Electric furnaces operate in a combined mode of resistance and electric arc, characterized by high electrode current values (tens of kiloamperes) and relatively low voltage, resulting in low active bath resistance.

To enhance energy-technological parameters and enable furnace operation at higher voltages, a smelting technology with an increased sub-electrode gap (exceeding the traditional values of 0.6 ÷ 0.9 electrode diameters) was proposed. This approach improves energy efficiency. By significantly increasing the bath depth, this technology eliminates the need to reduce electrode penetration into the charge while increasing active bath resistance, operating voltage, power factor, and the electrical and thermal efficiency of the furnace [8]. The critical challenge, however, lies in determining the optimal distance to which the electrode–substrate gap can be increased. Increasing this gap also expands the melting zone, including its vertical dimensions within the furnace bath, which necessitates a significant increase in bath depth.

The aim of this study was to smelt 45 % ferrosilicon using the carbon-thermal method and to determine the optimal value for the sub-electrode gap (electrode–substrate distance) in the bath of a single-electrode ferroalloy furnace. The goal was to achieve this without reducing electrode penetration into the charge or negatively affecting the smelting parameters for ferrosilicon. This investigation was conducted using a large-scale experimental electric furnace.

Research method

To study ferroalloy smelting technology, methods for measuring and adjusting the specific electrical resistance of charge materials at temperatures up to 1900 K are commonly applied. These methods have been used for various materials, including manganese alloys derived from Kazakh ores [9], carbonaceous ferrochrome, ferromanganese, 75 % ferrosilicon, ferrosilicomanganese MnSi17 [10], ferrosilicoaluminum [11], chromium alloys [12], and carbonaceous reductants [13]. Most research has concentrated on measuring the specific electrical resistance of non-traditional carbonaceous reductants for ferroalloys [14; 15] and silicon [16; 17].

In the present study, a series of heats was conducted to smelt 45 % ferrosilicon. Measurements were taken for useful voltage, electrode current, and power factor, while bath resistance and the reaction melting zone (melting crucible) were calculated to determine the specific electrical resistance in a single-electrode furnace under various sub-electrode gap conditions.

Before smelting, the furnace bath lining was gradually heated with current applied to coke for at least 24 h. After preheating, the current load was increased, and the first portions of the charge were introduced to initiate smelting with a closed arc. The first tapping of ferrosilicon through the spout occurred no earlier than two hours after the furnace started operating, with a gradual buildup of the burden level achieved by adding small portions of the charge. Subsequent ferrosilicon tappings were performed hourly, accompanied by periodic additions of the charge. Throughout the process, the electrode current (or current density) was maintained within consistent limits, close to the maximum allowable values for the 150 mm diameter graphitized electrode used in the furnace. During stable furnace operation, the working voltage and sub-electrode gap were gradually increased without changing the electrode penetration into the charge between tappings or reducing the ferrosilicon temperature at the furnace outlet [18].

Smelting unit description

The smelting unit was a single-electrode shaft furnace powered by alternating current at a frequency of 50 Hz, supplied to the working graphitized electrode and the electrically conductive carbon substrate. The furnace featured a tapping spout for ferrosilicon, with an electrode diameter of 150 mm and an electrode current

of approximately 4.7 kA. The insulating part of the lining was composed of fireclay bricks and granules, while the working layer of the walls was made of chromomagnesite bricks. To enhance durability, the furnace hearth (its lower section) was lined with carbon blocks up to a height of one electrode diameter. The substrate lining consisted of sheet asbestos, fireclay granules, four layers of fireclay bricks, two layers of carbon blocks, and a packing layer of electrode paste. The bath and electrically conductive substrate had a cross-section of 500×500 mm, with a bath depth of 1200 mm. During smelting, the smelting unit operated at a power range of 130 to 290 kV·A [8].

Results and discussion

The smelting of 45 % ferrosilicon was conducted using traditional charge materials, including quartzite, coke, and iron turnings. The electrode penetration into the charge was maintained at no less than 1.5 – 1.7 electrode diameters. As a baseline for comparison, the initial smelting was performed with a traditional sub-electrode gap of 0.6 ÷ 0.9 electrode diameters. During prolonged smelting, the electrode–substrate distance was gradually increased by incrementally raising the operating voltage while maintaining a constant electrode current. The maximum sub-electrode gap achieved was 6.0 electrode diameters. The active bath resistance increased from 4.8 to 12 mΩ, representing a 2.5-fold rise. Similarly, furnace power and voltage increased at this electrode–substrate distance without reducing the electrode penetration into the charge, facilitated by the significant increase in the furnace bath depth. Notably, the bath resistance did not change linearly with the increase in the electrode–substrate distance. Consequently, despite the significant rise in bath resistance, a decrease in the specific electrical resistance of the melting zone was observed [19] (see Figure).

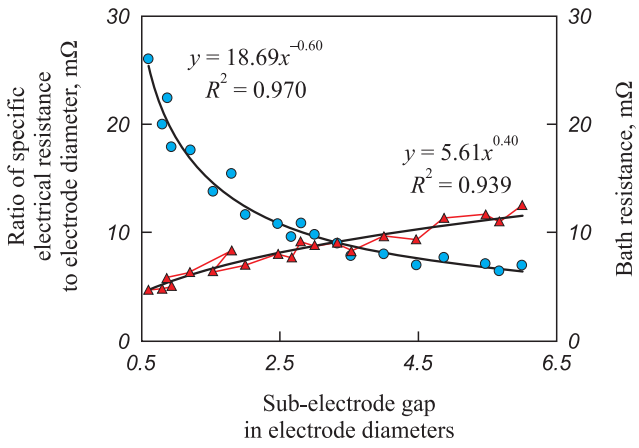

Changes in the bath active resistance and specific electrical resistance of the furnace melting zone depending on increase in sub-electrode gap when smelting 45 % ferrosilicon:
● – ratio of specific electrical resistance to the electrode diameter;
▲ – resistance of the furnace bath

Изменение активного сопротивления ванны и удельного электросопротивления плавильной зоны печи при выплавке 45 %-ного ферросилиция в зависимости от подэлектродного промежутка:
● – отношение удельного электросопротивления к диаметру электрода; ▲ – сопротивление ванны печи

The furnace power factor improved from 0.905 to 0.976, while electrical efficiency increased from 0.904 to 0.942. The relatively low thermal efficiency, typical of small furnaces, increased from 0.309 to 0.374. Specific energy consumption was reduced from 9020 to 7168 kW·h/ton due to the introduction of additional power into the furnace bath. Over the entire smelting campaign, silicon recovery into the alloy ranged from 91.9 – 92.1 %, with the tapping temperature of the alloy between 1650 and 1720 °C. The silicon content in the resulting alloy was 42.3 – 45.6 % Si, fully meeting the standard requirements.

Based on the studies of bath resistance and the specific electrical resistance of the melting zone as influenced by the sub-electrode gap during smelting in a ferroalloy furnace, the following relationships were derived:

$$R = 5.61\left(h/d_e\right)^{0.40}; \quad (1)$$

$$\rho/d_e = 18.69\left(h/d_e\right)^{-0.60}, \quad (2)$$

where R is the resistance of the furnace bath; h/d_e is the sub-electrode gap, expressed in electrode diameters; ρ/d_e is the ratio of the specific electrical resistance of the melting zone to the electrode diameter.

Despite the significant increase in bath resistance observed during the smelting of 45 % ferrosilicon, a notable decrease in the specific electrical resistance of the furnace melting zone was recorded as the sub-electrode gap (electrode–substrate distance) increased from 0.6 ÷ 0.9 to 6.0 electrode diameters (see Figure).

According to monographs by B.M. Strunsky [20; 21], which consolidate findings by P.V. Sergeev [22], W.H. Kelly, M.J. Morkramer, and other researchers on ferroalloy smelting in electric furnaces, the specific electrical resistance of various alloys spans the following ranges:

– 0.60 ÷ 0.95 Ω·cm for 45 % ferrosilicon;

– 0.50 ÷ 1.25 Ω·cm for 75 % ferrosilicon;

– 0 ÷ 2.00 Ω·cm for high carbon ferrochrome;

– 0.20 ÷ 0.55 Ω·cm for high carbon ferromanganese;

– 0.25 ÷ 0.38 Ω·cm for ferrosilicon manganese.

Given that the relative sub-electrode gap for standard ferroalloy smelting typically ranges from 0.6 ÷ 0.9 electrode diameters, variations in bath resistance are significant and substantially affect furnace regulation.

By solving the system of equations derived from equation (1) (reflecting an increase in bath resistance) and equation (2) (indicating a decrease in the specific electrical resistance of the melting zone), the optimal sub-electrode gap was calculated. The results showed that the optimal sub-electrode gap for smelting is 3.33 electrode diameters. Under these conditions, the furnace parameters for ferrosilicon smelting achieved favorable values: power factor up to 0.939; electrical efficiency up to 0.921; thermal efficiency up to 0.364. Allowing for a ±5 % deviation from this optimal sub-electrode gap, ferroalloy smelting can be effectively performed within the range of 3.2 – 3.5 electrode diameters. However, operating with a larger sub-electrode gap would necessitate further increasing the bath depth.

Conclusions

The smelting of 45 % ferrosilicon by the carbon-thermal method, with an increased sub-electrode gap ranging from 0.6 ÷ 0.9 to 6.0 electrode diameters, leads to a 2.5-fold increase in bath resistance, voltage, and power. This increase is accompanied by a noticeable reduction in the specific electrical resistance of the furnace melting zone. The optimal sub-electrode gap was determined to be 3.33 electrode diameters. With an allowable deviation of ±5 %, ferroalloy smelting can be effectively carried out within the range of 3.2 – 3.5 electrode diameters.

Список литературы / References

1. Syvachenko V., Yemchytskyy V., Nezhuryn V. Direction of saving energy resources in the technology of electrothermical processes. In: *Proceedings of the XIV Int. Ferroalloys Congress: INFACON XIV. Kiev, Ukraine. 31 May – 4 June 2015*. Kiev; 2015:700–702.
2. Degel R., Lux T., Joubert H. Furnace integrity of ferroalloy furnaces – synbiosis of process, cooling, refractory lining and furnace design. In: *Proceedings of the XV Int. Ferroalloys Congress: INFACON XV. Cape Town, South Africa. 25-28 February.* Cape Town; 2018:269–282.
3. Grishchenko S.G., Kutsin V.S., Kravchenko P.A. Ferroalloy industry of Ukraine: Current status, development trends and future prospects. In: *Proceedings of the XIV Int. Ferroalloys Congress: INFACON XIV. Kiev, Ukraine. 31 May – 4 June 2015*. Kiev; 2015:1–5.
4. Degel R., Frihling C., Koneke M. History and new milestones in submerged arc furnace technology for ferroalloy and silicon production. In: *Proceedings of the XIV Int. Ferroalloys Congress: INFACON XIV. Kiev, Ukraine. 31 May – 4 June 2015*. Kiev; 2015:7–16.
5. Gasik M. Handbook of Ferroalloys. Theory and Technology. Elsevier Ltd. 2013:520. https://doi.org/10.1016/C2011-0-04204-7
6. Gasik M., Dashevskii V., Bizhanov A. Ferroalloys. Theory and Practice. Springer Nature Switzerland; 2020:328. https://doi.org/10.1007/978-3-030-57502-1
7. Shkirmontov A.P. The role of sub-electrode gap in a ferroalloy furnace in improving the energy-technological parameters of smelting by carbon-thermal process. *Elektrometallurgiya*. 2017;(6):24–31. (In Russ.).

   Шкирмонтов А.П. Роль подэлектродного промежутка в ферросплавной печи в улучшении энерготехнологических параметров выплавки углеродотермическим процессом. *Электрометаллургия*. 2017;(6):24–31.
8. Shkirmontov A.P. Energy-Technological Parameters of Ferroalloy Smelting in Electric Furnaces. Moscow: NUST MISiS; 2018:216. (In Russ.).

   Шкирмонтов А.П. Энерготехнологические параметры выплавки ферросплавов в электропечах. Москва: НИТУ МИСиС; 2018:216.
9. Zhunusov A.K., Tolymbekov A.B. Metallurgical Processing of Manganese Ores from the TUR and Zapadny Kamys Deposits. Pavlodar: Keresku; 2016:209. (In Russ.).

   Жунусов А.К., Толымбеков А.Б. Металлургическая переработка марганцевых руд месторождения «ТУР» и Западный Камыс. Павлодар: Кереску; 2016:209.
10. Vorob'ev V.P. Electrothermy of Restorative Processes. Yekaterinburg: UB RAS; 2009:370. (In Russ.).

    Воробьев В.П. Электротермия восстановительных процессов. Екатеринбург: УрО РАН; 2009:370.
11. Bakirov A.G., Zhunusov A.K., Chekimbaev A.F., Shoshai Zh. Investigation of the electrical resistivity of charge mixtures for smelting ferrosilicoaluminium. *Nauka i Tekhnika Kazakhstana*. 2008;(2):14–19. (In Russ.).

    Бакиров А.Г., Жунусов А.К., Чекимбаев А.Ф., Шошай Ж. Исследование удельного электрического сопротивления шихтовых смесей для выплавки ферросиликоалюминия. *Наука и Техника Казахстана*. 2008;(2):14–19.
12. Kozhevnikov G.N., Zaiko V.P. Electrothermy of Chromium Alloys. Moscow: Nauka; 1980:188. (In Russ.).

    Кожевников Г.Н., Зайко В.П. Электротермия сплавов хрома. Москва: Наука; 1980:188.
13. Nurmukhanbetov Zh.U., Kim V.A., Tolymbekov M.Zh. Electrical resistance of carbon reducing agents. *Novosti nauki Kazakhstana*. 2005;(2):35–40. (In Russ.).

    Нурмуханбетов Ж.У., Ким В.А., Толымбеков М.Ж. Электросопротивление углеродистых восстановителей. *Новости науки Казахстана*. 2005;(2):35–40.
14. Vorob'ev V.P. Carborundum-bearing carbon reducing agents in silicon and silicon-ferroalloy production. *Steel in Translation*. 2015;45(6):439–442. https://doi.org/10.3103/S0967091215060157

    Воробьев В.П. Получение и применение карборундсодержащих углеродистых восстановителей в технологии кремния и ферросплавов. *Сталь*. 2015;(6):22–25.
15. Ul'eva G.A. Investigation of the physico-chemical properties of special types of coke and its application for smelting high-silicon alloys: Extended Abstract of Cand. Sci. Diss. Yekaterinburg; 2013:23. (In Russ.).

    Ульева Г.А. Исследование физико-химических свойств специальных видов кокса и его применения для выплавки высококремнистых сплавов: автореф. дисс. канд. техн. наук. Екатеринбург. 2013:23.
16. Isin D.K., Baisanov S.O., Mekhtiev A.D., Baisanov A.S., Isin B.D. Technology for the production of crystalline

silicon using non-traditional reducing agents. *Metallurg*. 2013;(11):88–93. (In Russ.).

Исин Д.К., Байсанов С.О., Мехтиев А.Д., Байсанов А.С., Исин Б.Д. Технология получения кристаллического кремния с применением нетрадиционных восстановителей. *Металлург*. 2013;(11):88–93.

17. Kim V.I. New types of carbon reducing agents for smelting of technical silicon. *Stal'*. 2017;(2):25–27. (In Russ.).

Ким В.И. Новые виды углеродистых восстановителей для выплавки технического кремния. *Сталь*. 2017;(2):25–27.

18. Shkirmontov A.P. Establishing the theoretical foundations and energy parameters for the production of ferroalloys with a larger-than-normal gap under the electrode. *Metallurgist*. 2009;53(5–6):300–308. https://doi.org/10.3103/s0967091222120117

19. Shkirmontov A.P. Change in active resistance of the bath and electrical resistivity of the reaction zone of ferrosilicon smelting with an increase in sub-electrode gap. In: *Physico-Chemical Fundamentals of Metallurgical Processes: Int. Sci. Conf.: Proceedings*. Moscow: IMET RAS; 2019:69. (In Russ.).

Шкирмонтов А.П. Изменение активного сопротивления ванны и удельного электросопротивления реакционной зоны выплавки ферросилиция при увеличении подэлектродного промежутка. В кн.: *Физико-химические основы металлургических процессов: Международная научная конференция: Сборник трудов*. Москва: ИМЕТ РАН; 2019:69.

20. Strunskii B.M. Calculations of Ore-Thermal Furnaces. Moscow: Metallurgiya; 1982:192. (In Russ.).

Струнский Б.М. Расчеты руднотермических печей. Москва: Металлургия; 1982:192.

21. Strunskii B.M. Ore-Thermal Melting Furnaces. Moscow: Metallurgiya; 1972:368. (In Russ.).

Струнский Б.М. Руднотермические плавильные печи. Москва: Металлургия; 1972:368.

22. Sergeev P.V. Energy Patterns of Ore-Thermal Electric Furnaces, Electrolysis and Electric Arc. Alma-Ata: Izdatel'stvo AS Kazakh SSR; 1963:251. (In Russ.).

Сергеев П.В. Энергетические закономерности руднотермических электропечей, электролиза и электрической дуги. Алма-Ата: Изд-во АН Казахской ССР; 1963:251.

Information about the Author / Сведения об авторе

Aleksandr P. Shkirmontov, *Dr. Sci. (Eng.), Director of the Editorial Center of Scientific Journals*, Financial University under the Government of the Russian Federation
E-mail: aps-panor@yandex.ru

Александр Прокопьевич Шкирмонтов, *д.т.н., директор Центра Редакции научных журналов*, Финансовый университет при Правительстве Российской Федерации
E-mail: aps-panor@yandex.ru

Received 26.04.2024
Revised 22.05.2024
Accepted 17.10.2024

Поступила в редакцию 26.04.2024
После доработки 22.05.2024
Принята к публикации 17.10.2024

METALLURGICAL TECHNOLOGIES / МЕТАЛЛУРГИЧЕСКИЕ ТЕХНОЛОГИИ

UDC 621.774
DOI 10.17073/0368-0797-2024-6-665-670

Original article
Оригинальная статья

FUNCTIONAL PROPERTIES OF PLASTIC DEFORMATION RESISTANCE OF 12KH18N10T STEEL

A. V. Vydrin[1, 2], A. V. Krasikov[3], A. A. Korsakov[2], E. A. Geim[1, 2] ✉

[1] **South Ural State University** (76 Lenina Ave., Chelyabinsk 454080, Russian Federation)
[2] **LLC "Research Center TMK"** (5 Bol'shoi Blvd., Skolkovo, Moscow 143026, Russian Federation)
[3] **JSC "Volzhskii Pipe Plant"** (6 Metallurgov Ave., Volzhskii, Volgograd Region 404119, Russian Federation)

✉ geymea@tmk-group.com

Abstract. The resistance of metals and alloys to plastic deformation has functional properties, since it depends on the history of the development of deformation over time. This is especially true for hot deformation processes. At the same time, complexity of the mathematical description and lack of the necessary experimental equipment for a long time did not allow us to design functionals of this type. Currently, due to the emergence of multifunctional research complexes like Gleeble, such an opportunity has appeared. Accordingly, a methodology was developed to study the functional properties of the resistance of metals and alloys of plastic deformation, which was applied to the study of 12Kh18N10T steel. The choice of steel grade is due to the fact that the behavior of austenitic stainless steel during plastic deformation differs significantly from carbon steels. On the other hand, at present, more and more attention is being paid to the production of metal products from stainless steels. This is due, on the one hand, to the tightening of the operating conditions of metal products, the development of new areas of their application and, on the other hand, a fairly high share of imports in the market of products made of austenitic stainless steels. Therefore, the study of the technological properties of such metals and alloys is relevant. At the same time, it should be noted that the most significant functional properties of the metal resistance to plastic deformation are manifested during hot deformation under continuous rolling conditions. Therefore, in this paper, the temperature range of hot plastic deformation is investigated. The results obtained can be used to determine the energy-power parameters in such processes as continuous rolling of strips in the finishing groups of strands and continuous rolling of sleeves in the lines of modern pipe rolling units.

Keywords: continuous rolling, metal resistance to plastic deformation, hot deformation, history of deformation, austenitic class, technological properties of metal, energy-power parameters

For citation: Vydrin A.V., Krasikov A.V., Korsakov A.A., Geim E.A. Functional properties of plastic deformation resistance of 12Kh18N10T steel. *Izvestiya. Ferrous Metallurgy*. 2024;67(6):665–670. https://doi.org/10.17073/0368-0797-2024-6-665-670

ФУНКЦИОНАЛЬНЫЕ СВОЙСТВА СОПРОТИВЛЕНИЯ ПЛАСТИЧЕСКОЙ ДЕФОРМАЦИИ СТАЛИ 12Х18Н10Т

А. В. Выдрин[1, 2], А. В. Красиков[3], А. А. Корсаков[2], Е. А. Гейм[1, 2] ✉

[1] **Южно-Уральский государственный университет** (Россия, 454080, Челябинск, пр. Ленина, 76)
[2] **ООО «Исследовательский центр ТМК»** (Россия, 143026, Москва, Инновационный центр Сколково, Большой бул., 5)
[3] **АО «Волжский трубный завод»** (Россия, 404119, Волгоградская область, Волжский, пр. Металлургов, 6)

✉ geymea@tmk-group.com

Аннотация. Сопротивление металлов и сплавов пластической деформации имеет свойства функционала, так как зависит от истории развития деформации во времени. Особенно это характерно для процессов горячей деформации. Вместе с тем сложность математического описания и отсутствие необходимого экспериментального оборудования долгое время не позволяли конструировать функционалы подобного типа. В настоящее время в связи с появлением многофункциональных исследовательских комплексов типа Gleeble такая возможность появилась. Соответственно была разработана методика исследования функциональных свойств сопротивления металлов и сплавов пластической деформации, которая была применена для исследования стали 12Х18Н10Т. Выбор марки стали обусловлен тем, что поведение нержавеющей стали аустенитного класса при пластическом деформировании существенно отличается от углеродистых сталей. С другой стороны, в настоящее время вопросам производства металлоизделий из нержавеющих марок стали уделяется все больше внимания. Это связано, с одной стороны, с ужесточением условий эксплуатации металлоизделий, освоением новых областей их применения и, с другой стороны, достаточно высокой долей импорта на рынке изделий из нержавеющих марок стали аустенитного класса. Поэтому исследование технологических свойств подобных металлов и сплавов является актуальным. При этом следует отметить, что наиболее заметно функциональные свойства сопротивления металла пластической деформации проявляются при

горячем деформировании в условиях непрерывной прокатки. Поэтому в данной работе исследован температурный интервал горячей пластической деформации. Полученные результаты могут быть использованы для определения энергосиловых параметров в таких процессах, как непрерывная прокатка полос в чистовых группах клетей и непрерывная раскатка гильз в линиях современных трубопрокатных агрегатов.

Ключевые слова: непрерывная прокатка, сопротивление металла пластической деформации, горячая деформация, история деформирования, аустенитный класс, технологические свойства металла, энергосиловые параметры

Для цитирования: Выдрин А.В., Красиков А.В., Корсаков А.А., Гейм Е.А. Функциональные свойства сопротивления пластической деформации стали 12Х18Н10Т. *Известия вузов. Черная металлургия*. 2024;67(6):665–670. https://doi.org/10.17073/0368-0797-2024-6-665-670

Introduction

The most productive and efficient method for manufacturing long metal products is continuous rolling. Recently, this method has been widely used in the production of rolled sections, strips, and pipes [1 – 3]. On the other hand, the quality of the final product rolled on continuous mills is significantly influenced by the adjustment of the mill's rate mode, which, in turn, determines the level of energy-power parameters. Therefore, to establish an optimal rate mode for the continuous rolling process, it is necessary to have relationships that link the kinematic parameters with the forces acting on the deformation zone boundaries.

Several studies [4 – 6] describe a methodology for determining such relationships. Analysis of the results obtained using this methodology for calculating rolling forces in continuous rolling has shown that the calculated values correspond quite well to actual values but are consistently underestimated. It should be noted that the rolling force is directly proportional to the metal's resistance to plastic deformation [7]. Further research has revealed that commonly used methods for calculating the resistance of metals to plastic deformation [8; 9] provide underestimated results when calculating the technological parameters of continuous rolling processes. This discrepancy arises because these methods do not account for the actual transformation of strength properties, particularly the residual strengthening after rolling in the previous stand of the mill. The effect of deformation history on the resistance of metals to plastic deformation during continuous hot strip rolling is also noted in [10]; however, the modeling employs expressions similar to those mentioned earlier. The above observations highlight the need for additional research into the resistance to plastic deformation of various steel grades.

One of the most in-demand types of metal products is seamless pipes made from stainless steel grades, particularly 12Kh18N10T [11]. Since continuous rolling is the most productive and economically efficient process for shell rolling in the production of seamless pipes [12; 13], studying the patterns of plastic deformation resistance formation in 12Kh18N10T steel during continuous rolling is highly relevant.

Research methods

In this study, experiments were conducted using the modern universal testing system Gleeble 3800 [14 – 16] in a vacuum environment (low vacuum) on the PocketJaw module, with chromel-alumel thermocouples welded to the samples (for temperature control during heating and measurement of deformation-induced heating). The samples were heated at a rate of 5 °C/s to the test temperature, followed by a 5-min hold, using electric current. High-temperature sensors for longitudinal and transverse deformation were used to measure deformation.

To determine the strain hardening rate of the steel, tensile tests were conducted at room temperature. The working hypothesis assumed that softening processes were absent under these conditions.

The behavior of metal resistance to plastic deformation during testing depends on its initial value, which, in turn, is influenced by the heating temperature. Therefore, a separate series of tensile tests was conducted on 12Kh18N10T steel samples at temperatures ranging from 800 to 1200 °C in 100 °C increments.

To determine the softening rate, stepwise tensile testing of cylindrical samples was performed with varying pause durations at temperatures from 800 to 1200 °C in 100 °C increments. It was assumed that during the pauses, no hardening processes occurred, and the decrease in stress characterized the softening rate.

All experimental data were processed using the least squares method in accordance with the methodology presented in [17].

Results

The general appearance of the strain hardening curves for 12Kh18N10T stainless steel, obtained from uniaxial tensile tests at various temperatures, is shown in Fig. 1.

The approximation of the strain hardening curve was based on results obtained at a temperature of 25 °C (Table 1).

In [18], it is noted that a power-law relationship is well-suited for approximating the dependence of the plastic deformation resistance of metals and alloys on strain

Table 1. **Plastic deformation resistance of 12Kh18N10T steel at 25 °C**

Таблица 1. **Сопротивление пластической деформации стали 12Х18Н10Т при температуре 25 °С**

Logarithmic strain	0.1	0.2	0.3	0.4	0.5	0.6	0.7	0.8	0.9	1.0
Stress, MPa	380	530	600	720	790	900	980	1100	1170	1270

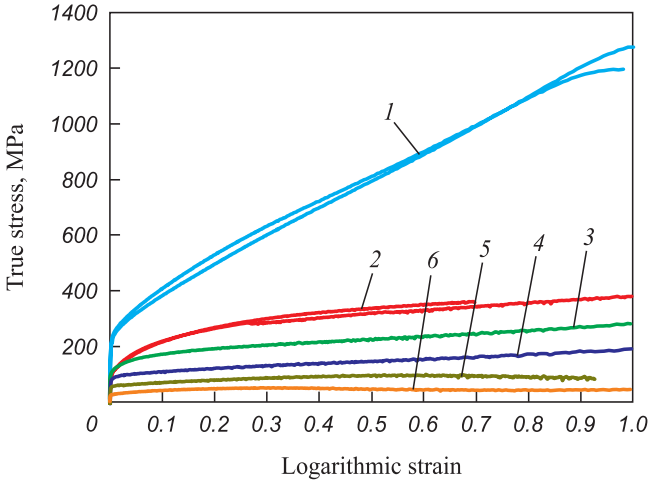

Fig. 1. Influence of logarithmic strain measure and temperature on plastic deformation resistance of 12Kh18N10T steel at temperature, °C:
1 – 25; *2* – 800; *3* – 900; *4* – 1000; *5* – 1100; *6* – 1200

Рис. 1. Влияние логарифмического показателя деформации и температуры на сопротивление пластической деформации стали 12Х18Н10Т при температуре, °С:
1 – 25; *2* – 800; *3* – 900; *4* – 1000; *5* – 1100; *6* – 1200

level in cold conditions. Processing the experimental data using the least squares method yielded the following equation for 12Kh18N10T steel

$$\sigma_{s0} = 200 + 1064\varepsilon^{0.78},$$

where ε is the logarithmic strain.

The statistical processing of experimental data (Table 2) also made it possible to determine the nature of the temperature's influence on the initial resistance of 12Kh18N10T steel to plastic deformation.

The resulting empirical relationship can be represented as:

$$\sigma_{s0}(\theta_0) = 200\left(\frac{1350-\theta_0}{1325}\right)^{0.87},$$

where θ_0 is the heating temperature of the sample.

It should be noted that the plastic deformation resistance of 12Kh18N10T steel in tensile tests has been previously studied. For example, in [19], based on extensive experimental research, an original methodology was proposed. According to this methodology, regardless of the steel grade, the ratio of the actual value of the metal's plastic deformation resistance σ_s to the average σ_{sc} for a given strain ε remains constant. The average plastic deformation resistance value is determined experimentally. Specifically, at South Ural State University, using this methodology and a cam plastometer, the following relationship was obtained for 12Kh18N10T steel:

$$\sigma_{sc} = 1892u^{0.0974}\varepsilon^{0.2637}\exp(-0.0022t),$$

where u is the strain rate; t is the heating temperature.

At the same time, it should be noted that the reliability of the results obtained thus far requires verification, as the equipment, methodologies, and measurement techniques used had certain errors.

On the other hand, the capabilities of modern research equipment significantly enhance the accuracy of results and broaden their applicability. In particular, stepwise loading of samples now enables the study of softening behavior during inter-deformation pauses. Similar studies using the Gleeble 3800 universal testing system are known [20], although they primarily focus on examining the metal structure. Therefore, stepwise tensile tests were conducted to obtain the relationship of the softening coefficient [8] as a function of temperature. As an example, Fig. 2 shows a record of the changes in the metal's plastic deformation resistance, taking into account the inter-deformation pause.

As a result, processing the presented experimental data using the least squares method yielded the following relationship:

$$k = 4.75\frac{1350-t}{t-25} - 0.93.$$

Table 2. **Initial value of plastic deformation resistance of 12Kh18N10T steel at different temperatures**

Таблица 2. **Начальное значение сопротивления пластической деформации стали 12Х18Н10Т при различных температурах**

Parameter	Temperature, °C				
	800	900	1000	1100	1200
Stress, MPa	100	100	60	40	30
Calculated value, MPa	93.07	78.16	62.81	46.87	30.05
Error, %	6.9	21.8	4.7	17.2	0.2

Analysis and discussion of results

The investigation of the plastic deformation resistance of 12Kh18N10T steel confirmed the existing information regarding the intensive strain hardening of this steel grade during cold deformation. The hardening behavior is accurately described by a power-law relationship.

The proposed new relationship for the initial plastic deformation resistance of 12Kh18N10T steel as a function of heating temperature provides a satisfactory qualitative and quantitative description of this dependence. A relatively large error is observed at a temperature of about 900 °C. However, on the other hand, the shell rolling process occurs at higher temperatures, where the proposed relationship shows good agreement with the actual data. Nevertheless, the search for a more suitable regression equation remains an open question.

The temperature dependence of the softening coefficient for 12Kh18N10T steel was determined for the first time. Previously, no attempts had been made to include a constant term in this equation. An analysis of the proposed relationship revealed that, according to calculations, the softening coefficient may take negative values at higher temperatures. This outcome lacks physical validity, as the softening coefficient represents the time required for the metal to fully soften. To address this issue, the constant term in the formula should be set to zero or higher. However, calculations indicate that this adjustment compromises the accuracy of the approximation at lower temperatures. Therefore, it is suggested to retain the current formula but assign a value of zero to the softening coefficient in cases where negative values are calculated. Alternatively, a more suitable regression equation could be developed to address this issue.

The investigation of the softening behavior of 12Kh18N10T steel at high temperatures revealed a distinct characteristic: it exhibits more intense softening between reductions compared to, for instance, ferritic-pearlitic steels [8].

As previously demonstrated [17], to determine the actual value of metal plastic deformation resistance while accounting for its time-dependent evolution, the entire duration of the deformation process, including pauses between reductions, is divided into discrete time intervals. For each i-th time interval, the plastic deformation resistance is calculated using a recursive formula.

The results of the study on the plastic deformation resistance of 12Kh18N10T steel allow for the proposal of the following recursive equation for determining this resistance within the temperature range of 900 – 1200 °C

$$\sigma_{si} = 200\left(\frac{1350-\theta_0}{1325}\right)^{0.87} + \sum_{i=1}^{m}\left\{1064\left(\varepsilon_i^{0.78}-\varepsilon_{i-1}^{0.78}\right)+\left(\sigma_{s(i-1)}-\sigma_0\right)\times\left[\exp\left(-\frac{\Delta\tau_i}{4.75\dfrac{1350-t}{t-25}}\right)-1\right]\right\},$$

where i is the number of the time interval into which the deformation time is divided; m is the total number

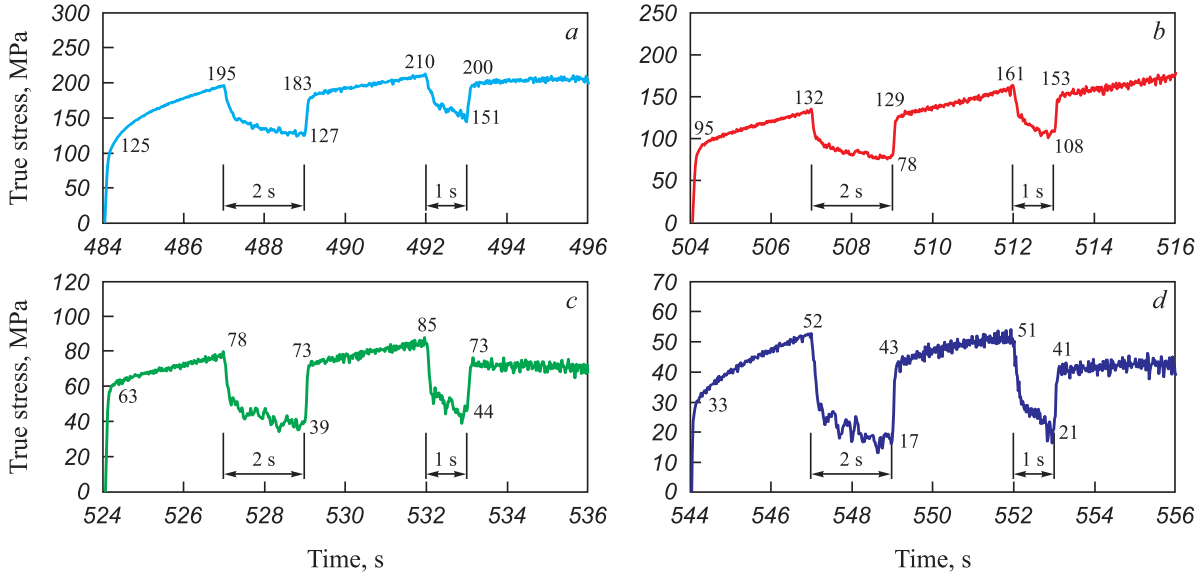

Fig. 2. Change in plastic deformation resistance of 12Kh18N10T steel under stepwise tension at temperature, °C:
a – 900; *b* – 1000; *c* – 1100; *d* – 1200

Рис. 2. Изменение сопротивления деформации стали 12Х18Н10Т при ступенчатом растяжении при температуре, °С:
a – 900; *b* – 1000; *c* – 1100; *d* – 1200

of time intervals into which the deformation time is divided; $\Delta\tau_i$ is the duration of the time interval.

Conclusions

The plastic deformation resistance of 12Kh18N10T steel in the hot state was studied. In addition to determining specific empirical coefficients, a notable characteristic of stainless steel deformation was identified – a significantly higher softening rate compared to ferritic-pearlitic steels.

The extensive experimental data collected can be used to calculate the deformation parameters and energy-power characteristics of the continuous shell rolling process for austenitic stainless steels on mills equipped with a controlled moving mandrel.

References / Список литературы

1. Cernuschi E. FQMTM: Danieli 3-roll pass retained mandrel mill for high quality seamless tube production. *Iron and Steel*. 2008;43(12):92–95.
2. Dukmasov V.G., Ageev L.M. State and Development of Technologies and Equipment in the World Ferrous Metallurgy. Chelyabinsk: SUSU; 2002:187. (In Russ.).

   Дукмасов В.Г., Агеев Л.М. Состояние и развитие технологий и оборудования в мировой черной металлургии. Челябинск: Издательство ЮУрГУ; 2002:187.
3. Dukmasov V.G., Il'ichev V.G. Efficiency of Modern Technologies in Metallurgy. Chelyabinsk: SUSU; 2006:178. (In Russ.).

   Дукмасов В.Г., Ильичев В.Г. Эффективность современных технологий в металлургии. Челябинск: Издательство ЮУрГУ; 2006:178.
4. Kolikov A.P., Romantsev B.A., Aleshchenko A.S. Metal Forming: Theory of Pipe Production Processes. Moscow: NUST MISIS; 2019:502. (In Russ.).

   Коликов А.П., Романцев Б.А., Алещенко А.С. Обработка металлов давлением: теория процессов трубного производства. Москва: Издательский дом НИТУ «МИСиС»; 2019:502.
5. Al-Jumaili M.J., Vydrin A.V., Shkuratov E.A. Elaboration of a digital model for estimation of power parameters of a rolling process in a continuous rolling mill. *AIP Conference Proceeding*. 2020;2213(1):020066. https://doi.org/10.1063/5.0000302
6. Vydrin A.V., Akhmerov D.A., Khramkov E.V. Simulation mathematical model of the pipe reduction process. *Chernye metally*. 2021;(10):56–60. (In Russ.).

   Выдрин А.В., Ахмеров Д.А., Храмков Е.В. Имитационная математическая модель процесса редуцирования труб. *Черные металлы*. 2021;(10):56–60.
7. Druyan V.M., Gulyaev Yu.G., Chukmasov S.A. Theory and Technology of Pipe Production. Dnepropetrovsk: Dnepr-VAL; 2001:544. (In Russ.).

   Друян В.М., Гуляев Ю.Г., Чукмасов С.А. Теория и технология трубного производства. Днепропетровск: РИА «Днепр-ВАЛ»; 2001:544.
8. Al-Khuzai A.S.O., Vydrin A.V., Shirokov V.V. Study of the resistance of metal to plastic deformation of steel pipe in a wide range of temperature variation. *Materials Today: Proceedings*. 2020;20(4):617–620. https://doi.org/10.1016/j.matpr.2019.09.199
9. Solod V.S., Beigel'zimer Ya.E., Kulagin R.Yu. Mathematical modeling of deformation resistance during hot rolling of carbon steels. *Metall i lit'e Ukrainy*. 2006;(7–8):52–56. (In Russ.).

   Солод В.С., Бейгельзимер Я.Е., Кулагин Р.Ю. Математическое моделирование сопротивления деформации при горячей прокатке углеродистых сталей. *Металл и литье Украины*. 2006;(7–8):52–56.
10. Aghasafari P., Salimi M., Daraei A. Flow stress evaluation in hot rolling of steel. *Journal of Materials Engineering and Performance*. 2014;23(8):2819–2828. http://doi.org/10.1007/s11665-014-1049-x
11. Volkova A.V. Steel Pipe Market – 2021. HSE University, 2021:69. (In Russ.).

    Волкова А.В. Рынок стальных труб – 2021. НИУ ВШЭ; 2021:69.
12. Kazaneki J. Wytwarzanie rur bez szwu. Krakow: Wydawnictwa AGN; 2003:622. (In Pol.).
13. Romantsev B.A., Goncharuk A.V., Vavilkin N.M., Samusev S.V. Metal Forming. Moscow: NUST MISIS; 2008:960. (In Russ.).

    Романцев Б.А., Гончарук А.В., Вавилкин Н.М., Самусев С.В. Обработка металлов давлением. Москва: МИСиС, 2008:960.
14. Kawulok R., Opela P., Schindler I., Kawulok P. Model of hot deformation resistance of the iron aluminide of the type Fe–40 at.%Al. In: *METAL 2013 – 22nd Int. Conf. on Metallurgy and Materials, Conference Proceedings 15–17.05.2013*, Brno, Czech Republic, EU: 444–449.
15. Dyya Kh., Knapinski M., Kovalek A. Modeling of metal forming processes and investigation of their mechanical properties using the Gleeble 3800 device. *Metallurgicheskaya i gornorudnaya promyshlennost'*. 2011;(7):16–20. (In Russ.).

    Дыя Х., Кнапиньски М., Ковалек А. Моделирование процессов обработки металлов давлением и исследование их механических свойств с помощью устройства Gleeble 3800. *Металлургическая и горнорудная промышленность*. 2011;(7):16–20.
16. Poliak E.I., Jonas J.J. Initiation of dynamic recrystallization in constant strain rate hot deformation. *ISIJ International*. 2003;43(5):684–61. https://doi.org/10.2355/isijinternational.43.684
17. Dukmasov V.G., Vydrin A.V. Mathematical Models and Processes of Rolling High-Quality Profiles. Chelyabinsk: SUSU; 2002:215. (In Russ.).

    Дукмасов В.Г., Выдрин А.В. Математические модели и процессы прокатки профилей высокого качества. Челябинск: Издательство ЮУрГУ; 2002:215.
18. Klimenko P.L. Hardening of Steel and Non-Ferrous Metals during Cold and Hot Deformation: Monograph. Dnepropetrovsk: Porogi; 2011:187. (In Russ.).

    Клименко П.Л. Упрочнение стали и цветных металлов при холодной и горячей деформации: Монография. Днепропетровск: Пороги; 2011:187.

19. Konovalov A.V., Vichuzhanin D.I., Partin A.S., Kozlov A.V. Determination of true stress-strain (hardening) curve for the fuel rod material. *Zavodskaya laboratoriya. Diagnostika materialov*. 2017;83(7):58–61. (In Russ.).

Коновалов А.В., Вичужанин Д.И., Партин А.С., Козлов А.В. Методика определения кривой упрочнения материала оболочек ТВЭЛов. *Заводская лаборатория. Диагностика материалов*. 2017;83(7):58–61.

20. Radionova L.V., Perevozchikov D.V., Makoveckii A.N., Eremin V.N., Akhmedyanov A.M., Rushchits S.V. Study of hot deformation behavior of stainless steel AISI 321. *Materials*. 2022;4057(15):4057. https://doi.org/10.3390/ma15124057

Information about the Authors

Aleksandr V. Vydrin, *Dr. Sci. (Eng.), Prof., Head of the Chair "Processes and Units of Metal Forming"*, South Ural State University; *Chief Researcher*, LLC "Research Center TMK"
E-mail: VydrinAV@susu.ru

Andrei V. Krasikov, *Cand. Sci. (Eng.), Chief Rollerman*, JSC "Volzhskii Pipe Plant"
E-mail: KrasikovAV@vtz.ru

Andrei A. Korsakov, *Cand. Sci. (Eng.), Head of Division of Seamless Pipes, Head of the Laboratory of Screw Rolling*, LLC "Research Center TMK"
E-mail: KorsakovAA@tmk-group.com

Evgenii A. Geim, *Postgraduate of the Chair "Processes and Units of Metal Forming"*, South Ural State University; *Junior Researcher*, LLC "Research Center TMK"
ORCID: 0000-0003-0856-0056
E-mail: geymea@tmk-group.com

Сведения об авторах

Александр Владимирович Выдрин, *д.т.н., профессор, заведующий кафедрой «Процессы и машины обработки металлов давлением»*, Южно-Уральский государственный университет; *главный научный сотрудник*, ООО «Исследовательский центр ТМК»
E-mail: VydrinAV@susu.ru

Андрей Владимирович Красиков, *к.т.н., главный прокатчик*, АО «Волжский трубный завод»
E-mail: KrasikovAV@vtz.ru

Андрей Александрович Корсаков, *к.т.н, начальник отдела бесшовных труб, заведующий лабораторией винтовой прокатки*, ООО «Исследовательский центр ТМК»
E-mail: KorsakovAA@tmk-group.com

Евгений Александрович Гейм, *аспирант кафедры «Процессы и машины обработки металлов давлением»*, Южно-Уральский государственный университет; *младший научный сотрудник*, ООО «Исследовательский центр ТМК»
ORCID: 0000-0003-0856-0056
E-mail: geymea@tmk-group.com

Contribution of the Authors

A. V. Vydrin – developing theoretical principles of functional properties of metal resistance to plastic deformation.

A. V. Krasikov – generalization of results.
A. A. Korsakov – processing experimental data.
E. A. Geim – conducting experimental studies.

Вклад авторов

А. В. Выдрин – разработка теоретических принципов функциональных свойств сопротивления металла пластической деформации.
А. В. Красиков – обобщение полученных результатов.
А. А. Корсаков – обработка экспериментальных данных.
Е. А. Гейм – проведение экспериментальных исследований.

Received 10.05.2023
Revised 04.10.2024
Accepted 23.10.2024

Поступила в редакцию 10.05.2023
После доработки 04.10.2024
Принята к публикации 23.10.2024

ECOLOGY AND RATIONAL USE OF NATURAL RESOURCES / ЭКОЛОГИЯ И РАЦИОНАЛЬНОЕ ПРИРОДОПОЛЬЗОВАНИЕ

UDC 669.054.83:66.094.2
DOI 10.17073/0368-0797-2024-6-671-678

Original article
Оригинальная статья

Effect of mechanical processing on reduction of iron oxides in man-made raw materials

M. V. Kleonovskii[1] ✉, O. Yu. Sheshukov[1, 2], M. A. Mikheenkov[1, 2], A. M. Mikheenkov[1], O. V. Matyukhin[1]

[1] **Ural Federal University named after the first President of Russia B.N. Yeltsin** (19 Mira Str., Yekaterinburg 620002, Russian Federation)
[2] **Institute of Metallurgy, Ural Branch of the Russian Academy of Science** (101 Amundsena Str., Yekaterinburg 620016, Russian Federation)

✉ kleonovskiy@yandex.ru

Abstract. The study considers ways to increase the efficiency of reduction of iron oxides from man-made waste (dust from electric arc furnaces) using mechanochemical activation (MCA), grinding and pressing. The analysis of chemical and phase compositions of the dust samples was carried out, which made it possible to identify their potential for processing. The experiments included a study of the effect of grinding and pressing at pressures up to 300 MPa on the materials' phase composition, as well as an assessment of the effects of coke addition during MCA. To study the effect of pressing pressure on the reduction processes, briquettes were fired at a temperature of 1200 °C. The results showed that the degree of iron metallization increases with an increase in pressing pressure: concentration of metallic iron reaches 19 % at a pressure of 300 MPa, which is higher compared to 17 % in the initial state without pressing. The novelty of the work lies in optimizing the pressing parameters and demonstrating its effect on the iron reduction process. The proposed conditions make it possible to increase the efficiency of processing man-made waste, which can be used to improve the environmental and economic components of production.

Keywords: mechanochemical activation, steelmaking dust, metallization, oxide reduction, zinc extraction, phase composition, secondary resources, waste recycling

For citation: Kleonovskii M.V., Sheshukov O.Yu., Mikheenkov M.A., Mikheenkov A.M., Matyukhin O.V. Effect of mechanical processing on reduction of iron oxides in man-made raw materials. *Izvestiya. Ferrous Metallurgy*. 2024;67(6):671–678.
https://doi.org/10.17073/0368-0797-2024-6-671-678

Воздействие механической обработки на процессы восстановления оксидов железа в техногенном сырье

М. В. Клеоновский[1] ✉, О. Ю. Шешуков[1, 2], М. А. Михеенков[1, 2], А. М. Михеенков[1], О. В. Матюхин[1]

[1] **Уральский Федеральный университет имени первого Президента России Б. Н. Ельцина** (Россия, 620002, Екатеринбург, ул. Мира, 19)
[2] **Институт металлургии Уральского отделения Российской академии наук** (Россия, 620016, Екатеринбург, ул. Амундсена, 101)

✉ kleonovskiy@yandex.ru

Аннотация. Рассмотрены способы повышения эффективности восстановления оксидов железа из техногенных отходов (пылей дуговой сталеплавильной печи) с применением механохимической активации, помола и прессования. Проведен анализ химического и фазового составов образцов пылей, что позволило выявить их потенциал для переработки. Эксперименты включали исследование влияния помола и прессования при давлениях до 300 МПа на фазовый состав материалов, а также оценку эффекта добавления кокса в процессе механохимической активации. Для изучения влияния давления прессования на восстановительные процессы был проведен обжиг брикетов при температуре 1200 °C. Полученные результаты показали, что степень металлизации железа возрастает при увеличении давления прес-

сования: содержание металлического железа достигает 19 % при давлении 300 МПа, что выше по сравнению с 17 % в исходном состоянии без прессования. Новизна работы заключается в оптимизации параметров прессования и демонстрации его влияния на процесс восстановления железа. Предложенные условия позволяют повысить эффективность переработки техногенных отходов, что может быть использовано для улучшения экологической и экономической составляющих производства.

Ключевые слова: механохимическая активация, сталеплавильные пыли, металлизация, восстановление оксидов, извлечение цинка, фазовый состав, вторичные ресурсы, переработка отходов

Для цитирования: Клеоновский М.В., Шешуков О.Ю., Михеенков М.А., Михеенков А.М., Матюхин О.В. Воздействие механической обработки на процессы восстановления оксидов железа в техногенном сырье. *Известия вузов. Черная металлургия*. 2024;67(6):671–678. https://doi.org/10.17073/0368-0797-2024-6-671-678

Introduction

The processing of man-made raw materials has become one of the key challenges in modern industry and environmental management. Man-made raw materials include various wastes and by-products generated during industrial processes. These materials often contain valuable components, such as metals, minerals, and chemical compounds, which can be extracted and reused. The efficiency of raw material processing can be enhanced through grinding and pressing, i.e., mechanochemical activation (MCA) [1; 2].

Mechanochemical activation is a process in which mechanical action is applied to solid substances, leading to changes in their physicochemical properties. This action can involve operations such as grinding, pressing, rolling, or other forms of mechanical impact. The MCA process is employed to enhance material reactivity [3], modify phase composition [4], improve interactions between components, and activate chemical reactions [5] that would otherwise occur slowly or not at all under standard conditions.

Outlined below are the key aspects of MCA.

• ***Grinding and lattice destruction.*** During grinding, the crystalline lattice of solid substances is disrupted, leading to the formation of defects and an increase in the specific surface area. This enhances the material's reactivity, as defects can serve as nucleation centers for new phases and initiate chemical reactions [6 – 8].

• ***Formation of active centers.*** Mechanical impact generates active centers on the particle surfaces, including free radicals, lattice defects, and surface irregularities. These active centers can trigger chemical reactions that would otherwise occur very slowly or require high temperatures and catalysts under normal conditions [9; 10].

• ***Phase composition changes.*** Mechanochemical activation can significantly alter a material's phase composition. For example, new phases that were absent in the initial material may form, or existing phases may transform into more stable or reactive forms [11 – 13].

• ***Increased chemical activity.*** Mechanochemically activated materials often demonstrate heightened chemical activity. This enhanced reactivity can be leveraged to accelerate the reduction of metals from oxides, synthesize new compounds, or break down otherwise stable chemical bonds [14 – 16].

• ***Lower reaction temperatures.*** Mechanochemical activation enables many chemical reactions to occur at lower temperatures than would otherwise be necessary. This effect is attributed to the accumulation of mechanical energy within the material, which helps to overcome the reaction's energy barrier [17; 18].

Thus, MCA is an important tool for controlling the physicochemical properties of materials, enabling the development of innovative technologies and processes.

In earlier experiments on the conditions of the pyrometallurgical reduction of oxide scale, it was found that increasing the pressing pressure of the scale during its preparation for firing from 0 to 300 MPa doubled its metallization degree during heating, while the onset temperature of metallization decreased by more than 40 °C [19]. It was hypothesized that the observed effects during the pyrometallurgical reduction of oxide scale result from the mechanochemical activation of iron oxides in the scale during pressing. Accordingly, the objective of this study is to confirm this hypothesis, optimize the pressing parameters, and demonstrate the impact of mechanical processing of raw materials on the iron reduction process.

Evaluation of franklinite decomposition potential during MCA

The effects of grinding and pressing pressure on the phase composition of electric arc furnace (EAF) dust were studied. To evaluate the influence of MCA on the phase composition of EAF dust, the tested dust samples were mixed to prepare an averaged sample, which was then ground for 2 min and pressed at pressures ranging from 0 to 300 MPa. The composition of the raw mixture in the first series and the processing conditions are presented in Table 1.

In the second series, coke was added to the dust, and the raw mixture was subjected to MCA. The composition of the raw mixture in the second series and the processing conditions are shown in Table 2.

Table 1. **Composition of raw material mixture of the first series and processing mode**

Таблица 1. **Состав сырьевой смеси первой серии и режимы обработки**

Sample ID	Composition				Grinding, min	Pressing pressure, MPa
	EAF dust		coke			
	%	g	%	g		
1.1	100	20	0	0	0	0
1.2					2	0
1.3					2	100
1.4					2	200
1.5					2	300

Таблица 2. **Состав сырьевой смеси второй серии и режимы обработки**

Table 2. **Composition of raw material mixture of the second series and processing mode**

Sample ID	Composition				Grinding, min	Pressing pressure, MPa
	EAF dust		coke			
	%	g	%	g		
2.1	80	16	20	4	0	0
2.2					2	0
2.3					2	100
2.4					2	200
2.5					2	300

The processed products were subjected to quantitative phase analysis.

Quantitative *X*-ray phase analysis was carried out using a STADI-P diffractometer (STOE, Germany). Data were collected with CuK_α radiation (40 kV, 30 mA), a graphite monochromator, within a scattering angle range of $2\theta = 10 \div 70°$, with a step size of 0.02° and a dwell time of 2 s per step. The results were analyzed using the PDF-2 database (Release 2008 RDB 2.0804).

Assessment of MCA's impact on the phase composition of EAF dust

The phase analysis results for samples 1.1 – 1.5 without coke are presented in Fig. 1.

Analysis of the ground and pressed samples reveals that the intensity of the *X*-ray spectrum varies cyclically with changes in pressing pressure. Table 3 and Fig. 1 illustrate the variations in the phase composition of the samples under different processing conditions.

The findings indicate an inverse relationship in compound content. As the pressing pressure increases to 150 MPa, the ZnO content in the sample rises, while the franklinite ($ZnO \cdot Fe_2O_3$) content decreases. Further increasing the pressing pressure to 300 MPa leads to a rise in franklinite ($ZnO \cdot Fe_2O_3$) content and a corresponding decrease in ZnO content. Therefore, it is crucial to monitor and maintain an optimal pressing pressure to achieve the desired compound composition in the final product.

Phase analysis results for samples 2.1 – 2.5 with coke are presented in Fig. 2.

Analysis of the phase composition of the ground and pressed samples indicates that, similar to the samples without coke, the intensity of the entire *X*-ray spectrum

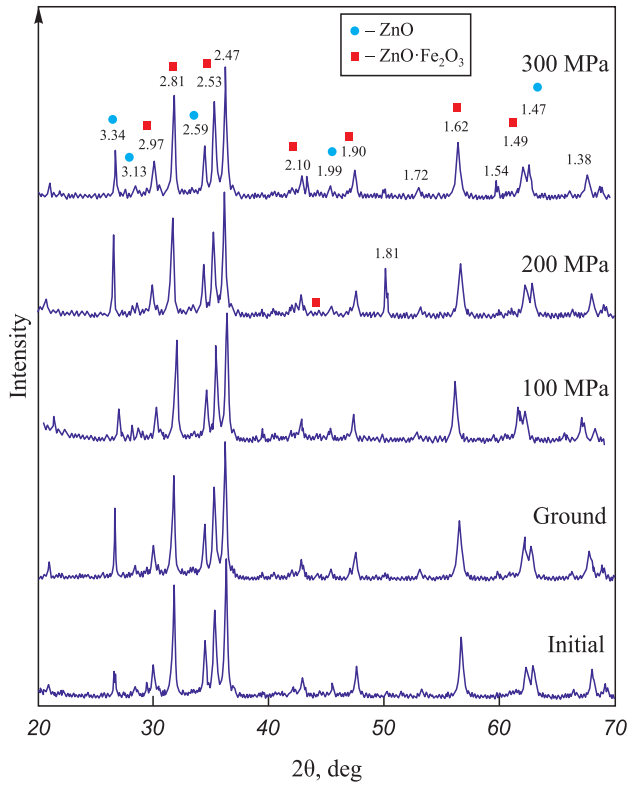

Fig. 1. Results of phase analysis of the samples 1.1 – 1.5

Рис. 1. Результаты фазового анализа проб 1.1 – 1.5

Table 3. **Phase composition in the samples depending on processing modes**

Таблица 3. **Содержания фаз в пробах в зависимости от режимов обработки**

Sample ID	Pressing pressure, MPa	Phase composition, wt. %	
		ZnO	$ZnO \cdot Fe_2O_3$
1.1	0	34.9	44.6
1.2	50*	36.1	43.0
1.3	100	42.6	37.3
1.4	200	38.0	39.1
1.5	300	34.9	44.5
* – grinding designation.			

changes cyclically depending on the pressing pressure. Table 4 and Fig. 2 present the variations in phase composition of the samples under different processing conditions.

The test results indicate that as the pressing pressure increases, the content of free ZnO initially decreases and then sharply rises. In the initial sample, the phase ratio of ZnO/ZnO·Fe_2O_3 is 37.4/40.7, whereas after complete MCA, this ratio shifts to 46.6/31.6. This change in phase quantities is likely due to interaction with coke according to the reaction

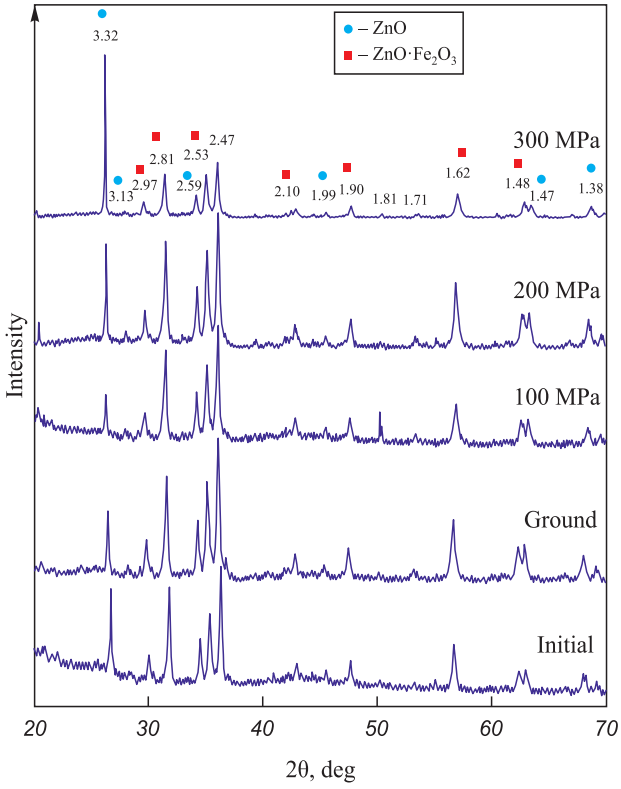

Fig. 2. Results of phase analysis of the samples 2.1 – 2.5

Рис. 2. Результаты фазового анализа проб 2.1 – 2.5

Table 4. **Phase composition in the samples 2.1 – 2.5 depending on processing modes**

Таблица 4. **Содержания фаз в пробах 2.1 – 2.5 в зависимости от режимов обработки**

Sample ID	Pressing pressure, MPa	Phase composition, wt. %	
		ZnO	ZnO·Fe_2O_3
2.1	0	37.4	40.7
2.2	50*	34.1	43.3
2.3	100	32.1	43.4
2.4	200	35.6	41.5
2.5	300	46.6	31.6

* – grinding designation.

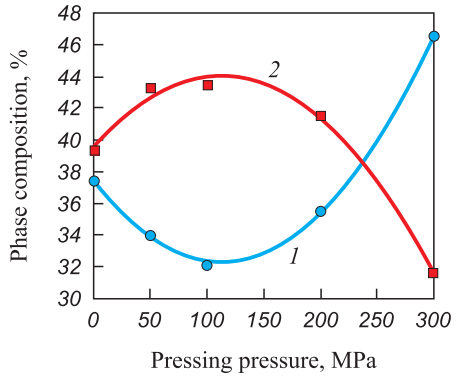

Fig. 3. Phase composition in the samples 2.1 – 2.5 depending on processing modes:
1 – ZnO; *2* – ZnO·Fe_2O_3

Рис. 3. Содержания фаз в пробах 2.1 – 2.5 в зависимости от режимов обработки:
1 – ZnO; *2* – ZnO·Fe_2O_3

$$3ZnFe_2O_4 + C = Fe_3O_4 + 3ZnO + CO\uparrow. \quad (1)$$

Fig. 3 shows the dependence of ZnO and ZnO·Fe_2O_3 phase content on pressing pressure.

Firing of pressed samples

To evaluate the effect of pressing pressure on the phase composition of fired products, a raw mixture was prepared using electric arc furnace (EAF) dust, coke, and a dry binder component with a content of 10 %. The components of the raw mixture were co-ground. After grinding, a liquid binder component was added to the raw mixture, which was then briquetted under pressures of 0, 100, 200 and 300 MPa. The composition of the binder is provided in the patent [20], while the composition of the raw mixture for firing and its processing conditions are listed in Table 5.

Before briquetting, a binder was introduced, consisting of ladle furnace slag (LFS), liquid glass, and hydrofluorosilicic acid (HFSA). The LFS contains approximately 40 % dicalcium silicate ($2CaOSiO_2$), which reacts with liquid glass, causing it to harden about 30 min after mixing and forming water-resistant tobermorite-like calcium-sodium hydrosilicates. This time is sufficient for briquetting to be carried out. Once briquetting and complete hardening are achieved, the briquettes gain high strength. Hydrofluorosilicic acid also reacts with liquid glass, promoting its hardening [21]. Additionally, the acid acts as a fluxing additive. It reacts with calcium oxide in the slag to form fluorite (fluorspar), which is a strong flux.

In [22], it was shown that when the binder content is less than 10 %, a non-diffusion reduction mode of iron oxides is implemented. In this mode, the degree of metallization is highly dependent on pressing pressure. When the binder content reaches 10 %, a liquid phase appears,

Table 5. **Composition of the raw mixture for firing and its processing mode**

Таблица 5. **Состав сырьевой смеси для обжига и режимы ее обработки**

Sample ID	Composition										Pressing pressure, MPa
	EAF dust		LFS slag		coke, (above 100 %)		Liquid glass-3.0 γ-1.2		HFSA γ-1.08		
	%	g	%	g	%	g	%	mL	%	mL	
3.1	90	18	10	2	20.0	4	7.5	1.5	3.75	0.75	0
3.2	90	18	10	2	20.0	4	7.5	1.5	3.75	0.75	100
3.3	90	18	10	2	20.0	4	7.5	1.5	3.75	0.75	200
3.4	90	18	10	2	20.0	4	7.5	1.5	3.75	0.75	300

and a diffusion reduction mode of iron oxides occurs. In this mode, the degree of metallization does not depend on pressing pressure and remains approximately the same across the entire pressure range.

The coke content corresponds to the stoichiometry of iron oxides and carbon, plus an additional 15 % to account for the ash content of the coke.

Dry briquettes were fired at temperatures up to 1200 °C for 1 h. The firing temperature matched the conditions for completing the metallization process [22]. An isothermal holding period of 30 min was maintained at 1200 °C. The overall appearance of the fired samples is shown in Fig. 4.

The fired samples in Fig. 4 clearly show droplets of metallic iron.

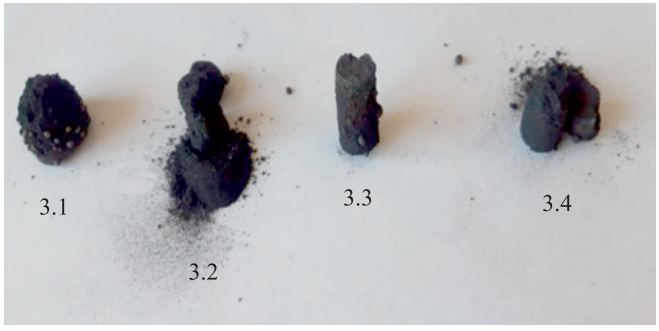

Fig. 4. General view of the fired samples

Рис. 4. Общий вид обожженных образцов

Table 6. **Phase composition in the studied samples**

Таблица 6. **Содержание фаз в исследованных пробах**

Sample ID	Phase composition, wt. %	
	Fe_{met}	$2CaO·SiO_2$, $3CaO·SiO_2$
3.1	17.1	82.9
3.2	16.3	83.7
3.3	17.4	82.6
3.4	19.0	80.8

The firing products were subjected to phase analysis, and the phase content of the studied samples is presented in Table 6.

The test results indicate that as the pressing pressure increases, the metallic iron content initially decreases but then rises, reaching 19 % at 300 MPa compared to 17 % in the initial state without pressing. Based on these findings, it is recommended to maintain a pressing pressure of 300 MPa, as lower pressures may negatively impact the degree of metallization.

Results and discussion

The research demonstrated a significant influence of pressing pressure on the phase composition and reduction processes of iron oxides in ASF dust. In the first series of experiments, conducted on samples without coke addition, cyclic variations in phase content were observed depending on the pressing pressure (Table 3). At pressures up to 150 MPa, the ZnO content increased, while the content of franklinite ($ZnO·Fe_2O_3$) decreased. However, at higher pressures up to 300 MPa, the opposite effect was noted: ZnO content decreased, and franklinite content increased. These findings highlight the necessity of controlling pressing pressure to achieve the desired phase ratio in the final product.

In the second series of experiments, involving samples with coke addition (Table 4), phase analysis results similarly demonstrated cyclic variations in the contents of ZnO and $ZnO·Fe_2O_3$ depending on pressing pressure. A substantial increase in free ZnO content at 300 MPa indicates the occurrence of the reduction reaction of franklinite ($ZnFe_2O_4$) involving carbon. The interaction, described by Equation (1), results in the formation of magnetite (Fe_3O_4), zinc oxide (ZnO), and carbon monoxide (CO), confirming the role of MCA in the breakdown of franklinite and the reduction of iron oxides.

The results of evaluating the effect of pressing pressure on firing processes (Table 6) showed that as pressure increased from 0 to 300 MPa, the metallic iron content initially decreased but subsequently increased, reaching

a maximum of 19 % at 300 MPa. These findings indicate that the optimal pressing pressure for maximizing iron metallization is 300 MPa. Lower pressures may adversely affect the reduction process, reducing the proportion of metallic iron in the final product.

Thus, the study confirms that MCA occurring during the pressing of EAF dust enhances the reduction processes of iron oxides. Optimizing pressing parameters, particularly maintaining a pressure of 300 MPa, ensures the highest metallization efficiency. This optimization offers promising opportunities to improve the productivity and environmental performance of pyrometallurgical waste processing.

Conclusions

It has been demonstrated that MCA significantly influences the phase composition of EAF dust, both with and without coke addition. In samples without coke, the phase composition changes cyclically with variations in pressing pressure. At pressures up to 150 MPa, the zinc oxide (ZnO) content increases, while the franklinite ($ZnO{\cdot}Fe_2O_3$) content decreases. However, with further pressure increases to 300 MPa, the franklinite content rises, and the free ZnO content decreases, indicating the need for precise pressure control to achieve the desired phase composition.

In samples with coke addition, a similar cyclic change in phase composition is observed depending on the pressing pressure. As the pressure increases, the free ZnO content initially decreases but then sharply rises. These changes are likely attributed to the reaction between franklinite and coke, resulting in the formation of magnetite (Fe_3O_4), ZnO, and carbon monoxide.

Firing of pressed samples revealed that as the pressing pressure increases, the metallic iron content initially decreases but subsequently rises, reaching a maximum at 300 MPa. This suggests that a pressing pressure of 300 MPa is optimal for achieving a high degree of metallization, while lower pressures may negatively affect the quality of the final product.

References / Список литературы

1. Saedi A., Jamshidi-Zanjani A., Mohseni M., Darban A., Nejati H. Mechanical activation of lead–zinc mine tailings as a substitution for cement in concrete construction. *Construction and Building Materials*. 2023;364:129973. https://doi.org/10.1016/j.conbuildmat.2022.129973
2. Yuan W., Wu Z., Song Q., Huang Q., Zhang C., Crittenden J. Lead recovery from waste CRT funnel glass by mechanochemical reaction with reductive Al powder. *Waste Management*. 2023;172:43–50. https://doi.org/10.1016/j.wasman.2023.09.008
3. Mañosa J., Alvarez-Coscojuela A., MarcoGibert J., Maldonado-Alameda A., Chimenos J.M. Enhancing reactivity in muscovitic clays: Mechanical activation as a sustainable alternative to thermal activation for cement production. *Applied Clay Science*. 2024;250:107266. https://doi.org/10.1016/j.clay.2024.107266
4. Penczner S., Kumar P., Patel M., Bouchard L., Iacopino D., Patel R. Innovations in mechanochemical synthesis: Luminescent materials and their applications. *Materials Today Chemistry*. 2024;38:102177. https://doi.org/10.1016/j.mtchem.2024.102177
5. Baki V.A., Ke X., Heath A., Calabria-Holley J., Terzi C., Sirin M. The impact of mechanochemical activation on the physicochemical properties and pozzolanic reactivity of kaolinite, muscovite and montmorillonite. *Cement and Concrete Research*. 2022;162:106962. https://doi.org/10.1016/j.cemconres.2022.106962
6. Kohobhange S.P., Manoratne C.H., Pitawala H.M., Rajapaks R.M. The effect of prolonged milling time on comminution of quartz. *Powder Technology*. 2018;330:266–274. https://doi.org/10.1016/j.powtec.2018.02.033
7. Yang X., Liu J., Chen G., Wu F., Liu J., Jiang X. Synergistic effects of mechanochemical activation and selective O-alkylation on the chemical structure and gaseous products evolution during coal flash pyrolysis. *Journal of Analytical and Applied Pyrolysis*. 2024;180:106553. https://doi.org/10.1016/j.jaap.2024.106553
8. Abed F.H., Zareei S.A., Kurdi N.H., Emami A. Enhancing geopolymer binder reactivity and performance via mechanochemical activation: A comprehensive study of rheological, mechanical, and microstructural properties. *Construction and Building Materials*. 2024;430:136456. https://doi.org/10.1016/j.conbuildmat.2024.136456
9. Yang C., Li Y., Tian Z., Qin W., Liu X., Wang X. Enhanced chalcopyrite leaching by mechanical activation: New insights from microstructure. *Minerals Engineering*. 2024;212:108719. https://doi.org/10.1016/j.mineng.2024.108719
10. Hosseini S., Brake N.A., Nikookar M., Günaydın-Şen Ö., Snyder H.A. Enhanced strength and microstructure of dredged clay sediment-fly ash geopolymer by mechanochemical activation. *Construction and Building Materials*. 2021;301:123984. https://doi.org/10.1016/j.conbuildmat.2021.123984
11. Singh A., Bhadauria S., Thakare A., Kumar A., Mudgal M., Chaudhary S. Durability assessment of mechanochemically activated geopolymer concrete with a low molarity alkali solution. *Case Studies in Construction Materials*. 2024;20:e02715. https://doi.org/10.1016/j.cscm.2023.e02715
12. Zhihan Z., Zhi W., Dong W., Yong L., Wanhai X., Chenghao L., Yang L., Jian W., Guobiao L. A green process for selective REEs recovery from Rare earth waste through mechanochemical activation. *Separation and Purification Technology*. 2023;315:123654. https://doi.org/10.1016/j.seppur.2023.123654
13. Zhang Y., Liu B., Gu X., Nehdi M.L., Zhang L.V. Mechanochemical activation of iron ore tailing-based ternary supplementary cementitious materials. *Construction and Building Materials*. 2022;346:128420. https://doi.org/10.1016/j.conbuildmat.2022.128420
14. Odebiyi O.S., Guo Y., Hao Du, Liu B., Wang S. Effect of mechanochemical activation parameters on vanadium

recovery from vanadium-bearing steel slag: Critical speed derivation for wet-ball milling. *Materials Chemistry and Physics*. 2024;324:129697.
https://doi.org/10.1016/j.matchemphys.2024.129697

15. Yu Y., Cui L., Zhang L., Wang Y. Efficient mechanochemical leaching of zinc from zinc oxide ores. *Transactions of Nonferrous Metals Society of China*. 2024;34:1976–1993.
https://doi.org/10.1016/S1003-6326(24)66520-9
16. Meng X., Hao J., Cao H., Lin X., Ning P., Zheng X., Chang J., Zhang X., Wang B., Sun Z. Recycling of $LiNi_{1/3}Co_{1/3}Mn_{1/3}O_2$ cathode materials from spent lithium-ion batteries using mechanochemical activation and solid-state sintering. *Waste Management*. 2019;84:54–63.
https://doi.org/10.1016/j.wasman.2018.11.034
17. Kriskova L., Pontikes Y., Cizer Ö., Mertens G., Veuleman W., Geysen D., Jones P.T., Vandewalle L., Van Balen K., Blanpain B. Effect of mechanical activation on the hydraulic properties of stainless steel slags. *Cement and Concrete Research*. 2012;42(6):778–788.
https://doi.org/10.1016/j.cemconres.2012.02.016
18. Gao P., Wu X., Zhang D., Sun X., Zhang G., Chen F. Mechanochemical activation of aryl diazonium salts: Synthesis of polycyclic (hetero)aromatics. *Journal of Organic Chemistry*. 2024;89(17):12197–12203.
https://doi.org/10.1021/acs.joc.4c01107
19. Sheshukov O.Yu., Mikheenkov M.A., Nekrasov I.V., Egiazar'yan D.V., Vedmid' L.B. Influence of pressing pressure on reduction of iron oxides of technogenic origin. In: *Proceedings of the Sci. and Pract. Conf. with Int. Part. and Elements of the School of Young Scientists: Dedicated to the 65th Anniversary of IMET UB RAS*. 2020:472–474. (In Russ.).

Шешуков О.Ю., Михеенков М.А., Некрасов И.В., Егиазарьян Д.В., Ведмидь Л.Б. Влияние давления прессования на процесс восстановления оксидов железа техногенного происхождения. *Труды научно-практической конференции с международным участием и элементами школы молодых ученых: 65-летию ИМЕТ УрО РАН посвящается*. 2020:472–474.
20. Vedmid' L.B. Mikheenkov M.A., Sheshukov O.Yu., Nekrasov I.V. Method of briquetting iron-containing waste in the form of scale. Patent RF no. 2705483. MPK C22B1/245. *Bulleten' izobretenii*. 2019;(31). (In Russ.).

Пат. 2705483 RU. Способ брикетирования железосодержащих отходов в виде окалины / Ведмидь Л.Б. Михеенков М.А., Шешуков О.Ю., Некрасов И.В.; заявл. 28.01.2019, опубл. 07.11.2019.
21. Borsuk P.A., Lyass A.M. Liquid Self-Hardening Mixtures. Moscow: Mashinostroenie; 1979:255. (In Russ.).

Борсук П.А., Лясс А.М. Жидкие самотвердеющие смеси. Москва: Машиностроение; 1979:255.
22. Sheshukov O., Mikheenkov M., Vedmid L., Nekrasov I., Egiazaryan D. Mechanism of ion-diffusion solid-phase reduction of iron oxides of technogenic origin in the presence of the liquid phase and without it. *Metals*. 2020; 10(12):1564.
https://doi.org/10.3390/met10121564

Information about the Authors / Сведения об авторах

Mikhail V. Kleonovskii, *Engineer of the Chair "Metallurgy of Iron and Alloys"*, Ural Federal University named after the first President of Russia B.N. Yeltsin
ORCID: 0000-0002-8874-9061
E-mail: kleonovskiy@yandex.ru

Oleg Yu. Sheshukov, *Dr. Sci. (Eng.), Prof., Director of the Institute of New Materials and Technologies*, Ural Federal University named after the first President of Russia B.N. Yeltsin; *Chief Researcher of the Laboratory of Powder, Composite and Nano-Materials*, Institute of Metallurgy, Ural Branch of the Russian Academy of Sciences
ORCID: 0000-0002-2452-826X
E-mail: o.j.sheshukov@urfu.ru

Mikhail A. Mikheenkov, *Dr. Sci. (Eng.), Prof.*, Ural Federal University named after the first President of Russia B.N. Yeltsin; *Senior Researcher of the Laboratory "Pyrometallurgy of Ferrous Metals"*, Institute of Metallurgy, Ural Branch of the Russian Academy of Sciences
ORCID: 0000-0002-7908-2955
E-mail: silast@mail.ru

Aleksandr M. Mikheenkov, *Postgraduate of the Chair "Metallurgy of Iron and Alloys"*, Ural Federal University named after the first President of Russia B.N. Yeltsin
E-mail: ma@osk66.ru

Oleg V. Matyukhin, *Cand. Sci. (Eng.), Assist. Prof. of the Chair "Thermal Physics and Informatics in Metallurgy"*, Ural Federal University named after the first President of Russia B.N. Yeltsin
E-mail: o.v.matiukhin@urfu.ru

Михаил Витальевич Клеоновский, *инженер 1-й категории кафедры «Металлургия железа и сплавов»*, Уральский федеральный университет имени первого Президента России Б.Н. Ельцина
ORCID: 0000-0002-8874-9061
E-mail: kleonovskiy@yandex.ru

Олег Юрьевич Шешуков, *д.т.н., профессор, директор Института новых материалов и технологий*, Уральский федеральный университет имени первого Президента России Б.Н. Ельцина; *главный научный сотрудник лаборатории порошковых, композиционных и нано-материалов*, Институт металлургии Уральского отделения РАН
ORCID: 0000-0002-2452-826X
E-mail: o.j.sheshukov@urfu.ru

Михаил Аркадьевич Михеенков, *д.т.н., профессор*, Уральский федеральный университет имени первого Президента России Б.Н. Ельцина; *старший научный сотрудник лаборатории пирометаллургии черных металлов*, Институт металлургии УрО РАН
ORCID: 0000-0002-7908-2955
E-mail: silast@mail.ru

Александр Михайлович Михеенков, *аспирант кафедры «Металлургия железа и сплавов»*, Уральский федеральный университет им. Первого Президента Б.Н. Ельцина
E-mail: ma@osk66.ru

Олег Владимирович Матюхин, *к.т.н., доцент кафедры теплофизики и информатики в металлургии*, Уральский федеральный университет имени первого Президента России Б.Н. Ельцина
E-mail: o.v.matiukhin@urfu.ru

Contribution of the Authors

M. V. Kleonovskii – development of the research concept and tasks, conducting the experiments, grinding and pressing of the studied samples at various pressures, analysis of the chemical and phase composition of EAF dusts and their changes during mechanochemical activation.
O. Yu. Sheshukov – scientific guidance, development of the methods for samples briquetting, firing them with subsequent analysis of the phase composition.
M. A. Mikheenkov – analysis of the effect of mechanochemical activation on the phase composition of EAF dust, study of the effect of grinding and pressing pressure on reduction of iron oxides, interpretation of the data obtained as a result of *X*-ray phase analysis of samples, study of interaction of the raw mixture components.

A. M. Mikheenkov – theoretical substantiation of the study, literary analysis, justification of importance of mechanochemical activation to increase the materials reactivity.

O. V. Matyukhin – processing and visualization of experimental data, plotting the dependence of phase composition on pressure and temperature, analysis of the research results, writing the conclusions, discussion of the results.

Вклад авторов

М. В. Клеоновский – разработка концепции исследования и постановка задач, проведение экспериментальной части работы, помол и прессование проб при различных давлениях, анализ химического и фазового состава пылей ДСП, а также их изменения в процессе механохимической активации.
О. Ю. Шешуков – научное руководство, разработка методов брикетирования образцов, их обжиг с последующим анализом фазового состава.
М. А. Михеенков – анализ воздействия механохимической активации на фазовый состав пыли ДСП, изучение влияния помола и давления прессования на процессы восстановления оксидов железа, интерпретация данных, полученных в результате рентгенофазового анализа проб и при исследовании взаимодействия компонентов сырьевой смеси.
А. М. Михеенков – теоретическое обоснование исследования, анализ литературных источников, обоснование важности механохимической активации для повышения реакционной способности материалов.
О. В. Матюхин – обработка и визуализация экспериментальных данных, построение графиков зависимости фазового состава от давления и температуры, анализ результатов исследований, формулировка выводов, обсуждение результатов.

Received 04.09.2024
Revised 23.09.2024
Accepted 23.10.2024

Поступила в редакцию 04.09.2024
После доработки 23.09.2024
Принята к публикации 23.10.2024

MATERIALS SCIENCE / МАТЕРИАЛОВЕДЕНИЕ

UDC 669:539.381.296
DOI 10.17073/0368-0797-2024-6-679-685

Original article
Оригинальная статья

INHOMOGENEITY OF DEFORMATION OF SURFACED STAINLESS STEEL

S. P. Buyakova[1], K. N. Kayurov[2], S. A. Barannikova[1]

[1] **Institute of Strength Physics and Materials Science, Siberian Branch of the Russian Academy of Sciences** (2/4 Akademicheskii Ave., Tomsk 634055, Russian Federation)
[2] **LLK Scientific Production Enterprise of Geophysical Equipment "Luch"** (34 2nd Yurginskaya Str., Novosibirsk 630051, Russian Federation)

bsa@ispms.ru

Abstract. The work is devoted to the study of the inhomogeneity of deformation of steel samples with laser surfacing. Highly nitrogenous austenitic stainless steel of the 08Kh18N6AG10S grade was selected as the substrate material in the state as received. To improve the mechanical properties of structural elements that operate under conditions of impact and abrasive wear, a surfacing of Ni–7Cr–6Fe + 60 % WC composite powder was applied to the steel. The surfacing was carried out with a change in the power of laser radiation from 1 to 3 kW and a change in the scanning speed from 0.005 to 0.040 m/s. The penetration depth of a single roller decreases with increasing the scanning speed. The microhardness varies widely in the surfacing thickness (from 7,000 ± 80 to 13,500 ± 70 MPa) and decreases with increasing scanning speed. Using the speckle photography method in the process of uniaxial extension of flat samples, it was found that the modes of laser surfacing also affect the level of inhomogeneity of deformation of micro-volumes of the deposited layer and the substrate. At the elastoplastic transition, the coefficient of variation of local deformations in the sample increases with an increase in the specific energy of laser surfacing. Coatings made of Ni–Cr–Fe+WC composite powder, obtained by laser surfacing under specified conditions, make it possible to increase the hardness and service life of structural elements of rotary controlled systems made of 08Kh18N6AG10S steel.

Keywords: plastic deformation, localization, surfacing, stainless steel, mechanical properties

Acknowledgements: The work was performed within the framework of the complex project "Organization of high-tech production of rotary controlled systems for opening complex plates and drilling wells with a large deviation from the vertical in difficult geological conditions in the Arctic" (grant agreement No. 075-11-2022-019 dated April 06, 2022), implemented by the Institute of Strength Physics and Materials Science of the Siberian Branch of the Russian Academy of Sciences with the financial support of the Ministry of Education and Science of the Russian Federation in the framework of Government Decree No. 218 dated 04.09.2010.

For citation: Buyakova S.P., Kayurov K.N., Barannikova S.A. Inhomogeneity of deformation of surfaced stainless steel. *Izvestiya. Ferrous Metallurgy*. 2024;67(6):679–685. *https://doi.org/10.17073/0368-0797-2024-6-679-685*

Исследование неоднородности деформации нержавеющей стали с наплавкой

С. П. Буякова[1], К. Н. Каюров[2], С. А. Баранникова[1]

[1] **Институт физики прочности и материаловедения Сибирского отделения РАН** (Россия, 634055, Томск, Академический пр., 2/4)
[2] **ООО Научно-производственное предприятие геофизической аппаратуры «ЛУЧ»** (Россия, 630051, Новосибирск, ул. 2-я Юргинская, 34)

bsa@ispms.ru

Аннотация. Работа посвящена изучению неоднородности деформации стальных образцов с лазерной наплавкой. В качестве материала подложки была выбрана высокоазотистая аустенитная нержавеющая сталь марки 08Х18Н6АГ10С в состоянии поставки. Для повышения механических свойств конструктивных элементов, работающих в условиях ударно-абразивного изнашивания, на сталь наносили наплавку из композиционного порошка Ni–7Cr–6Fe + 60 % WC. Наплавку проводили при изменении мощности лазерного излучения (1 – 3 кВт) и скорости сканирования (0,005 – 0,040 м/с). Глубина проплавления одиночного валика уменьшается с увеличением скорости сканирования. Микротвердость варьируется в широких пределах по толщине наплавки (с 7000 ± 80 до 13 500 ± 70 МПа) и уменьшается с увеличением скорости сканирования. С использованием метода спекл-фотографии в процессе одноосного растяжения плоских образцов установлено, что режимы лазерной наплавки также влияют на уровень неоднородности деформации микрообъемов наплавленного слоя и подложки. На упругопластическом переходе коэффициент вариации локальных деформаций в образце увеличивается

с ростом удельной энергии лазерной наплавки. Покрытия из композиционного порошка Ni–Cr–Fe+WC, полученные методом лазерной наплавки при заданных режимах, позволяют повысить твердость и ресурс конструктивных элементов роторных управляемых систем, изготовленных из стали марки 08Х18Н6АГ10С.

Ключевые слова: пластическая деформация, локализация, наплавка, нержавеющая сталь, механические свойства

Благодарности: Работа выполнена в рамках комплексного проекта «Организация высокотехнологичного производства роторных управляемых систем для вскрытия сложных пластов и бурения скважин с большим отходом от вертикали в сложных геологических условиях, Арктике» (соглашение о предоставлении субсидии от 06 апреля 2022 № 075-11-2022-019), реализуемого Институтом физики прочности и материаловедения Сибирского отделения РАН при финансовой поддержке Минобрнауки России в рамках постановления Правительства РФ от 09.04.2010 № 218.

Для цитирования: Буякова С.П., Каюров К.Н., Баранникова С.А. Исследование неоднородности деформации нержавеющей стали с наплавкой. *Известия вузов. Черная металлургия*. 2024;67(6):679–685. https://doi.org/10.17073/0368-0797-2024-6-679-685

Introduction

The increasing volume of hydrocarbon recovery requires complex well design profiles, where trajectories often include curved and inclined-rectilinear sections of significant length. For drilling such wells, rotary controlled systems (RCS) are employed as drill bit drives [1; 2]. The components of these systems are made from non-magnetic austenitic stainless steels [3; 4]. Under high loads, these elements develop defects that may lead to failures, with incidents most frequently occurring during rotary drilling operations in wells.

The hardness and wear resistance of steel surfaces can be enhanced by applying metal-ceramic (MC) coatings [5 – 7]. These coatings, a type of metal-matrix composite, consist of a metallic matrix reinforced with ceramic particles. Ceramic phases provide high hardness, while the relatively soft matrix holds the ceramic particles, imparting high fracture resistance and strength to the composite [8 – 11]. Metal-ceramic materials are highly resistant to abrasive wear.

One of the most widely used reinforcing materials for creating MC coatings is tungsten carbide (WC), known for its high hardness and strength [12 – 16]. These properties make WC-based coatings widely used for strengthening the working surfaces of wear-prone machine parts and mining tools. However, surfacing austenitic steels is challenging due to their tendency to form hot cracks during crystallization [17]. Solidification cracks in weld metal are considered the most detrimental and are more frequently observed than other types of cracking. The structure of austenitic steels is highly dependent on their chemical composition and the thermophysical conditions of crystallization, which are determined by the processing method [8; 17].

Technologies for additive manufacturing through layer-by-layer surfacing are rapidly developing [18 – 20]. These technologies enable the production of components with diverse geometric shapes, including large-scale parts, while also reducing material consumption. Such methods yield products with mechanical properties superior to those achieved through traditional manufacturing techniques. Layer-by-layer surfacing can be accomplished using various methods, with heat sources such as lasers, electron beams, electric arcs, and plasma arcs. Regardless of the method and type of material used, one of the critical features of additive manufacturing through layer-by-layer surfacing is the anisotropy of mechanical properties. This anisotropy arises from the crystallization process of the metal, leading to heterogeneous structures within the deposited layer and transcrystalline grain growth. Technologies utilizing concentrated energy sources offer significant potential for addressing these challenges.

Given that processes occurring near the interface during laser surfacing can impact the material's mechanical properties, this study aimed to investigate the effect of laser surfacing parameters on the inhomogeneity of plastic deformation in austenitic steel with surfacing.

Materials and methods

Forgings made of non-magnetic, high-nitrogen chromium-nickel-manganese stainless steel of the 08Kh18N6AG10S grade were used as the substrate material. The chemical composition of the steel was as follows, wt. %: <0.06 C; 16.0 – 18.0 Cr; 5.0 – 6.0 Ni; >0.4 N; 8.5 – 10.0 Mn; 0.6 – 1.2 Si; balance Fe. Currently, 08Kh18N6AG10S steel has demonstrated positive application experience in geophysical instruments, showing higher ductility and impact toughness compared to imported analogs while maintaining increased strength properties [21]. The austenitic stainless steel of the 08Kh18N6AG10S grade, in the as-received state, has an average yield strength of 800 MPa, an ultimate tensile strength of 1000 MPa, and an elongation at break of up to 20 %. The microstructure and phase composition of the steel have been described in detail in [21].

Laser surfacing of the Fe–Cr–Mn–Ni–N steel plates was performed using Ni–7Cr–6Fe + 60 % WC powder on an experimental setup at the Institute of Strength Physics and Materials Science of the Siberian Branch of the Russian Academy of Sciences (ISPMS SB RAS). The surfacing material was a nickel-based alloy with

a high content of tungsten carbide particles uniformly distributed within the solid matrix, which had a hardness exceeding 63 HRC. The particle size of tungsten carbide ranged from 10 to 45 μm, ensuring maximum resistance to abrasive and erosive wear. Surfacing parameters were selected to achieve a uniform, monolithic coating based on pre-established technological conditions. The beam diameter (d) was 4 mm, the power of the LS-15 fiber laser ranged from 1 to 3 kW, the scanning speed (V) ranged from 0.005 to 0.040 m/s, and the powder feed rate (F) was 20 mg/s.

Flat samples with dimensions of 50×8×2 mm in the working section were cut from the billets using the electro-spark method. The thickness of the Ni–7Cr–6Fe + 60 % WC surfacing layer was 1 mm, and the substrate layer (Fe–Cr–Mn–Ni–N) was 7 mm. The prepared samples were subjected to uniaxial tensile testing at room temperature on a Walter + Bai AG universal testing machine (LFM 125 series). The displacement rate of the movable grip V_{mach} was 0.4 mm/min, corresponding to a deformation rate of $1.67 \cdot 10^{-4}$ s^{-1}.

Structural studies were conducted using light microscopy (AXIOVERT-200MAT microscope) and X-ray diffraction analysis (DRON-07 diffractometer). The distribution of chemical elements across the thickness of the base and surfacing metal was measured using a LEO EVO 50 scanning electron microscope (Carl Zeiss, Germany) equipped with an Oxford Instruments attachment for X-ray dispersive microanalysis (Nanotech Center of ISPMS SB RAS). Microhardness measurements were performed using an instrumented indentation method in accordance with GOST R 8.748–2011 (ISO 14577-1:2002) on a PMT-3 microhardness tester.

Deformation fields on the surface of flat samples were recorded during mechanical testing using the speckle photography method outlined in [22–25]. The local elongation along the tensile axis of the sample, denoted as ε_{xx}, is typically the most intuitive parameter for visualizing and analyzing components of the plastic distortion tensor. To quantitatively evaluate the deformation inhomogeneity of the substrate and surfacing, the coefficient of variation was determined as the ratio of the standard deviation to the mean value [26].

Research results

During laser surfacing, powder granules melt, and the liquid alloy wets the tungsten carbide particles. As a result of subsequent high-speed crystallization, a metal-ceramic coating is formed. Mechanical testing revealed that surface hardening of the austenitic steel increased its tensile strength to 1500 MPa while reducing its ductility by 6 %.

To achieve metallurgical bonding between the surfacing material and the steel substrate while preventing dilution of the coating by the substrate material, surfacing must be performed under optimal conditions. Preventing crack formation requires applying different surfacing modes when depositing a single roller. The geometric parameters of the surfacing beads (coating thickness, penetration depth into the steel, and bead width) depend on the scanning speed, powder feed rate, and laser power. To optimize surfacing conditions, with constant powder feed rate and laser beam diameter, the scanning speed V and laser power P were chosen as variable factors (see Table). These parameters allow adjusting the specific energy, calculated as described in [17]:

$$E = \frac{P}{Vd},$$

where E is the specific energy, P is the laser power, d is the beam diameter, and V is the scanning speed.

Fig. 1 illustrates the effect of specific energy (E) on the penetration depth (L) of 08Kh18N6AG10S steel. The reduction in penetration depth with increasing scanning speed is attributed to the lower energy absorption during laser surfacing. As scanning speed increases, the proportion of the surface area covered by tungsten carbide (WC) particles grows, thereby reducing the mixing zone depth between the Ni–7Cr–6Fe + 60 % WC powder and the steel substrate.

X-ray diffraction analysis and dispersive microanalysis revealed that the content of the main alloying elements in the base metal corresponds to the nominal composition of 08Kh18N6AG10S steel. During heating, diffusion of alloying elements occurs from the base metal into the surfacing layer, while carbon diffuses in the opposite direction. At the interface on the austenitic steel side, reduced concentrations of manganese, chromium, and nitrogen were observed, along with an increased concentration of iron. No visible inclusions of ferrite or σ-phase were detected in the base metal (08Kh18N6AG10S) or the heat-affected

Effect of laser surfacing modes on the composite phase composition

Влияние режимов лазерной наплавки на фазовый состав композита

No.	P, kW	V, m/s	Phase
1	1.50	0.012	γ-Fe, $Me_{23}C_6$, WC, W_2C
2	1.50	0.016	γ-Fe, $Me_{23}C_6$, WC, W_2C
3	1.75	0.016	γ-Fe, $Me_{23}C_6$, WC, W_2C
4	2.00	0.020	γ-Fe, $Me_{23}C_6$, WC, W_2C
5	2.00	0.030	γ-Fe, $Me_{23}C_6$, WC, W_2C
6	2.00	0.035	γ-Fe, $Me_{23}C_6$, WC, W_2C
7	1.50	0.008	γ-Fe, $Me_{23}C_6$, WC, W_2C, Me_6C
8	2.00	0.008	γ-Fe, $Me_{23}C_6$, WC, W_2C, Me_6C

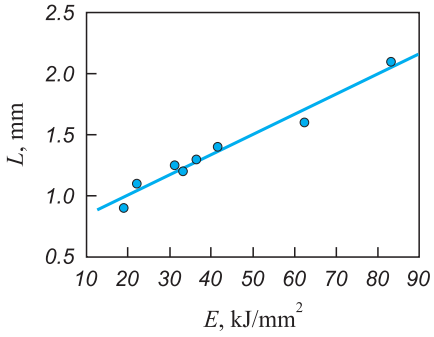

Fig. 1. Effect of specific energy (scanning speed and laser power) on the penetration depth of 08Kh18N6AG10S steel

Рис. 1. Влияние удельной энергии (скорости сканирования и мощности лазера) на глубину проплавления стали марки 08Х18Н6АГ10С

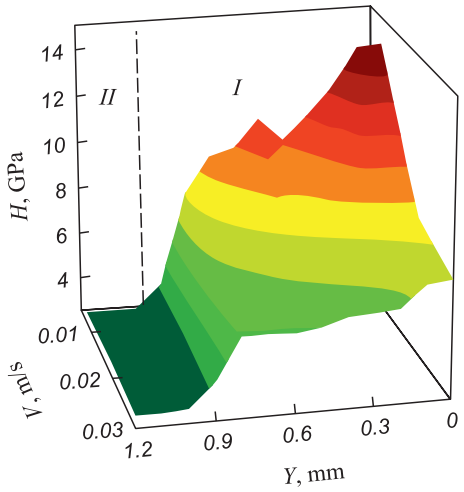

Fig. 2. Effect of scanning speed on microhardness distribution in the sample at a laser power of 2 kW (dashed line – connection zone):
I – Ni–Cr–Fe + WC surfacing layer; *II* – 08Kh18N6AG10S steel

Рис. 2. Влияние скорости сканирования на распределение микротвердости в образце при мощности лазера 2 кВт (зона соединения показана штриховой линией):
I – слой наплавки Ni–Cr–Fe + WC; *II* – сталь 08Х18Н6АГ10С

zone (HAZ). In the HAZ, a distinct dendrite junction line was observed. Microstructural analysis of the laser surfacing layer identified several zones: a columnar structure oriented normal to the interface with the substrate and a mixed structure comprising fine equiaxed dendrites and lamellar eutectic formations located at grain boundaries. The microstructure consists of various carbides, including undissolved (WC), partially dissolved (W_2C), and precipitated carbides ($Me_{23}C_6$ and Me_6C) within an austenitic matrix (refer to the Table, where *Me* = Cr, Fe, W, and Ni). The volume fraction of these precipitates varies depending on the surfacing parameters, directly influencing changes in microhardness.

Measurements indicated that the average microhardness of the base metal is 3285 ± 80 MPa, while in the connection zone with the surfacing layer, it reaches 3995 ± 70 MPa (Fig. 2). The microhardness of the surfacing layer, composed of Ni–Cr–Fe + WC, varies from 7000 ± 80 to 13,500 ± 70 MPa, depending on the surfacing modes (Fig. 2). The maximum microhardness is achieved at a low scanning speed during laser surfacing. This can be attributed to the high mass fraction of WC particles at lower scanning speeds and the enhanced dissolution of WC within the matrix. Increasing the scanning speed reduces the volumetric fraction of carbides, thereby decreasing the microhardness of the surfacing layer. Additionally, at low scanning speeds, a gradual decrease in microhardness is observed with increasing depth from the surface. This is explained by variations in the content and morphology of WC particles. Such a graded microstructure can be beneficial for maximizing wear resistance without compromising the strength of the surfacing layer. Conversely, higher scanning speeds result in a more uniform distribution of microhardness throughout the depth. These variations in microhardness are linked to the formation of composite microstructures consisting of various carbides dispersed within the stainless steel matrix.

Speckle photography data on local deformations ε_{xx} revealed areas of localized deformation in both the base metal and the surfacing layers (Fig. 3).

The analysis shows that plastic deformation is concentrated in specific zones of the sample, while other regions of the material remain nearly undeformed under the same increase in deformation. To quantitatively evaluate the degree of deformation inhomogeneity across different layers, the coefficient of variation of local deformations (ν) was used. For $\nu > 0.4$, the distribution of local elongations along the sample length $\varepsilon_{xx}(x_i)$ becomes significantly non-uniform, making the average value $\langle\varepsilon_{xx}\rangle$ unrepresentative [26].

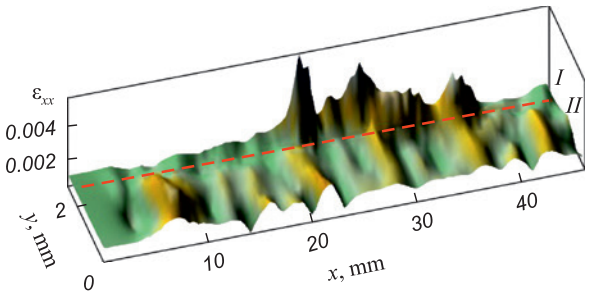

Fig. 3. Distribution of local deformations in the sample at scanning speed of 0.020 m/s and laser power of 2 kW (dashed line – connection zone):
I – Ni–Cr–Fe + WC surfacing layer; *II* – 08Kh18N6AG10S steel

Рис. 3. Распределение локальных деформаций в образце при скорости сканирования 0,020 м/с и мощности лазера 2 кВт (зона соединения показана штриховой линией):
I – слой наплавки Ni–Cr–Fe + WC; *II* – сталь 08Х18Н6АГ10С

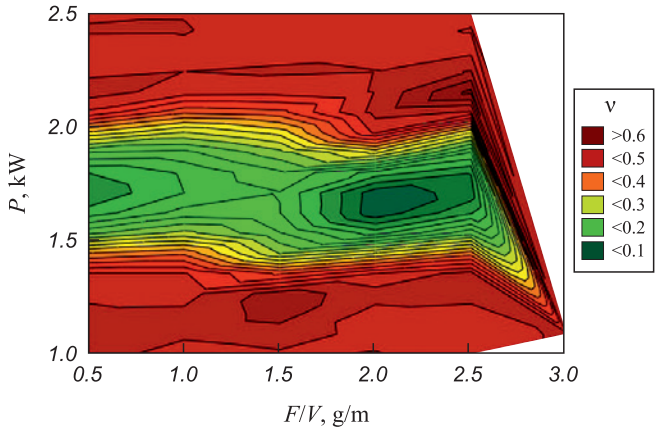

Fig. 4. Effect of laser surfacing modes on inhomogeneity degree of local deformations in the sample at total deformation of 0.01

Рис. 4. Влияние режимов лазерной наплавки на степень неоднородности локальных деформаций в образце при общей деформации 0,01

The structural inhomogeneity near the interface between the surfacing layer and the substrate significantly affects the development of localized deformation. For deformation compatibility at the composite interface, the deformations in the microvolumes adjacent to the boundary must be equal. As a result, the levels of deformation inhomogeneity in the microvolumes of different layers, measured by the coefficient of variation n, should also be balanced. Achieving this balance contributes to a more complex stress state in these regions.

Fig. 4 illustrates the variation in the deformation inhomogeneity n in a sample with surfacing under different modes during the initial stages of deformation, at a total deformation $\varepsilon = 0.01$. Upon reaching the yield strength, the levels of deformation inhomogeneity in the stainless steel and the surfacing layer differ significantly, depending on the increase in total deformation and specific energy.

A detailed analysis of microhardness distribution and deformation inhomogeneity in the composite revealed that laser surfacing modes with a laser power of 1.5 – 2.0 kW and scanning speeds of 0.007 – 0.040 m/s ensure satisfactory geometric parameters of the surfacing beads and the absence of cracks in the material.

Conclusions

To maintain the mechanical properties of the composite (steel – surfacing), it is crucial to select laser surfacing parameters that minimize deformation heterogeneity in the microvolumes of both the surfacing layer and the base metal.

The study demonstrated the effect of laser surfacing parameters on the distribution of microhardness and local deformations during the early stages of plastic deformation in 08Kh18N6AG10S stainless steel with a Ni – Cr – Fe + WC composite powder surfacing layer.

Coatings made from Ni – 7Cr – 6Fe + 60 % WC, composite powder, applied using laser surfacing at a power of 1.5 – 2.0 kW and scanning speeds of 0.007 – 0.040 m/s, are recommended to enhance the hardness and service life of structural elements in rotary controlled systems manufactured from 08Kh18N6AG10S steel.

References / Список литературы

1. Shevchenko I.A. Drilling wells with a large departure from the vertical, using a rotary-driven systems with control geophysical parameters in real-time. *Sovremennaya nauka: aktual'nye problemy teorii i praktiki. Seriya: estestvennye i tekhnicheskie nauki*. 2014;(1-2):36–39. (In Russ.).

   Шевченко И.А. Бурение скважин с большим отходом от вертикали с использованием роторных управляемых систем при контроле геофизических параметров в режиме реального времени. *Современная наука: актуальные проблемы теории и практики. Серия: естественные и технические науки*. 2014;(1-2):36–39.
2. Zakirov A.Ya. The first test results of Russian-made rotary-controlled systems. *Pro neft'. Professional'no o nefti*. 2016;(2(2)):43–47. (In Russ.).

   Закиров А.Я. Первые результаты испытаний роторно-управляемых систем российского производства. *Pro нефть. Профессионально о нефти*. 2016;(2(2)):43–47.
3. Speidel M., Speidel H. Austenitic stainless steels of high strength and ductility. *International Journal of Materials Research*. 2004;95(7):596–600. http://doi.org/10.1515/ijmr-2004-0115
4. Kostina M.V., Rigina L.G. Nitrogen-containing steels and methods of their production. *Izvestiya. Ferrous Metallurgy*. 2020;63(8):606–622. (In Russ.). https://doi.org/10.17073/0368-0797-2020-8-606-622

   Костина М.В., Ригина Л.Г. Азотосодержащие стали и способы их производства. *Известия вузов. Черная металлургия*. 2020;63(8):606–622. https://doi.org/10.17073/0368-0797-2020-8-606-622
5. Nurminen J., Näkki J., Vuoristo P. Microstructure and properties of hard and wear resistant MMC coatings deposited by laser cladding. *The International Journal of Refractory Metals and Hard Materials*. 2009;27(2):472–478. http://doi.org/10.1016/j.ijrmhm.2008.10.008
6. Zhong M., Liu W., Zhang Y., Zhu X. Formation of WC/Ni hard alloy coating by laser cladding of W/C/Ni pure element powder blend. *International Journal of Refractory Metals and Hard Materials*. 2006;24(6):453–460. http://doi.org/10.1016/j.ijrmhm.2005.09.002
7. Luo D., Hellman J., Luhulima D., Liimatainen J., Lindroos V.K. Interactions between tungsten carbide (WC) particulates and metal matrix in WC-reinforced composites. *Materials Science and Engineering: A*. 2003;340(1-2):155–162. http://doi.org/10.1016/S0921-5093(02)00173-9
8. Zhang Z., Yu T., Kovacevic R. Erosion and corrosion resistance of laser cladded AISI 420 stainless steel reinforced with VC. *Applied Surface Science*. 2017;410:225–240. http://doi.org/10.1016/j.apsusc.2017.03.137

9. Xiao Q., Sun W.-L., Yang K.-X., Xing X.-F., Chen Z.-H., Zhou H.-N., Lu J. Wear mechanisms and micro-evaluation on WC particles investigation of WC-Fe composite coatings fabricated by laser cladding. *Surface and Coatings Technology*. 2021;420:127341. http://doi.org/10.1016/j.surfcoat.2021.127341

10. Lee H.K. Effects of the cladding parameters on the deposition efficiency in pulsed Nd:YAG laser cladding. *Journal of Materials Processing Technology*. 2008;202(1-3):321–327. http://doi.org/10.1016/j.jmatprotec.2007.09.024

11. Hu G., Yang Y., Qi K., Lu X., Li J. Investigation of the microstructure and properties of NiCrBSi coating obtained by laser cladding with different process parameters. *Transactions of the Indian Institute of Metals*. 2020;73(10):2623–2634. http://doi.org/10.1007/s12666-020-02065-w

12. Huang S.W., Samandi M., Brandt M. Abrasive wear performance and microstructure of laser clad WC/Ni layers. *Wear*. 2004;256(11-12):1095–1105. https://doi.org/10.1016/S0043-1648(03)00526-X

13. Van Acker K., Vanhoyweghen D., Persoons R., Vangrunderbeek J. Influence of tungsten carbide particle size and distribution on the wear resistance of laser clad WC/Ni coatings. *Wear*. 2005;258(1-4):194–202. https://doi.org/10.1016/j.wear.2004.09.041

14. Yang J., Liu F., Miao X., Yang F. Influence of laser cladding process on the magnetic properties of WC-FeNiCr metal-matrix composite coatings. *Journal of Materials Processing Technology*. 2012;212(9):1862–1868. https://doi.org/10.1016/j.jmatprotec.2012.04.009

15. Si S.-H., Yuan X.-M., Liu Y.-L., He Y.-Z., Keesam Sh. Effect of laser power on microstructure and wear resistance of WCP/Ni cermet coating. *Journal of Iron and Steel Research International*. 2006;13:74–78. https://doi.org/10.1016/S1006-706X(06)60065-4

16. Guo Ch., Chen J., Zhou J., Zhao J., Wang L., Yu Y., Zhou H. Effects of WC–Ni content on microstructure and wear resistance of laser cladding Ni-based alloys. *Surface and Coatings Technology*. 2012;206(8-9):2064–2071. https://doi.org/10.1016/j.surfcoat.2011.06.005

17. Anandan S., Pityana L., Majumdar J.D. Structure-property-correlation in laser surface alloyed AISI 304 stainless steel with WC + Ni + NiCr. *Materials Science and Engineering: A*. 2012;536:159–169. https://doi.org/10.1016/j.msea.2011.12.095

18. Durst G. A new development in metal cladding. *JOM*. 1956; 8(3):328–333. https://doi.org/10.1007/BF03377692

19. Bogue R. Fifty years of the laser: its role in material processing. *Assembly Automation*. 2010;30(4):317–322. http://doi.org/10.1108/01445151011075771

20. Han T., Zhou K., Chen Z., Gao Y. Research progress on laser cladding alloying and composite processing of steel materials. *Metals*. 2022;12(12):2055. https://doi.org/10.3390/met12122055

21. Gordienko A.I., Abdulmenova E.V., Kozlova T.V., Gomorova Yu.F., Vlasov I.V., Fotin I.A., Kayurov K.N., Buyakova S.P. Effect of heat treatment modes on structure and properties of 08Kh18N6AG10S steel. *Izvestiya. Ferrous Metallurgy*. 2024;67(2):195–204. https://doi.org/10.17073/0368-0797-2024-2-195-204

Гордиенко А.И., Абдульменова Е.В., Козлова Т.В., Гоморова Ю.Ф., Власов И.В., Фотин И.А., Каюров К.Н., Буякова С.П. Влияние режимов термической обработки на структуру и свойства стали 08Х18Н6АГ10С. *Известия вузов. Черная металлургия*. 2024;67(2):195–204. https://doi.org/10.17073/0368-0797-2024-2-195-204

22. Zuev L.B., Barannikova S.A., Maslova O.A. The features of localized plasticity autowaves in solids. *Materials Research*. 2019;22(4):104–123. http://doi.org/10.1590/1980-5373-mr-2018-0694

23. Zuev L.B., Barannikova S.A. Autowave physics of material plasticity. *Crystals*. 2019;9(9):458. https://doi.org/10.3390/cryst9090458

24. Zuev L.B., Khon Yu.A. Plastic flow as spatiotemporal structure formation. Part I. Qualitative and quantitative patterns. *Physical Mesomechanics*. 2022;25(2):103–110. https://doi.org/10.1134/S1029959922020011

25. Zuev L.B., Gorbatenko V.V., Pavlichev K.V. Elaboration of speckle photography techniques for plastic flow analyses. *Measurement Science and Technology*. 2010;21(5):054014. http://doi.org/10.1088/0957-0233/21/5/054014

26. Mendenhall W.M., Sincich T.L. Statistics for Engineering and the Sciences. New York: Chapman and Hall/CRC; 2016:1182.

Information about the Authors / Сведения об авторах

Svetlana P. Buyakova, *Dr. Sci. (Eng.), Chief Researcher, Head of the Laboratory of Physical Mesomechanics and Non-Destructive Testing,* Institute of Strength Physics and Materials Science, Siberian Branch of the Russian Academy of Sciences
ORCID: 0000-0002-6315-2541
E-mail: sbuyakova@ispms.ru

Konstantin N. Kayurov, *General Director,* LLK Scientific Production Enterprise of Geophysical Equipment "Luch"
ORCID: 0000-0001-9545-5400
E-mail: kayurov@looch.ru

Svetlana A. Barannikova, *Dr. Sci. (Phys.-Math.), Leading Researcher of the Laboratory of Strength Physics,* Institute of Strength Physics and Materials Science, Siberian Branch of the Russian Academy of Sciences
ORCID: 0000-0001-5010-9969
E-mail: bsa@ispms.ru

Светлана Петровна Буякова, *д.т.н., главный научный сотрудник, заведующий лабораторией физической мезомеханики и неразрушающих методов контроля,* Институт физики прочности и материаловедения Сибирского отделения РАН
ORCID: 0000-0002-6315-2541
E-mail: sbuyakova@ispms.ru

Константин Николаевич Каюров, *генеральный директор,* ООО Научно-производственное предприятие геофизической аппаратуры «ЛУЧ»
ORCID: 0000-0001-9545-5400
E-mail: kayurov@looch.ru

Светлана Александровна Баранникова, *д.ф.-м.н. ведущий научный сотрудник лаборатории физики прочности,* Институт физики прочности и материаловедения Сибирского отделения РАН
ORCID: 0000-0001-5010-9969
E-mail: bsa@ispms.ru

Contribution of the Authors / Вклад авторов

S. P. Buyakova – concept formulation, literary review, analysis of the results.
K. N. Kayurov – selection of laser surfacing modes, discussion of the results.
S. A. Barannikova – conducting studies on mechanical characteristics and heterogeneity of deformation, discussion of the results, writing the text.

С. П. Буякова – формулирование концепции работы, обзор литературы, анализ результатов.
К. Н. Каюров – подбор режимов лазерной наплавки, обсуждение результатов.
С. А. Баранникова – проведение исследований механических характеристик и неоднородности деформации, обсуждение результатов, написание текста статьи.

Received 03.06.2024
Revised 21.08.2024
Accepted 20.09.2024

Поступила в редакцию 03.06.2024
После доработки 21.08.2024
Принята к публикации 20.09.2024

MATERIALS SCIENCE / МАТЕРИАЛОВЕДЕНИЕ

UDC 621:538.911:538.951
DOI 10.17073/0368-0797-2024-6-686-695

Original article
Оригинальная статья

Structural-phase state and properties of 56GM/(W + WC(Ni)) composite alloy obtained by wire electron beam additive manufacturing

A. V. Nikonenko, A. V. Vorontsov, N. N. Shamarin, V. R. Utyaganova, N. L. Savchenko, A. P. Zykova

Institute of Strength Physics and Materials Science, Siberian Branch of the Russian Academy of Sciences (2/4 Akademicheskii Ave., Tomsk 634055, Russian Federation)

aliska-nik@mail.ru

Abstract. The authors investigated the microstructure and mechanical characteristics of 56GM steel-based composite produced by wire electron-beam additive manufacturing with the addition of W + WC(Ni) powders during printing. The analysis demonstrates that 56GM/(W + WC(Ni)) composite alloy is characterised by a gradient structure consisting of 56GM base layer, 56GM – 56GM/(W + WC(Ni)) intermediate layer and 56GM/(W + WC(Ni)) composite layer. The base layer of 56GM steel is characterized by a multidirectional acicular structure, which corresponds to the ferrite-martensite state. In 56GM – 56GM/(W + WC(Ni)) intermediate layer the acicular structure becomes less pronounced. In 56GM/(W + WC(Ni)) composite layer an equiaxed grain structure is formed, with an average grain size of 8.59 μm, along the boundaries of which cracks are observed. WC particles are located mainly along the boundaries of small grains and in small quantities inside the grains themselves. It was found that 56GM/(W + WC(Ni)) composite is mainly composed of α-Fe (~80.6 vol. %), Ni (~6 vol. %), WC carbide phase (~10.3 vol. %) and γ-Fe (3 vol. %). The structure and properties of initial 56GM steel change both in the area of direct addition of alloying powder and in the underlying layers due to diffusion processes and infiltration of W + WC(Ni). Microhardness values increase from ~3.5 GPa to ~6.5 GPa with distance from the substrate to the composite layer. In uniaxial tensile tests, the ultimate tensile strength and yield strength values reached 1100 – 1200 MPa and 835 MPa in the intermediate layer, respectively.

Keywords: electron beam additive manufacturing, composite, 56GM steel, powder, WC(Ni) powder, structure, mechanical properties

Acknowledgements: The work was carried out within the framework of the state assignment of the Institute of Problems of Socio-Mechanical Problems of the Siberian Branch of the Russian Academy of Sciences, topic No. FWRW-2024-0001. The research was carried out using the equipment of the Nanotech Center of Collective Use of the Institute of Problems of Socio-Mechanical Problems of the Siberian Branch of the Russian Academy of Sciences.

For citation: Nikonenko A.V., Vorontsov A.V., Shamarin N.N., Utyaganova V.R., Savchenko N.L., Zykova A.P. Structural-phase state and properties of 56GM/(W + WC(Ni)) composite alloy obtained by wire electron beam additive manufacturing. *Izvestiya. Ferrous Metallurgy*. 2024;67(6):686–695. https://doi.org/10.17073/0368-0797-2024-6-686-695

Структурно-фазовое состояние и свойства композитного сплава 56GM/(W + WC(Ni)), полученного методом проволочного электронно-лучевого аддитивного производства

А. В. Никоненко, А. В. Воронцов, Н. Н. Шамарин, В. Р. Утяганова, Н. Л. Савченко, А. П. Зыкова

Институт физики прочности и материаловедения Сибирского отделения РАН (Россия, 634055, Томск, пр. Академический, 2/4)

aliska-nik@mail.ru

Аннотация. В работе исследовали микроструктуру и механические характеристики композита на основе стали 56GM, полученного методом проволочного электронно-лучевого аддитивного производства с введением при печати порошков W + WC(Ni). Показано, что композитный сплав 56GM/(W + WC(Ni)) характеризуется градиентной структурой, состоящей из основного слоя стали 56GM, промежуточного слоя 56GM – 56GM/(W + WC(Ni)) и композиционного слоя 56GM/(W + WC(Ni)). Основой слой 56GM характеризуется разнонаправленной игольчатой структурой, что соответствует феррито-мартенситному состоянию. В промежуточном слое 56GM – 56GM/(W + WC(Ni)) игольчатая структура становится менее выраженной. В композиционном слое 56GM/(W + WC(Ni)) формируется равноосная зеренная структура со средним размером зерен 8,59 мкм, по границам которых наблюдаются трещины. Частицы карбида вольфрама WC располагаются преимущественно по границам мелких зерен и в небольшом количестве внутри самих зерен. Методом рентгенофазового анализа установлено, что композит 56GM/(W + WC(Ni)) преимущественно состоит из α-Fe (~80,6 об. %), Ni (~6 об. %), карбидной фазы WC (~10,3 об. %) и незначительной доли γ-Fe (3 об. %). Структура и свойства исходной стали 56GM изменяются не только в области непосредственного добавления легирующего порошка, но и в нижележащих слоях из-за диффузионных процессов и инфильтрации порошка W + WC(Ni) при печати. Значения микротвердости по мере удаления от подложки до композиционного слоя увеличиваются примерно от 3,5 до 6,5 ГПа. Испытания на одноосное растяжение показали максимальные предел прочности и предел текучести в промежуточном слое, которые составили 1100 – 1200 и 835 МПа соответственно.

Ключевые слова: электронно-лучевое аддитивное производство, композит, сталь 56GM, порошок вольфрама, порошок WC(Ni), структура, механические свойства

Благодарности: Работа выполнена в рамках государственного задания Института физики прочности и материаловедения Сибирского отделения РАН, тема номер FWRW-2024-0001. Исследования выполнены с использованием оборудования ЦКП «Нанотех» Института физики прочности и материаловедения Сибирского отделения РАН.

Для цитирования: Никоненко А.В., Воронцов А.В., Шамарин Н.Н., Утяганова В.Р., Савченко Н.Л., Зыкова А.П. Структурно-фазовое состояние и свойства композитного сплава 56GM/(W + WC(Ni)), полученного методом проволочного электронно-лучевого аддитивного производства. *Известия вузов. Черная металлургия*. 2024;67(6):686–695. https://doi.org/10.17073/0368-0797-2024-6-686-695

Introduction

The incorporation of reinforcing materials (such as oxides, intermetallic compounds, nitrides, carbides, and borides) into a steel matrix enables the production of materials with enhanced performance characteristics due to the synergistic properties of the reinforcement and the matrix. These materials are known as metal-matrix composites (MMCs) [1]. The synthesis of MMCs is a highly effective approach to improving the mechanical properties of steel, including hardness, strength, fatigue life, and wear resistance [2].

Traditionally, MMCs are produced using casting or powder metallurgy methods. These techniques are time-consuming and challenging to control. Furthermore, the high cost of casting molds, coarse-grained microstructures, and limitations associated with the formation of undesirable interfacial compounds between the reinforcing particles and the matrix present significant challenges in the fabrication of MMCs [3].

Hybrid electron beam additive manufacturing technology, which involves the simultaneous or programmed feeding of wire and powder filaments, is an advanced additive manufacturing approach that enables the production of metallic components and composites with tailored microstructures. Recently, this technology has been the subject of intensive research and holds significant potential for creating novel metallic materials with unique properties [4 – 6].

Tungsten carbide (WC) is well-suited as a reinforcing particle for iron-based alloys due to its high melting point, thermal stability, strength, hardness, good wettability, and a coefficient of thermal expansion similar to that of iron. Consequently, there have been substantial efforts in recent years to fabricate WC/Fe composites using various methods, including additive manufacturing [7]. Particular attention has been paid to improving the microhardness and wear resistance of such composites, which result from the strong adhesion of tungsten carbide particles to the iron-based matrix via a reaction

layer. However, the development of high-performance MMCs has revealed challenges, such as the formation of thick, brittle reaction layers between the reinforcing particles and the matrix, driven by the formation of carbides like Me_3C [8]. These reaction layers frequently lead to cracks that propagate along the tungsten carbide/matrix interface [9]. As a result, the tungsten carbide particles lose their ability to effectively bear the load, compromising the mechanical properties of the composite material. Controlling the phase evolution at the interface between tungsten carbide reinforcing particles and the iron-based matrix must consider the diffusion of tungsten, carbon, iron, and other alloying elements, which is particularly challenging due to the non-equilibrium conditions of additive manufacturing associated with high energy input. Careful control of the reaction layer thickness is essential to ensure the load-bearing capacity of the tungsten carbide particles [10]. Furthermore, it is crucial to investigate how tungsten and carbon influence phase transformations in the iron-based matrix during rapid solidification in additive manufacturing, as they significantly expand the stability ranges of ferritic and austenitic phases, respectively [11].

It is well established that the nickel-tungsten carbide (Ni – WC) system exhibits superior properties when used for producing highly wear-resistant overlay deposits on various tools employed in the oil and gas industry [12]. In the Ni – WC system, tungsten carbide particles provide the desired wear resistance, while nickel alloys contribute relatively high impact toughness, mitigating the embrittlement of tungsten carbides [13].

It is also known that tungsten additions slow down the kinetics of carbide precipitation from steel alloying elements due to its low diffusion rate [14; 15]. In [16], the authors reported that introducing tungsten into hot-work tool steel alloyed with Cr – Mo – V improves mechanical properties during high-temperature tempering and increases resistance to softening by suppressing the coarsening of nanoscale carbides. Similarly, [17] demonstrated that adding tungsten to Cr – Mo alloyed steel enhances high-temperature strength by inhibiting dislocation recovery during tempering above 650 °C, resulting in a reduction in the size of $Me_{23}C_6$ carbides.

Recently, there has been a growing demand for materials capable of withstanding complex stresses, including thermal, mechanical, chemical, electromagnetic, and, potentially, neutron irradiation [18; 19]. The ability to function under such extreme conditions poses significant challenges in material development, often requiring combinations of multiple materials. When two or more materials are used, several challenges arise in integrating them into a compact composite. These include mismatched thermal and mechanical properties leading to stress concentration at the interface, physicochemical incompatibility, insufficient wettability or high mutual reactivity, and neutron-physical issues with some solders, among others [20 – 22].

The objective of this study is to investigate the microstructure and mechanical properties of steel matrix composites based on heat-resistant, highly alloyed steel with two types of reinforcing particles: tungsten particles and nickel-coated tungsten carbide particles. This composite was synthesized using a hybrid wire-and-powder electron beam additive manufacturing method.

Materials and methods

To produce the 56GM/(W + WC(Ni)) composite, 56GM steel wire (equivalent to 40Kh9S2 steel) with a diameter of 1 mm and the following chemical composition (wt. %) was used: Fe 86.9; Cr 9.24; Si 3.02; C 0.44; Mn 0.4.

Reinforcing powders of tungsten and nickel-coated tungsten carbide (WC(Ni)) were used in a mass ratio of 1:1. SEM images of tungsten powder particles and WC(Ni) particles are shown in Fig. 1, *a* and *c*. According to *X*-ray phase analysis, the tungsten powder particles contain a minor fraction of WO_3 oxide (Fig. 1, *b*). The *X*-ray phase analysis of WC(Ni) powder identified the presence of tungsten carbide (WC) and nickel phases (Fig. 1, *d*).

The 56GM/(W + WC(Ni)) composite was fabricated as follows. Using wire electron beam additive manufacturing (EBAM), layers of 56GM steel were deposited on a 12Kh18N10 stainless steel substrate (Fig. 2, *a*). After depositing nine layers of 56GM, 0.3 g of W + WC(Ni) powder was introduced onto the workpiece using a powder feeder (Fig. 2, *b*). A layer of 56GM wire was then deposited, which partially melted the W + WC(Ni) powders and the underlying 56GM layer (Fig. 2, *c*). Subsequently, another 0.3 g layer of W + WC(Ni) powder was applied using the powder feeder, followed by another layer of 56GM wire. This process was repeated three times, resulting in three layers of W + WC(Ni) powder alternated with layers of 56GM steel (each layer being 1 mm thick) (Fig. 2, *d*). The final samples measured 72×36×9 mm.

To study the structural-phase composition and mechanical properties of the 56GM/(W + WC(Ni)) composite, samples were extracted from three zones: the matrix, the intermediate layer, and the upper composite layer. The samples were prepared following standard procedures, which included grinding with sandpaper and polishing with diamond pastes (grit sizes 14/10, 3/2, and 1/0). To reveal microstructural elements, the polished sample surfaces were chemically etched using a reagent composed of $CuSO_4$ (0.008 kg) + H_2O (0.04 L) + HCl (0.04 L).

The macro- and microstructure of the samples were examined using an Altami Met 1S optical microscope, an Olympus confocal laser microscope, and scanning electron microscopy (SEM) (Thermo Fisher Scientific Apreo S LoVac equipped with an energydispersive spect-

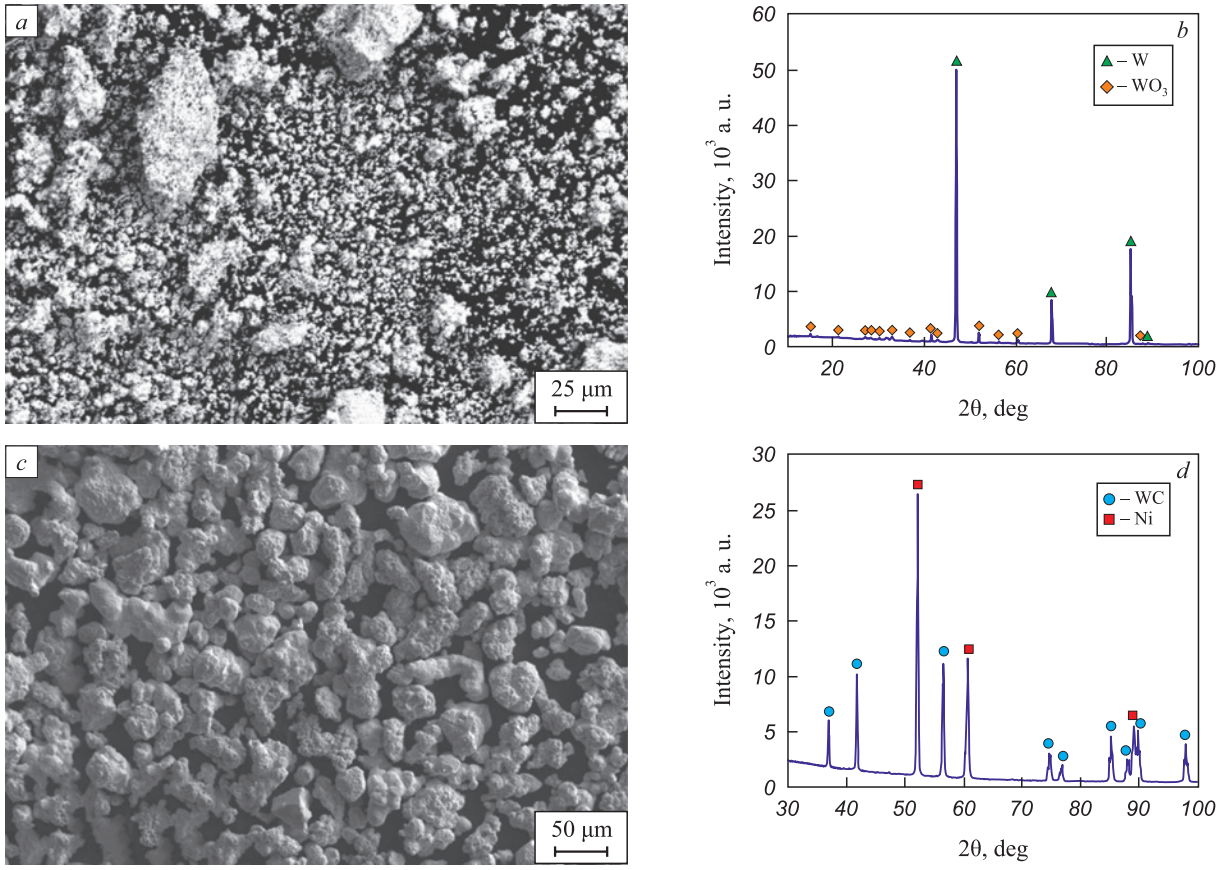

Fig. 1. SEM images (*a*, *c*) and *X*-ray diffraction patterns (*b*, *d*) of the initial W powder (*a*, *b*) and WC(Ni) powder (*c*, *d*)

Рис. 1. РЭМ-изображения (*a*, *c*) и рентгенограммы (*b*, *d*) исходного порошка вольфрама (*a*, *b*) и порошка карбида вольфрама WC(Ni) (*c*, *d*)

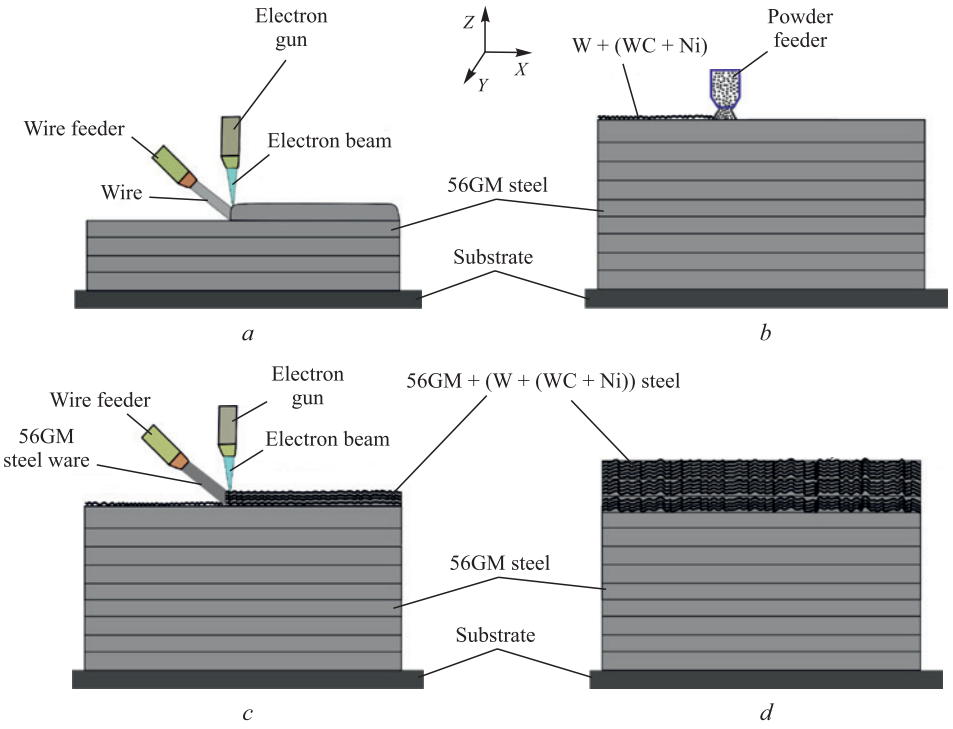

Fig. 2. Scheme of deposition of layers of the composite sample 56GM/(W + (WC(Ni))

Рис. 2. Схема нанесения слоев композиционного образца 56GM/(W + (WC(Ni))

rometer (EDS)). Particle sizes were measured using the secant method on prepared metallographic sections. *X*-ray phase analysis (XRD) was performed on a DRON-7 *X*-ray diffractometer (CoK_α radiation).

Microhardness was measured using a TBM 5215 A Tochline hardness tester with a 0.5 N load and a dwell time of 10 s. Uniaxial tensile tests were conducted on a UTS-110M-100 universal testing machine at room temperature with a crosshead speed of 1 mm/min. For tensile testing, flat specimens were cut along and across the printing direction, shaped as proportionally reduced blades according to GOST 1497, with working section dimensions of 12×2.7×1.5 mm. The specimens were extracted from characteristic regions of the composite material (matrix, intermediate layer, and upper composite layer).

Results and discussion

Fig. 3, *a* shows an optical image of the 56GM/(W + + WC(Ni)) composite alloy in the *ZOY* section, where several characteristic zones can be distinguished: *1* – stainless steel substrate (not considered in this study); *2* – layer of 56GM steel; *3* – intermediate layer 56GM – 56GM/(W + WC(Ni)); *4* – composite layer (W + WC(Ni))/56GM. In the *ZOY* cross-section of the 56GM/(W + WC(Ni)) sample (layer *2*), a significant number of melt pool boundaries, formed during the printing of 56GM steel layers, are observed. Layer *3*, the intermediate layer, features a distinct boundary between the printed matrix and the composite layers (Fig. 3, *a*). According to the results of *X*-ray tomography of the 56GM/(W + WC(Ni)) sample (Fig. 3, *b*), no macroscopic defects such as pores or cracks were detected in any of the analyzed zones (*1* – *3*) shown in Fig. 3, *a*.

X-ray phase analysis revealed that the 56GM/(W + WC(Ni)) composite primarily consists of α-Fe (~83.69 vol. %), Ni (~6 vol. %), and the WC carbide phase (~10.31 vol. %) (Fig. 3, *c*). Additionally, a small fraction of γ-Fe was observed in the composite layer, whereas no traces of γ-Fe were detected in the base alloy or the intermediate layer.

According to SEM analysis, the 56GM steel (layer *2*) exhibits a multidi-rectional acicular structure corresponding to a ferrite-martensite state (indicated by the red arrow, Fig. 4, *a*). The matrix of the composite alloy primarily consists of ~78 at. % Fe, ~12 at. % Cr, and ~6 at. % Si, which matches the initial steel composition (spectrum *3*, Fig. 4, *a*, *b*). The concentrations of tungsten and nickel in the base 56GM alloy are low, approximately 2 at. % each. Along the grain boundaries of the base layer of 56GM steel, fine particles are observed, which may result from infiltration along the grain boundaries or microcracks, as well as diffusion during composite printing (Fig. 4, *a*). EDS analysis of these particles shows ~66 at. % Fe, ~18 at. % Cr, ~7 at. % W, ~4 at. % Ni, and ~5 at. % Si (spectra *1* – *2*, Fig. 4, *a*, *b*). Since the EDS analysis captures a larger area, including both the particle and the matrix, it can be inferred based on XRD data that these particles are tungsten carbide (WC).

In the intermediate layer 56GM – 56GM/(W + WC(Ni)) (layer *3*, Fig. 3, *a*), the acicular structure becomes less pronounced (Fig. 4, *c*). However, the elemental composition of the grains in the transition zone is comparable

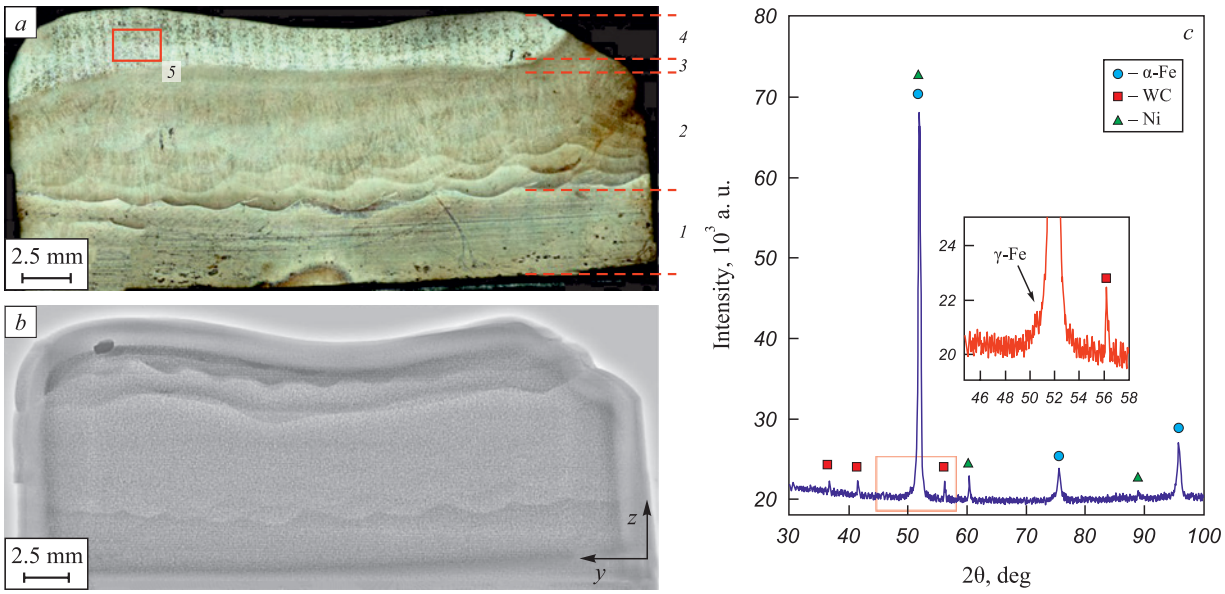

Fig. 3. Macrostructure (*a*), fluoroscopy (*b*) and *X*-ray pattern (*c*) of 56GM/(W + WC(Ni)) composite:
1 – substrate; *2* – layer of 56GM steel; *3* – intermediate layer; *4* – 56GM/(W + WC(Ni))composite layer; *5* – sample for XRD

Рис. 3. Макроструктура (*a*), рентгеноскопия (*b*) и рентгенограмма (*c*) композита 56GM/(W + WC(Ni)):
1 – подложка; *2* – слой стали 56GM; *3* – промежуточный слой; *4* – композиционный слой 56GM/(W + WC(Ni)); *5* – образец для РФА

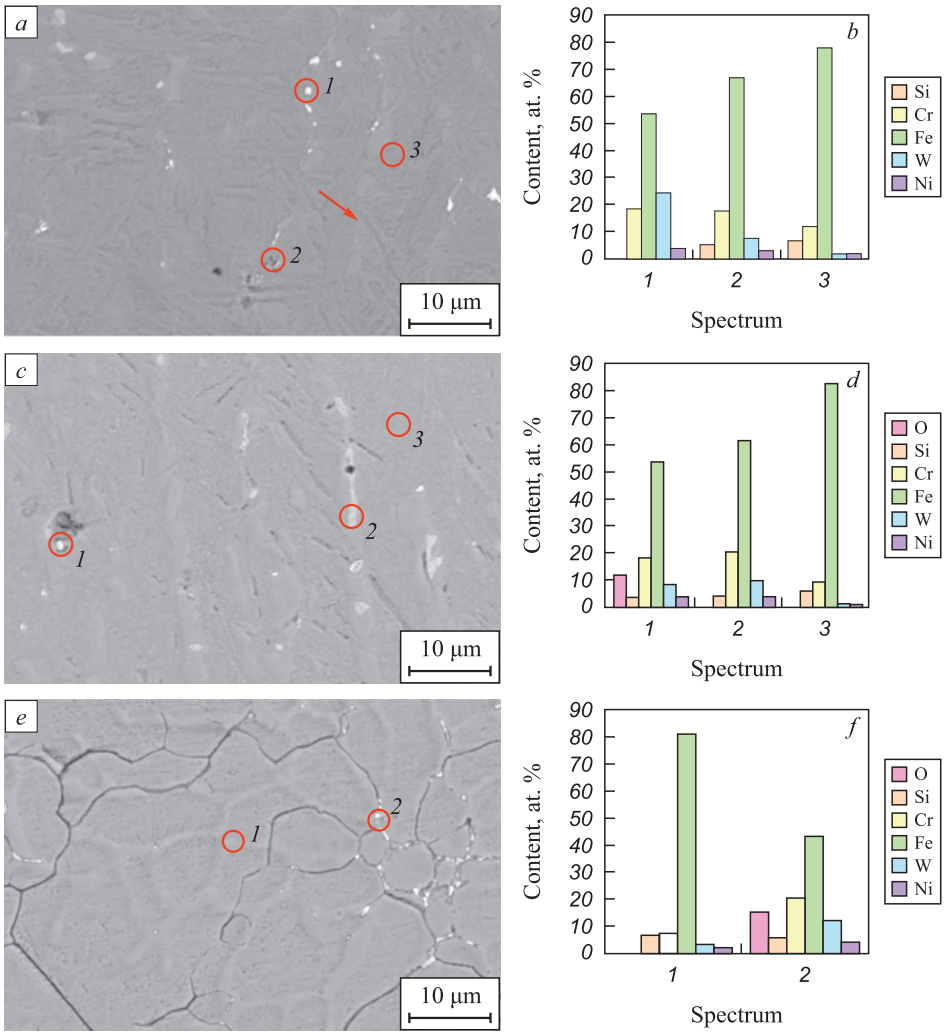

Fig. 4. SEM images and elemental composition of 56GM/(W + WC(Ni)) composite sample:
a, *b* – layer of 56GM steel (layer *2*); *c*, *d* – intermediate layer (layer *3*); *e*, *f* – 56GM/(W + WC(Ni)) composite layer

Рис. 4. РЭМ-изображения и элементный состав композиционного образца 56GM/(W + WC(Ni));
a, *b* – сталь 56GM (слой *2*); *c*, *d* – промежуточный слой (слой *3*); *e*, *f* – композиционный слой 56GM/(W + WC(Ni))

to that of the base layer of 56GM steel (spectrum *3*, Fig. 4, *c*, *d*). Similar to the base alloy, fine tungsten carbide (WC) particles are observed along the grain boundaries in the intermediate layer, with an average size of 2.64 μm (spectra *1* – *2*, Fig. 4, *c*, *d*).

In the composite layer 56GM/(W + WC(Ni)) (layer *4*, Fig. 3, *a*), an equiaxed grain structure is formed, with an average grain size of 8.59 μm. Cracks are observed along the grain boundaries (Fig. 4, *e*). EDS analysis of these grains also corresponds to the elemental composition of the base layer (spectrum *1*, Fig. 4, *e*, *f*): ~81 at. % Fe, ~7 at. % Cr, and ~7 at. % Si. WC powder particles are predominantly located within the cracks (along the boundaries of small grains) and, to a lesser extent, inside the grains (spectrum *2*, Fig. 4, *e*, *f*). The volume fraction of WC particles in the composite layer significantly increases compared to their fraction in the base alloy and the intermediate layer. According to XRD data, in addition to the main phases α-Fe (~80.6 vol. %), Ni (~6 vol. %), and WC (~10.3 vol. %), a minor fraction of γ-Fe (~3 vol. %) is present in the composite layer (Fig. 3, *c*).

Microhardness measurements were conducted on the cross-section *ZOY* of the 56GM/(W + WC(Ni)) composite in two regions (Fig. 5, *a*). In all cases, microhardness increased when measured in the direction from the substrate to the composite layer (Fig. 5, *a*). The microhardness values for the base intermediate and composite layers were approximately 3.5, 6.1, and 6.5 GPa, respectively.

Tensile tests on samples extracted from the base alloy and intermediate layer in the *ZOY* and *ZOX* cross-sections demonstrated ductile fracture behavior (samples 1.1, 2.1, 2.2, Fig. 5, *b* – *d*). For samples from the region of the base layer of 56GM steel, the ultimate tensile strength and yield strength were approximately 1000 and 650 MPa, respec-

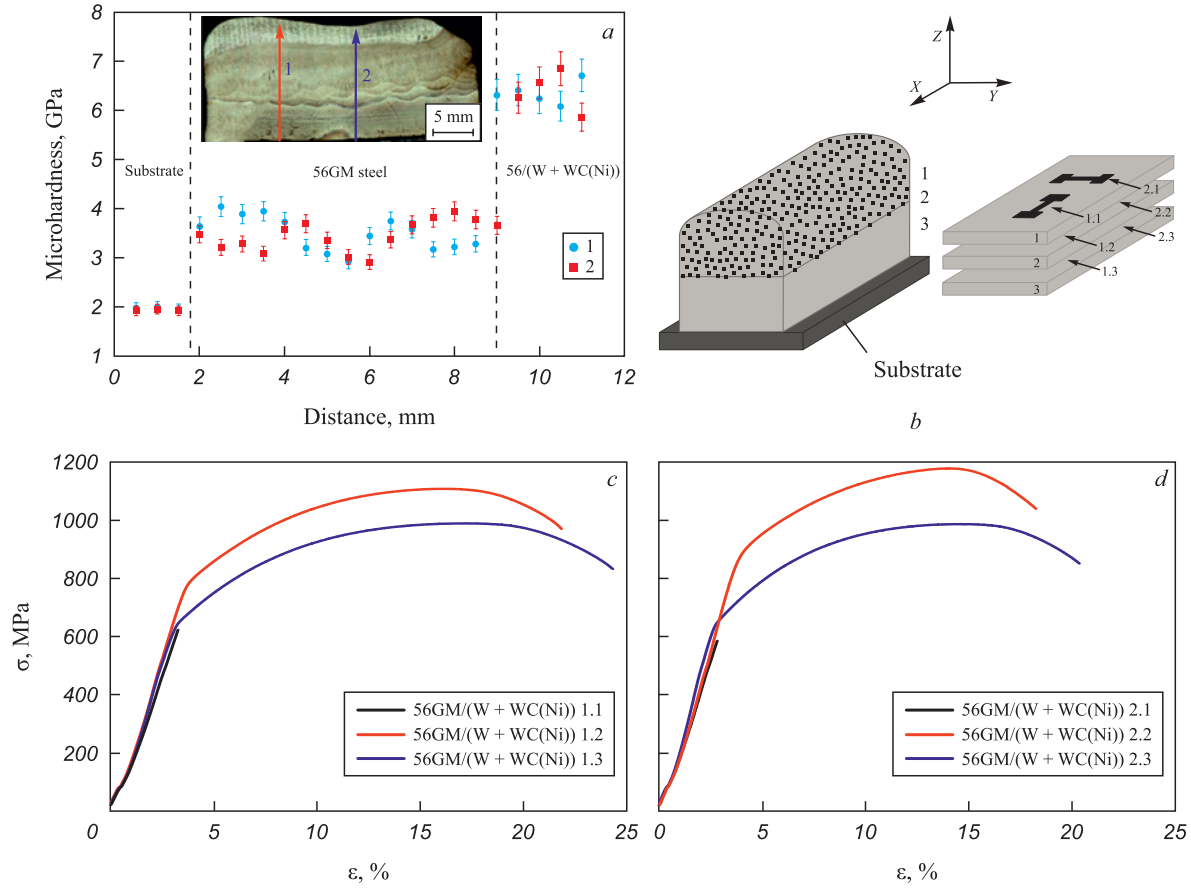

Fig. 5. Microhardness values (*a*), sample cutting diagram for tensile test (*b*), tensile values according to the sample cutting diagram (*c*, *d*)

Рис. 5. Значения микротвердости (*a*), схема вырезки образцов для испытания на растяжение (*b*), значения растяжения согласно схеме вырезки образцов (*c*, *d*)

tively (Fig. 5, *c*, *d*). For samples from the intermediate region (56GM – 56GM/(W + WC(Ni))), the ultimate tensile strength and yield strength reached 1100 – 1200 MPa and ~835 MPa, respectively – representing increases of 10 and 28 % compared to the base alloy (Fig. 5, *c*, *d*). For samples extracted from the composite layer region in the *ZOY* and *ZOX* cross-sections, the ultimate tensile strength values were 590 and 620 MPa, respectively, and the yield strength was ~570 MPa (samples 1.3, 3.1, Fig. 5, *b* – *d*). Due to the high volume fraction of brittle carbide particles located at the grain boundaries of 56GM steel, the relative elongation decreases to 3 %. A composite layer containing approximately 10 vol. % tungsten carbide is considered typical for metal-matrix composites, for which mechanical properties are traditionally assessed using compression rather than tensile testing [11].

It is well known that during additive manufacturing, significant diffusion of carbon from tungsten carbide (WC) particles into the α-Fe-based matrix occurs due to the formation of the melt pool. This diffusion significantly influences the phase formation of the matrix near the reinforcing carbide particles, as carbon is an austenite-promoting element. A substantial amount of diffused carbon likely integrates into the α-Fe matrix as interstitial atoms, driving the phase transformation from α-Fe to γ-Fe in the composite layer (Fig. 3, *c*). Furthermore, the nickel coating on the tungsten carbide particles is also an austenite-promoting element. For instance, additional nickel alloying in high-chromium steels can produce fully austenitic structures at room temperature under specific chromium-to-nickel ratios.

Numerous studies have reported that ferrite-martensite microstructures typically revert to austenite during the melting of the subsequent powder layer, as the temperature in some regions of the melt pool exceeds the austenite transformation finish temperature due to the constant heat flow from the molten zones to the substrate [23]. It is expected that the austenite would subsequently transform into martensite due to the high intrinsic cooling rate. As noted earlier, neither the base alloy nor the intermediate layer exhibited traces of γ-Fe, and their phase composition consisted entirely of α-Fe. However, in the composite layer, a small fraction of austenite did not transform into α-Fe during cooling due to the presence of tungsten carbide and nickel particles (Fig. 3, *c*).

The absence of interaction between iron and tungsten carbide (WC) form-ing carbides such as Me_3C, as

observed in this study, can be attributed to the beneficial effect of tungsten. Tungsten's slow diffusion rate reduced the kinetics of such carbide formation [14; 15].

Conclusions

The microstructure and mechanical properties of a composite alloy based on 56GM steel, produced using wire electron beam additive manufacturing with the incorporation of W + WC(Ni) powders during printing, were investigated. The 56GM/(W + WC(Ni)) composite alloy features a gradient structure consisting of the base layer of 56GM steel, an intermediate layer (56GM – 56GM/(W + WC(Ni))), and a composite layer (56GM/(W + WC(Ni))). The base layer of 56GM steel is composed of ferrite-martensite grains with isolated tungsten carbide (WC) particles located along the grain boundaries. The ultimate tensile strength and yield strength in the base metal zone were approximately 1000 and 650 MPa, respectively. In the composite layer, an equiaxed ferrite-martensite grain structure with a small fraction of austenite forms. was observed. Cracks were found along the grain boundaries, where tungsten carbide (WC) particles were concentrated. The volume fraction of WC particles in the composite layer was significantly higher than in the base layer of 56GM steel, resulting in a 40 % reduction in tensile strength and brittle fracture. Nonetheless, microhardness increased steadily from the substrate to the composite layer, ranging from 3.5 to 6.5 GPa.

The introduction of nickel-coated tungsten carbide (WC) particles shows considerable potential for fine-tuning the strength and ductility of steel materials by adjusting the volume fractions of austenitic and ferritic phases.

The results suggest that incorporating W + WC(Ni) powders into the surface layers of 56GM steel using electron beam additive manufacturing can enhance the tribological properties of the resulting composite material. This method holds significant promise for producing iron-based components with outstanding performance characteristics.

References / Список литературы

1. Tjong S.C. Recent progress in the development and properties of novel metal matrix nanocomposites reinforced with carbon nanotubes and graphene nanosheets. *Materials Science and Engineering: R: Reports*. 2013;74(10):281–350. https://doi.org/10.1016/j.mser.2013.08.001
2. Radhamani A.V., Lau H.C., Ramakrishna S. CNT-reinforced metal and steel nanocomposites: A comprehensive assessment of progress and future directions. *Composites Part A: Applied Science and Manufacturing*. 2018;114:170–187. https://doi.org/10.1016/j.compositesa.2018.08.010
3. AlMangour B., Grzesiak D., Yang J.-M. Selective laser melting of TiC reinforced 316L stainless steel matrix nanocomposites: Influence of starting TiC particle size and volume content. *Materials & Design*. 2016;104:141–151. https://doi.org/10.1016/j.matdes.2016.05.018
4. Filippov A.V., Khoroshko E.S., Shamarin N.N., Savchenko N.L., Moskvichev E.N., Utyaganova V.R., Kolubaev E.A., Smolin A.Yu., Tarasov S.Yu. Characterization of gradient CuAl–B_4C composites additively manufactured using a combination of wire-feed and powder-bed electron beam deposition methods. *Journal of Alloys and Compounds*. 2021;859:157824. https://doi.org/10.1016/j.jallcom.2020.157824
5. Zykova A., Chumaevskii A.V, Vorontsov A., Shamarin N., Panfilov A., Knyazhev E., Moskvichev E., Gurianov D., Savchenko N., Kolubaev E., Tarasov S. Microstructural evolution of AA5154 layers intermixed with Mo powder during electron beam wire-feed additive manufacturing (EBAM). *Metals*. 2022;12(1):109. https://doi.org/10.3390/met12010109
6. Utyaganova V.R., Chumaevskii A.V., Shamarin N.N., Moskvichev E.N., Vorontsov A.V., Gurianov D.A., Knyazhev E.O., Savchenko N.L. Regularities of structure formation and properties of composite materials based on aluminum–manganese bronze produced by electron beam additive manufacturing with the addition of iron, nickel, and tungsten powders during printing. *Russian Physics Journal*. 2023;65(9):1584–1591. https://doi.org/10.1007/s11182-023-02805-7
7. Yan X.C., Chen C.Y., Zhao R.X., Ma W.Y., Bolot R., Wang J., Ren Z.M., Liao H.L., Liu M. Selective laser melting of WC reinforced maraging steel 300: Microstructure characterization and tribological performance. *Surface and Coatings Technology*. 2019;371:355–365. https://doi.org/10.1016/j.surfcoat.2018.11.033
8. Gu D.D., Ma J., Chen H., Lin K., Xi L. Laser additive manufactured WC reinforced Fe-based composites with gradient reinforcement/matrix interface and enhanced performance. *Composite Structures*. 2018;192:387–396. https://doi.org/10.1016/j.compstruct.2018.03.008
9. Wang J.D., Li L.Q., Tao W. Crack initiation and propagation behavior of WC particles reinforced Fe-based metal matrix composite produced by laser melting deposition. *Optics and Laser Technology*. 2016;82:170–182. https://doi.org/10.1016/j.optlastec.2016.03.008
10. Kang N., Ma W., Heraud L., El Mansori M., Li F., Liu M., Liao H. Selective laser melting of tungsten carbide reinforced maraging steel composite. *Additive Manufacturing*. 2018;22:104–110. https://doi.org/10.1016/j.addma.2018.04.031
11. Chen H., Gu D., Kosiba K., Lu T., Deng L., Xi L., Kühn U. Achieving high strength and high ductility in WC-reinforced iron-based composites by laser additive manufacturing. *Additive Manufacturing*. 2020;35:101195. https://doi.org/10.1016/j.addma.2020.101195
12. Farahmand P., Kovacevic R. Corrosion and wear behavior of laser cladded Ni–WC coatings. *Surface and Coatings Technology*. 2015;276:121–135. https://doi.org/10.1016/j.surfcoat.2015.06.039
13. Liu W., Gao D. Microstructure and wear of Ni-WC hardfacing used for steel-body PDC bits. *International Journal of Refractory Metals and Hard Materials*. 2021;101:105683. https://doi.org/10.1016/j.ijrmhm.2021.105683
14. Ding H., Yuan Z., Liu T., Chen L., Zhou Y., Cao Y., Cao F., Luo R., Cheng X. Microstructure and high-temperature tensile behavior of modified H13 steel with the addition of tung-

sten, molybdenum, and lowering of chromium. *Materials Science and Engineering: A*. 2023;866:144655. https://doi.org/10.1016/j.msea.2023.144655

15. Won Y.-J., Kwon Y.-J., You J.-S., Park S.-S., Cho K.-S. Role of W addition in reducing heat checking and enhancing the mechanical properties of hot work tool steel. *Journal of Materials Research and Technology*. 2023;24:3413–3422. https://doi.org/10.1016/j.jmrt.2023.04.008

16. Xiang S., Wu R., Li W., Hu T., Huang S. Improved red hardness and toughness of hot work die steel through tungsten alloying. *Journal of Materials Engineering and Performance*. 2021;30(8):6146–6159. https://doi.org/10.1007/s11665-021-05793-2

17. Hong S.G., Lee W.B., Park C.G. The effects of tungsten addition on the microstructural stability of 9Cr–Mo Steels. *Journal of Nuclear Materials*. 2001;288(2-3):202–207. https://doi.org/10.1016/S0022-3115(00)00558-4

18. Matějíček J., Boldyryeva H., Brožek V., Sachr P., Chráska T., Pala Z. W–steel and W–WC–steel composites and FGMs produced by hot pressing. *Fusion Engineering and Design*. 2015;100:364–370. https://doi.org/10.1016/j.fusengdes.2015.06.154

19. Bolt H., Barabash V., Krauss W., Linke J., Neu R., Suzuki S., Yoshida N., Team A.U. Materials for the plasma-facing components of fusion reactors. *Journal of Nuclear Materials*. 2004;329-333(A):66–73. https://doi.org/10.1016/j.jnucmat.2004.04.005

20. Odegard B.C., Cadden C.H., Watson R.D., Slattery K.T. A review of the US joining technologies for plasma facing components in the ITER fusion reactor. *Journal of Nuclear Materials*. 1998;258-263(1):329–334. https://doi.org/10.1016/S0022-3115(98)00402-4

21. Merola M., Akiba M., Barabash V., Mazul I. Overview on fabrication and joining of plasma facing and high heat flux materials for ITER. *Journal of Nuclear Materials*. 2002; 307-311(2):1524–1532. https://doi.org/10.1016/S0022-3115(02)01070-X

22. Hamilton N.R., Wood J., Galloway A., Robbie M.B.O., Zhang Y. The metallurgy, mechanics, modelling and assessment of dissimilar material brazed joints. *Journal of Nuclear Materials*. 2013;432(1-3):42–51. https://doi.org/10.1016/j.jnucmat.2012.07.022

23. Holzweissig M.J., Taube A., Brenne F., Schaper M., Niendorf T. Microstructural characterization and mechanical performance of hot work tool steel processed by selective laser melting. *Metallurgical and Materials Transactions B*. 2015; 46:545–549. https://doi.org/10.1007/s11663-014-0267-9

Information about the Authors

Alisa V. Nikonenko, *Cand. Sci. (Eng.), Junior Researcher of the Laboratory of Structural Design of Advanced Materials,* Institute of Strength Physics and Materials Science of Siberian Branch of Russian Academy of Sciences
ORCID: 0000-0003-0937-1329
E-mail: aliska-nik@mail.ru

Andrei V. Vorontsov, *Cand. Sci. (Eng.), Research Associate of the Laboratory of Structural Design of Advanced Materials,* Institute of Strength Physics and Materials Science of Siberian Branch of Russian Academy of Sciences
ORCID: 0000-0002-4334-7616
E-mail: vav@ispms.ru

Nikolai N. Shamarin, *Junior Researcher of the Laboratory of Local Metallurgy in Additive Technologies,* Institute of Strength Physics and Materials Science of Siberian Branch of Russian Academy of Sciences
ORCID: 0000-0002-4649-6465
E-mail: shnn@ispms.ru

Veronika R. Utyaganova, *Cand. Sci. (Eng.), Research Associate of the Laboratory Local Metallurgy in Additive Technologies,* Institute of Strength Physics and Materials Science of Siberian Branch of Russian Academy of Sciences
ORCID: 0000-0002-2303-8015
E-mail: veronika_ru@ispms.ru

Nickolai L. Savchenko, *Dr. Sci. (Eng.), Leading Researcher of the Laboratory for Quality Control of Materials and Structures,* Institute of Strength Physics and Materials Science of Siberian Branch of Russian Academy of Sciences
ORCID: 0000-0001-8254-5853
E-mail: savnik@ispms.ru

Anna P. Zykova, *Cand. Sci. (Phys.-Math.), Senior Researcher, Head of the Laboratory of Structural Design of Advanced Materials,* Institute of Strength Physics and Materials Science of Siberian Branch of Russian Academy of Sciences
ORCID: 0000-0001-8779-3784
E-mail: zykovaap@mail.ru

Сведения об авторах

Алиса Владимировна Никоненко, *к.т.н., младший научный сотрудник лаборатории структурного дизайна перспективных материалов,* Институт физики прочности и материаловедения Сибирского отделения РАН
ORCID: 0000-0003-0937-1329
E-mail: aliska-nik@mail.ru

Андрей Владимирович Воронцов, *к.т.н., научный сотрудник лаборатории структурного дизайна перспективных материалов,* Институт физики прочности и материаловедения Сибирского отделения РАН
ORCID: 0000-0002-4334-7616
E-mail: vav@ispms.ru

Николай Николаевич Шамарин, *младший научный сотрудник лаборатории локальной металлургии в аддитивных технологиях,* Институт физики прочности и материаловедения Сибирского отделения РАН
ORCID: 0000-0002-4649-6465
E-mail: shnn@ispms.ru

Вероника Рифовна Утяганова, *к.т.н., научный сотрудник лаборатории локальной металлургии в аддитивных технологиях,* Институт физики прочности и материаловедения Сибирского отделения РАН
ORCID: 0000-0002-2303-8015
E-mail: veronika_ru@ispms.ru

Николай Леонидович Савченко, *д.т.н., ведущий научный сотрудник лаборатории контроля качества материалов и конструкций,* Институт физики прочности и материаловедения Сибирского отделения РАН
ORCID: 0000-0001-8254-5853
E-mail: savnik@ispms.ru

Анна Петровна Зыкова, *к.ф.-м.н., старший научный сотрудник, заведующий лабораторией структурного дизайна перспективных материалов,* Институт физики прочности и материаловедения Сибирского отделения РАН
ORCID: 0000-0001-8779-3784
E-mail: zykovaap@mail.ru

Contribution of the Authors / Вклад авторов

A. V. Nikonenko – performing microstructure studies by optical microscopy, formation of the main concept of the article, selection of illustrations, description of the results.
A. V. Vorontsov – analysis of *X*-ray diffraction data, performing mechanical tensile tests.
N. N. Shamarin – EBAM printing of samples, sample preparation.

V. R. Utyaganova – performing microstructure studies by scanning electron microscopy, description of the results.

N. L. Savchenko – *X*-ray analysis, processing and analysis of microstructural findings, editing the article final version.

A. P. Zykova – analysis of experimental data, revision of the text, formation of conclusions, editing of the final version of the article.

А. В. Никоненко – выполнение исследований микроструктуры методом оптической микроскопии, формирование основной концепции статьи, оформление иллюстраций, описание результатов.
А. В. Воронцов – анализ данных рентгеноструктурного анализа, проведение механических испытаний на растяжение.
Н. Н. Шамарин – печать образцов методом ЭЛАП, пробоподготовка образцов.
В. Р. Утяганова – выполнение исследований микроструктуры методом сканирующей электронной микроскопии; описание результатов.
Н. Л. Савченко – выполнение исследований методом рентгенофазового анализа, обработка и анализ результатов микроструктурных исследований, редактирование финальной версии статьи.
А. П. Зыкова – анализ экспериментальных данных, доработка текста, формирование выводов, редактирование финальной версии статьи.

Received 19.06.2024
Revised 21.08.2024
Accepted 17.10.2024

Поступила в редакцию 19.06.2024
После доработки 21.08.2024
Принята к публикации 17.10.2024

MATERIALS SCIENCE / МАТЕРИАЛОВЕДЕНИЕ

UDC 620.1
DOI 10.17073/0368-0797-2024-6-696-701

Original article
Оригинальная статья

Effect of 3D printing mode on structure and fatigue strength of 30CrMnSi steel

S. A. Mantserov, M. S. Anosov, Yu. S. Mordovina, M. A. Chernigin ✉

R.E. Alekseev Nizhny Novgorod State Technical University (24 Minina Str., Nizhny Novgorod 603022, Russian Federation)

✉ honeybadger52@yandex.ru

Abstract. The desire of modern manufacturers to reduce the cost of producing goods leads to an increased search for ways to obtain the raw materials for future products more efficiently. One promising method for obtaining raw materials is electric arc surfacing (WAAM), which is discussed in this paper. The aim of the study was to investigate the effect of electric arc surfacing on the structure and fatigue strength of 30CrMnSi steel. To obtain the samples, two walls were surfaced according to the specified modes: $I = 150$ A, $U = 25$ V, $Q = 600$ J/mm (mode *1*) and $I = 110$ A, $U = 17$ V, $Q = 300$ J/mm (mode *2*). During the study of the walls microstructure after milling, it was found that when the metal is surfaced according to the mode *1*, large accumulations of technological defects such as pores and bad welding form in the material. When the metal is treated according to the mode *2*, these macroscopic defects are practically not detected. During optical emission analysis, it was observed that during the surfacing process, alloying elements are consumed and the carbon content decreases most actively. It should be noted that the burnout of elements occurs more actively when the metal is surfaced using the mode *1*. This may be due to the higher energy input in this process. A predominant ferrite-sorbite structure was found in the metal surfaced using the mode *1*. However, local ferritic colonies were revealed on the surface of the samples due to their height. The microstructure of the samples produced using the mode *2* is mainly composed of ferrite and pearlite. Ferrite is isolated as closed grids along the boundaries of the austenitic grains, and traces of a Widmanstetten structure can also be seen. Perlite is present both as highly dispersed plates and partially spheroidized colonies. Despite the fact that the structure of the samples produced using the mode *1* is generally considered to be more favorable in terms of material properties, the fatigue strength of the samples produced according to the mode *2* exceeds that of the mode *1* by an average of 70 %. This may be due to the stronger influence of technological defects on the metal fatigue resistance than microstructural ones.

Keywords: 30CrMnSi steel, fatigue strength, structural defects, additive technologies, WAAM

Acknowledgements: The work was supported by the Ministry of Science and Higher Education of the Russian Federation (state assignment “Intelligent diagnostics of parts and structures obtained by additive cultivation in the process of their production and operation” No. FSWE-2023-0008).

For citation: Mantserov S.A., Anosov M.S., Mordovina Yu.S., Chernigin M.A. Effect of 3D printing mode on structure and fatigue strength of 30CrMnSi steel. *Izvestiya. Ferrous Metallurgy*. 2024;67(6):696–701. https://doi.org/10.17073/0368-0797-2024-6-696-701

Влияние режима 3D-печати на структуру и усталостную прочность стали 30ХГСА

С. А. Манцеров, М. С. Аносов, Ю. С. Мордовина, М. А. Чернигин ✉

Нижегородский государственный технический университет им. Р. Е. Алексеева (Россия, 603155, Нижний Новгород, ул. Минина, 24)

✉ honeybadger52@yandex.ru

Аннотация. Современное производство активно занимается поиском возможностей получения заготовок изделий наиболее экономически выгодными способами. Одним из перспективных методов получения заготовок является электродуговая наплавка (WAAM), применяемая в данной работе. Целью исследования являлось изучение влияние режима электродуговой наплавки на структуру и усталостную прочность образцов из стали 30ХГСА. Для получения образцов были наплавлены две стенки по следующим режимам: $I = 150$ А, $U = 25$ В, $Q = 600$ Дж/мм (режим *1*) и $I = 110$ А, $U = 17$ В, $Q = 300$ Дж/мм (режим *2*). В ходе изучения макроструктуры наплавленных стенок после фрезеровки установлено, что при наплавке по режиму *1* в металле образуются большие скопления технологических дефектов, таких, как поры и непровары. При наплавке металла по режиму *2* макродефекты практически не выявляются. Оптико-эмиссионный анализ показал, что в процессе наплавки происходит выгорание легирующих элементов, наиболее активно снижается содержание углерода. Следует отметить, что угар элементов происходит более активно при наплавке металла по режиму *1*, что может быть связано с большей погонной энергией процесса. В металле, наплавленном по данному режиму, выявлена преимущественно ферритно-сорбитная структура, однако по высоте образцов выявляются локальные ферритные колонии. Микроструктура образцов, изготовленных по режиму *2*, преимущественно представлена ферритом и перлитом. Феррит выделяется в виде замкнутых сеток по границам бывшего аустенитного зерна, также

выявлена видманштеттова структура. В микроструктуре перлит представлен как в пластинчатой, так и в частично сфероидизированной форме. Структура образцов, наплавленных по режиму *1*, считается более благоприятной. Однако усталостная прочность образцов, изготовленных по режиму *2*, превышает соответствующие значения для режима *1* в среднем на 70 %. Это может быть обусловлено более сильным влиянием на сопротивление усталости металла технологических дефектов, чем микроструктурных.

Ключевые слова: сталь 30ХГСА, усталостная прочность, дефекты структуры, аддитивные технологии, WAAM

Благодарности: Исследование выполнено при финансовой поддержке Министерства науки и высшего образования Российской Федерации (Государственное задание «Интеллектуальная диагностика деталей и конструкций, полученных методом аддитивного выращивания в процессе их получения и эксплуатации» № FSWE-2023-0008).

Для цитирования: Манцеров С.А., Аносов М.С., Мордовина Ю.С., Чернигин М.А. Влияние режима 3D-печати на структуру и усталостную прочность стали 30ХГСА. *Известия вузов. Черная металлургия*. 2024;67(6):696–701. https://doi.org/10.17073/0368-0797-2024-6-696-701

Introduction

Modern manufacturing is increasingly focused on reducing production costs. In this context, additive manufacturing methods are gaining widespread adoption due to their unique technological capabilities for producing complex-shaped preforms from a wide range of materials [1 – 3].

The main additive manufacturing methods currently known are selective laser melting (SLM) [4; 5], laser powder deposition (e.g., LENS/DMD) [6; 7], and wire arc additive manufacturing (WAAM) [8; 9]. Among these, WAAM is considered the most productive and technologically straightforward method [8; 10; 11].

Despite the significant advantages of additive manufacturing methods over traditional approaches, the processes occurring in the metal during surfacing (primarily structure formation) remain insufficiently studied. Literature [12; 13] indicates substantial differences in the microstructure and, consequently, the properties of metals in surfaced preforms compared to materials produced by traditional methods. These non-standard microstructures result from crystallization under non-equilibrium conditions during layer surfacing and the high number of high-temperature thermal cycles involved in surfacing. The main challenges in using WAAM for producing preforms include:

– selecting surfacing parameters considering the burnout of alloying elements;

– ensuring structural uniformity along the height of the surfaced metal;

– determining the optimal heat treatment (HT) mode that accounts for the altered chemical composition of the material after surfacing [14 – 16].

At the same time, achieving the desired combination of properties in products without additional heat treatment of preforms can significantly reduce production costs.

30CrMnSi steel is widely used in the manufacture of components operating at temperatures up to 200 °C. Products made from this steel (such as shafts, axles, levers, push rods, etc.) often work under alternating loads, which can lead to fatigue failure of structures. Achieving a sufficient level of fatigue strength without heat treatment (tempering) in this material is a promising goal for domestic industry.

Thus, the aim of this study is to investigate the effect of electric arc surfacing mode on the structure and fatigue strength of 30CrMnSi steel.

Materials and methods

The samples used in the study were surfaced as walls on an experimental WAAM test bench, which included a three-axis CNC gantry machine (IVCNC STL), an Alloy 275 ME Pulse welding power source, an exhaust hood, a welding table, and a welding torch. The 3D printing method used on this test bench is protected by patent RU 2696121C1. NP-30CrMnSi welding wire was used for surfacing the samples, with two walls surfaced as part of the sample preparation. The surfacing mode was defined by the following parameters: current (I, A), voltage (U, V), arc gap (z, mm), wire feed speed (V, mm/s), and shielding gas flow rate. The arc gap and wire feed speed were kept constant for all experiments at 11 mm and 300 mm/min, respectively. The shielding gas flow rate was also held constant.

The linear energy (Q) of the process (electrical energy per unit length of the weld) was determined based on the 3D printing modes as one of the key comprehensive parameters, calculated according to the formula provided in GOST R ISO 857-1-2009, considering an energy loss coefficient of 0.8:

$$Q = \frac{0.8IU}{V}. \quad (1)$$

Table 1 presents the surfacing modes for each surfaced wall and the corresponding values of the linear energy of the surfacing process.

Metallographic studies were conducted on transverse cross-sections relative to the surfacing direction at magnifications of 100× and 500× using an Altami MET1C optical microscope. Preparation of metallographic sec-

Table 1. **Surfacing modes**

Таблица 1. **Режимы наплавки**

Mode	*I*, A	*U*, V	*Q*, J/mm
1	150	25	600
2	110	17	300

tions followed a standard procedure involving mechanical grinding with abrasive paper of various grit sizes and polishing with paste. A 5 % alcoholic solution of nitric acid (nital) was used as the etchant for chemical etching [17].

Fatigue test samples were cut from the preforms along the surfacing direction. Fatigue tests were conducted using a cantilever bending scheme in accordance with the requirements of GOST 25.502–79. The sample had a thickness of 3 mm and a working zone size of 60×15 mm (Type IV according to GOST 25.502), tested at a frequency of 8.3 Hz.

The chemical composition of the surfaced metal was determined using optical emission spectrometry on a Foundry-Master spectrometer.

Results

The results of the chemical analysis of the surfaced metal and the composition of the initial wire are presented in Table 2.

As shown in Table 2, the surfacing process results in a reduction in the content of alloying elements, which is attributed to burnout, a phenomenon characteristic of casting and welding processes. The most significant reduction is observed in carbon content. It should be noted that the burnout of elements is more pronounced in samples surfaced using mode *1*, which may be associated with the higher linear energy of the process.

The microstructures of 30CrMnSi steel samples surfaced using both modes are shown in Fig. 1. The microstructure of the sample surfaced using mode *1* is represented by ferrite and troosto-sorbite, which may indicate quenching and tempering processes occurring during the surfacing of subsequent metal layers. This structure is favorable and, when considered layer by layer, uniform

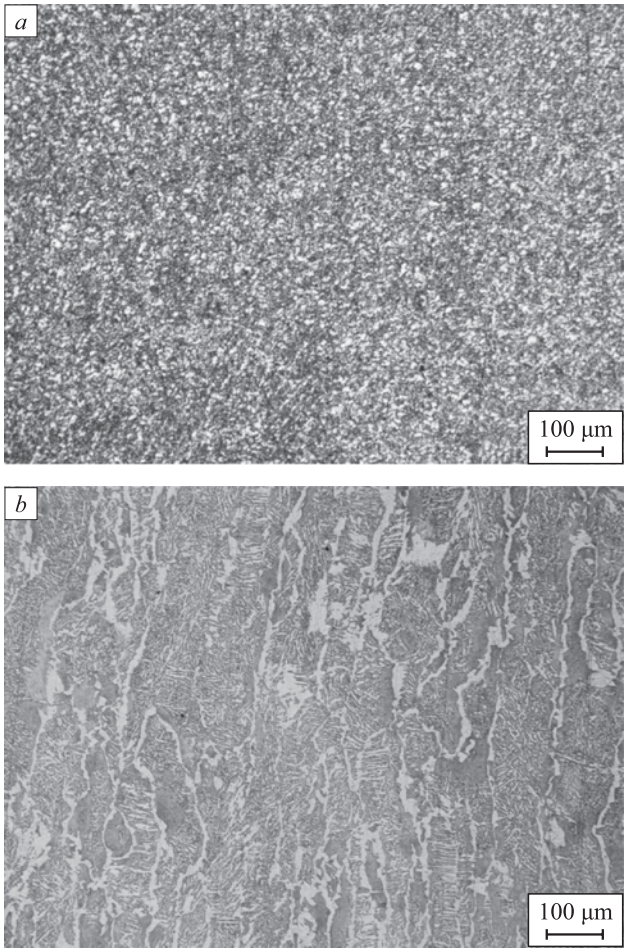

Fig. 1. Microstructure of 30CrMgSi steel samples: mode *1* (*a*); mode *2* (*b*)

Рис. 1. Микроструктура образцов из стали 30ХГСА: режим *1* (*a*); режим *2* (*b*)

within a single layer. However, structural heterogeneity is observed across the height of the sample, with distinct areas containing large ferritic colonies (Fig. 2).

In the metal surfaced using mode *2*, an anomalous ferrite-pearlite structure was observed. Due to significant overheating during surfacing and accelerated cooling, ferrite is distributed as closed networks along the boundaries of former austenitic grains, forming a Widmanstätten structure. Determining the morphology of pearlite at a magnification of 100× is challenging. At higher magnifications, the microstructure of the sample surfaced

Table 2. **Chemical composition of the surfaced metal and the initial wire**

Таблица 2. **Химический состав наплавленного металла и исходной проволоки**

Sample name	C	Si	Mn	Cr	Ni	S	P
Initial wire (30CrMnSi steel)	0.291	1.021	0.931	0.961	0.099	0.021	0.016
Surfaced metal (mode *1*)	0.260	0.941	0.901	0.942	0.096	0.013	0.018
Surfaced metal (mode *2*)	0.281	0.982	0.916	0.950	0.098	0.017	0.017

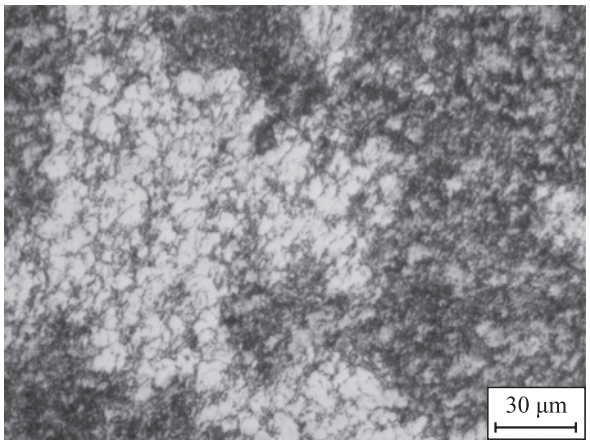

Fig. 2. Microstructure of the sample surfaced according to the mode *1*

Рис. 2. Микроструктура образца, наплавленного по режиму *1*

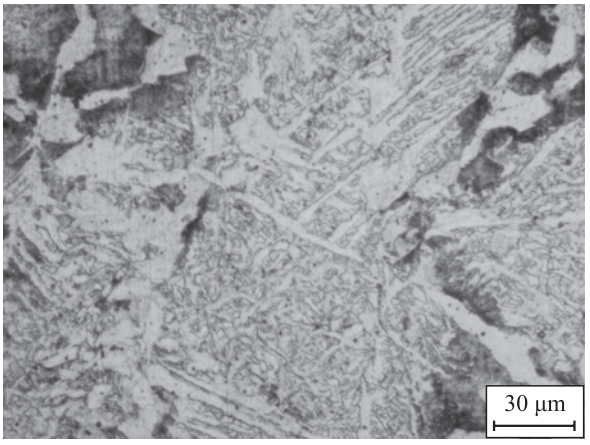

Fig. 3. Microstructure of the sample surfaced according to the mode *2*

Рис. 3. Микроструктура образца, наплавленного по режиму *2*

using mode *2* (Fig. 3) clearly reveals the Widmanstätten structure. Additionally, pearlite is observed in the form of highly dispersed plates and partially spheroidized colonies.

An analysis of the microstructures of samples surfaced under different modes (Figs. 1 – 3) showed that mode *1* leads to more active recrystallization of the structure in previously surfaced layers. This is attributed to the greater amount of thermal energy delivered to the material. Despite the more favorable structure achieved during surfacing, structural heterogeneity along the height of the sample is observed, which may lead to a reduction in the mechanical properties of the metal. Additionally, there is an increased risk of metal spattering, elevated porosity, and other technological defects during surfacing using mode *1*, which can further degrade the overall properties of the material.

Technological macrodefects are clearly visible on the surfaced walls after milling (Fig. 4). In the preform surfaced using mode *1*, significant clusters of macrodefects, including pores and lack of fusion [18; 19], are evident. These defect clusters evidently contribute to a reduction in the overall mechanical properties of the material [20; 21]. In contrast, macrodefects are almost entirely absent in preforms surfaced using mode *2*.

The data obtained from fatigue strength tests of samples surfaced under different modes are presented in Fig. 5.

Although the structure of the samples surfaced using mode *1* is considered more favorable in terms of material properties, the fatigue strength of the samples pro-

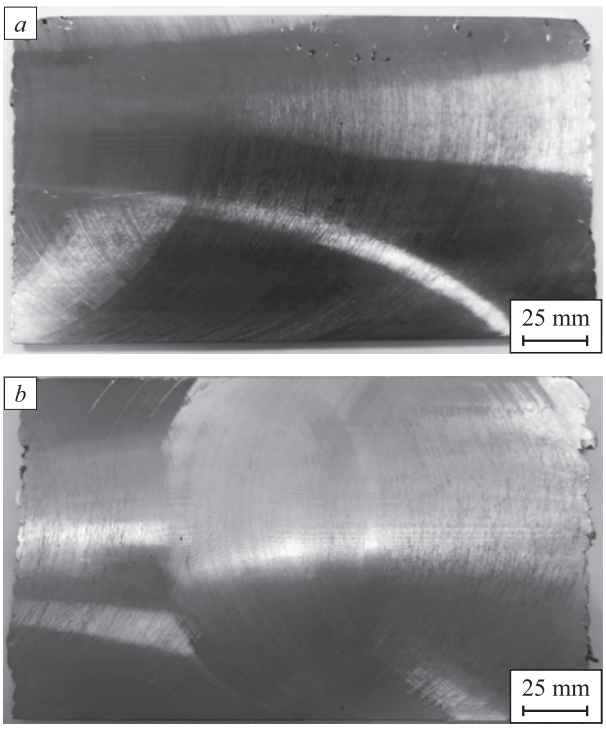

Fig. 4. Macrostructure of milled walls:
mode *1* (*a*); mode *2* (*b*)

Рис. 4. Макроструктура фрезерованных стенок:
режим *1* (*a*); режим *2* (*b*)

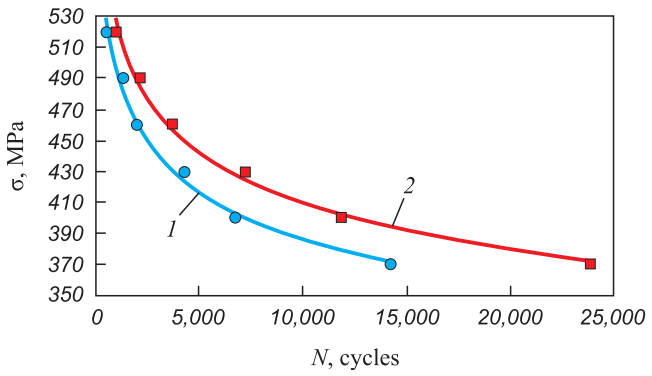

Fig. 5. Graph of low-cycle fatigue of the samples:
1 – mode *1*; *2* – mode *2*

Рис. 5. График малоцикловой усталости образцов:
1 – режим *1*; *2* – режим *2*

duced using mode *2* exceeds the corresponding values for mode *1* by an average of 70 % (Fig. 5). This effect may be attributed to the presence of macropores, bad welding, and other technological defects in the metal (mode *1*). Based on the data in Fig. 5, it can be concluded that technological defects have a greater impact on the fatigue strength of the metal than microstructural imperfections.

Conclusions

The study revealed that the surfacing mode significantly influences not only the metal's structure formation but also the presence of technological macrodefects (such as pores, incomplete fusion, lack of bonding, etc.). Although the structure of the metal surfaced using mode *1* is more favorable for the mechanical properties of the final product, the accumulation of macrodefects leads to a reduction in the overall property set of the preform.

Microstructural analysis showed that the structure of the metal surfaced using mode *1* (I = 150 A, U = 25 V, Q = 600 J/mm) is predominantly composed of ferrite and sorbite. However, localized ferritic colonies are observed along the height of the sample. The structure of samples surfaced using mode *2* (I = 110 A, U = 17 V, Q = 300 J/mm) exhibited an anomalous ferrite-pearlite structure formed as a result of significant overheating during surfacing and rapid cooling. In this case, ferrite is distributed as closed networks along the boundaries of the former austenitic grains, and a Widmanstätten structure is also observed. Pearlite is present as highly dispersed plates and partially spheroidized colonies.

The fatigue strength of samples produced using mode *2* is, on average, 70 % higher than that of mode *1*. This difference is primarily attributed to the greater impact of technological defects (such as pores, incomplete fusion, and bad welding) on the metal's fatigue strength compared to microstructural imperfections.

References / Список литературы

1. Herzog D., Seyda V., Wycisk E., Emmelmann C. Additive manufacturing of metals. *Acta Materialia*. 2016;117:371–392. https://doi.org/10.1016/j.actamat.2016.07.019
2. Zakay A., Aghion E. Effect of post-heat treatment on the corrosion behavior of AlSi10Mg alloy produced by additive manufacturing. *JOM*. 2019;71:1150–1157. https://doi.org/10.1007/s11837-018-3298-x
3. Ding D., Pan Z., Cuiuri D., Li H. Wire-feed additive manufacturing of metal components: Technologies, developments and future interests. *The International Journal of Advanced Manufacturing Technology*. 2015;81:465–481. https://doi.org/10.1007/s00170-015-7077-3
4. Kathiresan M., Karthikeyan M., Immanuel R.J. A short review on SLM-processed Ti6Al4V composites. *Proceedings of the Institution of Mechanical Engineers, Part E: Journal of Process Mechanical Engineering*. 2023;0(0). https://doi.org/10.1177/09544089231169380
5. Piekło J., Garbacz-Klempka A., Myszka D., Figurski K. Numerical and experimental analysis of strength loss of 1.2709 maraging steel produced by selective laser melting (SLM) under thermo-mechanical fatigue conditions. *Materials*. 2023;16(24):7682. https://doi.org/10.3390/ma16247682
6. Kumar S.P., Anand K., Chealvan S.H., Muthu S.K. Review on surface characteristics of components produced by direct metal deposition process. *Journal of Mechanical Engineering and Sciences*. 2022;16(4):9197–9229. https://doi.org/10.15282/jmes.16.4.2022.05.0729
7. Zhao P., Yi Z., Liu W., Kaiyuan Z., Luo Y. Influence mechanism of laser defocusing amount on surface texture in direct metal deposition. *Journal of Materials Processing Technology*. 2022;312:117822. https://doi.org/10.1016/j.jmatprotec.2022.117822
8. Li J., Alkahari M.R., Rosli N.A., Hasan R., Sudin M.N., Ramli F.R. Review of wire arc additive manufacturing for 3D metal printing. *International Journal of Automation Technology*. 2019;13(3):346–353. https://doi.org/10.20965/ijat.2019.p0346
9. Pant H., Arora A., Gopakumar G.S., Chadha U., Saeidi A., Patterson A.E. Applications of wire arc additive manufacturing (WAAM) for aerospace component manufacturing. *The International Journal of Advanced Manufacturing Technology*. 2023;127:4995–5011. https://doi.org/10.1007/s00170-023-11623-7
10. Jackson M.A., Van Asten A., Morrow J.D., Min S., Pfefferkorn F.E. Energy consumption model for additive-subtractive manufacturing processes with case study. *International Journal of Precision Engineering and Manufacturing-Green Technology*. 2018;5(4):459–466. https://doi.org/10.1007/s40684-018-0049-y
11. Pinto-Lopera J.E., Motta J.M., Absi Alfaro S.C. Real-time measurement of width and height of weld beads in GMAW processes. *Sensors*. 2016;16(9):1500. https://doi.org/10.3390/s16091500
12. Shah A., Aliyev R., Zeidler H., Krinke S. A review of the recent developments and challenges in wire arc additive manufacturing (WAAM) process. *Journal of Manufacturing and Materials Processing*. 2023;7(3):97. https://doi.org/10.3390/jmmp7030097
13. Lan B., Wang Y., Liu Y., Paul H., Hooper P., Hopper C., Zhang G., Zhang X., Jiang J. The influence of microstructural anisotropy on the hot deformation of wire arc additive manufactured (WAAM) Inconel718. *Materials Science and Engineering: A*. 2021;823:141733. https://doi.org/10.1016/j.msea.2021.141733
14. Svetlizky D., Das M., Zheng B., Vyatskikh A.L., Bose S., Bandyopadhyay A., Schoenung J.M., Lavernia E.J., Eliaz N. Directed energy deposition (DED) additive manufacturing: physical characteristics, defects, challenges and applications. *Materials Today*. 2021;49:271–295. https://doi.org/10.1016/j.mattod.2021.03.020
15. Kennedy J., Davis A., Caballero A.E. Microstructure transition gradients in titanium dissimilar alloy (Ti-5Al-5V-5Mo-3Cr/Ti-6Al-4V) tailored wire-arc additively manufactured components. *Materials Characterization*. 2021;182:111577. https://doi.org/10.1016/j.matchar.2021.111577

16. Tomar B., Shiva S., Nath T. A review on wire arc additive manufacturing: Processing parameters, defects, quality improvement and recent advances. *Materials Today Communications*. 2022;31:103739. https://doi.org/10.1016/j.mtcomm.2022.103739

17. Beckert M., Klemm H. Handbuch der metallographischen Ätzverfahren. Leipzig: VEB, Deutscher Verlag für Grundstoffindustrie: 1966:388. (In Germ.).

18. Vasin O.E., etc. Atlas of Defects. Scientific and Technical Collection. Yekaterinburg: Izdatel'skie resheniya; 2008:56. (In Russ.).

Васин О.Е. и др. Атлас дефектов. Научно-технический сборник. Екатеринбург: Издательские решения; 2008:56.

19. Kalinichenko N.P., Vasilyeva M.A., Radostev A.Yu. Atlas of Defects in Welded Joints and Base Metal: Textbook. Tomsk: Tomsk Polytechnic University; 2011:71. (In Russ.).

Калиниченко Н.П., Васильева М.А., Радостев А.Ю. Атлас дефектов сварных соединений и основного металла: Учебное пособие. Томск: Издательство Томского политехнического университета; 2011:71.

20. Nguyen N., Ruban A.R. Influence of defects in welds on mechanical properties of steel frame specified under static loading. *Vestnik of Astrakhan State Technical University. Series: Marine engineering and Technology*. 2015;(2): 14–22. (In Russ.).

Нгуен Н., Рубан А.Р. Влияние дефектов сварных швов на механические свойства корпусной стали, определяемые при статическом нагружении. *Вестник АГТУ. Серия: Морская техника и технология*. 2015;(2):14–22.

21. Sarkeeva A.A., Kruglov A.A., Muxametraximov M.X., Pore effect on mechanical properties of layered material from titanium alloy. *Letters on Materials*. 2013;3(1):12–15. (In Russ.). https://doi.org/10.22226/2410-3535-2013-1-12-15

Саркеева А.А., Круглов А.А., Мухаметрахимов М.Х. Влияние пор на механические свойства слоистого материала из титанового сплава ВТ6. *Письма о материалах*. 2013;3(1):12–15. https://doi.org/10.22226/2410-3535-2013-1-12-15

Information about the Authors / Сведения об авторах

Sergei A. Mantserov, *Cand. Sci. (Eng.), Assist. Prof., Head of the Chair "Automation of Mechanical Engineering", Director of the Institute of Industrial Technologies of Mechanical Engineering"*, R.E. Alekseev Nizhny Novgorod State Technical University
E-mail: mca_9@nntu.ru

Maksim S. Anosov, *Cand. Sci. (Eng.), Assist. Prof. of the Chair "Technology and Equipment Engineering"*, R.E. Alekseev Nizhny Novgorod State Technical University
E-mail: anosov-maksim@list.ru

Yuliya S. Mordovina, *Engineer of the Chair "Technology and Equipment Engineering", Postgraduate*, R.E. Alekseev Nizhny Novgorod State Technical University
E-mail: ips4@nntu.ru

Mikhail A. Chernigin, *Engineer of the Chair "Technology and Equipment Engineering", Postgraduate*, R.E. Alekseev Nizhny Novgorod State Technical University
E-mail: honeybadger52@yandex.ru

Сергей Александрович Манцеров, *к.т.н., доцент, заведующий кафедрой «Автоматизация машиностроения», директор Института промышленных технологий машиностроения*, Нижегородский государственный технический университет им. Р.Е. Алексеева
E-mail: mca_9@nntu.ru

Максим Сергеевич Аносов, *к.т.н., доцент кафедры «Технология и оборудование машиностроения»*, Нижегородский государственный технический университет им. Р.Е. Алексеева
E-mail: anosov-maksim@list.ru

Юлия Сергеевна Мордовина, *инженер кафедры «Технология и оборудование машиностроения», аспирант*, Нижегородский государственный технический университет им. Р.Е. Алексеева
E-mail: ips4@nntu.ru

Михаил Алексеевич Чернигин, *инженер кафедры «Технология и оборудование машиностроения», аспирант*, Нижегородский государственный технический университет им. Р.Е. Алексеева
E-mail: honeybadger52@yandex.ru

Contribution of the Authors / Вклад авторов

S. A. Mantserov – drawing up an experimental research plan, scientific guidance, editing the article, cutting the samples.

M. S. Anosov – scientific guidance, editing the article, conducting fatigue tests, analyzing the results of fatigue tests, conducting surfacing on the samples.
Yu. S. Mordovina – performing metallographic analysis, analyzing changes in the alloy chemical composition, designing and editing the article.
M. A. Chernigin – conducting metallographic analysis and chemical analysis on the billets after surfacing, designing and editing the article.

С. А. Манцеров – составление плана экспериментального исследования, научное руководство, редактирование статьи, вырезка образцов.
М. С. Аносов – научное руководство, редактирование статьи, проведение усталостных испытаний, анализ результатов усталостных испытаний, проведение наплавки образцов.
Ю. С. Мордовина – металлографический анализ, анализ изменения химического состава сплава, оформление и редактирование статьи.
М. А. Чернигин – металлографический анализ, проведение химического анализа заготовок после наплавки, оформление и редактирование статьи.

Received 06.04.2024
Revised 22.04.2024
Accepted 23.10.2024

Поступила в редакцию 06.04.2024
После доработки 22.04.2024
Принята к публикации 23.10.2024

MATERIALS SCIENCE / МАТЕРИАЛОВЕДЕНИЕ

UDC 669.046:533.9
DOI 10.17073/0368-0797-2024-6-702-709

Original article
Оригинальная статья

STRUCTURAL-PHASE COMPOSITION AND MECHANICAL PROPERTIES OF STAINLESS STEEL – LOW CARBON STEEL METAL COMPOSITE

V. I. Danilov[1] ✉, D. V. Orlova[1], G. V. Shlyakhova[1], Yu. P. Mironov[1], E. D. Petrova[2]

[1] **Institute of Strength Physics and Materials Science, Siberian Branch of the Russian Academy of Sciences** (2/4 Akademicheskii Ave., Tomsk 634055, Russian Federation)
[2] **Saint-Petersburg State Marine Technical University** (3 Lotsmanskaya Str., St. Petersburg 190121, Russian Federation)

✉ dvi@ispms.tsc.ru

Abstract. The subject of the study is a metal composite obtained by electric arc surfacing in argon of corrosion–resistant steel on low-carbon steel. Powdered chromium-nickel steel was deposited with an increased content of silicon and molybdenum relative to the traditional composition. In this work, we studied the elemental and structural-phase compositions, as well as the mechanical properties of both components of the material and the composite as a whole in the initial state and after annealing at 680 °C for 3 h. The main part of the corrosion-resistant component is a two-phase austenitic-ferritic mixture with a ratio of 65 % HCC phase and 30 % BCC phase. The material has high microhardness (more than 4000 MPa). The highest microhardness (4550 MPa) is observed in a narrow strip of deposited metal with a width of 25 μm, where the phase composition is represented by martensite (BCC), and austenite is absent. The transition across the boundary into carbon steel is accompanied by a decrease in microhardness to 1225 MPa. Here, a decarbonized zone with a width of 180 μm was formed near the fusion line. The resulting non-equilibrium stress-strain state of the composite led to low strength, low plasticity and brittle fracture of the deposited layer during tensile testing. After annealing, microstructure of the corrosion-resistant component became more uniform in size of both austenitic and ferritic structural elements. As a result of these transformations, internal stresses decreased and microhardness decreased to 3100 MPa. At the same time, the width of the decarbonized zone in the base metal increased. All these changes led to the fact that, although the tensile stress of the annealed material increased by 8 %, and the deformation to rupture – by 27 %, however, nature of the fracture remained brittle and rupture still occurs along the deposited layer. This is determined by the austenitic-ferritic phase composition of the stainless component, which, in turn, is determined by chemical composition of the deposited material.

Keywords: electric arc surfacing, corrosion-resistant steel – carbon steel composite, microstructure, microhardness, phase composition, mechanical properties, annealing

Acknowledgements: The work was performed within the framework of the state assignment of the Institute of Strength Physics and Materials Science SB RAS using the equipment of the Nanotech Center of Collective Use, topic No. FWRW-2021-0011.

For citation: Danilov V.I., Orlova D.V., Shlyakhova G.V., Mironov Yu.P., Petrova E.D. Structural-phase composition and mechanical properties of stainless steel – low carbon steel metal composite. *Izvestiya. Ferrous Metallurgy*. 2024;67(6):702–709.
https://doi.org/10.17073/0368-0797-2024-6-702-709

Исследование структурно-фазового состава и механических свойств металлокомпозита нержавеющая сталь – низкоуглеродистая сталь

В. И. Данилов[1], Д. В. Орлова[1], Г. В. Шляхова[1], Ю. П. Миронов[1], Е. Д. Петрова[2]

[1] **Институт физики прочности и материаловедения Сибирского отделения РАН** (Россия, 634055, Томск, пр. Академический, 2/4)
[2] **Санкт-Петербургский государственный морской технический университет** (Россия, 190121, Санкт-Петербург, ул. Лоцманская, 3)

dvi@ispms.tsc.ru

Аннотация. Предмет изучения – металлический композит, полученный электродуговой наплавкой в аргоне коррозионностойкой стали на низкоуглеродистую сталь. Наплавлялась порошковая хромоникелевая сталь с повышенным относительно традиционного состава содержанием кремния и молибдена. В настоящей работе исследованы элементный и структурно-фазовый составы, а также механические свойства обоих компонентов материала и композита в целом в исходном состоянии и после отжига при 680 °С в течение 3 ч. Основная часть коррозионностойкого компонента является двухфазной аустенитно-ферритной смесью с соотношением 65 % ГЦК-фазы и 30 % ОЦК-фазы. Материал обладает высокой микротвердостью (более 4000 МПа). Наибольшая микротвердость (4550 МПа) наблюдается в узком слое наплавленного металла шириной 25 мкм, где фазовый состав представлен мартенситом (ОЦК), а аустенит отсутствует. Переход через границу в углеродистую сталь сопровождается уменьшением микротвердости до 1225 МПа. Здесь вблизи линии сплавления образовалась обезуглероженная зона шириной 180 мкм. Сформировавшееся неравновесное напряженно-деформированное состояние композита привело к низкой прочности, малой пластичности и хрупкому разрушению наплавленного слоя при испытании на растяжение. После отжига микроструктура коррозионностойкого компонента стала более однородной по размерам как аустенитных, так и ферритных структурных элементов. В результате этих преобразований снизились внутренние напряжения и уменьшилась микротвердость до 3100 МПа. В то же время увеличилась ширина обезуглероженной зоны в основном металле. Все эти изменения привели к тому, что, хотя напряжение разрушения при растяжении отожженного материала увеличилось на 8 %, а деформация до разрыва – на 27 %, однако характер разрушения остался хрупким и разрыв по-прежнему происходит по наплавленному слою. Это определяется аустенитно-ферритным фазовым составом нержавеющего компонента, который, в свою очередь, задается химическим составом наплавляемого материала.

Ключевые слова: электродуговая наплавка, композит коррозионностойкая сталь – углеродистая сталь, микроструктура, микротвердость, фазовый состав, механические свойства, отжиг

Благодарности: Работа выполнена в рамках государственного задания Института физики прочности и материаловедения Сибирского отделения РАН с использованием оборудования ЦКП «Нанотех», тема № FWRW-2021-0011.

Для цитирования: Данилов В.И., Орлова Д.В., Шляхова Г.В., Миронов Ю.П., Петрова Е.Д. Исследование структурно-фазового состава и механических свойств металлокомпозита нержавеющая сталь – низкоуглеродистая сталь. *Известия вузов. Черная металлургия*. 2024;67(6):702–709. https://doi.org/10.17073/0368-0797-2024-6-702-709

Introduction

The strict and often contradictory requirements for materials in specialized mechanical engineering, chemical, nuclear, electrical, and electronics industries frequently make it impossible to rely on existing homogeneous metals and alloys. This challenge has driven the development and widespread adoption of layered metal composites. These composites, widely used in mechanical engineering, are valued for their high structural strength, corrosion resistance, heat resistance, and weldability – all achieved at relatively low cost. In large-scale industrial production, layered metal composites are typically manufactured as sheets, tubes, strips, and rods through casting followed by joint hot rolling of the components [1 – 4]. For applications with limited production volumes, various protective coatings – such as gas-thermal, ion-plasma diffusion, or electroplated coatings – are often more practical [5 – 8].

Among the most commonly used layered metal composites are those featuring a base layer of low-carbon or low-alloy steel, with cladding layers made of corrosion-resistant steel, copper, nickel, titanium, or other metals and alloys. This combination is designed to ensure that the base layer provides the required strength characteristics, while the cladding layer protects against aggressive environmental conditions. A cost-effective and accessible method for producing such composites is electric arc surfacing using a consumable austenitic electrode applied to low-alloy carbon steel [9]. This method makes it possible to create cladding layers with the desired physical and mechanical properties and precise geometric parameters. The use of powdered electrodes has proven particularly effective [10; 11]. Moreover, the process is

compatible with standard welding machines, leveraging well-established operating modes [12].

Despite its advantages, the production of such metal composites is not without challenges. Issues such as residual stresses, anisotropy, and the formation of porosity remain significant concerns. It is well known that during surfacing or welding, the cladding layer can acquire either a cast structure (in single-layer surfacing) or a structure modified by additional thermal treatment in specific zones (in multi-pass surfacing). When corrosion-resistant steel is surfaced onto carbon steel, the fusion zone may form martensitic or austenitic-ferritic structures, depending on the carbon content and diffusion processes [13 – 15]. Insufficient nickel and chromium in the deposited metal can lead to a secondary austenitic-martensitic structure [12]. These structures inevitably contribute to a complex stress state in and around the contact zone. Furthermore, the degree of mixing between the base and deposited metals significantly influences the stress-strain state of the bimetal composite. Ultimately, these factors play a decisive role in determining the overall performance characteristics of the layered metal composite.

This study aimed to assess the structure and stress-strain state of a layered metal composite made from corrosion-resistant steel and low-carbon steel, produced via electric arc surfacing, and to identify optimal thermal treatment parameters to enhance the structural strength of the material.

Materials and methods

The subject of this study is a metal composite obtained through automatic electric arc surfacing in an argon atmosphere, performed in two passes using a consumable powdered electrode on a plate of standard carbon steel grade 20 (as per GOST 1050–88) [16]. The electrode diameter was 1.5 mm, the plate thickness was 8 mm, the width of the deposited bead was 20 mm, and the average bead height was 10 mm. The chemical composition of the powdered electrode was as follows (wt. %: ≤0.12 C; ~18.0 Cr; ~1.0 Mn; ~5.0 Si; ~9.0 Ni; ~1.0 Mo; ~0.2 Ti; <0.04 S; <0.04 P; with the balance being iron. To prevent cracking during surfacing, the plate was preheated to approximately 300 °C.

For mechanical testing, a series of "*dog bone*" samples were cut from the resulting workpiece along the axis of the bead using the electro-erosion method.

The sample design and the scheme for measuring microhardness and evaluating structural-phase characteristics are shown in Fig. 1. The dimensions of the working section of the sample were 40×6×2 mm. In the working area of the sample, the fractions of the deposited metal and the base metal were approximately equal. Some of the prepared samples were annealed in a vacuum at a temperature of 680 °C for 3 h, followed by furnace

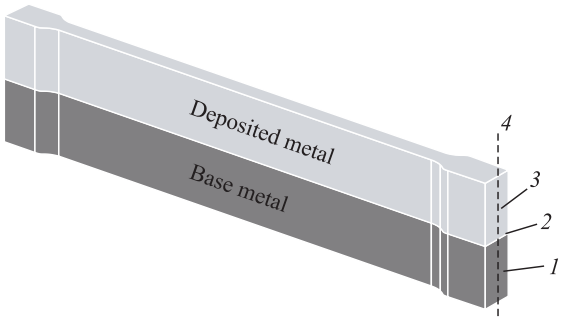

Fig. 1. A sample of metal composite for mechanical testing and determination of structural and phase characteristics: *1* – base metal; *2* – fusion line; *3* – deposited metal; *4* – line for measuring microhardness and certification of structural and phase characteristics

Рис. 1. Образец металлокомпозита для механических испытаний и определения структурно-фазовых характеристик: *1* – основной металл; *2* – линия сплавления; *3* – наплавленный металл; *4* – линия измерения микротвердости и аттестации структурно-фазовых характеристик

cooling (the initial state of the samples without heat treatment is referred to as "State *1*" and the state after annealing is referred to as "State *2*"). For structural analysis, cross-sectional samples were prepared in accordance with RD 24.200.04–90. The analysis of the cross-sections was conducted using a Neophot-21 microscope (Zeiss, Germany). The elemental composition of the deposited and base metals was determined using a LEO EVO 50 scanning electron microscope (Zeiss, Germany). Microhardness was measured with a PMT-3 microhardness tester (1 N load on the indenter), and phase composition was analyzed with a DRON-8 *X*-ray diffractometer (copper radiation).

Uniaxial tensile tests at room temperature were conducted on a Walter + Bai AG, model LFM-125 machine (Switzerland) at a crosshead speed of 0.2 mm/min.

Results and discussion

Fig. 2, *a* shows the macrostructure of the metal composite sample in State *1*. A strongly etched fusion boundary is distinctly visible. The deposited metal exhibits a layered structure with well-defined boundaries (Fig. 2, *a*). The layers are numbered starting from the fusion boundary, and their dimensions are provided in Table 1.

Table 1. **Layers of deposited metal**

Таблица 1. **Слои наплавленного металла**

Sample state	Layer thickness, mm			
	I	*II*	*III*	*IV*
Initial (*1*)	0.025	1.50	1.35	1.25
After annealing (*2*)	0.050	1.10	1.90	1.30

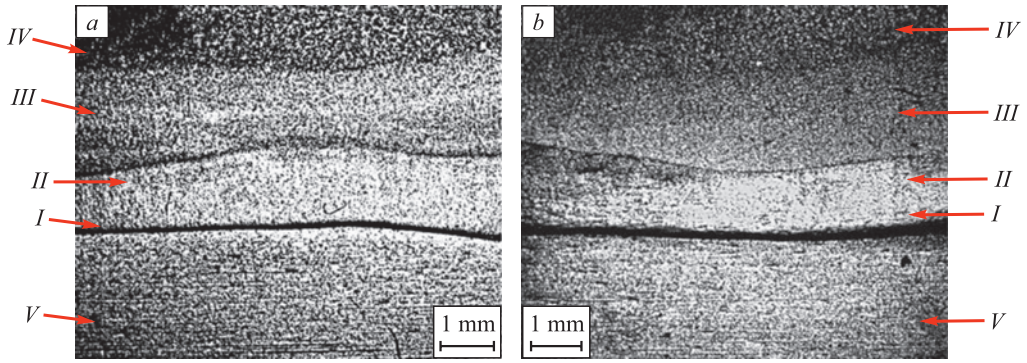

Fig. 2. Macrostructural image of the metal composite:
a – initial state; *b* – state after annealing; *I – IV* – layer of deposited metal; *V* – base metal

Рис. 2. Макроструктурное изображение металлокомпозита:
a – исходное состояние; *b* – состояние после отжига; *I – IV* – слои наплавленного металла; *V* – основной металл

Layer *I* is located immediately adjacent to the fusion line, where the deposited metal underwent the most significant structural and phase transformations. The material in this layer etches poorly, giving it an unstructured appearance. The formation of such "white zones" is typical for welded joints between high-alloy corrosion-resistant steels and carbon steels. According to previous studies [17 – 19], these zones exhibit a martensitic structure. In the macroscopic image (Fig. 2, *a*), layers *II* and *III* appear visually similar but are separated by a clearly distinguishable boundary.

Microstructural analysis revealed that in State *1*, the deposited metal has a cast structure, with the size and morphology of structural elements differing across layers *II – IV* (Fig. 3, *a*). In layers *II* and *III*, the deposited metal displays a dendritic structure with dark inter-dendritic regions. Near the boundary between layers *I* and *II*, the dendrites transition into polyhedral grains, while the inter-dendritic regions transform into inter-granular boundaries. The boundary of layer *I* is marked with a red dashed line in Fig. 3. As the boundary of layer *III* is approached, the thickness of the inter-dendritic regions increases, the transverse size of the dendrites decreases, and dark particles begin to form within them. Overall, in layer *III*, the dendritic structure is most pronounced and relatively uniform. The structure of layer *IV* is heterogeneous. The transverse sizes of the dendrites can vary significantly, differing by several times. The dark regions between the dendrites are spatially oriented and appear to have a phase composition distinct from that of the dendrites themselves.

Figs. 2, *a* and 3, *a* show that the macro- and microstructure of the base metal (layer *V*) is generally typical. The microstructure corresponds to that of high-quality carbon steel grade 20, consisting of polyhedral ferrite grains with a small amount of pearlite (Fig. 3, *a*). In State *1*, the average grain size was 21 ± 5 μm, corresponding to a grain size number of 8 ÷ 9. Notable struc-

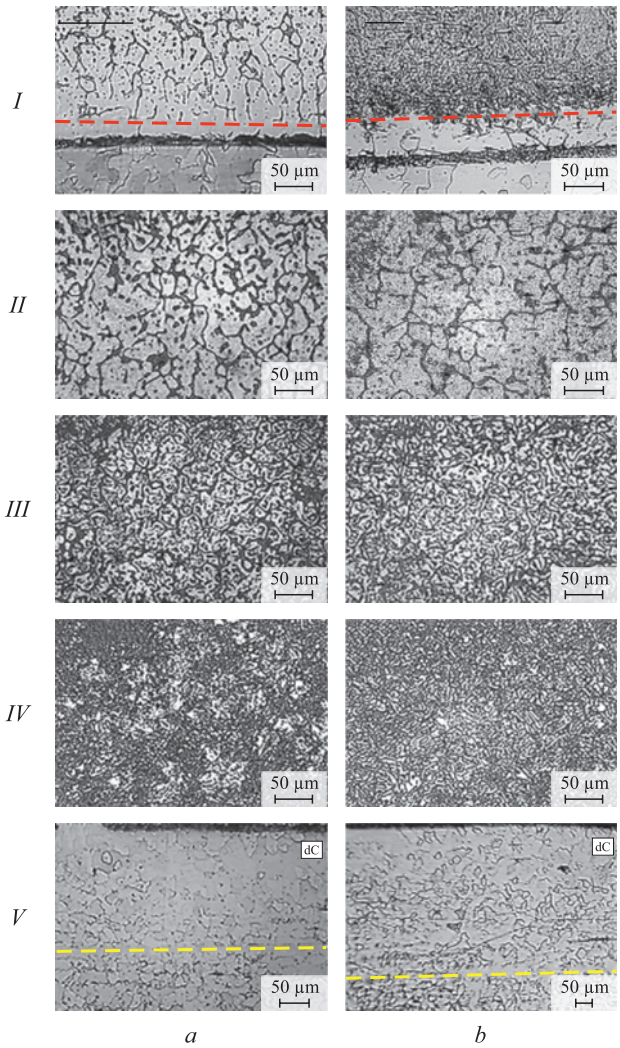

Fig. 3. Microstructure in layers *I – IV* of the deposited metal and base metal *V*:
a – initial state *1*; *b* – state after annealing *2*;
dC – decarburized zone of the base metal

Рис. 3. Микроструктура в слоях *I – IV* наплавленного металла и основного металла *V*:
a – исходное состояние *1*; *b* – состояние после отжига *2*;
dC – обезуглероженная зона основного металла

tural changes were observed near the fusion line, where a decarbonized zone (dC) formed, characterized by the absence of pearlite. This zone is 180 μm wide, with its boundary indicated by a yellow dashed line in Fig. 3.

The microhardness of the composite varies according to the structural characteristics of its layers (Fig. 4, curve *1*). The deposited metal exhibits a microhardness more than double that of the base metal, approximately 4000 MPa compared to 1700 MPa. The highest microhardness, 4550 MPa, is observed in the non-etching layer *I*. Moving toward the middle of layer *II*, the microhardness decreases but begins to rise again, reaching a nominal value of about 4000 MPa in layer *III*. At the fusion boundary, the microhardness measures 2550 MPa, while its lowest value of 1225 MPa corresponds to the decarbonized zone (dC) in the base metal.

The structural characteristics of the deposited metal layers and the microhardness distribution are closely tied to changes in phase composition. Fig. 5 shows the diffraction pattern obtained for the main portion of the deposited metal (curve *1*), indicating the presence of two dominant phases: FCC and BCC. At the farthest distance from the fusion boundary (layer *IV*), the FCC phase (~65 %, austenite) predominates, while the BCC phase (ferrite) makes up no more 30 %, with no signs of tetragonal distortions. In Fig. 3, *a*, the bright structural elements in layer *IV* are identified as austenite, while the darker, oriented features correspond to ferrite. The remaining ~5 % of the volume consists of a mixture of low-symmetry phases, silicides, and carbides. Near the fusion boundary, the phase composition reverses: in layer I, the BCC phase dominates, while austenite accounts for no more than 5 % of the volume and exhibits significant texturing.

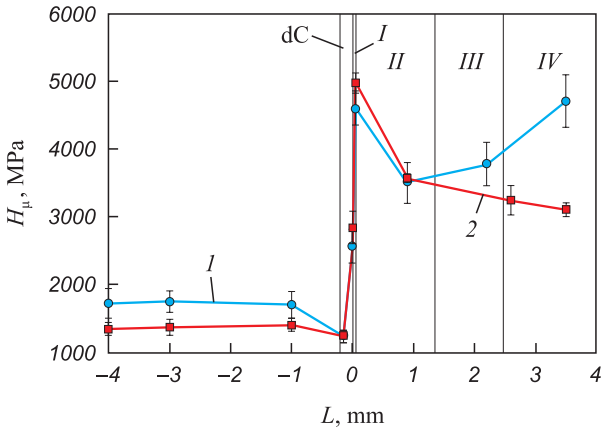

Fig. 4. Microhardness in different layers of the metal composite in initial state (*1*) and after annealing (*2*):
I – IV – numbers of layers of deposited metal;
dC – decarburized zone of the base metal

Рис. 4. Микротвердость в разных слоях металлокомпозита в исходном состоянии (*1*) и в состоянии после отжига (*2*):
I – IV – слои наплавленного металла;
dC – обезуглероженная зона основного металла

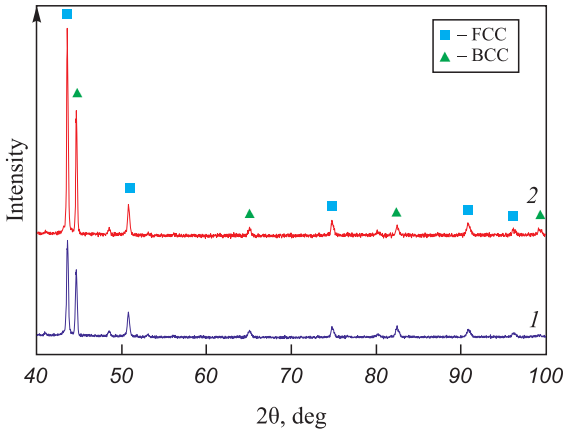

Fig. 5. *X*-ray diffraction patterns of the deposited layer in initial state (*1*) and after annealing (*2*)

Рис. 5. Рентгеновские дифрактограммы наплавленного слоя в исходном состоянии (*1*) и в состоянии после отжига (*2*)

The proportion of low-symmetry phases also decreases to around 2 %. As expected, the base metal consists primarily of the BCC phase. However, near the fusion boundary, the 220 diffraction peaks exhibit significant broadening, likely caused by tetragonal lattice distortions and internal stresses. This observation aligns with previous studies [17; 18] which describe a martensitic structure in the non-etching zone near the fusion boundary.

The observed structural-phase characteristics and microhardness distribution are driven by the diffusion-driven redistribution of carbon and alloying elements near the fusion line (between the base and deposited metals). This is supported by the results of elemental analysis (Table 2).

In layers *III* and *IV* of the deposited metal, the alloying element content closely matches the chemical composition of the powdered electrode. Using the concepts of Cr_{eq} and Ni_{eq} and the A. Schaeffler structural diagram for chromium-nickel stainless steels [20], the two-phase structure of these layers becomes clear. According to this diagram, the FCC phase corresponds to austenite, while the BCC phase corresponds to ferrite. In layer *II*, the nickel content decreases by a factor of three, silicon content by nearly half, and chromium content by half. As a result, the phase composition is a mixture of mar-

Table 2. **Chemical composition of the deposited metal**

Таблица 2. **Элементный состав наплавленного металла**

Metal layers	Content of alloying elements, wt. %			
	Si	Cr	Mn	Ni
III – IV	5.4	15.3	1.3	10.3
II	3.3	7.6	1.6	3.6
I	1.8	5.2	1.5	1.8

tensite and austenite, consistent with microstructural analysis findings. In layer *I*, the chromium and silicon content drops by a factor of three, and the nickel content decreases by a factor of 5.5, leaving only martensite. This result aligns with both microstructural observations and *X*-ray diffraction analysis.

The analysis of structure, microhardness, *X*-ray diffraction, and elemental composition in the initial State *1* reveals a significant heterogeneity in the material's stress-strain state, which adversely affects the composite's structural strength. The stress-strain curve from uniaxial tensile testing is shown in Fig. 6 (curve *1*). The material displays low plasticity, which is unusual for both carbon and stainless steels. At a strain of ε = 3.6 %, the deposited layer fails, forming a crack that extends through the entire layer. The crack opening reaches up to 1 mm. The diagram shows that the stress calculated for the full cross-section of the composite drops from 554.2 to 219.5 MPa. The base metal layer remains intact and continues to deform plastically. The remaining undamaged cross-sectional area of the sample is 6.33 mm^2, meaning that the stress acting in this area equals the stress in the entire sample at the moment the crack forms. This indicates that the failure of the deposited layer is brittle. The low fracture toughness of the deposited layer is likely due to high internal stresses. This issue can be addressed by annealing, which, as described earlier, was performed for 3 h at 680 °C.

The macroscopic image of the annealed material (Fig. 2, *b*) shows that the layered structure of the deposited metal is largely preserved, although the boundary between layers *III* and *IV* is noticeably blurred. The width of layer *I* has increased to 50 μm (Table 1). Layer *I* remains non-etching (Fig. 3, *b*). The adjacent layer *II*, as in State *1*, exhibits a grain structure that gradually transitions into a dendritic structure. The evolution of the microstructure from layer *II* to layer *III* after annealing follows the same pattern observed in the initial state. The dendritic structure of layer *III* remains unchanged between the initial and annealed states. However, significant changes occur in the microstructure of layer *IV* (Figs. 3, *a* and 3, *b*). The microstructure becomes more uniform, with the bright austenitic structural elements becoming more consistent in size, while the dark ferritic elements thicken and lose their preferred orientation.

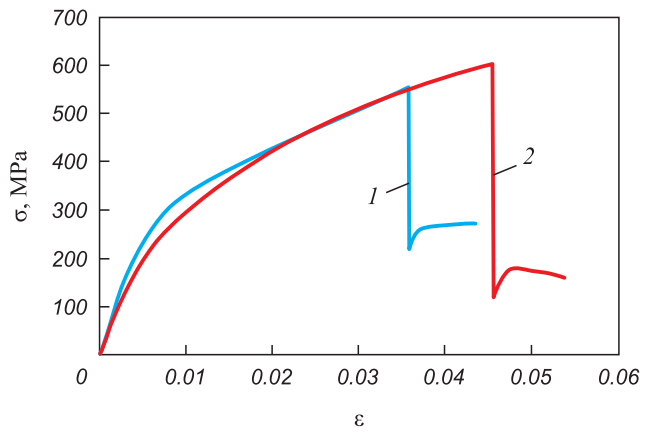

Fig. 6. Loading curves for the composite in initial state (*1*) and after annealing (*2*)

Рис. 6. Диаграммы нагружения композита в исходном состоянии (*1*) и в отожженном состоянии (*2*)

The microhardness distribution of the composite after annealing (State *2*) is shown in Fig. 4, curve *2*. The most notable changes are observed in layer *IV*, where the microhardness decreases from 4700 to 3100 MPa. Conversely, the microhardness of layer *I* increases by 400 MPa compared to the initial state, while the microhardness of the base metal shows a slight decrease. It is also noteworthy that, while the microhardness of the decarbonized zone remains unchanged after annealing, the width of this zone expands to approximately 500 μm.

The phase composition in layers *III* and *IV* remains unchanged after annealing (Fig. 5, *b*), consisting of austenite, ferrite, and less than 5 % of low-symmetry phases. The half-width of the main peaks for the BCC and FCC phases decreases compared to the initial state, indicating a reduction in second-order internal stresses. Furthermore, in layer *I*, the content of the FCC phase decreases significantly (to about 2 %), and the proportion of low-symmetry phases drops to less than 2 %. After annealing, the base metal consists of a more refined BCC phase, reflecting the absence of elastic distortions.

Overall, the deposited metal, fusion boundary, and the composite as a whole transition to a more equilibrated stress-strain state, which has a positive effect on the material's structural strength. As shown by curve *2* in Fig. 6, while the deposited metal still fractures in a brittle manner, the tensile stress at failure increases to 603 MPa, and the relative elongation improves to 4.56 %.

Conclusions

Studies of the composite produced by electric arc surfacing in an argon atmosphere, combining stainless steel and low-carbon structural steel, showed that the corrosion-resistant component has a two-phase austenitic-ferritic structure. The component features a dendritic structure, with an elemental composition matching that of the electrode wire. The ferritic phase is concentrated in the inter-dendritic regions. Closer to the fusion boundary, the dendritic structure transitions into a grain structure, and the FCC phase content decreases to zero. At the same time, the concentration of alloying elements drops by a factor of 3 to 5, resulting in the formation of a martensitic structure within a few micrometers of the fusion boundary. Overall, the deposited layer exhibits high hardness and brittleness due to significant internal stresses.

Annealing at 680 °C for 3 h improves the microstructure of the deposited layer, reduces hardness, and increases relative elongation at failure. However, the composite remains brittle.

During electric arc surfacing of the corrosion-resistant layer onto low-carbon steel grade 20, a porosity-free layer is formed that is strongly bonded to the base metal. This layer exhibits an austenitic-ferritic phase composition with substantial internal stresses, leading to brittle fracture under load. This brittleness is attributed to the elevated silicon and molybdenum content in the powdered electrode wire compared to traditional compositions for chromium-nickel stainless steels. Although annealing relieves internal stresses in the deposited layer, it does not fully eliminate the composite's brittleness.

References / Список литературы

1. Golovanenko S.A., Meandrov L.V. Bimetal Production. Moscow: Metallurgiya; 1966:297. (In Russ.).

   Голованенко С.А., Меандров Л.В. Производство биметаллов. Москва: Металлургия; 1966:297.
2. Dhib Z., Guermazi N., Gaspérini M., Haddar N. Cladding of low-carbon steel to austenitic stainless steel by hot-roll bonding: Microstructure and mechanical properties before and after welding. *Materials Science and Engineering: A*. 2016;656:130–141. http://doi.org/10.1016/j.msea.2015.12.088
3. Hu K., Xia Y., Zhu F., Noda N.A. Evaluation of thermal breakage in bimetallic work roll considering heat treated residual stress combined with thermal stress during hot rolling. *Steel Research International*. 2017;89(4):1700368. http://doi.org/10.1002/srin.201700368
4. Mittler T., Greb T., Feistle M., Krinninger M., Hofmann U., Riedle J., Golle R., Volk W. Fabrication and processing of metallurgically bonded copper bimetal sheets. *Journal of Materials Processing Technology*. 2019;263:33–41. https://doi.org/10.1016/j.jmatprotec.2018.08.008
5. Hocking M.G., Vasantasree V., Sidky P.S. Metallic and Ceramic Coatings. NY: Longman Scientific & Technical Publisher; 1989:670.

   Хокинг М., Васантасри В., Сидки П. Металлические и керамические покрытия: Получение, свойства и применение / Под ред. Р.А. Андриевского. Москва: Мир; 2000:518.
6. Khmelevskaya V.B., Moseiko E.S., Ol'khovik E.O. Study of strengthening of ship propeller parts by plasma spray coating with ultrasonic treatment. *Vestnik gosudarstvennogo universiteta morskogo i rechnogo flota im. admirala S.O. Makarova*. 2013;(3):81–87. (In Russ.).

   Хмелевская В.Б., Мосейко Е.С., Ольховик Е.О. Исследование упрочнения деталей судового валопровода методом покрытия плазменным напылением с ультразвуковой обработкой. *Вестник государственного университета морского и речного флота им. адмирала С.О. Макарова*. 2013;(3):81–87.
7. Monceau D., Oquab D., Estournes C., Boidot M., Selezneff S., Ratel-Ramond N. Thermal barrier systems and multi-layered coatings fabricated by spark plasma sintering for the protection of Ni-base superalloys. *Materials Science Forum*. 2010;654–656:1826–1831. https://doi.org/10.4028/www.scientific.net/MSF.654-656.1826
8. Gotz W., Heinisch T. Leyendecker: Steckverbinder – Hohe Zuverlässigkeit bei reduziertem Edelmetalleinsatz. *Galvanotechnik*. 2003;4(9):2139–2140. (In Germ.).
9. Bandyopadhyay A., Heer B. Additive manufacturing of multi-material structures. *Materials Science and Engineering: R: Reports*. 2018;129:1–16. https://doi.org/10.1016/j.mser.2018.04.001
10. Kozyrev N.A., Kibko N.V., Umanskii A.A., Titov D.A. Improving the quality of deposited layer of rolling rolls by optimizing the composition of flux-cored wires. *Svarochnoe proizvodstvo*. 2017;7:29–34. (In Russ.).

    Козырев Н.А., Кибко Н.В., Уманский А.А., Титов Д.А. Повышение качества наплавленного слоя прокатных валков за счет оптимизации состава порошковых проволок. *Сварочное производство*. 2017;(7):29–34.
11. Usol'tsev A.A., Kozyrev N.A., Bashchenko L.P., Kryukov R.E., Zhukov A.V. Development of flux-cored wire of Fe–C–Si–Mn–Cr–W–V system with additives of carbon-fluorine-containing material and titanium. *Izvestiya. Ferrous Metallurgy*. 2023;66(4):403–409. https://doi.org/10.17073/0368-0797-2023-4-403-409

    Усольцев А.А., Козырев Н.А., Бащенко Л.П., Крюков Р.Е., Жуков А.В. Разработка порошковой проволоки системы Fe–C–Si–Mn–Cr–W–V с присадками углеродфторсодержащего материала и титана. *Известия вузов. Черная металлургия*. 2023;66(4):403–409. https://doi.org/10.17073/0368-0797-2023-4-403-409
12. Sidorov V.P., Mel'zitdinova A.V. Methodology for determining the requirements for welding parameters accuracy. *Svarka i diagnostika*. 2014;(3):10–13. (In Russ.).

    Сидоров В.П., Мельзитдинова А.В. Методика определения требований к точности параметров сварки. *Сварка и диагностика*. 2014;(3):10–13.
13. Boronenkov V.N., Korobov Yu.S. Basics of Arc Metallization. Physico-Chemical Patterns. Ekaterinburg: Izd. Ural. un-ta; 2012:268. (In Russ.).

    Бороненков В.Н., Коробов Ю.С. Основы дуговой металлизации. Физико-химические закономерности. Екатеринбург: Изд. Урал. ун-та; 2012:268.
14. Zernin E.A., Petrova E.D., Danilov V.I., Shlyakhova G.V. Structure and properties of a metal deposited by a powder wire in a plasma stream. *Svarka i diagnostika*. 2024;(2):28–33. (In Russ.). https://doi.org/10.52177/2071-5234_2024_02_28

    Зернин Е.А., Петрова Е.Д., Данилов В.И., Шляхова Г.В. Структура и свойства металла, наплавленного порошковой проволокой в потоке плазмы. *Сварка и диагностика*. 2024;(2):28–33. https://doi.org/10.52177/2071-5234_2024_02_28
15. Wielage B., Pokhmurska H., Student M., Gvozdeckii V., Stupnyckyj T., Pokhmurskii V. Iron-based coatings arc-sprayed with cored wires for applications at elevated temperatures. *Surface & Coatings Technology*. 2013; 220:27–35. https://doi.org/10.1016/j.surfcoat.2012.12.013
16. Sorokin V.G., etc. Steels and Alloys. Grade Guide: Reference Book. Moscow: Intermet Inzhiniring; 2001:608. (In Russ.).

    Стали и сплавы. Марочник: Справ. изд. / В.Г. Сорокин и др. Москва: Интермет Инжиниринг; 2001:608.

17. Gel'man A.S., Chudnovskii A.D., Tsemakhovich B.D., Kharin I.L. Cladding of Steel by Explosion. Moscow: Mashinostroenie; 1978:191. (In Russ.).

Плакирование стали взрывом / Под ред. А.С. Гельмана, А.Д. Чудновского, Б.Д. Цемаховича, И.Л. Харина. Москва: Машиностроение; 1978:191.

18. Trudov A.F., Trykov Yu.P., Klochkov S.V., Dontsov D.Yu., Voinov M.O. The effect of heat treatment on the structural and mechanical heterogeneity of explosion-welded bimetal St.3+12Kh18N10T. *Deformatsiya i razrushenie materialov*. 2009;12:41–44. (In Russ.).

Трудов А.Ф., Трыков Ю.П., Клочков С.В., Донцов Д.Ю., Войнов М.О. Влияние термообработки на структурно-механическую неоднородность сваренного взрывом биметалла Ст.3+12Х18Н10Т. *Деформация и разрушение материалов*. 2009;(12):41–44.

19. Shlyakhova G.V., Barannikova S.A., Bochkareva A.V., Li Yu.V., Zuev L.B. Study of the structure of bimetal construction carbon steel – stainless steel. *Izvestiya. Ferrous Metallurgy*. 2018;61(4):219–223. (In Russ.). https://doi.org/10.17073/0368-0797-2018-4-300-305

Шляхова Г.В., Баранникова С.А., Бочкарёва А.В., Ли Ю.В., Зуев Л.Б. Исследование структуры биметалла конструкционная углеродистая сталь – нержавеющая сталь. *Известия вузов. Черная металлургия*. 2018;61(4):300–305. https://doi.org/10.17073/0368-0797-2018-4-300-305

20. Schaeffler M. Constitution diagram for stainless steel weld metal. *Metal Progress*. 1949:56:680–681.

Information about the Authors / Сведения об авторах

Vladimir I. Danilov, *Dr. Sci. (Phys.-Math.), Prof., Chief Researcher of the Laboratory of Strength Physics*, Institute of Strength Physics and Materials Science, Siberian Branch of the Russian Academy of Sciences
ORCID: 0000-0002-5741-7574
E-mail: dvi@ispms.ru

Dina V. Orlova, *Cand. Sci. (Phys.-Math.), Research Associate of the Laboratory of Strength Physics*, Institute of Strength Physics and Materials Science, Siberian Branch of the Russian Academy of Sciences
ORCID: 0000-0003-0068-2542
E-mail: dvo@ispms.ru

Galina V. Shlyakhova, *Cand. Sci. (Eng.), Research Associate of the Laboratory of Strength Physics*, Institute of Strength Physics and Materials Science SB RAS
ORCID: 0000-0001-9578-2989
E-mail: shgv@ispms.ru

Yurii P. Mironov, *Cand. Sci. (Phys.-Math.), Research Associate of the Laboratory of Materials Science of Shape Memory Alloys*, Institute of Strength Physics and Materials Science SB RAS
ORCID: 0000-0002-2351-3592
E-mail: myp@ispms.ru

Ekaterina D. Petrova, *Assistant of the Chair of Welding of Ship Structures*, Saint-Petersburg State Marine Technical University
ORCID: 0009-0002-2302-8359
E-mail: petrowa.ket@yandex.ru

Владимир Иванович Данилов, *д.ф.-м.н., профессор, главный научный сотрудник лаборатории физики прочности*, Институт физики прочности и материаловедения Сибирского отделения РАН
ORCID: 0000-0002-5741-7574
E-mail: dvi@ispms.ru

Дина Владимировна Орлова, *к.ф.-м.н., научный сотрудник лаборатории физики прочности*, Институт физики прочности и материаловедения Сибирского отделения РАН
ORCID: 0000-0003-0068-2542
E-mail: dvo@ispms.ru

Галина Витальевна Шляхова, *к.т.н. научный сотрудник лаборатории физики прочности*, Институт физики прочности и материаловедения Сибирского отделения РАН
ORCID: 0000-0001-9578-2989
E-mail: shgv@ispms.ru

Юрий Петрович Миронов, *к.ф.-м.н., научный сотрудник лаборатории материаловедения сплавов с памятью формы*, Институт физики прочности и материаловедения Сибирского отделения РАН
ORCID: 0000-0002-2351-3592
E-mail: myp@ispms.ru

Екатерина Дмитриевна Петрова, *ассистент кафедры сварки судовых конструкций*, Санкт-Петербургский государственный морской технический университет
ORCID: 0009-0002-2302-8359
E-mail: petrowa.ket@yandex.ru

Contribution of the Authors / Вклад авторов

V. I. Danilov – formation of the article main concept, scientific guidance, revising and writing the article final version.
D. V. Orlova – analysis and discussion of experimental results, writing the article draft version.
G. V. Shlyakhova – carrying out metallographic studies, describing composite structures.
Yu. P. Mironov – carrying out *X*-ray studies, describing the material phase composition.
E. K. Petrova – performing surfacing in specified modes, obtaining a composite.

В. И. Данилов – идея работы, научное руководство, написание окончательного варианта рукописи.
Д. В. Орлова – анализ и обсуждение экспериментальных результатов, написание первичного варианта рукописи.
Г. В. Шляхова – проведение металлографических исследований, описание структур композита.
Ю. П. Миронов – проведение рентгеновских исследований, описание фазового состава материала.
Е. К. Петрова – выполнение наплавки по заданным режимам, получение композита.

Received 13.08.2024
Revised 05.09.2024
Accepted 20.09.2024

Поступила в редакцию 13.08.2024
После доработки 05.09.2024
Принята к публикации 20.09.2024

MATERIALS SCIENCE / МАТЕРИАЛОВЕДЕНИЕ

UDC 621.791.927.5
DOI 10.17073/0368-0797-2024-6-710-715

Original article
Оригинальная статья

STRUCTURE AND PROPERTIES OF COATINGS OBTAINED BY GAS-THERMAL SPRAYING

A. V. Kolubaev, **O. V. Sizova** ✉

Institute of Strength Physics and Materials Science, Siberian Branch of the Russian Academy of Sciences (2/4 Akademicheskii Ave., Tomsk 634055, Russian Federation)

✉ ovs@ispms.tsc.ru

Abstract. The authors investigated the microstructure and mechanical properties of wear-resistant coatings applied by the method of gas-thermal spraying with heating of the metal to a liquid state and its subsequent spraying with a gas jet. Nowadays, thermal spraying is increasingly an alternative to various methods of surfacing due to the high costs of consumables, the complexity of maintenance and safety during repairs. By this method, it is possible to reliably solve a variety of technological tasks, which include spraying of wear-resistant, antifriction and corrosion-resistant coatings; alitizing by spraying (increasing heat resistance); increasing the size of products; surfacing and soldering; elimination of casting defects; manufacture of molds, etc. The tribotechnical properties of the vibration damper rod of a railway carriage with reinforcing surface layers applied to the working surface by methods of gas-thermal spraying with 40Kh13 steel and galvanic chromium plating were investigated. Structure and thickness of the coatings, microhardness distribution in the coating-substrate zone, as well as the features of the coatings destruction under the same test conditions were studied. The criterion for comparing the coatings' wear resistance was the operating time of the samples before the beginning of the coating destruction. Wear of the rollers was determined by the change in diameter, and wear of the pads – by the depth and width of the grooves formed on their surface during the experiment. The coating applied to the vibration damper rod by spraying 40Kh13 steel wire has high wear resistance in conditions of boundary friction with grease and can be an alternative to electroplated chrome coating. The high wear resistance of the coating makes it possible to recommend it for restoring the dimensions of worn parts and increasing the durability of new ones, as well as for replacing special anti-friction bearing alloys.

Keywords: structural steel, dimensional defect, wear-resistant coating, thermal spraying, tribotechnical properties, sliding friction

Acknowledgements: The work was performed within the framework of the state assignment of the Institute of Strength Physics and Materials Science of the Siberian Branch of the Russian Academy of Sciences, project No. FWRW 2021-0006.

For citation: Kolubaev A.V., Sizova O.V. Structure and properties of coatings obtained by gas-thermal spraying. *Izvestiya. Ferrous Metallurgy*. 2024;67(6):710–715. *https://doi.org/10.17073/0368-0797-2024-6-710-715*

СТРУКТУРА И СВОЙСТВА ПОКРЫТИЙ, ПОЛУЧЕННЫХ СПОСОБОМ ГАЗОТЕРМИЧЕСКОГО НАПЫЛЕНИЯ

А. В. Колубаев, **О. В. Сизова** ✉

Институт физики прочности и материаловедения Сибирского отделения РАН (Россия, 634055, Томск, пр. Академический, 2/4)

✉ ovs@ispms.tsc.ru

Аннотация. В работе исследовались микроструктура и механические свойства износостойких покрытий, нанесенных способом газотермического напыления с нагревом металла до жидкого состояния и последующим его распылением газовой струей. Газотермическое напыление в настоящее время все чаще выступает альтернативой различным методам наплавки из-за высоких затрат на расходуемые материалы, сложность обслуживания и обеспечения безопасности при выполнении ремонта. С помощью этого способа можно надежно решать разнообразные технологические задачи, к которым относятся: напыление износостойких, антифрикционных и коррозионностойких покрытий; алитирование напылением (повышение жаростойкости); наращивание размеров изделий; наплавка и пайка; устранение литейных дефектов; изготовление пресс-форм и др. Авторы исследовали триботехнические свойства штока виброгасителя железнодорожного вагона с нанесенными на рабочую поверхность упрочняющих поверхностных слоев способами газотермического напыления стали 40Х13 и гальванического хромирования. Изучали строение и толщину покрытий, распределение микротвердости в зоне покрытие – подложка, а также особенности разрушения покрытий при одинаковых условиях испытаний. Критерием для сравнения износостойкости покрытий является время работы образцов до начала разрушения покрытия. Износ роликов определялся по изменению диаметра, а колодок – по глубине и ширине канавок, образовавшихся на их поверхности за время проведения эксперимента. Покрытие,

нанесенное на шток виброгасителя распылением проволоки из стали 40Х13, обладает высокой износостойкостью в условиях граничного трения со смазкой и способно быть альтернативой гальваническому хромовому покрытию. Высокая износостойкость покрытия позволяет рекомендовать его для восстановления размеров изношенных деталей и повышения долговечности новых, а также для замены специальных антифрикционных подшипниковых сплавов.

Ключевые слова: конструкционная сталь, размерный дефект, износостойкое покрытие, газотермическое напыление, триботехнические свойства, трение скольжения

Благодарности: Работа выполнена в рамках государственного задания Института физики прочности и материаловедения Сибирского отделения РАН, номер темы FWRW 2021-0006.

Для цитирования: Колубаев А.В., Сизова О.В. Структура и свойства покрытий, полученных способом газотермического напыления. *Известия вузов. Черная металлургия*. 2024;67(6):710–715. https://doi.org/10.17073/0368-0797-2024-6-710-715

Introduction

Structural steels of various chemical compositions are traditional materials for manufacturing components of mechanisms and equipment. During operation, under conditions of sliding friction on working surfaces, the geometric dimensions of such components change, which consequently leads to disruptions in the operating modes of mechanisms and the occurrence of hazardous situations. The intensity of the wear process depends on several factors: chemical composition of the steel, its operational characteristics, load, and sliding speed of the working surface against the counterbody. A critical task in modern mechanical engineering is to develop a scientifically grounded set of measures for creating technologies to restore the working surfaces of machine components and tooling. One of the most promising methods is gas-thermal restoration of worn surfaces by applying metallic, non-metallic, and composite coatings. This involves heating the source material to a liquid or plastic state and spraying it with a gas jet. This method includes the previously known metallization process by spraying and similar processes for applying various materials. The spraying process consists of several stages: the initial stages ensure the atomization of the source materials, and in the final stage, they are deposited onto a target.

The gas-thermal spraying process is defined by distinct thermodynamic and aerodynamic characteristics [1], which are of practical importance as they directly influence the quality of the deposited material layer and its functional performance [2 – 9].

The gas-thermal spraying (GTS) process consists of four sequential stages: melting the source material in quantities sufficient to ensure continuous and uninterrupted spraying; atomizing the molten material into fine particles using jets of compressed air or other gases; creating a directed flow (spray plume) of these molten and atomized particles; and depositing the particles to form a material layer. During deposition, the particles, propelled by their kinetic energy, bombard the target surface, embedding themselves in its irregularities and adhering to previously deposited particles. Gas-thermal spraying is increasingly emerging as an alternative to traditional surfacing methods, which are often associated with high consumable costs, complex maintenance requirements, and significant safety challenges during repairs [10 – 16].

This study presents a comparative analysis of the structure and properties of gas thermal coatings made from high-chromium steel, applied to the working surface of a vibration damper rod in a passenger railway carriage. The coatings were applied using GTS, where the metal was heated to a liquid state and sprayed with a gas jet, and electroplated chrome coatings for comparison.

Materials and methods

The tribotechnical properties of the vibration damper rod of a railway carriage were investigated, with reinforcing surface layers applied to the working surface using gas-thermal spraying with 40Kh13 steel and electroplated chrome coatings. The chemical composition of the coatings was determined by *X*-ray fluorescence analysis, and the results were compared with the chemical composition of 40Kh13 steel according to GOST 5632 – 72. The study examined the structure and thickness of the coatings, the distribution of microhardness in the coating-substrate zone, and the characteristics of coating destruction under identical test conditions. Metallographic studies of the friction surfaces were conducted using a NEOPHOT-21 optical microscope, and the microhardness was measured with a PMT-3 microhardness tester.

The chemical composition of the coating obtained by gas-thermal spraying of 40Kh13 wire was as follows (wt. %): C 0.38, Si 0.21, Mn 0.64, Cr 0.87. A comparison of the primary element content, particularly chromium, showed that the coating material after spraying corresponded to the standard composition of 40Kh13 steel as per GOST 4543 – 71.

The wear of the rollers was determined by measuring the change in diameter, while the wear of the pads was evaluated based on the depth and width of the grooves formed on their surface during the experiment. A comparative analysis of the tribotechnical properties of electroplated and gas-thermal coatings was performed using a SMT-1 tribometer, following a roller-to-pad configuration. The rollers were the test samples, and the pads

were made of SCh 32-52 grade cast iron. The test conditions closely simulated the real operating conditions of vibration dampers, including the lubricant used in this design (VMGZ oil). Tests were conducted until the onset of coating destruction, which was monitored by observing changes in surface topography and detecting initial signs of coating failure. After every three hours of experimentation, the structure of the coating and substrate was analyzed, microhardness was measured, and changes in the dimensions of rollers and pads were recorded.

The implementation of new high-velocity gas-flame spraying systems offers significant potential for further development of this method, particularly in protecting critical machine and mechanism components from abrasive wear, corrosion, and other types of degradation [6 – 12]. One such critical component is the vibration damper of a railway carriage (Fig. 1), a large oilfilled shock absorber designed to dampen carriage oscillations during motion. A passenger carriage typically has four vibration dampers. Generally, within six months of operation, these dampers begin to fail due to the destruction of the chrome coating and oil leakage. The cumulative costs of oil loss, rod replacement, and carriage downtime are substantial. It should be noted that worn rods are typically not repaired but discarded. Improving the wear resistance of these critical components can significantly reduce railway maintenance costs and enhance the safety of railway operations [13 – 16].

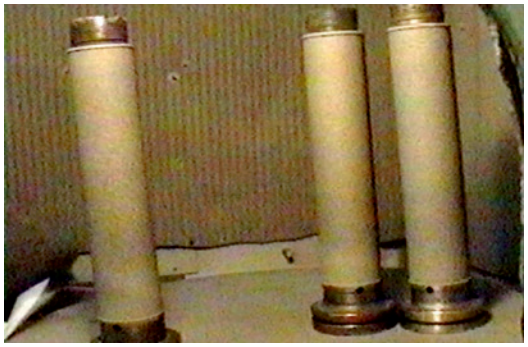

a

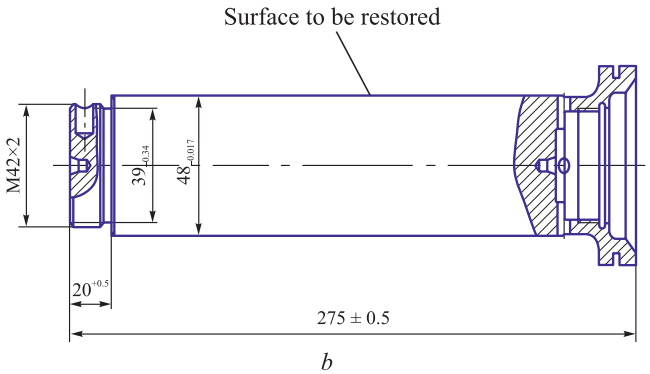

b

Fig. 1. General view (*a*) and diagram (*b*) of the vibration damper rod

Рис. 1. Общий вид (*a*) и схема штока (*b*) виброгасителя

Samples for the structural and tribotechnical studies were prepared from two types of vibration damper rods: the first was a worn rod restored using GTS with 40Kh13 steel wire, and the second was a rod coated with a protective layer applied through standard electroplating in a liquid electrolyte.

The wear rates of the electroplated and gas-thermal coatings on the test samples were determined through comparative wear tests conducted on a 2070 SMT-1 tribometer, following the previously described roller-to-pad configuration. The experimental scheme is shown in Fig. 2.

The performance criterion for comparison was the duration of sample operation until the onset of coating failure under a load of $P = 400$ N and a shaft rotation speed of $\omega = 350$ rpm. The degree of wear was evaluated using the following parameters: for the rollers, by the change in diameter; and for the pads, by the depth and width of the grooves formed on their surface during the experiment.

Results

The structural analysis of the coatings revealed notable differences. The thickness of the dense electroplated chrome coating did not exceed 0.1 mm, with a sharp and well-defined boundary observed between the coating and the substrate (Fig. 3, *a*). In contrast, the thickness of the coating applied through GTS reached approximately 2 mm, with a similarly distinct boundary evident in this case. The metal structure within the gas thermal sprayed coating zone comprised mixed layers of the sprayed metal, varying in thickness (Fig. 3, b). Discontinuities, such as cracks and pores, were observed at the boundaries between these layers. The calculated porosity of the material was determined to be 5 – 6 %. Microhard-

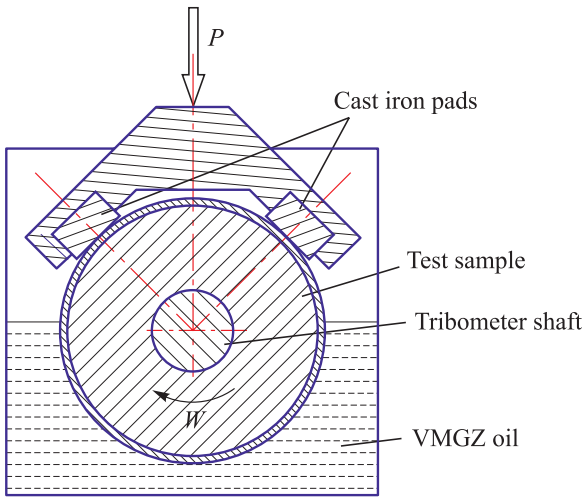

Fig. 2. Experimental scheme

Рис. 2. Схема проведения эксперимента

ness measurements indicated that the chrome coating exhibited a hardness of approximately 700 HV, while the gas-thermal sprayed coating demonstrated a hardness range of 340 – 400 HV. The substrate material (45 steel) had a hardness within the range of 150 – 180 HV.

During the first three hours of testing, no significant changes were observed in either sample. However, after six hours of testing, the sample with the chrome coating began to exhibit the initial signs of substrate material deformation and localized chipping of the coating. These signs included the formation of a deformed layer beneath the coating, measuring 0.8 – 0.9 mm in depth, and the detachment of coating fragments along the boundary (Fig. 3, *c*). The image clearly illustrates that the failure of the chrome coating occurred through the detachment of small particles in areas where substrate material (the rod) deformation had occurred beneath the coating.

The coating applied through GTS retained its original structure throughout the entire testing period (9 h) without any visible signs of damage. Wear occurred gradually, with the removal of thin surface layers, avoiding the formation of localized areas with significant material loss.

Analysis and discussion of results

The analysis of the results revealed that the coating applied to the vibration damper rod through GTS of 40Kh13 steel wire demonstrated excellent wear resistance under conditions of boundary friction with lubrication. This highlights its potential as a viable alternative to electroplated chrome coatings. The exceptional wear resistance of the gas thermal coating makes it suitable not only for restoring the dimensions of worn components and enhancing the durability of new ones but also as a replacement for specialized anti-friction bearing alloys. The findings suggest that, in most cases, GTS is the most economically viable method for applying anti-friction coatings on components operating under sliding friction with either limited or abundant liquid lubrication [17 – 20].

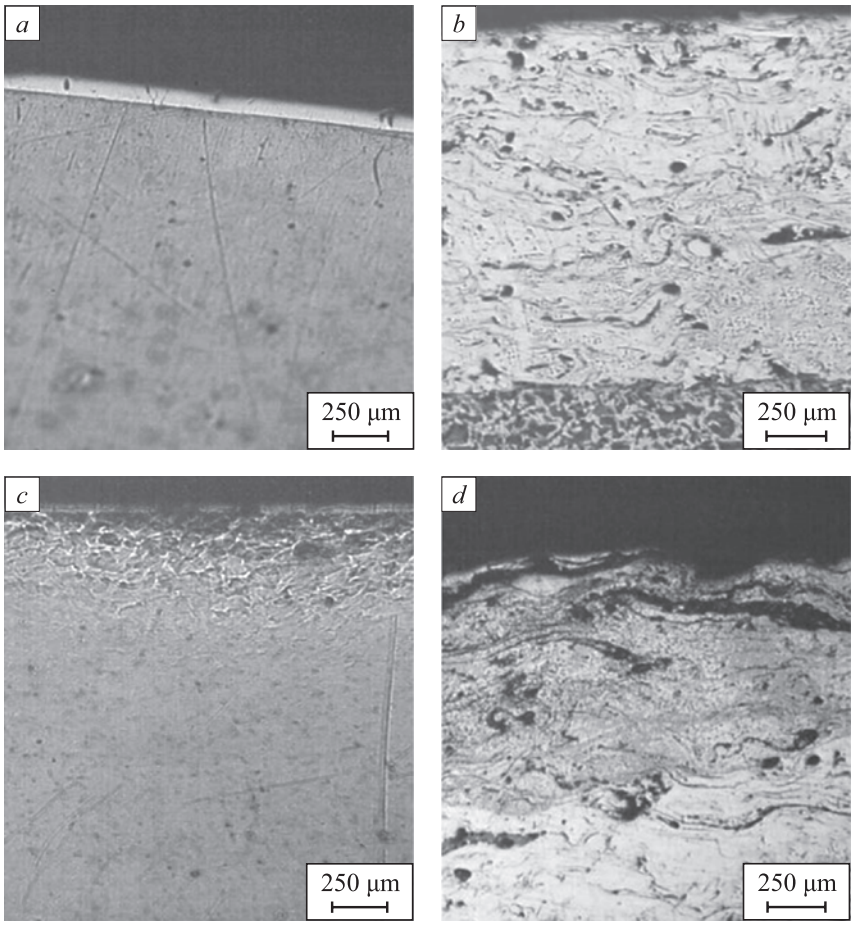

Fig. 3. Microstructure of the samples in cross section:
a – chrome coating applied by galvanic method; *b* – coating obtained by gas-thermal spraying;
c and *d* – destruction of chrome and of sprayed coatings

Рис. 3. Микроструктура образцов в поперечном сечении:
a – хромовое покрытие, нанесенное гальваническим способом; *b* – покрытие, полученное газотермическим напылением;
c и *d* – разрушение хромового и напыленного покрытия

Conclusions

It has been established that the GTS method, which involves heating the metal to a liquid state followed by its atomization using a gas jet, can be effectively employed to restore the worn surfaces of steel components.

Comparative studies of the tribotechnical properties of coatings applied through GTS and electroplating indicate that the gas thermal method reliably addresses a wide range of technological applications, including application of wear-resistant, anti-friction, and corrosion-resistant coatings; alitizing through spraying (to enhance heat resistance); increasing the dimensions of components; surfacing and soldering through spraying; rectification of casting defects.

References / Список литературы

1. Belotserkovskii M.A. Tribotechnical characteristics of gas-flame coatings. *Friction and Wear*. 2000;21(5):534–539. (In Russ.).

   Белоцерковский М.А. Триботехнические характеристики газопламенных покрытий. *Трение и износ*. 2000; 21(5):534–539.
2. Vityaz P.A., Belotserkovskii M.A., Kukareko V.A., Kalinovskii D.M., Sukhotskii P.G., Kovalevskaya Zh.G. Structure and properties of 40Kh13 steel coatings obtained using various methods of gas-thermal spraying. *Fizicheskaya Mezomekhanika*. 2002;5(1):29–36. (In Russ.).
   https://doi.org/10.24411/1683-805X-2002-00072

   Витязь П.А., Белоцерковский М.А., Кукареко В.А., Калиновский Д.М., Сухоцкий П.Г., Ковалевская Ж.Г. Структура и свойства покрытий из стали 40Х13, полученных с использованием различных методов газотермического напыления. *Физическая мезомеханика*. 2002;5(1):29–36. https://doi.org/10.24411/1683-805X-2002-00072
3. Baldaev P.Kh., Shesterkin N.G., Lupakov V.I., Shatov A.P. Features of high-speed gas plasma spraying processes. *Svarochnoe proizvodstvo*. 2003;(5):43–46. (In Russ.).

   Балдаев П.Х., Шестеркин Н.Г., Лупаков В.И., Шатов А.П. Особенности процессов высокоскоростного газоплазменного напыления. *Сварочное производство*. 2003;(5):43–46.
4. Belotserkovskii M.A., Pryadko A.S. Activated plasma gas and electric arc spraying of coatings with conductive materials. *Uprochnyayushchie tekhnologii i pokrytiya*. 2006;(12):17–23. (In Russ.).

   Белоцерковский М.А., Прядко А.С. Активированное газоплазменное и электродуговое напыление покрытий проволочными материалами. *Упрочняющие технологии и покрытия*. 2006;(12):17–23.
5. Zavareh M.A., Sarhan A.A.D.M., Binti A.R.B., Basirun W.J. Plasma thermal spray of ceramic oxide coating on carbon steel with enhanced wear and corrosion resistance for oil and gas applications. *Ceramics International*. 2014;40(9A): 14267–14277.
   https://doi.org/10.1016/j.ceramint.2014.06.017
6. Belotserkovskii M.A. Strength reliability and tribotechnical properties of gas-thermal coatings used in friction units. *Fizicheskaya Mezomechanika*. 2007;10(2):103–108. (In Russ.). https://doi.org/10.24411/1683-805X-2007-00037

   Белоцерковский М.А. Прочностная надежность и триботехнические свойства газотермических покрытий, используемых в узлах трения. *Физическая мезомеханика*. 2007;10(2):103–108.
   https://doi.org/10.24411/1683-805X-2007-00037
7. Chu Z., Yang Y., Chen X., Yan D., Huang D., Lei W., Liu Z. Characterization and tribology performance of Fe-based metallic glassy composite coatings fabricated by gas multiple-tunnel plasma spraying. *Surface and Coatings Technology*. 2016;292:44–48.
   https://doi.org/10.1016/j.surfcoat.2016.03.024
8. Kolubaev A.V., Belyi A.V., Buyanovskii I.A. Mechanisms of deformation and destruction of hard coatings under frictional heating conditions. *Izvestiya vuzov. Fizika*. 2019;62(8): 53–75. (In Russ.).
   http://doi.org/10.17223/00213411/62/8/52

   Колубаев А.В., Белый А.В., Буяновский И.А. Механизмы деформирования и разрушения твердых покрытий в условиях фрикционного нагрева. *Известия вузов. Физика*. 2019;62(8):53–75.
   http://doi.org/10.17223/00213411/62/8/52
9. Gusev A.I., Usol'tsev A.A., Kozyrev N.A., Kibko N.V., Bashchenko L.P. Development of flux-cored wire for surfacing of parts operating under conditions of wear. *Izvestiya. Ferrous Metallurgy*. 2018;61(11):898–906. (In Russ.).
   https://doi.org/10.17073/0368-0797-2018-11-898-906

   Гусев А.И., Усольцев А.А., Козырев Н.А., Кибко Н.В., Бащенко Л.П. Разработка порошковой проволоки для наплавки деталей, работающих в условиях износа. *Известия вузов. Черная Металлургия*. 2018;61(11):898–906. https://doi.org/10.17073/0368-0797-2018-11-898-906
10. Belotserkovskii V.A., Grigorchik A.N., Kukareko V.A., Konstantinov V.M. The structural and phase state and wear resistance of nitrogen ion-modified thermal gas coatings made of high-chromium steels applied using high-enthalpy combustible gas. *Metallovedenie i termicheskaya obrabotka*. 2019;(9(771)):46–54. (In Russ.).

    Белоцерковский В.А., Григорчик А.Н., Кукареко В.А., Константинов В.М. Структурно-фазовое состояние и износостойкость модифицированных ионами азота газотермических покрытий из высокохромистых сталей, нанесенных с использованием высокоэнтальпийного горючего газа. *Металловедение и термическая обработка*. 2019;(9(771)):46–54.
11. Kolubaev A.V., Sizova O.V., Fortuna S.V., Vorontsov A.V., Ivanov A.N., Kolubaev E.A. Weld structure of low-carbon structural steel formed by ultrasonic-assisted laser welding. *Journal of Constructional Steel Research*. 2020;172:160190.
    https://doi.org/10.1016/j.jcsr.2020.106190
12. Kukareko V.A., Belotserkovskii V.A., Grigorchik A.N., Sosnovskii A.V. Structure and tribological properties of the coating Ti–TiN, obtained by high-speed deposition. *Friction and Wear*. 2022;43(5):458–465. (In Russ.).
    https://doi.org/10.32864/0202-4977-2022-43-5-458-465

    Кукареко В.А., Белоцерковский В.А., Григорчик А.Н., Сосновский А.В. Структура и триботехнические свойства покрытия Ti-TiN, полученного высокоскоростным

напылением. *Трение и износ*. 2022;43(5):458–465. https://doi.org/10.32864/0202-4977-2022-43-5-458-465

13. Artemenko S.A., Orlik G.V., Orlik A.G. The use of wear-resistant cord material for the restoration of worn teeth of a quarry excavator. *Svarochnoe proizvodstvo*. 2021;(10):63–69. (In Russ.). https://doi.org/10.26160/2658-3305-2021-10-63-69

    Артеменко С.А., Орлик Г.В., Орлик А.Г. Применение износостойкого шнурового материала по восстановлению изношенных зубьев карьерного экскаватора. *Сварочное производство*. 2021;(10):63–69. https://doi.org/10.26160/2658-3305-2021-10-63-69
14. Zharkevich A.M., Nurzhanova O.A., Bessonov A.V. Determination of the optimal technological modes of surfacing when restoring parts such as bodies of revolution. *Svarochnoe proizvodstvo*. 2022;(5):35–40. (In Russ.).

    Жаркевич А.М., Нуржанова О.А., Бессонов А.В. Определение оптимальных технологических режимов наплавки при восстановлении деталей типа тел вращения. *Сварочное производство*. 2022;(5):35–40.
15. Liu S.-H., Trelles J.P., Li C.-J., Li C.-X., Guo H.-B. A review and progress of multiphase flows in atmospheric and lowe pressure plasma spray advanced coating. *Materials Today Physics*. 2022;27:100832. https://doi.org/10.1016/j.mtphys.2022.100832
16. Singh S., Goyal K., Bhatia R. A review on protection of boiler tube steels with thermal spray coatings from hot corrosion. *Materials Today: Proceedings*. 2022;56(1):379–383. https://doi.org/10.1016/j.matpr.2022.01.219
17. Li N., Tariq N. ul H., Che Y., Liu S., Wang J., Cui X., Xiong T. Corrosion-resistant thermal spray coatings for low-alloy steel in contact with molten nitrate salts in solar power plants. *Solar Energy Materials and Solar Cells*. 2023;59:112432. https://doi.org/10.1016/j.solmat.2023.112432
18. Samal S., Zeman J., Kopeček J., Šittner P. Thermal plasma spraying of NiTi powder for thick coating of shape memory alloy. *Journal of Alloys and Compounds*. 2024;984:173962. https://doi.org/10.1016/j.jallcom.2024.173962
19. Gupta M., Li X.-H., Peng R., Ottosson A., Gillberge P., Girgulisf J. Understanding the effect of bondcoat surface treatment on enhanced lifetime of suspension plasma sprayed thermal barrier coatings. *Surface and Coatings Technology*. 2024;482:130716. https://doi.org/10.1016/j.surfcoat.2024.130716
20. Lakkannavar V., Yogesha K.B., Prasad C.D., Phanden R.K., Srinivasa G., Prasad S.C. Thermal spray coatings on high-temperature oxidation and corrosion applications – A comprehensive review. *Results in Surfaces and Interfaces*. 2024;16:100250. https://doi.org/10.1016/j.rsurfi.2024.100250

Information about the Authors

Aleksandr V. Kolubaev, *Dr. Sci. (Phys.-Math.), Chief Researcher*, Institute of Strength Physics and Materials Science, Siberian Branch of the Russian Academy of Sciences
ORCID: 0000-0002-2839-5249

Ol'ga V. Sizova, *Dr. Sci. (Phys.-Math.), Chief Researcher*, Institute of Strength Physics and Materials Science, Siberian Branch of the Russian Academy of Sciences
ORCID: 0000-0001-9177-6602
E-mail: ovs@ispms.tsc.ru

Сведения об авторах

Александр Викторович Колубаев, *д.ф.-м.н., главный научный сотрудник*, Институт физики прочности и материаловедения Сибирского отделения РАН
ORCID: 0000-0002-2839-5249

Ольга Владимировна Сизова, *д.ф.-м.н., главный научный сотрудник*, Институт физики прочности и материаловедения Сибирского отделения РАН
ORCID: 0000-0001-9177-6602
E-mail: ovs@ispms.tsc.ru

Received 21.08.2024
Revised 03.10.2024
Accepted 17.10.2024

Поступила в редакцию 21.08.2024
После доработки 03.10.2024
Принята к публикации 17.10.2024

MATERIALS SCIENCE / МАТЕРИАЛОВЕДЕНИЕ

UDC 669.018.25:539.219:539.25
DOI 10.17073/0368-0797-2024-6-716-724

Original article
Оригинальная статья

Impact strength and fracture features of 12 % chromium ferritic-martensitic steel EP-823 in temperature range from –196 to 100 °C

K. V. Spiridonova[1] ✉, I. Yu. Litovchenko[1], N. A. Polekhina[1], V. V. Osipova[2], S. A. Akkuzin[1], V. M. Chernov[3]

[1] **Institute of Strength Physics and Materials Science, Siberian Branch of Russian Academy of Sciences** (2/4 Akademicheskii Ave., Tomsk 634055, Russian Federation)
[2] **National Research Tomsk State University** (36 Lenina Ave., Tomsk 634050, Russian Federation)
[3] **JSC "A.A. Bochvar High-Technology Scientific-Research Institute of Inorganic Materials"** (5a Rogova Str., Moscow 123098, Russian Federation)

✉ almaevakv@ispms.ru

Abstract. The authors investigated the patterns of fracture during impact bending tests and determined the values of impact strength and temperature of the ductile-brittle transition in temperature range from –196 to 100 °C of heat-resistant 12 % chromium ferritic-martensitic steel EP-823 in structural states after traditional heat (THT) and high-temperature thermomechanical (HTMT) treatments. After THT, temperature of the ductile-brittle transition T_{dbt} is approximately –45 °C, after HTMT – approximately –40 °C. At these temperatures, the impact energy (*KCV*) after THT is approximately 36 J/cm^2, after HTMT – 32 J/cm^2. Fractographic studies conducted by scanning electron microscopy of the fracture features of impact steel samples after two treatments (THT and HTMT) in the low-temperature test area (at cryogenic temperatures) showed a predominantly brittle nature of fracture, while fracture occurs by the mechanism of a transcrystalline quasi-cleavage. In the temperature range of the ductile-brittle transition, a mixed nature of fracture is observed, which passes through the mechanism of a transcrystalline quasi-cleavage with elements of ductile dimple fracture. In the temperature range from 50 to 100 °C, the extremely ductile nature of the fracture was detected, realized by the transcrystalline dimple fracture mechanism. After HTMT, there is a slight decrease (relative to THT) in the steel impact strength in almost the entire temperature range under consideration and, accordingly, an increase in the temperature of its ductile-brittle transition. This is due to the tests' geometry, in which the direction of impact occurs in the plane of the layered structure, and it facilitates the formation of delamination cracks.

Keywords: ferritic-martensitic steel EP-823, microstructure, impact test, impact strength, ductile-brittle transition temperature, fracture features

Acknowledgements: The work was performed within the framework of the state task of the Institute of Strength Physics and Materials Science, Siberian Branch of Russian Academy of Sciences, project No. FWRW-2021-0008. The research was carried out with the equipment of the Share Use Centre "Nanotech" of the ISPMS SB RAS.

For citation: Spiridonova K.V., Litovchenko I.Yu., Polekhina N.A., Osipova V.V., Akkuzin S.A., Chernov V.M. Impact strength and fracture features of 12 % chromium ferritic-martensitic steel EP-823 in temperature range from –196 to 100 °C. *Izvestiya. Ferrous Metallurgy*. 2024;67(6):716–724. https://doi.org/10.17073/0368-0797-2024-6-716-724

Ударная вязкость и особенности разрушения 12 % хромистой ферритно-мартенситной стали ЭП-823 в температурном интервале от –196 до 100 °С

К. В. Спиридонова[1], И. Ю. Литовченко[1], Н. А. Полехина[1], В. В. Осипова[2], С. А. Аккузин[1], В. М. Чернов[3]

[1] **Институт физики прочности и материаловедения Сибирского отделения РАН** (Россия, 634055, Томск, пр. Академический, 2/4)
[2] **Национальный исследовательский Томский государственный университет** (Россия, 634050, Томск, пр. Ленина, 36)
[3] **АО «Высокотехнологический научно-исследовательский институт неорганических материалов им. акад. А.А. Бочвара»** (Россия, 123098, Москва, ул. Рогова, 5а)

almaevakv@ispms.ru

Аннотация. В настоящей работе исследованы закономерности разрушения при испытаниях на ударный изгиб, определены значения ударной вязкости и температура вязко-хрупкого перехода в температурном интервале от –196 до 100 °С жаропрочной 12 %-ной хромистой ферритно-мартенситной стали ЭП-823 в структурных состояниях после традиционной термической (ТТО) и высокотемпературной термомеханической (ВТМО) обработок. После ТТО температура вязко-хрупкого перехода $T_{хв}$ составляет приблизительно –45 °С, после ВТМО – приблизительно –40 °С. При этих температурах энергия удара (*KCV*) после ТТО составляет приблизительно 36 Дж/см^2, после ВТМО – 32 Дж/см^2. Проведенные методом растровой электронной микроскопии фрактографические исследования особенностей разрушения ударных образцов стали после двух обработок (ТТО и ВТМО) в низкотемпературной области испытаний (при криогенных температурах) показали преимущественно хрупкий характер разрушения, при этом разрушение происходит по механизму транскристаллитного квазискола. В области температур вязко-хрупкого перехода наблюдается смешанный характер разрушения, который проходит по механизму транскристаллитного квазискола с элементами вязкого ямочного разрушения. В интервале температур от 50 до 100 °С обнаружен преимущественно вязкий характер разрушения, реализуемый по транскристаллитному ямочному механизму разрушения. После ВТМО наблюдается незначительное снижение (относительно ТТО) ударной вязкости стали практически во всем рассматриваемом температурном диапазоне и, соответственно, повышение температуры ее вязко-хрупкого перехода. Это обусловлено геометрией испытаний, при которой направление удара происходит в плоскости слоистой структуры, что облегчает зарождение трещин расслоения.

Ключевые слова: ферритно-мартенситная сталь ЭП-823, микроструктура, ударные испытания, ударная вязкость, температура вязко-хрупкого перехода, особенности разрушения

Благодарности: Работа выполнена в рамках государственного задания Института физики прочности и материаловедения Сибирского отделения РАН, тема номер FWRW-2021-0008. Исследования выполнены с использованием оборудования центра коллективного пользования ИФПМ СО РАН «Нанотех».

Для цитирования: Спиридонова К.В., Литовченко И.Ю., Полехина Н.А., Осипова В.В., Аккузин С.А., Чернов В.М. Ударная вязкость и особенности разрушения 12 % хромистой ферритно-мартенситной стали ЭП-823 в температурном интервале от –196 до 100 °С. *Известия вузов. Черная металлургия*. 2024;67(6):716–724. https://doi.org/10.17073/0368-0797-2024-6-716-724

Introduction

In recent decades, ferritic-martensitic steels containing 9 – 12 % chromium have been considered as structural materials for next-generation reactors [1 – 6]. Studies [7 – 10] on this class of steels have shown that they exhibit a combination of favorable mechanical properties, high creep resistance, corrosion resistance, thermal conductivity, resistance to radiation-induced swelling, and relatively low thermal expansion compared to previously used austenitic steels [11 – 15].

The key challenges in the development of ferritic-martensitic steels are improving their high-temperature strength above 600 °C and reducing their susceptibility to low-temperature embrittlement. Special attention is given to the phenomenon of cold brittleness in these steels, as body-centered cubic (BCC) metals transition from a high-energy ductile fracture mode to a low-energy brittle fracture mode via quasi-cleavage as the test temperature decreases [16; 17]. This transition is associated with the ductile-brittle transition temperature (T_{dbt}). Moreover, under operating conditions, radiation exposure can lead to a reduction in fracture toughness and a shift of T_{dbt} to higher temperatures (300 – 400 °C) [17; 18], increasing the risk of premature structural failure. Therefore, developing methods to mitigate embrittlement and enhance the material's resistance to low temperatures remains a critical research objective.

One of the Russian representatives of the ferritic-martensitic steel class with 12 % chromium is EP-823 steel (Fe–12Cr–Mo–Nb–W–V–B) [8]. This steel has been studied after different treatment methods, including traditional heat treatment (THT) and high-temperature thermomechanical treatment (HTMT) [8; 12; 19]. According to [8], HTMT enhances the strength and plastic properties of EP-823 steel over a wide temperature range (from –70 to 720 °C) compared to THT. The improvement in mechanical properties after HTMT is correlated with

the following microstructural changes: a 1.5 – 2.0-fold reduction in the average size of martensitic blocks and ferritic grains; a threefold decrease in the average size of martensitic lamellae; an increase in dislocation density to $(3 – 6)\cdot10^{10}$ cm^{-2} in the ferrite phase and to $(6 – 9)\cdot10^{10}$ cm^{-2} in the martensite phase; and a 1.5-fold increase in the volume fraction of nanoscale *MeX*-type particles (*Me* = Nb, Mo; *X* = C, N) compared to THT [8]. It is important to note that, regardless of the treatment method, the primary hardening mechanisms of EP-823 steel include: dispersion hardening by nanoscale *MeX* carbonitrides via the Orowan mechanism; grain boundary hardening due to martensitic block boundaries and ferrite grain boundaries; and substructural hardening due to low-angle boundaries of martensitic lamellae and an increased dislocation density [19].

It is well known that the strength, plasticity, and impact properties of a material are interrelated. The mechanical properties of EP-823 steel under tensile testing conditions have been sufficiently studied [8]; however, the effect of processing regimes on its impact properties has not been previously investigated.

It is worth noting that when examining samples after hot rolling (specifically, those cut perpendicular to the rolling plane), a layered structure is observed (referred to in international literature as a "*pancake structure*") [8; 15; 20 – 22]. This structure is characterized by a reduction in the effective grain size. It has been shown that this structural feature has a positive effect on impact toughness and the ductile-brittle transition temperature when the impact direction is perpendicular to the layers and, in particular cases, to the rolling plane, due to crack arrest within the layered structure [15; 20 – 22].

To investigate the effect of low-temperature embrittlement, Charpy impact tests were conducted in this study on 12 % chromium ferritic-martensitic EP-823 steel in structural states after THT and HTMT.

Materials and methods

EP-823 steel has the following chemical composition (wt. %): C 0.14; Cr 11.56; Mn 0.58; Mo 0.74; Nb 0.40; V 0.34; W 0.68; Ni 0.68; N 0.03; Si 1.09; Ce 0.10; Ti 0.01; B 0.006; Al 0.02; with iron as the balance [8; 10; 12; 19]. The processing schemes are as follows:

• THT consisted of heating to $T = 1100$ °C, holding for 1 h, air quenching, and tempering at $T = 720$ °C for 3 h;

• HTMT involved austenitization at $T = 1100$ °C for 1 h, followed by hot plastic deformation via rolling in the austenitic region to $\varepsilon \approx 50$ % in a single pass, with subsequent water quenching. After deformation, the steel was tempered at $T = 720$ °C for 1 h [8; 12; 15; 19].

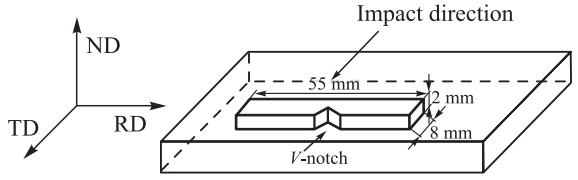

Fig. 1. Scheme of cutting samples for impact tests: ND – direction normal to the rolling plane; RD – rolling direction; TD – transverse direction

Рис. 1. Схема вырезания образцов для испытаний на удар: ND – направление нормали к плоскости прокатки; RD – направление прокатки; TD – поперечное направление

Impact toughness tests were carried out on an automated Instron 450MP pendulum impact tester using *V*-notched Charpy samples in structural states after THT and HTMT over a temperature range from –196 to 100 °C. According to GOST 9454–78, the sample dimensions were 55.0×2.0×8.0 mm, with a notch depth of 2.0 mm. Samples after HTMT were cut according to the designated scheme (Fig. 1), and the pendulum impact was applied in the transverse direction (TD). Cooling was performed in a KO-70 metal sample cooling chamber for 10 min immediately before testing. The testing time for cooled samples did not exceed 5 s. At test temperatures of 50–100 °C, the samples were additionally preheated. The impact toughness values were averaged based on the test results of at least three identical samples. The variation in the obtained impact toughness values did not exceed ±5 %.

The temperature dependence of impact toughness $KCV(T)$ exhibits two plateaus: the upper plateau KCV_{max} and the lower plateau KCV_{min}. The ductile-brittle transition temperature (T_{dbt}) is defined as the average value between KCV_{max} and KCV_{min}.

Fractographic analysis of the fracture surfaces of the tested steel samples was conducted using scanning electron microscopy with an Apreo 2S microscope. Additionally, in accordance with ASTM E23-05, the rates of brittle and ductile fracture components in EP-823 steel were calculated across the entire investigated temperature range, and the brittle transition temperature T_{50} was determined, corresponding to the temperature at which the rate of brittle fracture reaches 50 %).

Results

The results of Charpy impact tests for EP-823 steel in structural states after THT and HTMT over a temperature range from –196 to 100 °C are presented in Fig. 2.

At elevated temperatures, the maximum impact toughness values are observed in EP-823 steel samples after both treatment methods. Specifically, the upper plateau energy (at $T = 50 – 100$ °C) is approximately 65 J/cm^2 for THT-treated steel and 60 J/cm^2 for HTMT-treated steel.

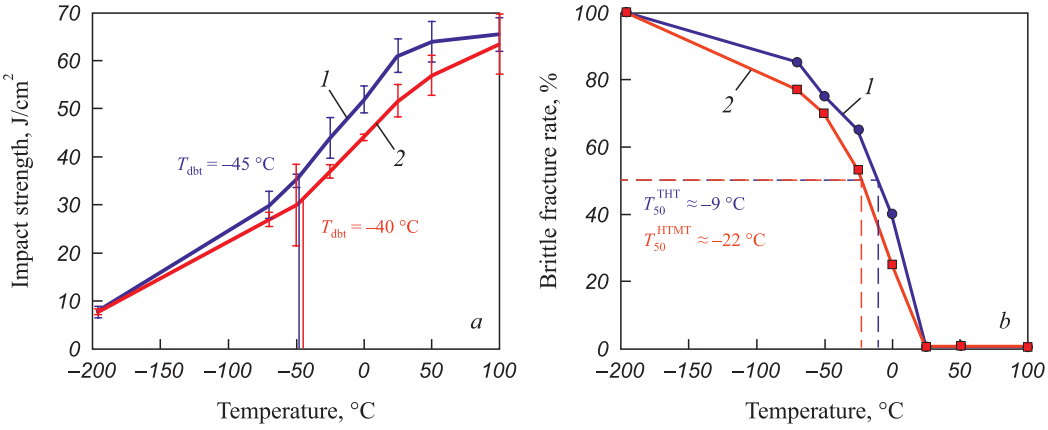

Fig. 2. Temperature dependences of EP-823 steel after THT (*1*) and HTMT (*2*) in the temperature range from –196 to 100 °C: *a* – impact strength; *b* – brittle fracture rate

Рис. 2. Температурные зависимости стали ЭП-823 после ТТО (*1*) и ВТМО (*2*) в интервале температур от –196 до 100 °C: *a* – ударная вязкость; *b* – доля хрупкого разрушения

As the test temperature decreases, the impact toughness declines, reaching approximately 7.7 J/cm^2 at cryogenic temperatures (T = –196 °C) for both treatments. Across almost the entire investigated temperature range (except at T = –196 °C), the *KCV* values of steel after THT are higher than those obtained after HTMT.

The ductile-brittle transition temperature of EP-823 steel after THT and HTMT is –45 and –40 °C, respectively, with *KCV* values of approximately 36 and 32 J/cm^2, respectively.

To establish a correlation between impact toughness values and fracture mechanisms, fractographic studies were conducted on EP-823 steel samples after impact tests in structural states following THT and HTMT, with fractures occurring within the temperature range of –196 to 100 °C. It is important to note that, after both treatments, the fractographic features and fracture mechanisms of EP-823 steel are qualitatively similar.

At a test temperature of –196 °C, after both treatment modes, the unstable crack propagation zone occupies the entire fracture surface. At this temperature, the fracture occurs by the transcrystalline (brittle) quasi-cleavage mechanism, with no ductile fracture regions observed (Fig. 3). The fracture surface exhibits quasi-cleavage facets, differing in size, shape, and orientation. A river -like pattern is frequently observed. The average facet

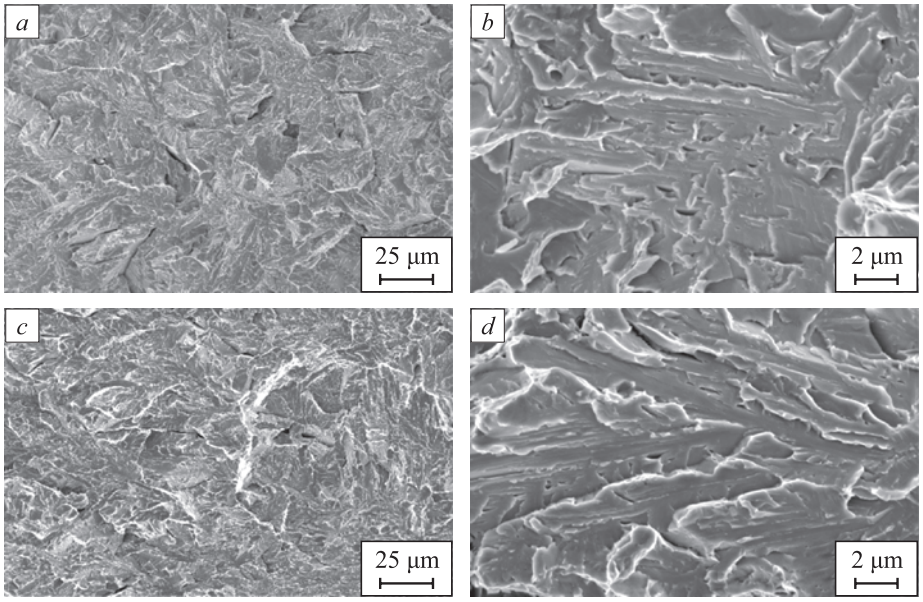

Fig. 3. SEM fractographic images of steel samples after impact tests at –196 °C after THT (*a*, *b*) and after HTMT (*c*, *d*)

Рис. 3. Фрактографические изображения образцов стали после ударных испытаний при –196 °C, полученные методом РЭМ, после ТТО (*a*, *b*) и после ВТМО (*c*, *d*)

width ranges from 3 to 7 μm, and additionally, narrow elongated facets approximately 10 μm in length are present on the fracture surface.

At test temperatures near T_{dbt}, the unstable crack propagation zone is significantly reduced compared to that at lower temperatures. In this zone, the fracture exhibits a mixed character, occurring through a combination of the transcrystalline quasi-cleavage mechanism and ductile dimple fracture elements (Fig. 4). Within the temperature range of –70 to 22 °C, multiple delamination microcracks are observed in HTMT-treated samples, propagating in the direction of the pendulum impact. These microcracks can reach lengths of up to 500 μm, with their widths not exceeding 0.2 μm. In contrast, THT-treated samples display only isolated cracks, oriented perpendicular to the fracture plane.

At the upper plateau of the impact toughness curve, the fracture occurs predominantly through the ductile transcrystalline dimple fracture mechanism, which involves the nucleation, growth, and coalescence of micropores. The average dimple size ranges from 1 to 5 μm, with some dimples reaching up to 10 μm in size

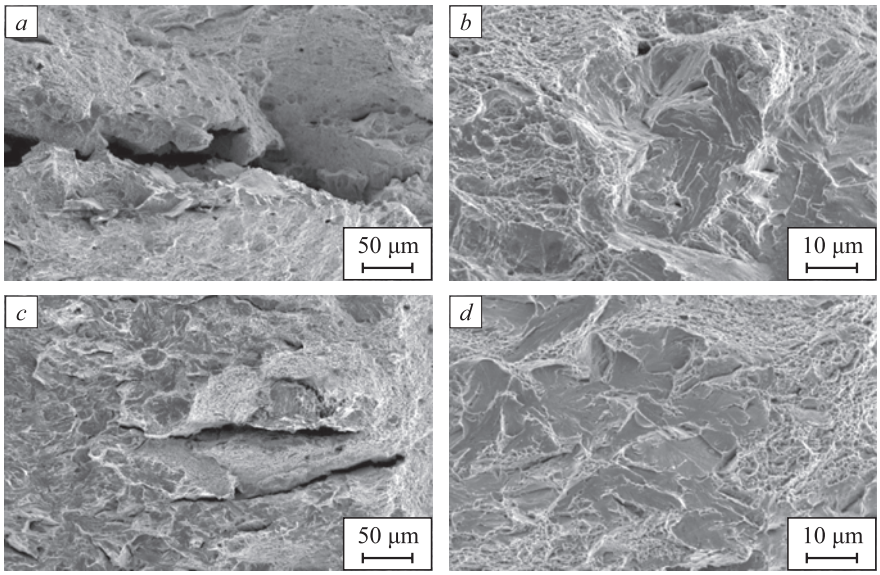

Fig. 4. SEM fractographic images of steel samples after impact tests at – 50 °C, after THT (*a*, *b*) and after HTMT (*c*, *d*)

Рис. 4. Фрактографические изображения образцов стали после ударных испытаний при температуре –50 °C, полученные методом РЭМ, после ТТО (*a*, *b*) и после ВТМО (*c*, *d*)

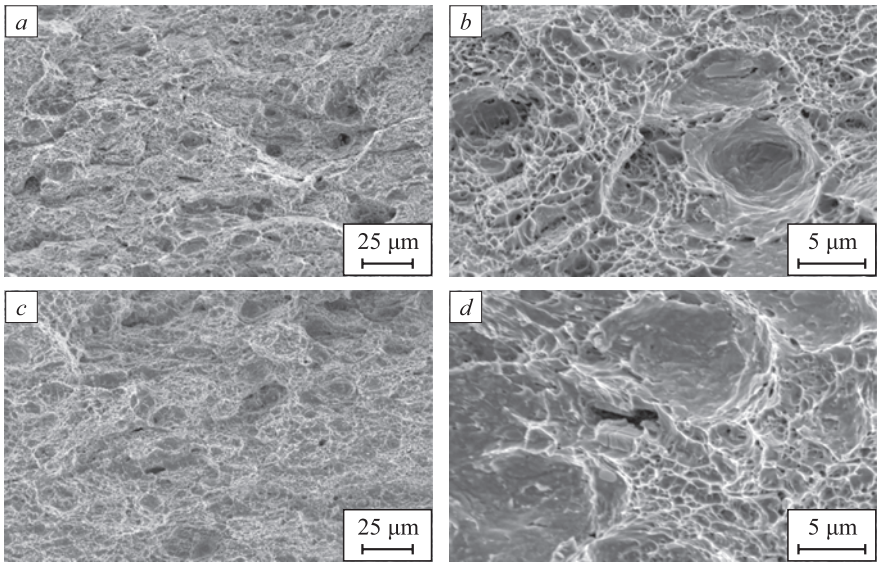

Fig. 5. SEM fractographic images of steel samples after impact tests at 100 °C, after THT (*a*, *b*) and after HTMT (*c*, *d*)

Рис. 5. Фрактографические изображения образцов стали после ударных испытаний при 100 °C, полученные методом РЭМ, после ТТО (*a*, *b*) и после ВТМО (*c*, *d*)

(Fig. 5). Non-metallic inclusions are commonly found at the bottom of the dimples, while delamination cracks are absent at these elevated temperatures.

Fig. 2, *b* shows the brittle fracture fraction across the temperature range from –196 to 100 °C, based on fractographic analysis. The T_{50} temperature, where the brittle fracture fraction reaches 50 %, is –9 °C for THT-treated EP-823 steel and –22 °C for HTMT-treated steel. These findings suggest that the transition in fracture mechanism occurs at higher temperatures in THT-treated steel compared to HTMT-treated steel.

Discussion of the results

After HTMT, a slight decrease in impact toughness and an increase in T_{dbt} are observed compared to THT (Fig. 2, *a*). This behavior is clearly related to the microstructural features of the steel formed as a result of HTMT. It has been shown [8] hat in EP-823 steel after THT, the microstructure consists of equiaxed prior-austenite grains containing martensitic blocks and lamellae. After HTMT, the prior-austenite grains and martensitic blocks become elongated in the rolling plane, with a reduction in their average cross-sectional size. Fig. 6 presents EBSD images of the microstructure (the EBSD method using SEM is described in detail in [8]) of EP-823 steel in a section parallel to the rolling plane (Fig. 6, *a*) and in a section perpendicular to the rolling plane (Fig. 6, *b*), along with a schematic representation of the microstructure indicating the direction of the pendulum impact used in this study. Notably, after HTMT, the average grain size in the transverse section (Fig. 6, *b*) decreases by a factor of 2.2 ($d \approx 1.4$ μm) compared to the corresponding value after THT ($d \approx 3.1$ μm) [8].

Numerous studies [20 – 23] have reported that reducing grain size leads to an increase in impact toughness. The formation of a high density of grain boundaries helps to retard quasi-cleavage crack propagation, thereby enhancing the material's toughness.

Another critical factor influencing impact toughness and T_{dbt}, is the test geometry relative to the layered structure formed during HTMT. When the impact direction is perpendicular to the layers (i.e., the rolling plane), the layered structure acts as a *crack – arrester*, inhibiting the propagation of the main crack and promoting the formation of secondary cracks along the layers (*crack – arrester – type delamination*) [20; 24 – 26]. This mechanism results in an increase in impact toughness and a decrease in T_{dbt}. Conversely, when the impact is applied along the layers, the crack propagates in a *crack – divider*, where the main crack splits mode (*crack – divider – type delamination*), leading to relatively low fracture toughness values [20 – 22; 24 – 26].

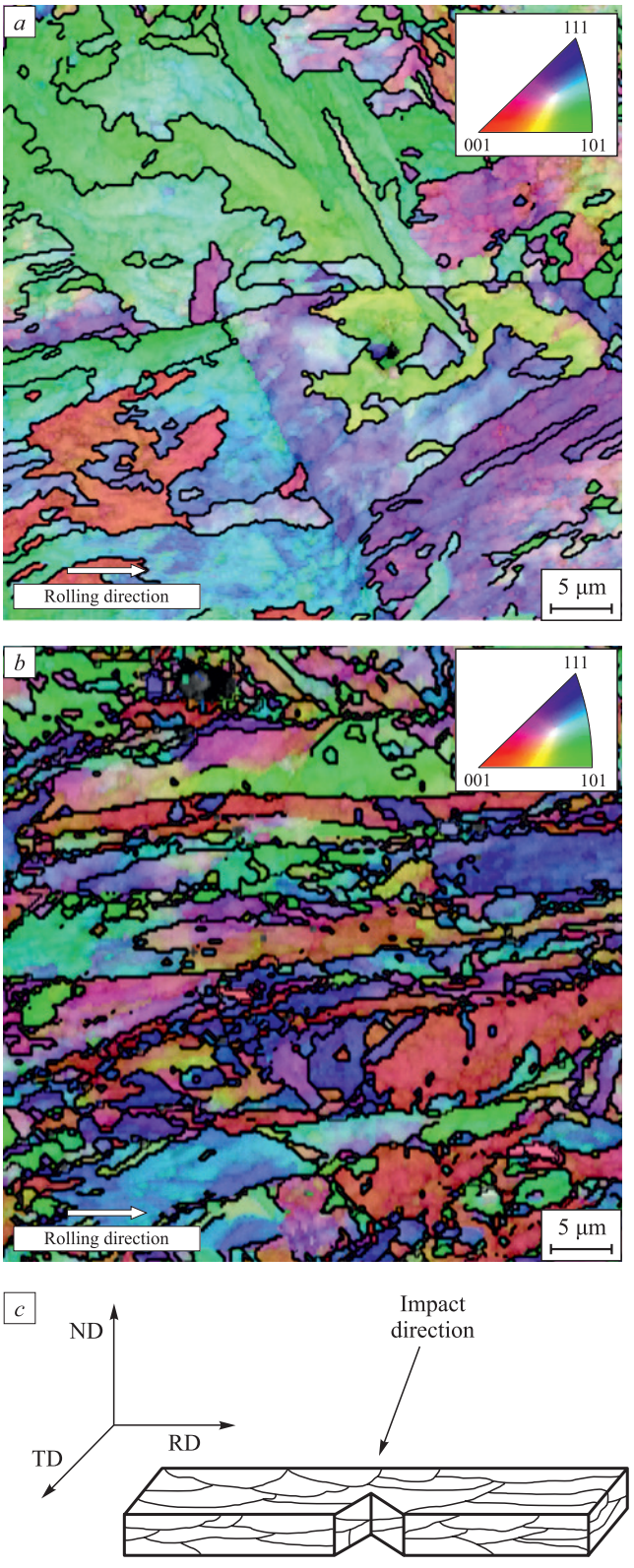

Fig. 6. Microstructure of EP-823 steel after HTMT, obtained by the SEM EBSD method:
a and *b* – in a section parallel and perpendicular to the rolling plane;
c – scheme of a sample for impact tests with illustrated layered structure

Рис. 6. Микроструктура стали ЭП-823 после ВТМО, полученная методом РЭМ EBSD:
a и *b* – в сечении, параллельном и перпендикулярном плоскости прокатки; *c* – схема образца для ударных испытаний с проиллюстрированной слоистой структурой

In the present case, the impact toughness of EP-823 steel after HTMT is determined by the interaction of two competing factors: the reduction in grain size compared to THT may contribute to an increase in impact toughness, while the formation of delamination cracks in the direction of the pendulum impact, parallel to the layered structure, tends to reduce it. The predominance of the second factor results in a slight reduction in impact toughness after HTMT and an increase in T_{dbt} compared to THT (Fig. 2, *a*).

Thus, despite the anisotropy of the microstructure formed after HTMT, the steel demonstrates satisfactory impact toughness under the selected unfavorable impact test geometry.

Conclusions

Based on Charpy impact tests conducted on EP-823 steel in structural states after THT and HTMT over the temperature range of –196 to 100 °C, the impact and the ductile-brittle transition temperature were determined. The results showed that after THT, $T_{dbt} \approx -45$ °C with $KCV \approx 36$ J/cm^2, while after HTMT, $T_{dbt} \approx -40$ °C, $KCV \approx 32$ J/cm^2.

Fractographic analysis using scanning electron microscopy revealed that in the low-temperature region ($T = -196$ °C), the steel exhibited a predominantly brittle fracture mode characterized by the transcrystalline quasi-cleavage mechanism. In the ductile-brittle transition region ($T = -70$ to 20 °C), a mixed fracture mode was observed, while at higher temperatures (50 – 100 °C), the fracture demonstrated a predominantly ductile character.

The slight reduction in impact toughness and the increase in T_{dbt} observed after HTMT, compared to THT, are attributed to the formation of multiple delamination cracks under the specific impact test geometry, where the impact direction is parallel to the planes of the layered structure.

Regardless of the treatment method (THT or HTMT), the investigated EP-823 steel demonstrates sufficiently low T_{dbt} values and satisfactory impact toughness, even under unfavorable impact test conditions.

References / Список литературы

1. Cabet C., Dalle F., Gaganidze E., Henry J., Tanigawa H. Ferritic-martensitic steels for fission and fusion applications. *Journal of Nuclear Materials*. 2019;523:510–537. https://doi.org/10.1016/j.jnucmat.2019.05.058
2. Yvon P. Structural Materials for Generation IV Nuclear Reactors. Amsterdam, Netherlands: Elsevier; 2017:664.
3. Odette R.G., Zinkle S.J. Structural Alloys for Nuclear Energy Applications. Amsterdam, Netherlands: Elsevier; 2019:655.
4. Zinkle S.J., Ghoniem N.M. Operating temperature windows for fusion reactor structural materials. *Fusion Engineering and Design*. 2000;51-52:55–71. https://doi.org/10.1016/S0920-3796(00)00320-3
5. Klueh R.L., Harries D.R. High-Chromium Ferritic and Martensitic Steels for Nuclear Applications. ASTM International; 2001:220. https://doi.org/10.1520/MONO3-EB
6. Yan W., Wang W., Shan Y., Yang K., Sha W. 9-12Cr Heat-Resistant Steels. Engineering Materials, Springer; 2015:223.
7. Ioltukhovsky A.G., Leontyeva-Smirnova M.V., Kazennov Y.I., Medvedeva E.A., Tselishchev A.V., Shamardin V.K., Povstyanko A.V., Ostrovsky S.E., Dvoryashin A.M., Porollo S.I., Vorobyev A.N., Khabarov V.S. Influence of operation conditions on structure and properties of 12 % Cr steels as candidate structural materials for fusion reactor. *Journal of Nuclear Materials*. 1998;258-263(2):1312–1318. https://doi.org/10.1016/S0022-3115(98)00396-1
8. Litovchenko I., Almaeva K., Polekhina N., Akkuzin S., Linnik V., Moskvichev E., Chernov V., Leontyeva-Smirnova M. The microstructure and mechanical properties of ferritic-martensitic steel EP-823 after high-temperature thermomechanical treatment. *Metals*. 2022;12(1):79. https://doi.org/10.3390/met12010079
9. Polekhina N.A., Litovchenko I.Y., Almaeva K.V., Tymentsev A.N., Chernov V.M., Leontieva-Smirnova M.V. Microstructure, structural-phase transformations, and mechanical properties of low-activation 12 % chromium ferritic-martensitic steel EK-181 depending on the treatment conditions. *Inorganic Materials*. 2022;13:1247–1260. https://doi.org/10.1134/S2075113322050355
10. Belomyttsev M.Yu., Molyarov V.G. Creep resistance of ferritic-martensitic steel 16Cr12MoWSiVNbB (EP-823). *Izvestiya. Ferrous Metallurgy*. 2019;62(4):290–302. (In Russ.). https://doi.org/10.17073/0368-0797-2019-4-290-302

Беломытцев М.Ю., Моляров В.Г. Исследование сопротивления ползучести феррито-мартенситной стали 16Х12МВСФБР (ЭП-823). *Известия вузов. Черная Металлургия*. 2019;62(4):290–302. https://doi.org/10.17073/0368-0797-2019-4-290-302
11. Vivas J., San-Martin D., Caballero F.G., Capdevila C. High-chromium (9–12Cr) steels: Creep enhancement by conventional thermo-mechanical treatments. In: *Metal Heat Treatments*. Intechopen; 2020:1–23. https://doi.org/10.5772/intechopen.91931
12. Polekhina N.A., Litovchenko I.Yu., Almaeva K.V., Akkuzin S.A., Linnik V.V., Moskvichev E.N., Chernov V.M., Naumenko I.A., Saifutdinova M.S., Leontieva-Smirnova M.V. Special features of the surface layer structure of ferritic-martensitic EP-823-Sh steel after prolonged exposure to the flowing lead at 630 °C under low oxygen concentration. *Journal of Nuclear Materials*. 2022;572:154039. https://doi.org/10.1016/j.jnucmat.2022.154039
13. Saini N., Pandey Ch., Mahapatra M.M., Narang H.K., Mulik R.S., Kumar P. A comparative study of ductile-brittle transition behavior and fractography of P91 and P92 steel. *Engineering Failure Analysis*. 2017;81:245–253. http://dx.doi.org/10.1016/j.engfailanal.2017.06.044
14. Abe F., Kern T.-U., Viswanathan R. Creep-Resistant Steels. Cambridge, UK: Woodhead; 2008;700.
15. Polekhina N., Linnik V., Litovchenko I., Almaeva K., Akkuzin S., Moskvichev E., Chernov V., Leontyeva-Smirnova M., Degtyarev N., Moroz K. The microstructure, tensile and impact

properties of low-activation ferritic-martensitic steel EK-181 after high-temperature thermomechanical treatment. *Metals*. 2022;12(11):1928. https://doi.org/10.3390/met12111928

16. Kurtz R.J., Odette G.R. Chapter 3 – Overview of reactor systems and operational environments for structural materials in fusion reactors. In: *Structural Alloys for Nuclear Energy Applications*. 2019:51–102. https://doi.org/10.1016/B978-0-12-397046-6.00003-4
17. Chatterjee A., Chakrabarti D., Moitra A., Mitra R., Bhaduri A.K. Effect of deformation temperature on the ductile-brittle transition behavior of a modified 9Cr-1Mo steel. *Materials Science and Engineering: A*. 2015;630:58–70. https://doi.org/10.1016/j.msea.2015.01.076
18. Chatterjee A., Chakrabarti D., Moitra A., Mitra R., Bhaduri A.K. Effect of normalization temperatures on ductile-brittle transition temperature of a modified 9Cr-1Mo steel. *Materials Science and Engineering: A*. 2014;618:219–231. https://doi.org/10.1016/j.msea.2014.09.021
19. Almaeva K.V., Litovchenko I.Yu., Polekhina N.A., Linnik V.V. Mechanisms of hardening of 12 % chromium ferritic-martensitic steel EP-823. *Izvestiya. Ferrous Metallurgy*. 2022;65(12):887–894. (In Russ.). https://doi.org/10.17073/0368-0797-2022-12-887-894

Алмаева К.В., Литовченко И.Ю., Полехина Н.А., Линник В.В. Механизмы упрочнения 12 %-ой хромистой ферритно-мартенситной стали ЭП-823. *Известия вузов. Черная Металлургия*. 2022;65(12):887–894. https://doi.org/10.17073/0368-0797-2022-12-887-894

20. Yuzbekova D., Dudko V., Pydrin A., Gaidar S., Mironov S., Kaibyshev R. Effect of tempforming on strength and toughness of medium-carbon low-alloy steel. *Materials*. 2023;16(3):1202. https://doi.org/10.3390/ma16031202
21. Haskel H.L., Pauletti E., Martins J.P., de Carvalho A.L.M. Microstructure and microtexture assessment of delamination phenomena in Charpy impact tested specimens. *Materials Research*. 2014;17(5):1238. http://dx.doi.org/10.1590/1516-1439.268314
22. Kimura Y., Inoue T. Influence of warm tempforming on microstructure and mechanical properties in an ultrahigh-strength medium-carbon low-alloy steel. *Metallurgical and Materials Transactions A*. 2013;44:560–576. http://dx.doi.org/10.1007/s11661-012-1391-2
23. Pallaspuro S., Kaijalainen A., Mehtonen S., Kömi J., Zhang Zh., Porter D. Effect of microstructure on the impact toughness transition temperature of direct-quenched steels. *Materials Science and Engineering: A*. 2018;712:671–680. https://doi.org/10.1016/j.msea.2017.12.037
24. Inoue T., Yin F., Kimura Y., Tsuzaki K., Ochiai S. Delamination effect on impact properties of ultrafine-grained low-carbon steel processed by warm caliber rolling. *Metallurgical and Materials Transactions: A*. 2010;41:341–355. https://doi.org/10.1007/s11661-009-0093-x
25. Kimura Y., Inoue T. Mechanical property of ultrafine elongated grain structure steel processed by warm tempforming and its application to ultrahigh-strength bolt. *ISIJ International*. 2020;60(6):1108–1126. https://doi.org/10.2355/isijinternational.ISIJINT-2019-726
26. Dolzhenko A., Kaibyshev R., Belyakov A. Tempforming as an advanced processing method for carbon steels. *Metals*. 2020;10(12):1566. https://doi.org/10.3390/met10121566

Information about the Authors / Сведения об авторах

Kseniya V. Spiridonova, *Cand. Sci. (Phys.-Math.), Research Associate of the Laboratory of Materials Science of Shape Memory Alloys*, Institute of Strength Physics and Materials Science, Siberian Branch of Russian Academy of Sciences
ORCID: 0000-0002-9181-4362
E-mail: almaevakv@ispms.ru

Igor' Yu. Litovchenko, *Dr. Sci. (Phys.-Math.), Assist. Prof., Head of the Laboratory of Materials Science of Shape Memory Alloys*, Institute of Strength Physics and Materials Science, Siberian Branch of Russian Academy of Sciences
ORCID: 0000-0002-5892-3719
E-mail: litovchenko@ispms.ru

Nadezhda A. Polekhina, *Cand. Sci. (Phys.-Math.)., Senior Researcher of the Laboratory of Materials Science of Shape Memory Alloys*, Institute of Strength Physics and Materials Science, Siberian Branch of Russian Academy of Sciences
ORCID: 0000-0001-9076-5469
E-mail: nadejda89tsk@yandex.ru

Valeriya V. Osipova, *Postgraduate*, National Research Tomsk State University
ORCID: 0000-0001-8975-1553
E-mail: lera.linnik.1999@mail.ru

Sergei A. Akkuzin, *Junior Researcher of the Laboratory of Materials Science of Shape Memory Alloys*, Institute of Strength Physics and Materials Science, Siberian Branch of Russian Academy of Sciences
ORCID: 0000-0002-2078-4194
E-mail: s.akkuzin@ispms.ru

Ксения Викторовна Спиридонова, *к.ф.-м.н., научный сотрудник лаборатории материаловедения сплавов с памятью формы,* Институт физики прочности и материаловедения Сибирского отделения РАН
ORCID: 0000-0002-9181-4362
E-mail: almaevakv@ispms.ru

Игорь Юрьевич Литовченко, *д.ф.-м.н., доцент, заведующий лабораторией материаловедения сплавов с памятью формы,* Институт физики прочности и материаловедения Сибирского отделения РАН
ORCID: 0000-0002-5892-3719
E-mail: litovchenko@ispms.ru

Надежда Александровна Полехина, *к.ф.-м.н., старший научный сотрудник лаборатории материаловедения сплавов с памятью формы,* Институт физики прочности и материаловедения Сибирского отделения РАН
ORCID: 0000-0001-9076-5469
E-mail: nadejda89tsk@yandex.ru

Валерия Васильевна Осипова, *аспирант,* Национальный исследовательский Томский государственный университет
ORCID: 0000-0001-8975-1553
E-mail: lera.linnik.1999@mail.ru

Сергей Александрович Аккузин, *младший научный сотрудник лаборатории материаловедения сплавов с памятью формы,* Институт физики прочности и материаловедения Сибирского отделения РАН
ORCID: 0000-0002-2078-4194
E-mail: s.akkuzin@ispms.ru

Vyacheslav M. Chernov, *Dr. Sci. (Phys.-Math.), Prof., Chief Researcher,* JSC "A.A. Bochvar High-Technology Scientific-Research Institute of Inorganic Materials"
ORCID: 0000-0002-9558-3055
E-mail: VMChernov@bochvar.ru

Вячеслав Михайлович Чернов, *д.ф.-м.н, профессор, главный научный сотрудник,* АО «Высокотехнологический научно-исследовательский институт неорганических материалов имени академика А.А. Бочвара»
ORCID: 0000-0002-9558-3055
E-mail: VMChernov@bochvar.ru

Contribution of the Authors

K. V. Spiridonova – conducting impact tests, data analysis, writing the text.
I. Yu. Litovchenko – scientific guidance, conceptualization, editing of the text.
N. A. Polekhina – conceptualization, conducting fractographic studies, editing the text.
V. V. Osipova – preparing samples for impact tests, analysis of results.

S. A. Akkuzin – conducting impact tests, analysis of results.

V. M. Chernov – editing the text.

Вклад авторов

К. В. Спиридонова – проведение ударных испытаний, анализ данных, написание текста статьи.
И. Ю. Литовченко – научное руководство, разработка концепции статьи, редактирование текста статьи.
Н. А. Полехина – разработка концепции статьи, проведение фрактографических исследований, редактирование текста статьи.
В. В. Осипова – подготовка образцов для ударных испытаний, анализ результатов.
С. А. Аккузин – проведение ударных испытаний, анализ результатов.
В. М. Чернов – редактирование текста статьи.

Received 07.10.2024
Revised 15.11.2024
Accepted 15.11.2024

Поступила в редакцию 07.10.2024
После доработки 15.11.2024
Принята к публикации 15.11.2024

PHYSICO-CHEMICAL BASICS OF METALLURGICAL PROCESSES / ФИЗИКО-ХИМИЧЕСКИЕ ОСНОВЫ МЕТАЛЛУРГИЧЕСКИХ ПРОЦЕССОВ

UDC 669
DOI 10.17073/0368-0797-2024-6-725-730

Original article
Оригинальная статья

Thermodynamic modeling of converter sludge sintering

E. V. Protopopov ✉, I. A. Rybenko, E. A. Belenetskii

Siberian State Industrial University (42 Kirova Str., Novokuznetsk, Kemerovo Region – Kuzbass 654007, Russian Federation)

✉ protopopov_ev@sibsiu.ru

Abstract. Currently, a promising area is the development of technologies for sintering or briquetting of converter sludge. Recycling of this sludge into production will allow solving a number of important tasks for modern metallurgy in the utilization of man-made waste, saving raw materials and reducing the cost of steel. The efficiency of utilizing useful components in the composition of briquettes is significantly higher than in any other state (in a fine or polydisperse fraction, in sorted form). In this paper, we consider the development and justification of an integrated approach to thermochemical sintering of converter sludge based on conditioning of iron-containing sludge by non-thermal adsorption dehydration and thermochemical sintering with simultaneous reduction of iron from oxides. Adsorption dehydration to a moisture content of 2 – 3 % is provided by a short-term contact of iron-containing slimes with a porous energy carrier, brown coal semi-coke, which is separated by pneumoseparation and sent for energy technological use, and the iron-containing product mixed with coals is subjected to thermo-oxidative coking. Coking is carried out in an annular furnace with a rotating hearth, where, when temperatures reach 1050 – 1100 °C, a large and durable lump material is formed with 55 – 60 % of the iron-containing product with almost complete reduction. Thermodynamic modeling of converter sludge sintering with coals was carried out. A tool for performing computational experiments using methods of thermodynamic modeling of the studied object was the Terra software package designed to calculate the thermodynamic properties and composition of the phases of equilibrium state of arbitrary systems with chemical and phase transformations. The results of thermodynamic modeling were fully confirmed by the experimental studies. The obtained material is an analog of ferrocox containing 35 – 39 % of iron and 45 – 49 % of carbon, while the zinc oxide content does not exceed 0.017 %.

Keywords: converter sludge, thermochemical sintering, thermodynamic modeling, instrumental system, ferrocoke

For citation: Protopopov E.V., Rybenko I.A., Belenetskii E.A. Thermodynamic modeling of converter sludge sintering. *Izvestiya. Ferrous Metallurgy*. 2024;67(6):725–730. https://doi.org/10.17073/0368-0797-2024-6-725-730

Термодинамическое моделирование процессов окускования конвертерного шлама

Е. В. Протопопов ✉, И. А. Рыбенко, Е. А. Беленецкий

Сибирский государственный индустриальный университет (Россия, 654007, Кемеровская обл. – Кузбасс, Новокузнецк, ул. Кирова, 42)

✉ protopopov_ev@sibsiu.ru

Аннотация. В настоящее время перспективным направлением является разработка технологий окускования или брикетирования конвертерных шламов. Рециклинг этих шламов в производство позволит решить ряд важнейших для современной металлургии задач утилизации техногенных отходов, экономии сырья и снижения себестоимости стали. Эффективность использования полезных компонентов в составе брикетов значительно выше, чем в каком-либо другом состоянии (в мелкой или полидисперсной фракции, в сортированном виде). В настоящей работе рассматриваются развитие и обоснование комплексного подхода термохимического окускования конвертерного шлама, основанного на кондиционировании железосодержащих шламов нетермическим адсорбционным обезвоживанием и термохимическим окускованием с одновременным восстановлением железа из оксидов. Адсорбционное обезвоживание до содержания влаги 2 – 3 % обеспечивается кратковременным контактом железосодержащих шламов с пористым энергоносителем – буроугольным полукоксом, который отделяется пневмосепарационным способом и направляется для энерготехнологического использования, а железосодержащий продукт в смеси с углями – на термоокислительное коксование. Коксование осуществляется в кольцевой печи с вращающимся подом, где при достижении температур 1050 – 1100 °С происходит формирование крупного и прочного кускового материала с 55 – 60 % железосодержащего продукта с практически полным восстановлением. Проведено термодинамическое моделирование процесса спекания конвертерного шлама с углями. Инструментом при выполнении вычислительных экспериментов с использованием методов термодинамического моделирования объекта исследования являлся программный комплекс «Терра», предназначенный для расчета термодинами-

ческих свойств и состава фаз равновесного состояния произвольных систем с химическими и фазовыми превращениями. Результаты термодинамического моделирования полностью подтвердили экспериментальные исследования. Полученный материал представляет собой аналог феррококса, содержащий 35 – 39 % железа и 45 – 49 % углерода, при этом содержание оксида цинка не превышает 0,017 %.

Ключевые слова: конвертерный шлам, термохимическое окускование, термодинамическое моделирование, инструментальная система, феррококс

Для цитирования: Протопопов Е.В., Рыбенко И.А., Беленецкий Е.А. Термодинамическое моделирование процессов окускования конвертерного шлама. *Известия вузов. Черная металлургия*. 2024;67(6):725–730. https://doi.org/10.17073/0368-0797-2024-6-725-730

Introduction

In modern practices, the oxygen-converter process plays a dominant role in global steelmaking [1 – 4]. The development and refinement of converter unit designs, coupled with accumulated knowledge on the use of combined melt blowing, have significantly enhanced the versatility of the converter process. This includes smelting technologies involving liquid-phase reduction of industrial waste and the use of multipurpose additives or briquettes [5 – 8].

Studies [9 – 12] indicate that steel production in oxygen converters generates approximately 12 – 25 kg of fine dust per ton of steel, which is a valuable iron-containing industrial by-product. For example, converter sludge from EVRAZ United West Siberian Metallurgical Plant JSC (EVRAZ ZSMK) contains up to 57 – 63 % Fe_2O_3 and 46.8 % total Fe [13]. Recycling this sludge back into production addresses critical metallurgical challenges, including waste utilization, raw material conservation, and steel production cost reduction [14 – 15]. However, despite the clear potential of converter sludge recycling, its direct introduction into the charge of oxygen converters or blast furnaces in fine-dispersed form is infeasible.

Iron-containing materials for the blast furnace or converter are typically introduced in lump form. Therefore, industrial waste (e.g., mill scale, dust, and dewatered sludge) is traditionally utilized, for instance, by adding it to charge [13]. However, introducing fine-particle materials into the charge in significant quantities is generally accompanied by a decrease in process productivity and a deterioration in the strength characteristics of the final sinter [14].

For this reason, the development of technologies for sintering or briquetting converter sludge remains a promising direction. Briquetting has several advantages: it enables the conversion of industrial waste with diverse chemical compositions and properties into standard products with controlled fraction sizes and technological characteristics. This increases the density of the composite material, prevents caking and blockages of fine waste in hoppers and dosing equipment, and reduces dust during transportation and use [14]. Moreover, the efficiency of utilizing valuable components in briquettes is significantly higher than in fine or polydisperse fractions, sorted forms, or other states.

Thus, briquetting converter sludge for subsequent recycling has distinct advantages over its use in sinter mix. However, the sludge must first undergo dehydration. Currently, various sludge dehydration methods exist, but they are typically bulky, complex, and energy-intensive, involving preliminary mechanical moisture removal (to below 20 – 25 %) through thickening or filtration, followed by thermal drying [14].

This paper proposes a new integrated approach to the thermochemical sintering of converter sludge, based on conditioning iron-containing sludge through non-thermal adsorption dehydration and thermochemical sintering with simultaneous reduction of iron from oxides.

Adsorption dehydration to a moisture content of 2 – 3 % is achieved by short-term contact between iron-containing sludge and a porous energy carrier – brown coal semi-coke (BCSC). After dehydration, BCSC is separated by pneumoseparation and directed for energy-technological use, while the iron-containing product, mixed with coal (grades GZh or Zh), undergoes thermo-oxidative coking in an annular furnace with a rotating hearth. At temperatures of 1050 – 1100 °C, a large, durable lump material is formed containing 55 – 60 % iron with almost complete reduction.

Brown coal semi-coke is a relatively new product for metallurgy, but numerous laboratory and industrial studies have demonstrated its effectiveness in pig iron and steel production, thermal energy generation, and recycling of high-moisture waste. In this case, BCSC is a low-ash, low-sulfur product with high energy potential and increased reactivity and adsorption capacity, making it suitable for preliminary dehydration of converter sludge [15; 16]. After preliminary dehydration, the proposed technological scheme suggests a thermochemical sintering method in a mixture with sinterable coals in an annular furnace with a rotating hearth.

Research methods

To address optimization tasks, thermodynamic modeling of the converter sludge sintering process with coals was conducted. The Terra software package, developed at Bauman Moscow State Technical University, was selected as the tool for computational experiments using thermodynamic modeling methods for the studied system. This software is designed to calculate the thermo-

dynamic properties and phase composition of equilibrium states in arbitrary systems with chemical and phase transformations [17; 18]. The program demonstrates consistently good convergence when modeling processes in elementary systems, including the direct reduction of metals in complex multicomponent heterogeneous systems [19; 20].

Computational experiments were conducted for two types of mixtures:

– 50 % Kuznetsk enrichment plant concentrate (coal grades Zh and GZh) and 50 % converter sludge;

– 50 % concentrate of grade Zh coal from the Mezhegey deposit and 50 % converter sludge.

The composition of the converter sludge is as follows (wt. %): Fe_2O_3 64.05; FeO 1.82; MgO 4.59; CaO 16.68; SiO_2 5.75; K_2O 0.19; V_2O_5 0.07; Cr_2O_3 0.10; C 0.63; S 0.24; ZnO 1.11; CuO 0.06; PbO 0.11; MnO 1.08; Al_2O_3 1.93; Na_2O 0.88; P_2O_5 0.32; TiO_2 0.21; W 1.35. The table below presents the characteristics of the coal concentrates, where W^r is moisture content; A^d is ash content; V^{daf} is volatile matter yield; S^d is sulfur content [14].

Characteristics of coal concentrates

Характеристика угольных концентратов

Concentrate	W^r, %	A^d, %	V^{daf}, %	S^d, %
GZh + Zh	10.5	7.8	38.0	0.56
Zh	8.6	8.1	38.2	0.67

Results and discussion

The results of the thermodynamic modeling (Fig. 1) were nearly identical for the tested conditions and demonstrated that the reduction of iron begins at a temperature of approximately 873 K. At temperatures above 1073 K, the chemical composition of the briquettes stabilizes. The iron content reaches a maximum of approximately 39 %, and the carbon content is 45 %. Additionally, the semi-product contains, (wt. %): CaO 6.9, MgO 4.3, $MgAl_2O_4$ 1.0. The briquette mass amounts to 0.6 kg per kg of the initial mixture.

The zinc and lead content drops to nearly zero at temperatures above 1073 K, as compounds of these elements presumably transition to the gas phase. Copper content remains at approximately 0.04 %. Other elements (titanium, chromium, vanadium, sodium, potassium) are present in the system in trace amounts as oxides (less than 0.1 %).

This information is fully supported by experimental studies, where the mixtures were heated in an annular furnace to a temperature of 1003 K and then in a Tamman furnace for 30 min at the final process temperature

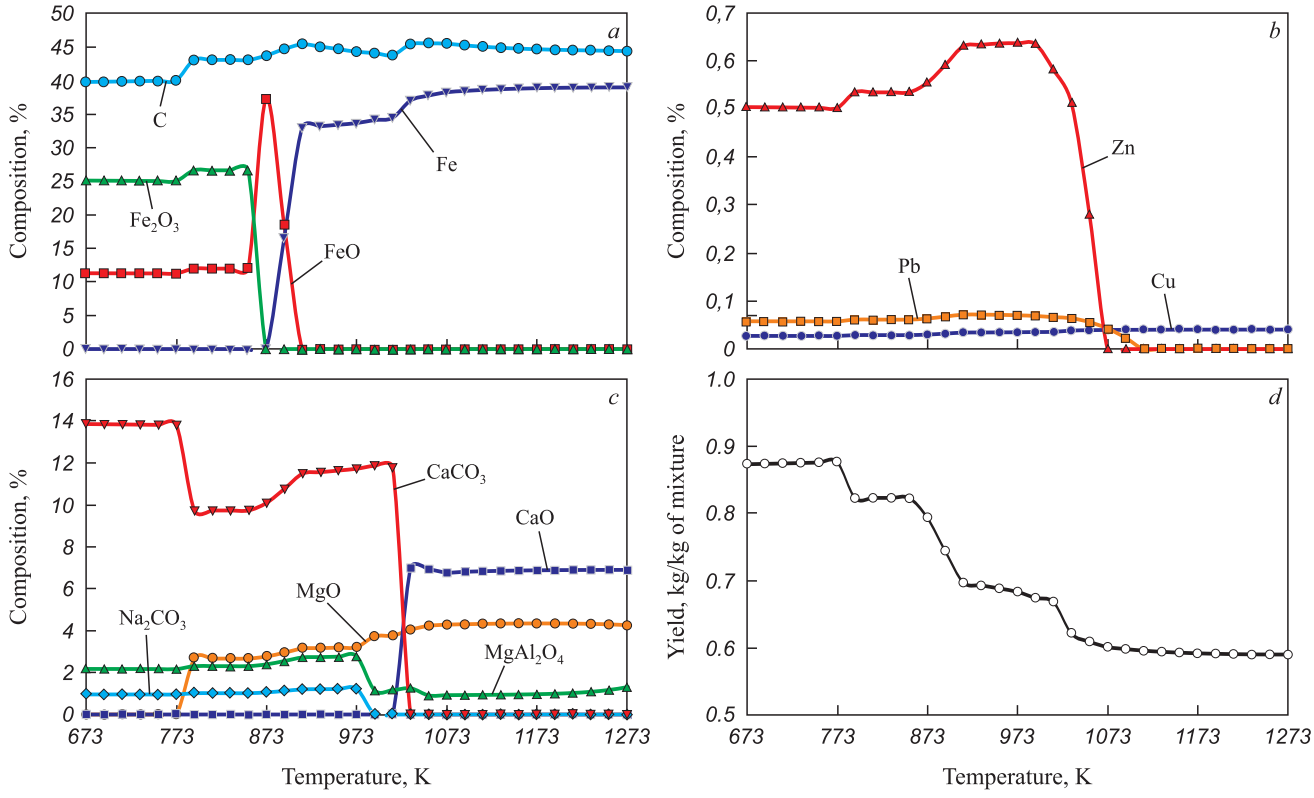

Fig. 1. Results of thermodynamic modeling of converter sludge sintering with coal

Рис. 1. Результаты термодинамического моделирования процесса спекания конвертерного шлама с углем

of 1373 K. The data indicate that the briquetted material resembles ferrocoke (Fig. 2), containing 35 – 39 wt. % Fe and 45 – 49 wt. % C, while the zinc oxide content does not exceed 0.017 wt. %.

Further studies using the Terra software investigated the parameters of the semi-product at various ratios of converter sludge to coal in the composite charge within a temperature range of 873 – 1273 K. The results (Fig. 3) indicate that the carbon content in the product stabilizes at temperatures above 1073 K, reaching 50, 45 and 27 % for converter sludge proportions of 40, 50 and 60 % in the charge, respectively. The iron content is 26.5 % for a sludge proportion of 40 % in the charge and remains nearly constant at approximately 39 – 40 % for sludge proportions of 50 and 60 % at temperatures above 1073 K. Similar trends are observed for the yield of ferrocoke-type briquettes as a function of temperature at different ratios of charge components. The yield of the semi-product at the final reduction temperatures is 0.6 kg per kg of charge for a sludge proportion of up to 40 %. For sludge proportions of 50 and 60 %, the product yield shows only slight variation, ranging between 0.67 and 0.69 kg per kg of charge.

Thus, the optimal ratio of converter sludge to charge for achieving the desired yield and composition of the semi-product should be 1:1. Increasing the proportion of sludge in the charge results in only minor changes to the amount of reduced iron and product yield; however, it leads to a decrease in carbon content in the semi-product.

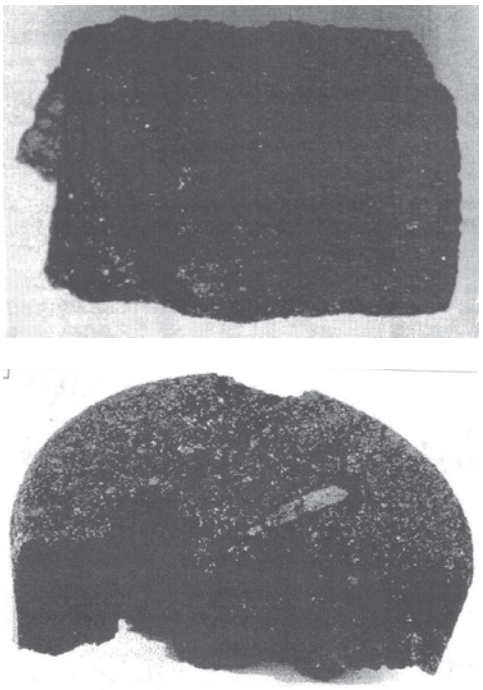

Fig. 2. Experimental samples of ferrocox briquettes

Рис. 2. Опытные образцы брикетов типа феррококса

The practical application of the resulting briquettes lies in their use as additives to the charge in the converter process, serving as an iron-containing material, an additional heat carrier, and a reducing agent.

Conclusions

The issues of thermochemical sintering of converter sludge with simultaneous iron reduction from oxides were analyzed. Thermodynamic and physical modeling of the processes of sludge sintering with various coals allowed us to consider the resulting material as an effec-

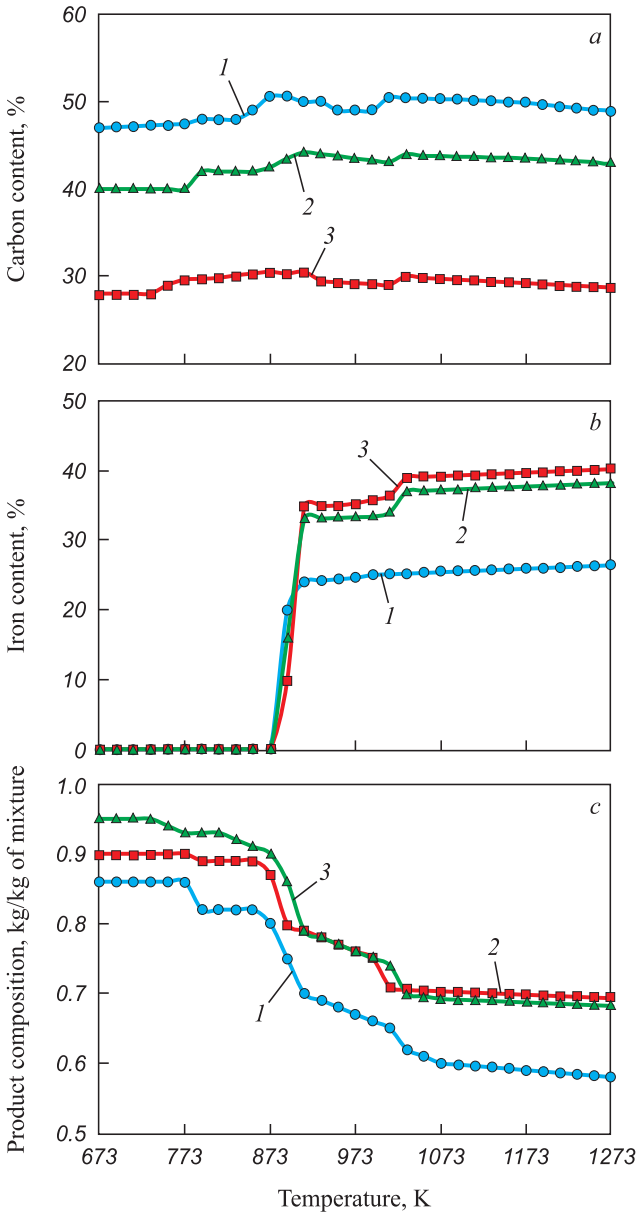

Fig. 3. Results of the study of converter sludge sintering with coal using the Terra software package:
1 – 40 %; *2* – 50 %; *3* – 60 %

Рис. 3. Результаты исследования процесса спекания конвертерного шлама с углем с использованием программного комплекса «Терра»:
1 – 40 %; *2* – 50 %; *3* – 60 %

tive heat carrier and reducing agent for converter smelting. The rational composition of the initial charge for composite briquettes of the ferrocox type was determined.

References / Список литературы

1. Budanov I.A., Ustinov V.S. Prospects for development of metallurgical production in Russia. *Ferrous Metallurgy. Bulletin of Scientific, Technical and Economic Information*. 2014;(5(1373)):3–12. (In Russ.).

   Буданов И.А., Устинов В.С. Перспективы развития металлургического производства в России. *Черная металлургия. Бюллетень научно-технической и экономической информации*. 2014;(5(1373)):3–12.
2. Grigorovich K.V. Current state of ferrous metallurgy and directions of its development in digital economy. In: *Proceedings of the XV Int. Congress of Steelmakers and Metal Manufacturers*. 2018:42–59. (In Russ.).

   Григорович К.В. Современное состояние черной металлургии и направления ее развития в цифровой экономике. В кн.: *Сборник трудов XV международного Конгресса сталеплавильщиков и производителей металла*. 2018:42–59.
3. Brun L.C. Overcapacity in Steel: China's Role in Global Problem. Center of Globalization, Governance & Competitiveness, Duke University; 2016:54.
   https://doi.org/10.13140/RG.2.2.11923.48161
4. Osaba E., Carballedo R., Diaz F., Perallos A. Simulation tool based on a memetic algorithm to solve a real instance of a dynamic TSP. In: *Proceedings of IASTED Int. Conf. of Applied Simulation and Modelling*. 2012:27–33.
   https://doi.org/10.2316/P.2012.776-029
5. Sakthivel R., Vasumathi N., Sahu D., Mishra B.K. Synthesis of magnetite powder from iron ore tailings. *Powder Technology*. 2010;201(2):187–190.
   https://doi.org/10.1016/j.powtec.2010.03.005
6. Sanakulov K. Scientific-Technical Basis of Processing Mining-Metallurgical Wastes. Tashkent: FAN; 2009:404.

   Санакулов К. Научно-технические основы переработки отходов горно-металлургического производства. Ташкент: ФАН; 2009:404.
7. Yusupkhodjayev A.A. Theory Waste Free Technology on the Ferrous Metallurgy. Tashkent: TSTU; 2017:4.
8. Jiabin C., Wenlong J., Lianghui Y. Survey and evaluation of the iron tailings resources in China. *Mineral Resources Development*. 2010;(3):60–62.
9. Yusupkhodzhaev A.A., Valiev Kh.R., Khudoyarov S.R., Matkarimov S.T. Efficiency rise of steel making production via additional recovery of valuable components from utilized slags. *Chernye metally*. 2015;(1):19–22.

   Юсупходжаев А.А., Валиев Х.Р., Худояров С.Р., Маткаримов С.Т. Повышение эффективности сталеплавильного производства доизвлечением ценных компонентов из утилизируемых шлаков. *Черные металлы*. 2015;(1):19–22.
10. Chong Y.T., Teo K.M., Tang L.C. A lifecycle-based sustainability indicator framework for waste-to-energy systems and a proposed metric of sustainability. *Renewable and Sustainable Energy Reviews*. 2016;56:797–809.
    https://doi.org/10.1016/j.rser.2015.11.036
11. Su F., Lampinen H.-O., Robinson R. Recycling of sludge and dust to the BOF converter by cold bonded pelletizing. *ISIJ International*. 2004;44(4):770–776.
    https://doi.org/10.2355/isijinternational.44.770
12. Matsubae-Yokoyama K., Kubo H., Nagasaka T. Recycling effects of residual slag after magnetic separation for phosphorus recovery from hot metal dephosphorization slag. *ISIJ International*. 2009;95(3):306–312.
    https://doi.org/10.2355/tetsutohagane.95.306
13. Volynkina E.P., Kuznetsov S.N., Protopopov E.V., etc. Metallurgical Technologies for Processing Technogenic Deposits of Industrial and Household Waste. Novosibirsk: Publishing House of the SB RAS; 2014:294. (In Russ.).

    Металлургические технологии переработки техногенных месторождений промышленных и бытовых отходов / Е.П. Волынкина, С.Н. Кузнецов, Е.В. Протопопов и др. Новосибирск: Изд-во СО РАН; 2014:294.
14. Kuznetsov S.N., Shkoller M.B., Protopopov E.V., Temlyantsev M.V., Feiler S.V. Technological basics of adsorption dehydration and thermochemical sintering of BOF sludge. *Izvestiya. Ferrous Metallurgy*. 2017;60(4):268–275. (In Russ.).
    https://doi.org/10.17073/0368-0797-2017-4-268-275

    Кузнецов С.Н., Школлер М.Б., Протопопов Е.В., Темлянцев М.В., Фейлер С.В. Технологические основы адсорбционного обезвоживания и термохимического окускования конверторных шламов. *Известия вузов. Черная металлургия*. 2017;60(4):268–275.
    https://doi.org/10.17073/0368-0797-2017-4-268-275
15. Shkoller M.B. Research and development of a method for recycling high-moisture and high-ash coal sludge. In: *Modeling and High-Tech Information Technologies in Technical and Socio-Economic Systems. Proceedings of the V Int. Sci. and Pract. Conf*. Novokuznetsk: IC SibSIU; 2021:213–217. (In Russ.).

    Школлер М.Б. Исследование и разработка способа рециклинга высоковлажных и высокозольных угольных шламов. В сб.: *Моделирование и наукоемкие информационные технологии в технических и социально-экономических системах. Труды V Международной научно-практической конференции*. Новокузнецк: ИЦ СибГИУ; 2021:213–217.
16. Shkoler M.B. Theory and Practice of Using Fine-Grained Semi-Coke from Brown Coals to Produce Various Grades of Coke, Process Fuels, Composites and Solid Waste Recycling. Role: Open Science Publishing; 2019:134. (In Russ.).

    Школлер М.Б. Основы теории и практики использования мелкозернистого полукокса из бурых углей для получения разных сортов кокса, технологического топлива, композитов и рециклинга твердых отходов. Роли: Open Science Publishing; 2019:134.
17. Belov G.V., Trusov B.G. Thermodynamic Modeling of Chemically Reacting Systems. Moscow: Bauman MSTU; 2013;96. (In Russ.).

    Белов Г.В., Трусов Б.Г. Термодинамическое моделирование химически реагирующих систем. Москва: Изд. МГТУ им. Н.Э. Баумана; 2013;96.
18. Belov G.V. Thermodynamic Modeling: Methods, Algorithms, Programs. Moscow: Nauchnyi Mir; 2002:184. (In Russ.).

Белов Г.В. Термодинамическое моделирование: методы, алгоритмы, программы. Москва: Научный Мир; 2002:184.

19. Rybenko I.A. Thermodynamic Modeling of Processes in Elementary Systems. Novokuznetsk: SibSIU; 2016:97. (In Russ.).

Рыбенко И.А. Термодинамическое моделирование процессов в элементарных системах. Новокузнецк: Изд. центр СибГИУ; 2016:97.

20. Rybenko I.A. Development of optimal technological modes for the production of metals using mathematical modeling methods and instrumental systems. *Ferrous Metallurgy. Bulletin of Scientific, Technical and Economic Information*. 2018;(2):57–61. (In Russ.).

Рыбенко И.А. Разработка оптимальных технологических режимов получения металлов с использованием методов математического моделирования и инструментальных систем. *Черная металлургия. Бюллетень научно-технической и экономической информации*. 2018;(2):57–61.

Information about the Authors / Сведения об авторах

Evgenii V. Protopopov, *Dr. Sci. (Eng.), Prof. of the Chair of Ferrous Metallurgy and Chemical Technology*, Siberian State Industrial University
ORCID: 0000-0002-7554-2168
E-mail: protopopov@sibsiu.ru

Евгений Валентинович Протопопов, *д.т.н., профессор кафедры металлургии черных металлов и химической технологии*, Сибирский государственный индустриальный университет
ORCID: 0000-0002-7554-2168
E-mail: protopopov@sibsiu.ru

Inna A. Rybenko, *Prof., Head of the Chair of Applied Information Technologies and Programming*, Siberian State Industrial University
ORCID: 0000-0003-1679-0839
E-mail: rybenkoi@mail.ru

Инна Анатольевна Рыбенко, *д.т.н., профессор, заведующий кафедрой прикладных информационных технологий и программирования*, Сибирский государственный индустриальный университет
ORCID: 0000-0003-1679-0839
E-mail: rybenkoi@mail.ru

Evgenii A. Belenetskii, *MA Student of the Chair of Ferrous Metallurgy and Chemical Technology*, Siberian State Industrial University
E-mail: info@vpk-oil.ru

Евгений Анатольевич Беленецкий, *магистрант кафедры металлургии черных металлов и химической технологии*, Сибирский государственный индустриальный университет
E-mail: info@vpk-oil.ru

Contribution of the Authors / Вклад авторов

E. V. Protopopov – technological description of the task, justification of the research direction, analysis of the results.

I. A. Rybenko – conducting thermodynamic calculations, processing calculation results.
E. A. Belenetskii – conducting thermodynamic calculations, processing calculation results.

Е. В. Протопопов – технологическое описание поставленной задачи, обоснование направления исследований, анализ полученных результатов.
И. А. Рыбенко – проведение термодинамических расчетов, обработка результатов расчетов.
Е. А. Беленецкий – проведение термодинамических расчетов, обработка результатов расчетов.

Received 13.09.2024
Revised 03.10.2024
Accepted 10.10.2024

Поступила в редакцию 13.09.2024
После доработки 03.10.2024
Принята к публикации 10.10.2024

Innovation in metallurgical industrial and laboratory equipment, technologies and materials / **Инновации в металлургическом промышленном и лабораторном оборудовании, технологиях и материалах**

UDC 621.891
DOI 10.17073/0368-0797-2024-6-731-734

Short Report
Краткое сообщение

Improving operation of a drawing mill

A. G. Nikitin[1], A. R. Fastykovskii[1], S. P. Gerasimov[2]

[1] **Siberian State Industrial University** (42 Kirova Str., Novokuznetsk, Kemerovo Region – Kuzbass 654007, Russian Federation)
[2] **JSC "EVRAZ – Joint West Siberian Metallurgical Plant"** (16 Kosmicheskoe Route, Kemerovo Region – Kuzbass 654007, Russian Federation)

nikitin1601@yandex.ru

Abstract. The report considers the purpose of drawing mills and possible violations of the technological process associated with the design flaws of drawing mill drive. We analyzed the design of a planetary gearbox with a common carrier used in the drive of the stretching drum of a drawing mill. During the operation of such a transmission, there are disadvantages: due to the imbalance of links of the mechanism relative to the central axis, additional dynamic forces arise. This design transmits movement from the leading link to the carrier only through one satellite, the teeth of which perceive all the force transmitted by the torque, which reduces the reliability of the gearbox and the drive as a whole. The design of a three-satellite balanced self-aligning planetary gearbox, free from these disadvantages, is described.

Keywords: drawing mill, drive, planetary gearbox, torque, dynamic force, carrier, satellite, reliability

For citation: Nikitin A.G., Fastykovskii A.R., Gerasimov S.P. Improving operation of a drawing mill. *Izvestiya. Ferrous Metallurgy*. 2024;67(6): 731–734. https://doi.org/10.17073/0368-0797-2024-6-731-734

Совершенствование работы волочильного стана

А. Г. Никитин[1], А. Р. Фастыковский[1], С. П. Герасимов[2]

[1] **Сибирский государственный индустриальный университет** (Россия, 654007, Кемеровская обл. – Кузбасс, Новокузнецк, ул. Кирова, 42)
[2] **АО «ЕВРАЗ Объединенный Западно-Сибирский металлургический комбинат»** (Россия, 654043, Кемеровская обл. – Кузбасс, Новокузнецк, ш. Космическое, 16)

nikitin1601@yandex.ru

Аннотация. В сообщении рассматривается назначение волочильных станов и возможные нарушения технологического процесса, связанные с недостатками конструкции привода волочильного барабана. Проведен анализ конструкции планетарного редуктора с общим водилом, используемым в приводе протягивающего барабана волочильного стана. В процессе работы такой передачи возникают недостатки: из-за неуравновешенности звеньев механизма относительно центральной оси возникают дополнительные динамические силы. Такая конструкция передает движение от ведущего звена на водило лишь через один сателлит, зубья которого воспринимают всю силу, передаваемую крутящим моментом, что снижает надежность редуктора и привода в целом. Описана конструкция трехсателлитного уравновешенного самоустанавливающегося планетарного редуктора, свободного от указанных недостатков.

Ключевые слова: волочильный стан, привод, планетарный редуктор, крутящий момент, динамическая сила, водило, сателлит, надежность

Для цитирования: Никитин А.Г., Фастыковский А.Р., Герасимов С.П. Совершенствование работы волочильного стана. *Известия вузов. Черная металлургия*. 2024;67(6):731–734. https://doi.org/10.17073/0368-0797-2024-6-731-734

Drawing represents the fourth stage of metallurgical production and is used to create cold-drawn products such as wire, shaped profiles, and tubes. The process involves pulling an initial billet through a tapered channel in the drawing die under the influence of a pulling force. This reduces the cross-section of the material, shaping it to match the die's outlet. Drawing dies are manufactured with high precision using tungsten carbide hard alloys.

The drawing process is performed in a cold state with mandatory lubrication. The stability of the drawing process, product quality, and scrap generation largely depend on the application of the external force needed to execute the operation. This force is supplied by the drum of the drawing mill, which is typically driven by an electric motor through a cylindrical gearbox. The drum drive system plays a critical role in influencing friction conditions in the die, ensuring stable load application during acceleration and steady-state operation, and ultimately determining the overall feasibility of the drawing process [1; 2].

Currently, the drawing process is used to produce wires, small-diameter tubes, and certain types of specialized profiles. The primary equipment for this operation is the drawing mill, whose main components include the die and the stretching drum. The drum receives rotation from an electric motor via a gearbox [3; 4].

An analysis of the AZTM VN 2-550 drawing mill, operated in the steel rolling shop of EVRAZ United West-Siberian Metallurgical Plant JSC (EVRAZ ZSMK), identified the need for modernization to extend its service life and enhance productivity. The modernization involved replacing the existing drive system – comprising two bevel gears, a cylindrical gearbox, and a belt transmission – with a three-satellite planetary gearbox, model MPO-1M-10-5.74-7.5/250 [5].

However, the newly installed three-satellite planetary gearbox with a common carrier exhibited significant shortcomings. The imbalance of the transmission components relative to the central axis caused additional dynamic forces. Furthermore, the design transmitted motion from the driving link to the carrier through a single satellite, whose teeth bore the full torque-transmitted load. These drawbacks reduced the reliability of the gearbox and the drive system overall [6; 7]. Consequently, critical technological challenges remained unresolved, such as shortening profile changeover times, achieving smooth acceleration to steady-state drawing speeds, and reducing the occurrence of breakages.

To address these shortcomings, researchers at the Siberian State Industrial University developed a design for a three-satellite balanced self-aligning planetary gearbox [8] (see Figure).

The three-satellite planetary gearbox consists of a central input drive wheel (1), satellites (*2 – 4*), an output link (carrier) (*5*), three-pair articulated levers (*6*, *7*), and a central wheel with internal teeth (*8*), around which motion occurs. Since the mass centers of the three-pair articulated levers are located along the axes of the satellites they connect, the system becomes balanced, reducing dynamic forces in the gear meshing zones.

The three-satellite balanced planetary gearbox operates as follows: rotation from the electric motor is transmitted to the central input drive wheel (*1*), which evenly transfers motion to all satellites (*2 – 4*) through the three-pair articulated levers (*6*, *7*) connected with the output

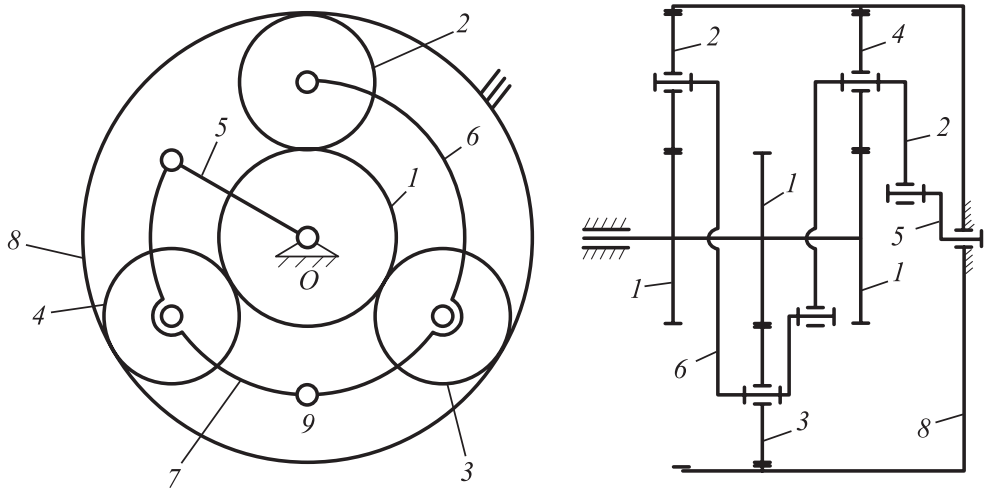

a *b*

General view (*a*) and kinematic scheme (*b*) of a balanced three-satellite planetary transmission:
1 – central input drive wheel; *2 – 4* – satellites; *5* – output link (carrier);
6, *7* – three-pair articulated levers, which are connected with satellites *2 – 4* and with the carrier *5* by five rods;
8 – central wheel with internal teeth; *9* – additional hinge

Общий вид (*a*) и кинематическая схема (*b*) уравновешенной трехсателлитной планетарной передачи:
1 – центральное входное ведущее колесо; *2 – 4* – сателлиты; *5* – выходное звено (водило);
6, *7* – трехпарные шарнирные рычаги, которые пятью шарнирами соединены с сателлитами *2 – 4* и с водилом *5*;
8 – центральное колесо с внутренними зубьями; *9* – дополнительный шарнир

link (carrier) (*5*). In this process, the torque from the central input drive wheel (*1*) is uniformly distributed among all satellites.

The mobility of the developed gearbox design is determined using P.L. Chebyshev's formula:

$$W = 3n - 2p_5 - p_4,$$

where W is the degrees of freedom (mobility) of the mechanism; n is the number of links; p_5 and p_4 are the numbers of fifth-class (hinge) and fourth-class (gear meshing) pairs.

The kinematic chain of the transmission contains seven links ($n = 7$), connected by seven hinges ($p_5 = 7$) and six gear meshes ($p_4 = 6$). Substituting these values yields $W = 1$. This indicates that the planetary transmission is statically determinate, and all three satellites reliably participate in transmitting power from the central wheel to the output link. This reduces forces and, consequently, stresses in the gear teeth.

Integrating the three-satellite balanced self-aligning planetary gearbox into the drawing mill drive system can significantly reduce profile changeover times, lower scrap rates and downtime caused by breakages, increase drawing speed, and enhance the overall productivity of the drawing mill.

Conclusions

The analysis of the drawing mill operation revealed that to improve its productivity, the drive of the drawing drum must be modernized. The developed design of the drawing mill drive, featuring a three-satellite balanced self-aligning planetary transmission, extends the service life, reduces profile changeover time, increases drawing speed, minimizes equipment downtime due to failures, and decreases scrap rates, thereby enhancing the overall productivity of the mill.

References / Список литературы

1. Rodionova L.V., Rodionova A.A. The current situation and perspectives the development of wire-drawing steel wire. *Mashinostroenie*. 2013;1(1):3–11. (In Russ.).

   Родионова Л.В., Родионова А.А. Современное состояние и перспективы развития волочильного производства стальной проволоки. *Машиностроение*. 2013;1(1):3–11.
2. Vega G., Haddi A., Imad A. Investigation of process parameters effect on the copper-wire drawing. *Materials and Design*. 2009;30(8):3308–3312. https://doi.org/10.1016/j.matdes.2008.12.006
3. Pertsikov Z.I. Drawing Mills. Moscow: Metallurgiya; 1986:208. (In Russ.).

   Перциков З.И. Волочильные станы. Москва: Металлургия; 1986:208.
4. Haddi A., Imad A., Vega G. Analysis of temperature and speed effects on the drawing stress for improving the wire drawing process. *Materials and Design*. 2011;32(8-9): 4310–4315. https://doi.org/10.1016/j.matdes.2011.04.010
5. Nikitin A.G., Bazhenov I.A., Gerasimov S.P. Analysis of the drawing mill drive operation. *Izvestiya. Ferrous Metallurgy*. 2022;65(6):434–436. (In Russ.). https://doi.org/10.17073/0368-0797-2022-6-434-436

   Никитин А.Г., Баженов И.А., Герасимов С.П. Анализ эксплуатационного ресурса привода волочильного стана. *Известия вузов. Черная металлургия*. 2022;65(6): 434–436. https://doi.org/10.17073/0368-0797-2022-6-434-436
6. Lai T.-S. Design and machining of the epicycloid planetary gear of cycloid drives. *The International Journal of Advanced Manufacturing Technology*. 2006;28(7-8):665–670. https://doi.org/10.1007/s00170-004-2423-x
7. Yang B.-D., Meng C.-H. Modeling of friction contact and its application to the designing of shroud contact. *Journal of Engineering for Gas Turbines and Power*. 1997;119(4):958–963. https://doi.org/10.1115/1.2817082
8. Dvornikov L.T., Gerasimov S.P. The method of assembling a multi-satellite balanced planetary transmission. Pat. 2526738 RF. *Bulleten' izobretenii*. 2020;22.

   Пат. 2526738 РФ. Способ сборки многосателлитной уравновешенной планетарной передачи / Л.Т. Дворников, С.П. Герасимов; заявл. 09.01.2020, опубл. 31.07.2020.

Information about the Authors / Сведения об авторах

Aleksandr G. Nikitin, *Dr. Sci. (Eng.), Prof. of the Chair of Mechanics and Machine Engineering*, Siberian State Industrial University
ORCID: 0000-0001-9198-6386
E-mail: nikitin1601@yandex.ru

Andrei R Fastykovskii, *Dr. Sci. (Eng.), Assist. Prof., Prof. of the Chair of Metal Forming and Metal Science. OJSC "EVRAZ ZSMK"*, Siberian State Industrial University
ORCID: 0000-0001-9259-9038
E-mail: omd@sibsiu.ru

Semen P. Gerasimov, *Senior Technician on Equipment Repair*, JSC "EVRAZ – Joint West Siberian Metallurgical Plant"
ORCID: 0000-0001-5012-2565
E-mail: knikitos@mail.ru

Александр Григорьевич Никитин, *д.т.н., профессор кафедры механики и машиностроения*, Сибирский государственный индустриальный университет
ORCID: 0000-0001-9198-6386
E-mail: nikitin1601@yandex.ru

Андрей Ростиславович Фастыковский, *д.т.н., доцент, профессор кафедры «Обработка металлов давлением и металловедение. ЕВРАЗ ЗСМК»*, Сибирский государственный индустриальный университет
ORCID: 0000-0001-9259-9038
E-mail: omd@sibsiu.ru

Семен Павлович Герасимов, *старший мастер по ремонту оборудования*, АО «ЕВРАЗ Объединенный Западно-Сибирский металлургический комбинат»
ORCID: 0000-0001-5012-2565
E-mail: knikitos@mail.ru

Contribution of the Authors

A. G. Nikitin – formation of the basic concept, formulation of conclusions, scientific guidance.
A. R. Fastykovskii – revision of the text, correction of conclusions, discussion of the experiments.
S. P. Gerasimov – performing the experiments, writing the text.

Вклад авторов

А. Г. Никитин – формирование основной концепции, формулирование выводов, научное руководство.
А. Р. Фастыковский – доработка текста, корректировка выводов, обсуждение экспериментальной части.
С. П. Герасимов – выполнение экспериментальной части работы, написание текста.

Received 27.12.2023
Revised 12.09.2024
Accepted 17.10.2024

Поступила в редакцию 27.12.2023
После доработки 12.09.2024
Принята к публикации 17.10.2024

Innovation in metallurgical industrial and laboratory equipment, technologies and materials

Инновации в металлургическом промышленном и лабораторном оборудовании, технологиях и материалах

UDC 669.187
DOI 10.17073/0368-0797-2024-6-735-737

Short report
Краткое сообщение

Re-engineering of ball mill at Novotroitsk Plant of Chromium Compounds

A. V. Nefedov[1], R. E. Ishmukhametov[1], N. A. Chichenev[2]

[1] **Novotroitsk Branch of the National University of Science and Technology "MISIS"** (8 Frunze Str., Novotroitsk, Orenburg Region 426359, Russian Federation)
[2] **National University of Science and Technology "MISIS"** (4 Leninskii Ave., Moscow 119049, Russian Federation)

chich38@mail.ru

Abstract. Novotroitsk Plant of Chromium Compounds (NPCC) specializes in the processing of chromite and dolomite ores. Operating experience showed that the loss of operability of the ball mill installed in this workshop leads to unplanned downtime due to the failure of drive elements, which account for 11.3 % of the rated operating time of the workshop. To improve the reliability of technological equipment, it was proposed to replace the existing electric drive with a modern geared motor, which transmits rotation to the mill drum through a gear coupling. As a result of the new drive engineering, it was possible to simplify its design and reduce the labor intensity of maintenance and repair. Additional capital expenditures do not exceed RUB 3.4 million and pay off in less than 3 months.

Keywords: foundry, beneficiation production, crushing and grinding processes, tube ball mill, electromechanical drive, geared motor

For citation: Nefedov A.V., Ishmukhametov R.E., Chichenev N.A. Re-engineering of ball mill at Novotroitsk Plant of Chromium Compounds. *Izvestiya. Ferrous Metallurgy*. 2024;67(6):735–737. https://doi.org/10.17073/0368-0797-2024-6-735-737

Реинжиниринг шаровой мельницы Новотроицкого завода хромовых соединений

А. В. Нефедов[1], Р. Э. Ишмухаметов[1], Н. А. Чиченев[2]

[1] **Новотроицкий филиал Национального исследовательского технологического университета «МИСИС»** (Россия, 426359, Оренбургская обл., Новотроицк, ул. Фрунзе, 8)
[2] **Национальный исследовательский технологический университет «МИСИС»** (Россия, 119049, Москва, Ленинский пр., 4)

chich38@mail.ru

Аннотация. Новотроицкий завод хромовых соединений специализируется на переработке хромитовых и доломитовых руд. Опыт эксплуатации показал, что потеря работоспособности шаровой мельницы, установленной в данном цехе, приводит к незапланированным простоям из-за отказа элементов привода, которые составляют 11,3 % от номинального времени работы цеха. Для повышения надежности технологического оборудования предложена замена действующего электропривода на современный мотор-редуктор, передающий вращение барабану мельницы через зубчатую муфту. В результате разработки нового привода удалось упростить его конструкцию и уменьшить трудоемкость технического обслуживания и ремонта. Дополнительные капитальные затраты не превышают 3,4 млн руб и окупаются менее, чем за три месяца.

Ключевые слова: обогатительное производство, процессы дробления и измельчения, трубчатая шаровая мельница, электромеханический привод, мотор-редуктор

Для цитирования: Нефедов А.В., Ишмухаметов Р.Э., Чиченев Н.А. Реинжиниринг шаровой мельницы Новотроицкого завода хромовых соединений. *Известия вузов. Черная металлургия*. 2024;67(6):735–737. https://doi.org/10.17073/0368-0797-2024-6-735-737

Modern metallurgical enterprises place significant emphasis on re-engineering existing equipment [1 – 3]. This includes the introduction of advanced technologies, automation of metallurgical process management using modern computer systems, improvements in labor organization, and enhancement of personnel qualifications [4 – 6].

Novotroitsk Plant of Chromium Compounds (NPCC) specializes in the processing of chromite ore. After the initial crushing of large pieces, the ore is transported via conveyor to a dry grinding mill, where chromite and dolomite ores are ground. From the ball mill, the material is conveyed to the next elevator and, finally, to a hopper in the batch preparation area.

Currently, the grinding section operates a ball mill model SMM2061, equipped with a 4A series electric motor, which is now discontinued, and a special gearbox. Physical and functional obsolescence results in unplanned downtime due to failures in the drive components, which account for 11.3 % of the nominal operating time of the workshop.

With the growing demand for NPCC products, it has become necessary to increase the productivity of technological equipment, including enhancing the power of the electric drive and the drum rotation speed of the ball mill. Operational experience with ball mills indicates that productivity increases (without altering the drum design) are possible within a range of 10 – 15 %. This technical solution will allow NPCC, a chemical-metallurgical company, to increase the production of sodium monochromate by processing a larger volume of chromite and dolomite ores in the first shop's crushing section, thereby reducing production costs.

To achieve this, a replacement of the existing electric drive with a modern R167DV280V4/BVG122 geared motor with a power of 30 kW and a low-speed shaft rotation frequency of 22 rpm has been proposed. The drive is mounted on a welded sheet metal frame. A general-purpose gear coupling is used to connect the transmission shaft between the output shaft of the geared motor and the mill's drive shaft.

To assess the economic efficiency of implementing the upgraded drive for the tube ball mill, a capital cost estimate was prepared. The total investment required, including the cost of purchasing and installing the new equipment, amounts to approximately RUB 3.4 million. The expected economic effect of implementing the new drive is associated with a reduction in the time required for capital and routine repairs, leading to an increase in the ball mill's productivity by 3 t/h. The proposed modernization of the drive will reduce the cost of processing 1 ton of ore by 0.02 %, increase production profitability by 1.37 %, and boost sales profit by 1.29 %. At the current production volume, this will result in a significant economic benefit. The costs of implementing the proposed equipment will be recouped in less than three months from the start of its operation. These indicators demonstrate the economic efficiency of the developed project.

Conclusions

As a result of the modernization of the tube ball mill drive, its design was simplified, and the labor intensity of maintenance and repair was reduced. Replacing the old drive, which included an electric motor and a gearbox, with a new drive consisting of a geared motor and a gear coupling, allows for an extended maintenance interval, thereby reducing operational costs. Calculations show that the implementation of the proposed design solutions leads to a 0.02 % reduction in the cost of processing 1 ton of ore, a 1.37 % increase in production profitability, and a 1.29 % increase in sales profit. Additional capital expenditures do not exceed RUB 3.4 million and are recouped in less than three months.

References / Список литературы

1. Efremov D.B., Stepanov V.M., Chicheneva O.N. Modernization of rapid pressing of DUO rolling stand rolls in mill 2800 of JSC Ural Steel. *Stal'*. 2020; (8):44–47. (In Russ.).
Ефремов Д.Б., Степанов В.М., Чиченева О.Н. Модернизация механизма быстрого отжима валков прокатной клети ДУО стана 2800 АО «Уральская Сталь». *Сталь*. 2020;(8):44–47.
2. Nefedov A.V., Kitanov A.A., Chichenev N.A. Reengineering of the roller hardening machine of the sheet-rolling shop of JSC Ural Steel. *Chernye metally*. 2022;(3):22–26. https://doi.org/10.17580/chm.2022.05.04
Нефедов А.В., Китанов А.А., Чиченев Н.А. Реинжиниринг роликовой закалочной машины листопрокатного цеха АО «Уральская Сталь». *Черные металлы*. 2022;(3):22–26. https://doi.org/10.17580/chm.2022.05.04
3. Nefedov A.V., Tanchuk A.V., Chichenev N.A. Modification of car tippler drive at Donskoy Ore Mining and Processing Plant. *Gornyi zhurnal*. 2022;(8):52–56. (In Russ.). https://doi.org/10.17580/gzh.2022.08.07
Нефедов А.В., Танчук А.В., Чиченев Н.А. Модернизация привода опрокидывателя рудных вагонеток Донского ГОК АО «ТНК Казхром». *Горный журнал*. 2022;(8):52–56. https://doi.org/10.17580/gzh.2022.08.07
4. Bardovskiy A.D., Gorbatyuk S.M., Keropyan A.M., Bibikov P.Ya. Assessing parameters of the accelerator disk of a centrifugal mill taking into account features of particle motion on the disk surface. *Journal of Friction and Wear*. 2018;39(4): 326–329. https://doi.org/10.3103/S1068366618040037
5. Zinyagin A.G. Use of machine learning methods for determination of the boundary conditions coefficients in a FEM task for the case of accelerated cooling of hot-rolled sheet metal. *CIS Iron and Steel Review*. 2023;(1):58–66. https://doi.org/10.17580/cisisr.2023.01.10
6. Nefedov A.V., Svichkar V.V., Chicheneva O.N. Re-engineering of equipment to feed the melting furnace with aluminum Charge. In: *Proceedings of the 6th Int. Conf. on Industrial Engineering (ICIE 2020)*. 2021:1198–1204. https://doi.org/10.1007/978-3-030-54817-9_139

Information about the Authors / Сведения об авторах

***Andrei V. Nefedov*,** *Cand. Sci. (Pedagogical), Assist. Prof., Deputy Director*, Novotroitsk Branch of the National University of Science and Technology "MISIS"
E-mail: cosnovotr@rambler.ru

***Roman E. Ishmukhametov*,** *Student*, Novotroitsk Branch of the National University of Science and Technology "MISIS"
E-mail: peretz_97@mail.ru

***Nikolai A. Chichenev*,** *Dr. Sci. (Eng.), Prof. of the Chair "Engineering of Technological Equipment"*, National University of Science and Technology "MISIS"
ORCID: 0000-0002-9019-4675
E-mail: chich38@mail.ru

***Андрей Викторович Нефедов*,** *к.пед.н., доцент, заместитель директора*, Новотроицкий филиал НИТУ «МИСИС»
E-mail: cosnovotr@rambler.ru

***Роман Эдуардович Ишмухаметов*,** *студент*, Новотроицкий филиал НИТУ «МИСИС»
E-mail: peretz_97@mail.ru

***Николай Алексеевич Чиченев*,** *д.т.н., профессор кафедры инжиниринга технологического оборудования*, Национальный исследовательский технологический университет «МИСИС»
ORCID: 0000-0002-9019-4675
E-mail: chich38@mail.ru

Contribution of the Authors / Вклад авторов

A. V. Nefedov – formulation of the article idea, definition of the purpose and objectives of the research.
R. E. Ishmukhametov – analysis and generalization of the results.

N. A. Chichenev – search and analysis of publications, formation of the article concept, writing the text.

А. В. Нефедов – формулировка идеи работы, определение цели и задачи исследования.
Р. Э. Ишмухаметов – анализ и обобщение полученных результатов.
Н. А. Чиченев – поиск и анализ литературных источников, формирование концепции статьи, подготовка текста.

Received 13.07.2024
Revised 18.07.2024
Accepted 23.10.2024

Поступила в редакцию 13.07.2024
После доработки 18.07.2024
Принята к публикации 23.10.2024

INFORMATION TECHNOLOGIES AND AUTOMATIC CONTROL IN FERROUS METALLURGY / **ИНФОРМАЦИОННЫЕ ТЕХНОЛОГИИ И АВТОМАТИЗАЦИЯ В ЧЕРНОЙ МЕТАЛЛУРГИИ**

UDC 519.876.2
DOI 10.17073/0368-0797-2024-6-738-743

Original article
Оригинальная статья

Planning BOF repair system in conditions of quasi-periodic operation of units

M. E. Kornet[1], A. V. Zimin[2], I. V. Burkova[3], V. V. Zimin[2]

[1] **National University of Science and Technology "MISIS"** (4 Leninskii Ave., Moscow 119049, Russian Federation)
[2] **Siberian State Industrial University** (42 Kirova Str., Novokuznetsk, Kemerovo Region – Kuzbass 654007, Russian Federation)
[3] **V.A. Trapeznikov Institute of Control Sciences, Russian Academy of Sciences** (65 Profsoyuznaya Str., Moscow 117997, Russian Federation)

marya.kornet@gmail.com

Abstract. Using the example of the steelmaking production of JSC EVRAZ United West Siberian Metallurgical Plant, the paper considers the task of synchronous calendar planning in the interval of several planned periods of operation of basic oxygen furnace (BOF), BOF shops, production as a whole, as well as ongoing repairs of BOF for steelmaking production (two BOF shops with two and three BOFs). Scheduled stops of the BOF for repair depend on the actual achieved duration of the lining campaign and production schedules of the units and are performed when the current duration of the BOF campaign reaches a given standard value. Thus, the current duration of the BOF campaign is described by a discrete, nonlinear quasi-periodic function that does not have a fixed period, but has some regularity. Technological limitations were formalized, determining the minimum and maximum values of the number of melts per day that each of the workshops can produce with one or two BOFs operating simultaneously. The authors formulated the conditions to avoid performing two "cold" repairs in one shop in one planned period and ensuring daily processing by BOF shops of all cast iron coming from the blast furnace shop. In the proposed mathematical formulation of the problem, it is required to find such schedules of BOF repairs and such calendar plans of their work that satisfy the formulated constraints and optimize the non-linear criterion. The proposed criterion is aimed at ensuring the constant readiness of the shops for implementation of the production program and design productivity. The task is formulated for the conditions of trouble-free operation and stable provision of the shops with liquid cast iron as the main component of the metal charge of BOF smelting.

Keywords: steelmaking, BOF, campaign duration, BOF shop, quasi-periodicity, calendar plan, design productivity

For citation: Kornet M.E., Zimin A.V., Burkova I.V., Zimin V.V. Planning BOF repair system in conditions of quasi-periodic operation of units. *Izvestiya. Ferrous Metallurgy*. 2024;67(6):738–743. https://doi.org/10.17073/0368-0797-2024-6-738-743

Планирование системы ремонтов конвертеров в условиях квазипериодического функционирования агрегатов

М. Е. Корнет[1], А. В. Зимин[2], И. В. Буркова[3], В. В. Зимин[2]

[1] **Национальный исследовательский технологический университет «МИСИС»** (Россия, 119049, Москва, Ленинский пр., 4)
[2] **Сибирский государственный индустриальный университет** (Россия, 654007, Кемеровская область – Кузбасс, Новокузнецк, ул. Кирова, 42)
[3] **Институт проблем управления им. В.А. Трапезникова РАН** (Россия, 117997, Москва, ул. Профсоюзная, 65)

marya.kornet@gmail.com

Аннотация. На примере сталеплавильного производства АО «ЕВРАЗ Объединенный Западно-Сибирский металлургический комбинат» рассматривается задача синхронного календарного планирования в интервале нескольких плановых периодов работы конвертеров, конвертерных цехов, производства в целом, а также текущих ремонтов конвертеров сталеплавильного производства (два конвертерных цеха с двумя и тремя конвертерами). Плановые остановки конвертера на ремонт зависят от реальной достигнутой продолжительности кампании по футеровке и производственных календарных планов работы агрегатов. Ремонты выполняются при достижении текущей длительности кампании конвертера заданного нормативного значения. Таким образом, текущая длительность кампании конвертера описывается дискретной, нелинейной квазипериодической функцией, не имеющей фиксированного периода, но обладающей некоторой регулярностью. Формализованы технологические ограничения, определяющие минимальные и максимальные значения количества

плавок в сутки, которое может провести каждый из цехов при одном или двух одновременно работающих конвертерах. Сформулированы условия, позволяющие избежать выполнения в одном цехе двух «холодных» ремонтов в одном плановом периоде и обеспечивающие ежесуточную переработку конвертерными цехами всего поступающего из доменного цеха чугуна. В предлагаемой математической постановке задачи требуется найти такие графики ремонтов конвертеров и такие календарные планы их работы, которые удовлетворяют сформулированным ограничениям и оптимизируют нелинейный критерий. Предложенный критерий направлен на обеспечение постоянной подготовленности цехов для выполнения производственной программы и проектной производительности. Задача сформулирована для условий безаварийной работы и стабильного обеспечения цехов жидким чугуном как основной составляющей металлозавалки конвертерной плавки.

Ключевые слова: сталеплавильное производство, конвертер, длительность кампании, конвертерный цех, квазипериодичность, календарный план, проектная производительность

Для цитирования: Корнет М.Е., Зимин А.В., Буркова И.В., Зимин В.В. Планирование системы ремонтов конвертеров в условиях квазипериодического функционирования агрегатов. *Известия вузов. Черная металлургия*. 2024;67(6):738–743. https://doi.org/10.17073/0368-0797-2024-6-738-743

Introduction

The basic oxygen furnace (BOF) process is widely regarded as the most effective method for improving economic efficiency and enhancing the quality of metallurgical products [1 – 3].

In Russia, BOF production mirrors the key challenges faced globally, including optimizing the composition of processed charges and reducing losses and resource consumption in the process [4 – 6]. Modern economic conditions demand improvements in production planning, technological advancements, the development of new refractory materials, and innovative BOF lining repair methods. These efforts aim to significantly extend unit campaign durations and reduce refractory consumption [6 – 9]. As a result, planning production metrics, along with the maintenance and repair of equipment and auxiliary systems, remains a critical focus for achieving the highest possible technical and economic performance in BOF shops [10 – 12].

Planning BOF repairs in steelmaking production presents unique challenges, as it requires multifactorial solutions when developing a calendar plan for BOF operations. In the case of other metallurgical units, the BOF repair schedule is a key input for their overall calendar planning [13 – 15]. This distinction stems from the fact that BOFs are taken offline for repairs once the number of melts conducted on a given lining reaches the defined standard campaign duration [16; 17]. The timing of this milestone depends on the unit's operational calendar and often results in repairs being carried out at irregular intervals under production conditions [18 – 20].

Key concepts and notations

Let $O = \{O_I, O_{II}\}$ represent the structure of the steelmaking production, which includes two BOF shops: $O_I = \{o_1, o_2, o_3\}$ and $O_{II} = \{o_4, o_5\}$. The first shop operates three BOFs of the same type, while the second shop operates two. The planning interval for BOF repairs depends on the standard campaign durations of the BOFs, their charge capacities, and the monthly volumes of cast iron supplied for processing. Let $(T_1, T_2, ..., T_j, ..., T_P)$ denote the sequence of months in the BOF repair planning interval; $T_j = \left(\Delta t_{s_j} | s_j = \overline{1, S_j}\right)$; and S_j represent the number of days in the j-th month. The volumes of cast iron processed per melt cycle by the BOFs in the first and second shops are denoted as $g(O_I)$ and $g(O_{II})$ respectively. The cast iron consumption coefficients for producing one ton of steel in the corresponding shops are ρ_I, ρ_{II} and the standard campaign durations of the BOFs are K_I and K_{II}. Let $\left\{\left(s_j^{r_{ic}^n}, s_{j'}^{r_{ic}^e}\right) | c = \overline{1,2,...}\right\}$, $i = \overline{1,5}$ represent the planned intervals for BOF repairs, where $s_j^{r_{ic}^n}$ and $s_{j'}^{r_{ic}^e}$ are the days when the c-th repair of the i-th BOF begins and ends, respectively. If $j = j'$, the repair starts and finishes within the same planning period j. If $j \neq j'$, the repair begins in period j and ends in period j', with the repair lasting $\left(S_j - s_j^{r_{ic}^n}\right)$ days in period j and $s_{j'}^{r_{ic}^e}$ days in period j'.

It is important to note that the reduction in scrap metal supply under current market conditions has made scrap metal prices comparable to the cost of cast iron production. As a result, the cast iron consumption coefficients ρ_I and ρ_{II} are no longer considered constants and are now given as interval-based estimates:

$$\begin{aligned} \rho_I &\in \left(\rho_I^{\min}, \rho_I^{\max}\right); \\ \rho_{II} &\in \left(\rho_I^{\min}, \rho_I^{\max}\right). \end{aligned} \quad (1)$$

Advancements in BOF production technology – such as the introduction of secondary steelmaking, real-time monitoring of BOF lining conditions, and periodic "hot" repairs between scheduled overhauls involving lining replacement – have significantly extended BOF campaign durations, which now often exceed 6000 melts. At the same time, the total number of "cold" BOF repairs has decreased. Additionally, different suppliers of specia-

lized materials for "hot" repairs offer varying guarantees on BOF campaign durations, leading to the widespread use of the term "guaranteed BOF durability." In modern practice, campaign duration is typically determined by the refractory supplier under a specific contractual agreement:

$$K_I = \left(K_1^{\min},\ K_1^{\max}\right);$$
$$K_{II} = \left(K_{1I}^{\min},\ K_{1I}^{\max}\right). \quad (2)$$

The understanding of "cold" repairs has also evolved. Previously, this term referred exclusively to the time required to replace the BOF lining. Today, such repairs are generally combined with maintenance of auxiliary equipment and other metallurgical units. As a result, BOF stop for repairs may exceed the duration of the current planned production period.

Unless otherwise specified, the evaluations of the parameters introduced will be treated as point estimates rather than interval estimates.

Let us denote the number of melts produced daily by BOF i in shops O_I and O_{II} as $m_{ij}\left(\Delta t_{s_j}\right)$, $m_{Ij}\left(\Delta t_{s_j}\right)$, $m_{IIj}\left(\Delta t_{s_j}\right)$. It is evident that:

$$\sum_{i=1}^{3} m_{ij}\left(\Delta t_{s_j}\right) = m_{Ij}\left(\Delta t_{s_j}\right);$$
$$\sum_{i=4}^{5} m_{ij}\left(\Delta t_{s_j}\right) = m_{IIj}\left(\Delta t_{s_j}\right). \quad (3)$$

The calendar plan for the operation of the i-th BOF in the j-th month is defined as the sequence

$$m_{ij}\left(\Delta t_{s_j}\right) \mid s = \overline{1,S}_j. \quad (4)$$

The joint operation of BOFs in the shops is governed by technological constraints that define the range of daily melts in each shop, depending on whether one or two BOFs are operating simultaneously:

$$\underline{m_I^1} \le m_{ij}\left(\Delta t_{s_j}\right) \le \overrightarrow{m_I^1},\ i = \overline{1,3},\ j = \overline{1,P}; \quad (5)$$

$$\underline{m_{II}^1} \le m_{ij}\left(\Delta t_{s_j}\right) \le \overrightarrow{m_{II}^1},\ i = \overline{4,5},\ j = \overline{1,P}; \quad (6)$$

$$2\underline{m_I^1} \le \left(m_{ij}(\Delta t_s) + m_{i'j}(\Delta t_s)\right) \le \overline{2m_I^1};$$
$$i \ne i',\ i,\ i' = \overline{1,3},\ j = \overline{1,P}; \quad (7)$$

$$2\underline{m_{II}^1} \le \left(m_{4j}(\Delta t_s) + m_{5j}(\Delta t_s)\right) \le \overline{2m_{II}^1},\ j = \overline{1,P}, \quad (8)$$

where $\underline{m_I^1}$, $\overrightarrow{m_I^1}$, $\underline{m_{II}^1}$, $\overrightarrow{m_{II}^1}$, $2\underline{m_I^1}$, $\overline{2m_I^1}$, $2\underline{m_{II}^1}$, $\overrightarrow{2m_{II}^1}$ are the minimum and maximum numbers of melts produced in the first and second shops, respectively, when operating a single BOF, as well as the minimum and maximum numbers of melts produced when two BOFs are in operation.

Operating three BOFs in the first shop is technologically challenging to implement.

We define the function $k_{ij}(s_j)$, which represents the number of melts produced by the i-th BOF by the end of day s_j in the j-th period. The number of melts is limited by the campaign durations of the BOFs

$$k_{ij}\left(s_j\right) \le \begin{cases} K_I,\ i = \overline{1,3}; \\ K_{II},\ i = \overline{4,5}. \end{cases} \quad (9)$$

The set of possible start times $s_j^{r_{i_c}^n}$ for BOF repairs is determined by the following relationships

$$\left\{ s_j^{r_{i_c}^n} \mid k_{ij}\left(s_j\right) \ge K_I \right\},\ i = \overline{1,3};$$
$$\left\{ s_j^{r_{i_c}^n} \mid k_{ij}\left(s_j\right) \ge K_{II} \right\},\ i = \overline{4,5}. \quad (10)$$

The completion time $s_j^{r_{i_c}^e}$ for repairs is determined by their specified duration r_{i_c}, $c = \overline{1,2,\ldots}$

In steelmaking production, the design and repair management system ensures that no two "cold" repairs are carried out in the same shop during a single planned period. Additionally, the first shop is designed to maintain the continuous operation of two BOFs, while the third is either under repair or held in reserve. As a result, during each planned period T_j one of the following four operating modes is implemented in each shop:

1. No repairs are performed on either of the two operational BOFs

$$\left(s_j^{r_{i_c}^n}, s_j^{r_{i_c}^e}\right) \not\subset T_j. \quad (11)$$

2. One of the operational BOFs is undergoing repairs

$$\left(s_j^{r_{i_c}^n}, s_j^{r_{i_c}^e}\right) \subset T_j. \quad (12)$$

3. Repairs on one of the operational BOFs, started in a previous period, are completed

$$T_{j-1}\left(s_{j-1}^{r_{i_c}^n}, s_j^{r_{i_c}^e}\right) \bigcap T_j = \overline{1, s_j^{r_{i_c}^e}}. \quad (13)$$

4. Repairs on one of the operational BOFs are initiated and will be completed in a subsequent period

$$T_{j+1}\left(s_j^{r_{i_c}^n}, s_{j+1}^{r_{i_c}^e}\right) \bigcap T_j = \overline{s_{j+1}^{r_{i_c}^n}, S_j}. \quad (14)$$

Let k_{ij}^n represent the number of melts produced by the *i*-th BOF at the beginning of the *j*-th planning period. Based on expression (4), the number of melts k_{ij}^e, produced by the *i*-th BOF by the end of the *j*-th planning period, for each operating mode, is described by the following functions

$$k_{ij}^e = k_{ij}^n + \sum_{l=1}^{S_j} m_i\left(\Delta t_{s_j}\right); \quad (15)$$

$$k_{ij}^e = k_{ij}^n + \sum_{l=1}^{s_j^{r_{ic}^n}} m_i\left(\Delta t_{s_j}\right) + \sum_{l=s_j^{r_{ic}^e}+1}^{S_j} m_i\left(\Delta t_{s_j}\right); \quad (16)$$

$$k_{ij}^e = k_{ij}^n + \sum_{l=s_j^{r_{ic}^e}+1}^{S_j} m_i\left(\Delta t_{s_j}\right); \quad (17)$$

$$k_{ij}^e = k_{ij}^n + \sum_{l=1}^{s_j^{r_{ic}^n}} m_i\left(\Delta t_{s_j}\right). \quad (18)$$

The function $k_{ij}(s_j)$, which represents the number of melts produced by the *i*-th BOF by the end of day s_j exhibits quasi-periodic behavior (irregular periodicity). It has a "sawtooth" shape, with a maximum value of K_I for BOFs in the first shop and K_{II} for BOFs in the second shop. The length of the "sawtooth base" depends on the number of melts produced daily by the BOF until the function reaches its maximum value, at which point it resets to zero. The spacing between the "teeth" of the saw corresponds to the BOF repair duration, during which the function also equals zero.

The oscillations of $k_{ij}(s_j)$ follow a regular pattern but lack a fixed period.

Using the sequences

$$\left(g_j^{\text{in}}\left(\Delta t_{s_j}\right)|s_j = \overline{1,S_j}\right),$$

$$\left(g_{Ij}^{\text{in}}\left(\Delta t_{s_j}\right)|s_j = \overline{1,S_j}\right),$$

$$\left(g_{IIj}^{\text{in}}\left(\Delta t_{s_j}\right)|s_j = \overline{1,S_j}\right)$$

we can describe the daily inflow of liquid iron from blast furnace production to the steelmaking facilities as a whole, as well as to the first and second shops during the *j*-th period. It is evident that $g_{Ij}^{\text{in}}\left(\Delta t_{s_j}\right) + g_{IIj}^{\text{in}}\left(\Delta t_{s_j}\right) = g^{\text{in}}\left(\Delta t_{s_j}\right)$, $s_j = \overline{1,S_j}$. Let

$$\sum_{s_0=1}^{S_j} g_j^{\text{in}}\left(\Delta t_{s_j}\right) = G_{T_j}^{\text{in}},$$

where $G_{T_j}^{\text{in}}$ is the monthly volume of cast iron requiring processing. Similarly, we define the values $G_{IT_j}^{\text{in}}$ and $G_{IIT_j}^{\text{in}}$, $G_{IT_j}^{\text{in}} + G_{IIT_j}^{\text{in}} = G_{T_j}^{\text{in}}$. To calculate the number of melts required to process the incoming cast iron on day s_j described by the sequence $\left(g_{Ij}^{\text{in}}\left(\Delta t_{s_j}\right)|s_j = \overline{1,S_j}\right)$, we use the following recursive procedure:

$$m_{Ij}^{\text{in}}(\Delta t_1) = \left[\frac{g_{Ij}^{\text{in}}(\Delta t_1)}{g(O_I)}\right];$$
$$m_{Ij}^{\text{in}}(\Delta t_2) = \left[\frac{g_{Ij}^{\text{in}}(\Delta t_2) + g_{Ij}^{\text{in}}(\Delta t_1)}{g(O_I)} - \frac{m_{Ij}^{\text{in}}(\Delta t_1)\, g(O_I)\rho_I}{g(O_I)}\right] \quad (19)$$

continuing until $s_j = S_j$.

This results in a sequence $\left(m_{Ij}^{\text{in}}\left(\Delta t_{s_j}\right)|s_j = \overline{1,S_j}\right)$, that describes the daily number of melts the first shop must produce. A similar sequence can be calculated $\left(m_{IIj}^{\text{in}}\left(\Delta t_{s_j}\right)|s_j = \overline{1,S_j}\right)$ for the second shop. Let us represent the monthly volumes of cast iron requiring processing in the $M_{IT_j} = \sum_{s_j=1}^{S_j} m_I^{\text{in}}\left(\Delta t_{s_j}\right)$ and $M_{IIT_j} = \sum_{s_j=1}^{S_j} m_{II}^{\text{in}}\left(\Delta t_{s_j}\right)$ first and second shops, respectively, expressed as the number of melts. It is evident that $M_{IT_j} g(O_I) + M_{IIT_j} g(O_{II}) = G_{T_j}^{\text{in}}$.

The current campaign durations of the BOFs are significantly higher than the monthly production volume of their respective shops:

$$M_{IT_j} \ll K_I;\ M_{IIT_j} \ll K_{II}. \quad (20)$$

Now, let us define a condition to prevent two "cold" repairs from being carried out in the same shop during a single planning period. We will start with the second shop, which operates two BOFs. Due to the quasi-periodic nature of the functions $k_{4j}(s_j)$ and $k_{5j}(s_j)$, and because the campaign durations K_{II} of the BOFs are identical, the maximum possible difference between the values $k_{4j}(s_j)$ and $k_{5j}(s_j)$ of these functions is $K_{II}/2$:

$$\left|k_{4j}(s_j) - k_{5j}(s_j)\right| \le K_{II}/2. \quad (21)$$

Therefore, the best way to stagger the repairs of the fourth and fifth BOFs is to maintain the approximate equality

$$\left|k_{4j}(s_j) - k_{5j}(s_j)\right| \approx K_{II}/2. \quad (22)$$

Equation (20) also indicates that if one BOF is taken offline for repair, the remaining BOF has enough capacity to handle the entire production plan for the current planning period.

For the first shop, which operates three BOFs, the design provides for the continuous operation of two BOFs, while the third is either under repair or held in

reserve. The reserved BOF is brought online whenever one of the operating BOFs is taken offline for repair. Under this scheme, with two BOFs operating continuously, the condition for staggering their repairs, similar to that of the second shop, can be written as

$$\left|k_{ij}\left(s_j\right)-k_{i'j}\left(s_j\right)\right|\approx K_I/2;\ i,\ i'\in\{1,2,3\}, \qquad (23)$$

where i, $i'\in\{1, 2, 3\}$ are the BOFs operating in the first shop on day s_j.

Task formulation for planning BOF repairs and operations across planned periods (T_1, T_2, ..., T_j, ..., T_P)

The objective is to determine sequences

$$\left(m_{ij}\left(\Delta t_{s_j}\right)\,|\,s_j=\overline{1,S_j}\right),\ i=\overline{1,5},\ j=\overline{1,P} \qquad (24)$$

and BOF repair schedules

$$\left(s_j^{r_{i_c}^n},\ s_j^{r_{i_c}^e}\right)\subset\bigcup_{j=1}^{P}T_j,\ i=\overline{1,5},\ c=\overline{1,2,\ldots}, \qquad (25)$$

that satisfy equations (5) – (8), the constraint

$$g(O_I)\sum_{i=1}^{3}m_{ij}\left(\Delta t_{s_j}\right)+g(O_{II})\sum_{i=4}^{5}m_{ij}\left(\Delta t_{s_j}\right)=g_j^{\text{in}}\left(\Delta t_{s_j}\right), \qquad (26)$$

and conditions (11) – (14) for performing repairs under specific operational modes, while minimizing criterion

$$Q=\sum_{j=1}^{P}\left\{\left(\left|k_{ij}^e-k_{i'j}^e\right|-0{,}5K_1\right)+\right.$$
$$\left.+\left(\left|k_{4j}^e-k_{5j}^e\right|-0{,}5K_{II}\right)\right\}\to\min, \qquad (27)$$

where i, $i'\in\{1, 2, 3\}$ denote the indices of the BOFs operating in the first shop on day S_j, and the values k_{ij}^e are determined in accordance with rules (15) – (18).

The criterion is designed to ensure conditions that enable the shops to achieve their design production capacities during each planning period.

Conclusions

Using the steelmaking production at JSC EVRAZ United West Siberian Metallurgical Plant as an example, the problem of synchronous calendar planning is examined. This planning covers multiple periods, including the operation of BOFs, BOF shops, and the production process as a whole, as well as ongoing BOF repairs. Scheduled BOF stops for repairs depend on the actual duration of the lining campaign achieved and the production schedules of the units. Repairs are carried out when the current campaign duration of a BOF reaches the specified standard value.

References / Список литературы

1. Grigorovich K.V. Metallurgy of the XXI century: Current state and directions of development. In: *Proceedings of the XIV Int. Congress of Steelmakers. Moscow, Elektrostal, October 17-21, 2016*. Moscow: Metallurgical Plant "Elektrostal'"; 2016:56–65. (In Russ.).

   Григорович К.В. Металлургия XXI века: современное состояние и направления развития. В кн.: *Труды XIV международного конгресса сталеплавильщиков. Москва; Электросталь, 17-21 октября 2016 г.* Москва: Изд-во: АО «Металлургический завод «Электросталь»; 2016:56–65.
2. Guzela D., Oliveira J., Staudinger G., Muller J. The latest model of the oxygen converter as a result of half a century of technology development. In: *Proceedings of the IX Congress of Steelmakers*. Moscow: Chermetinformatsiya; 2014:153–163. (In Russ.).

   Гузела Д., Оливейра Дж., Стаудингер Г., Муллер Дж. Новейшая модель кислородного конвертера как результат полувекового развития технологии. В кн.: *Труды IX конгресса сталеплавильщиков*. Москва: Черметинформация; 2014:153–163.
3. Petrushka R., Manley S. Improvement in oxygen lance life. In: *Steelmaking Conference Proceedings*. 2000:245–250.
4. Tabata Y., Marsh R.C., Kelly P., etc. Impovement of BOP steel refining blowing control using wide angle lance nozzles. In: *Steelmaking Conference Proceedings*. 1998:451–457.
5. Brun L. Overcapacity in steel: China's Role in a Global Problem. Center on Globalization, Governance & Competitiveness, Duke University; 2016:54. https://doi.org/10.13140/RG.2.2.11923.48161
6. Mutumi Ohji. Recent trends and future in steelmaking technology in Japan. *ISIJ International*. 1996;36:S2–S5. https://doi.org/10.2355/isijinternational.36.Suppl_S2
7. Springorum D. The management of research and technology in the German steel industry with respect to the European Union. *ISIJ Intemational*. 1998;38(9):935–942. https://doi.org/10.2355/isijinternational.38.935
8. Macanley D. Engineering developments lead to greater economy. *Steel Times International*. 1996;(5):12–14.
9. Rymarchyk N. Post combustion lances in Basic Oxygen Furnace (BOF) operations. In: *Steelmaking Conference Proceedings*. 1998:445–449.
10. Messina C.J. Slag splashing in the BOF – world wide status, practices and results. *Iron and Steel Engineer*. 1996;(5):17–19.
11. Protopopov E.V., Temlyantsev M.V. Improving the Technology of Increasing the Durability of Oxygen Converter Lining. Novosibirsk: SB RAS; 2023:324. (In Russ.).

    Протопопов Е.В., Темлянцев М.В. Совершенствование технологии повышения стойкости футеровки кислородных конвертеров. Новосибирск: СО РАН; 2023:324.
12. Shoukhin' T., Yan'ven' Yu. Reuse and restoration of used refractories. *Ogneupory i tekhnicheskaya keramika*. 2007;(5):29–34.

    Шоухинь Т., Яньвэнь Ю. Повторное использование и восстановление отработанных огнеупоров. *Огнеупоры и техническая керамика*. 2007;(5):29–34.

13. Lasdon Leon S. Optimization Theory for Large Systems. New York: Macmillan; 1970:523.

14. Russell R.O., Donaghy N., Meyer E.C., Goodson K.M. Everlasting BOF linings at LTV Steel? In: *Proceedings of the 1st European Oxygen Steelmaking Congress, Düsseldorf/Neuss, June 21–23, 1993*. Verlag Stahleisen GmbH; 1993:220–225.

15. Prokhorov I.M., Zimin A.V., Burkova I.V., Zimin V.V. Formulation and decomposition of the task of calendar planning of repairs and operation of steelmaking converters. *Sistemy upravleniya i informatsionnye tekhnologii*. 2024;(2(96)): 38–40. (In Russ.).

Прохоров И.М., Зимин А.В., Буркова И.В., Зимин В.В. Постановка и декомпозиция задачи календарного планирования ремонтов и работы конвертеров сталеплавильного производства. *Системы управления и информационные технологии*. 2024;(2(96)):38–40.

16. Prokhorov I.M., Zimin A.V., Burkova I.V., Zimin V.V. On the procedure for solving the problem of scheduling repairs of converters of a steelmaking workshop with two units. *Sistemy upravleniya i informatsionnye tekhnologii*. 2024;(2(96)): 64–67. (In Russ.).

Прохоров И.М., Зимин А.В., Буркова И.В., Зимин В.В. О процедуре решения задачи построения расписания ремонтов конвертеров сталеплавильного цеха с двумя агрегатами. *Системы управления и информационные технологии*. 2024;(2(96)):64–67.

17. Zimin V.V. Building coordinated schedules for production units of the steel-rolled complex: Extended Abstract of Cand. Sci. Diss. Moscow: MISiS; 1979:21.

Зимин В.В. Построение согласованных расписаний для производственных звеньев комплекса «сталь-прокат»: автореф. канд. дис. 05.13.06. Москва: МИСиС; 1979:21.

18. Lohmer J., Lasch R. Production planning and scheduling in multi-factory production networks: A systematic literature review. *International Journal of Production Research*. 2021;59(7):2028–2054. https://doi.org/10.1080/00207543.2020.1797207

19. Moghaddam M., Moosavi E. A view on recent developments for production scheduling optimization. In: *Proceedings of the 26th Int. Mining Congress and Exhibition of Turkey (IMCET 2019)*. 2019:166–173.

20. Li Y., Goga K., Tadei R., Terzo O. Production scheduling in industry 4.0. In: *Complex, Intelligent and Software Intensive Systems, Advances in Intelligent Systems and Computing*. Barolli L., Poniszewska-Maranda A., Enokido T. eds. 2020;1194.

Information about the Authors / Сведения об авторах

Maria E. Kornet, *Senior Lecturer of the Chair of Engineering Cybernetics*, National University of Science and Technology "MISIS"
ORCID: 0000-0003-4100-5644
E-mail: marya.kornet@gmail.com

Aleksei V. Zimin, *Dr. Sci. (Eng.), Assist. Prof., Head of the Chair of Automation and Information Systems*, Siberian State Industrial University
ORCID: 0000-0002-0485-9846
E-mail: zimin.0169@yandex.ru

Irina V. Burkova, *Dr. Sci. (Eng.), Assist. Prof., Leading Researcher*, V.A. Trapeznikov Institute of Control Sciences, Russian Academy of Sciences
ORCID: 0000-0002-4671-0847
E-mail: irbur27@gmail.com

Valerii V. Zimin, *Dr. Sci. (Eng.), Prof. of the Chair of Automation and Information Systems*, Siberian State Industrial University
ORCID: 0000-0003-4152-3572
E-mail: zimin1945@sibsiu.ru

Мария Евгеньевна Корнет, *старший преподаватель кафедры инженерной кибернетики*, Национальный исследовательский технологический университет «МИСИС»
ORCID: 0000-0003-4100-5644
E-mail: marya.kornet@gmail.com

Алексей Валерьевич Зимин, *д.т.н., доцент, заведующий кафедрой автоматизации и информационных систем*, Сибирский государственный индустриальный университет
ORCID: 0000-0002-0485-9846
E-mail: zimin.0169@yandex.ru

Ирина Владимировна Буркова, *д.т.н., доцент, ведущий научный сотрудник*, Институт проблем управления им. В.А. Трапезникова РАН
ORCID: 0000-0002-4671-0847
E-mail: irbur27@gmail.com

Валерий Викторович Зимин, *д.т.н., профессор кафедры автоматизации и информационных систем*, Сибирский государственный индустриальный университет
ORCID: 0000-0003-4152-3572
E-mail: zimin1945@sibsiu.ru

Contribution of the Authors / Вклад авторов

M. V. Kornet – formulation of research tasks, development and implementation of the algorithm, analysis of the results.
A. V. Zimin – formulation of the problem, formation of conclusions.
I. V. Burkova – formulation of research tasks, data analysis.
V. V. Zimin – technological description of the task, justification of the research direction, analysis of the results.

М. В. Корнет – постановка задачи исследования, разработка и реализация алгоритма, анализ полученных результатов.
А. В. Зимин – постановка проблемы, формирование выводов.
И. В. Буркова – постановка задач исследования, анализ данных.
В. В. Зимин – технологическое описание поставленной задачи, обоснование направления исследований, анализ полученных результатов.

Received 16.09.2024
Revised 24.09.2024
Accepted 25.09.2024

Поступила в редакцию 16.09.2024
После доработки 24.09.2024
Принята к публикации 25.09.2024

Index of articles "Izvestiya. Ferrous Metallurgy" for 2024, Vol. 67

HISTORY OF METALLURGY

METALLURGICAL TECHNOLOGIES

RESOURCE SAVING IN FERROUS METALLURGY

ECOLOGY AND RATIONAL USE OF NATURAL RESOURCES

SUPERDUTY STEEL

MATERIAL SCIENCE

INNOVATIONS IN METALLURGICAL INDUSTRIAL AND LABORATORY EQUIPMENT, TECHNOLOGIES AND MATERIALS

PHYSICO-CHEMICAL BASICS OF METALLURGICAL PROCESSES

INFORMATION TECHNOLOGIES AND AUTOMATIC CONTROL IN FERROUS METALLURGY

BASED ON THE MATERIALS OF THE INTERNATIONAL CONFERENCE "SCIENTIFIC AND PRACTICAL SCHOOL FOR YOUNG METALLURGISTS"

Указатель статей, помещенных в журнале «Известия высших учебных заведений. Черная металлургия» за 2024 год, том 67

ИСТОРИЯ ОТРАСЛИ

МЕТАЛЛУРГИЧЕСКИЕ ТЕХНОЛОГИИ

РЕСУРСОСБЕРЕЖЕНИЕ В ЧЕРНОЙ МЕТАЛЛУРГИИ

ЭКОЛОГИЯ И РАЦИОНАЛЬНОЕ ПРИРОДОПОЛЬЗОВАНИЕ

СТАЛИ ОСОБОГО НАЗНАЧЕНИЯ

МАТЕРИАЛОВЕДЕНИЕ

ИННОВАЦИИ В МЕТАЛЛУРГИЧЕСКОМ ПРОМЫШЛЕННОМ И ЛАБОРАТОРНОМ ОБОРУДОВАНИИ, ТЕХНОЛОГИЯХ И МАТЕРИАЛАХ

ФИЗИКО-ХИМИЧЕСКИЕ ОСНОВЫ МЕТАЛЛУРГИЧЕСКИХ ПРОЦЕССОВ

ИНФОРМАЦИОННЫЕ ТЕХНОЛОГИИ И АВТОМАТИЗАЦИЯ В ЧЕРНОЙ МЕТАЛЛУРГИИ

ПО МАТЕРИАЛАМ МЕЖДУНАРОДНОЙ КОНФЕРЕНЦИИ «НАУЧНО-ПРАКТИЧЕСКАЯ ШКОЛА ДЛЯ МОЛОДЫХ МЕТАЛЛУРГОВ»

Над номером работали:

Л.И. Леонтьев, *главный редактор*

Е.В. Протопопов, *заместитель главного редактора*

Е.А. Ивани, *ответственный секретарь*

Л.П. Бащенко, *заместитель ответственного секретаря*

Е.Ю. Потапова, *заместитель главного редактора по развитию*

О.А. Долицкая, *научный редактор*

Е.М. Запольская, *ведущий редактор*

В.В. Расенець, *верстка, иллюстрации*

Г.Ю. Острогорская, *менеджер по работе с клиентами*

Подписано в печать 20.12.2024. Формат 60×90 $^{1}/_{8}$. Бум. офсетная № 1.
Печать цифровая. Усл. печ. л. 15,25. Заказ 21240. Цена свободная.

Отпечатано в типографии Издательского Дома МИСИС.
119049, Москва, Ленинский пр-кт, д. 4, стр. 1.
Тел./факс: +7 (499) 236-76-17

Зарегистрирован Федеральной службой по надзору в сфере связи, информационных технологий и массовых коммуникаций. Свидетельство о регистрации ПИ № ФС77-35456.

Подписной индекс 70383.